The role of Vitamin D metabolic enzymes in bone development and repair

by

Roy Pascal Naja

Department of Human Genetics

McGill University

Montreal, Quebec

Canada

October 2008

A thesis submitted to McGill University in partial fulfillment of the requirements of the Degree of Doctor of Philosophy.

Your file Votre référence
ISBN: 978-0-494-66619-7
Our file Notre référence
ISBN: 978-0-494-66619-7

To my Parents

Table of contents

Abstract

The *CYP27B1* enzyme that synthesizes 1α,25-$(OH)_2$D, is expressed in chondrocytes, suggesting that local production of 1α,25-$(OH)_2$D could play an autocrine or paracrine role in the differentiation of these cells. To test this hypothesis, we have engineered mutant mice that do not express the Cyp27b1 gene in chondrocytes. This led to increased width of the hypertrophic zone of the growth plate at E15.5, increased bone mass in neonatal long bones, and increased expression of the chondrocytic differentiation markers Indian Hedgehog and PTH/PTHrP receptor. VEGF mRNA levels were decreased, accompanied by decreased PECAM-1 immunostaining, suggesting a delay in vascularization. We have also engineered mice overexpressing a Cyp27b1 transgene in chondrocytes. The transgenic mice showed a partial mirror image phenotype compared to the tissue-specific inactivation model. These results support an autocrine/paracrine role of 1α,25-$(OH)_2$D in endochondral ossification and chondrocyte development *in vivo*.

The *CYP24A1* enzyme is involved in the catabolic breakdown of 1α,25-$(OH)_2$D but also synthesizes the 24R,25-$(OH)_2$D metabolite. Studies in chicken suggest a role for 24R,25-$(OH)_2$D in fracture repair. We induced stabilized transverse mid-diaphysial fractures of the tibia in four-month-old wild-type and Cyp24a1-deficient mice. Examination of the callus sections showed delayed hard callus formation in the homozygous mutant animals compared to wild-type littermates. RT-qPCR showed perturbed levels of type X collagen transcripts in mutant mice at 14 and 21 days post-fracture, reflecting the delayed healing. Rescue of the impaired healing by subcutaneous

injection of 24R,25-$(OH)_2D_3$ normalized the histological appearance of the callus, static histomorphometric index and type X collagen mRNA expression, while 1α,25-$(OH)_2D_3$ did not. These results show that Cyp24a1 deficiency delays fracture repair and strongly suggest that vitamin D metabolites hydroxylated at position 24, such as 24R,25-$(OH)_2D$, play an important role in the mechanisms leading to normal fracture healing.

Resumé

CYP27B1 est une enzyme qui produit la 1α,25-$(OH)_2$D. Elle est exprimée dans les chondrocytes, suggérant que la production locale de la 1α,25-$(OH)_2$D peut jouer un rôle autocrine ou paracrine dans la différenciation des chondrocytes. Afin de tester cette hypothèse, nous avons généré une lignée de souris qui n'exprime pas le gène Cyp27b1 dans les chondrocytes. L'inactivation des deux allèles Cyp27b1 conduit à: (a) une augmentation de l'épaisseur de la zone hypertrophique dans la plaque de croissance à l'age de 15.5 jours post-conception, (b) une augmentation de la masse osseuse dans les os longs des nouveau-nés, et (c) une augmentation de l'expression des marqueurs de la différenciation chondrocytiques tels que Indian Hedgehog et le récepteur PTH/PTHrP. L'expression des niveaux d'ARNm du marqueur angiogénique VEGF était diminuée, étant aussi accompagnée d'une diminution de PECAM-1, suggérant un retard dans le processus de la vascularisation. Nous avons aussi généré des lignées de souris qui surexpriment Cyp27b1 dans les chondrocytes sous l'effet du promoteur du collagène α_1(II). Ces souris montrent un phénotype partiellement opposé comparé aux souris dont le gène Cyp27b1 est inactivé dans les chondrocytes. Ces résultats suggèrent un rôle autocrine/paracrine de la 1α,25-$(OH)_2$D dans l'ossification endochondrale et dans le dévelopment des chondrocytes *in vivo*.

L'enzyme *CYP24A1* est non seulement impliquée dans le catabolisme de la 1α,25-$(OH)_2$D, mais aussi dans la synthèse du métabolite 24R,25-$(OH)_2$D. Des études chez le poulet ont suggéré un rôle pour la 24R,25-$(OH)_2$D dans la réparation des fractures. Nous avons soumis des souris contrôles et des souris déficientes en Cyp24a1 à

une fracture transversale stabilisée dans la diaphyse du tibia. L'examen des sections du callus montre que les animaux homozygotes mutants présentaient un délai dans la formation du callus par rapport aux animaux sauvages. L'expression des ARNm du collagène de type X est perturbée chez les souris mutantes aux jours 14 et 21 après la fracture, en accordance avec le délai de formation du callus observé. Pour essayer de corriger ceci, l'injection sous-cutanée de 24R,25-$(OH)_2D$ a normalisée l'apparance histologique du callus, les paramètres histomorphométriques, et l'expression du collagène de type X, tandis que la 1α,25-$(OH)_2D_3$ n'a pas eu cet effet. Ces résultats montrent que la déficience en Cyp24a1 retarde la réparation des fractures et suggèrent fortement que les métabolites de la vitamine D hydroxylés en position 24, tel le 24R,25-$(OH)_2D$, jouent un rôle important dans les mécanismes de réparation des fractures.

Acknowledgements

First and foremost, I would like to sincerely thank Dr. René St-Arnaud for taking me into his lab and offering me the opportunity to pursue a doctorate degree. He supervised me through every step of the way and provided me with all the tools necessary to conduct my work. Dr. St-Arnaud created and maintained a pleasant working environment for me and other members of the lab. I was privileged to have him as a mentor over the years and always enjoyed our stimulating scientific and social conversations. Thank you René.

I would like to thank Alice Arabian for all her intellectual and technical guidance. Alice was instrumental in arming me with many molecular biology skills in my first year of graduate work. Thank you Alice for always being there for me as a friend and a second mentor.

I would like to thank Dr. Benoit St-Jacques who always welcomed me in his lab and treated me as one of his graduate students. Dr. St-Jacques provided me with invaluable scientific advice at many occasions throughout my graduate training years. I would also like to thank Dr. Francis Glorieux and Dr. John White for serving as members of my graduate committee and offering me scientific guidance and support.

I would like to thank Dr. Omar Akhouayri for being a friend and a helpful colleague. An acknowledgment also goes to many past and present members of the Shriners research unit namely, Marco Cardelli, Anthony Ciarallo, Jad El-Hoss, Meg Debarats, Behareh Hekmatnejad, Barbara Small, Adamo Petosa, Dr. Thomas Meury, Claude Gauthier, Fares Hamadeh, Mireille Dussault, Micheline Vachon, Dr. Vice Mandic, Dr. Eunice

Lee, Dr. Peter Roughley and others. Also many thanks to Mia Esser, Louise Marineau and other members of the Shriners animal health group for breeding and maintaining my different mouse strains and helping in sample collections.

I would like to thank Guylaine Bedard for her help in the preparation of the figures shown in this work.

In the end, words are not enough to thank my parents Nicolas and Viviane and my siblings Carl and Chrytelle. My family and especially my parents provided me with every kind of support without which I wouldn't be able to get where I am today.

List of Figures

List of Tables

Abbreviations

μCT	microcomputed tomography
1α,25-$(OH)_2$D	1-alpha-25-dihydroxyvitamin D
24R,25-$(OH)_2$D	24R-25-dihydroxyvitamin D
25-(OH)D	25-hydroxyvitamin D
AF-2	activating function-2
BSP	bone sialoprotein
BV/TV	bone volume/tissue volume
C	carbon
CasR	calcium sensing receptor
CDK8	cyclin dependent kinase 8
Col10a1	collagen type X
Col1a1	collagen type I
Col2a1	collagen type α_1(II)
CYP24A1	human/chicken 25-hydroxyvitamin D-24-hydroxylase
Cyp24a1	mouse 25-hydroxyvitamin D-24-hydroxylase
CYP27B1	human 25-hydroxyvitamin D-1alpha-hydroxylase
Cyp27b1	mouse 25-hydroxyvitamin D-1alpha-hydroxylase
CYP2R1	human 25-hydroxylase
DBD	DNA binding domain
ECF	extra cellular fluid
ECM	extra cellular matrix

ERK1/2	extracellular-signal regulated kinase ½
FGF23	human fibroblast growth factor 23
Fgf23	mouse fibroblast growth factor 23
H&E	hematoxylin and eosin
Hif1α	hipoxia induced factor 1 alpha
Ihh	indian hedgehog
Kdr/VEGFR2	vascular endothelial growth factor receptor 2
LBD	ligand binding domain
MAPK	mitogen activated protein kinase
MMA	methyl methacrylate
MMP9	matrix metallopeptidase 9
NPT2a	sodium phosphate cotrasporter 2 a
NPT2b	sodium phosphate cotrasporter 2 b
OPN	osteopontin
PBS	phosphate buffered saline
PCNA	proliferating cell nuclear antigen
PECAM-1/CD31	platelet and endothelial cell adhesion molecule-1
PFA	paraformaldehyde
P_i	inorganic phosphate
PKC	protein kinase C
PLC	phospholipase C
PTH	parathyroid hormone
Pthr1	PTH/PTHrP receptor 1

PTHrP	parathyroid hormone related peptide
RANKL	receptor activator of NF-κB ligand
RXR	retinoid X receptor
TFIIB	transcription factor II beta
TRAP	tartrate resistant acid phosphatase
TRPV5	kidney epithelial calcium channel
TRPV6	intestinal epithelial calcium channel
UV	ultraviolet
VDBP	vitamin D binding protein
VDR	vitamin D receptor
VDRE	vitamin D response element
VEGF	vascular endothelial growth factor
VIP	VDR interacting-proteins

Foreword

This thesis has been written in the traditional format and meets all the requirements according to the "Guidelines Concerning Thesis Preparation" issued by the Faculty of Graduate Studies and Research. The thesis contains all the components listed in the "Guidelines", which are the following: 1) originality, 2) a properly formated title page, 3) a detailed table of contents, 4) a brief abstract in both English and French, 5) an acknowledgements section, 6) an introduction with detailed review of the subject matter, 7) a final conclusion and summary, 8) a thorough bibliography, and 9) an appendix section containing all the biosafety & ethics certificates.

We anticipate that two manuscripts will result from the work presented herein. The first part of the results section (Role of locally synthesized 1α,25-$(OH)_2$D in chondrocyte development and function) has been submitted for publication in the journal *Endocrinology* under the following title:

CHONDROCYTE-SPECIFIC MODULATION OF THE EXPRESSION OF CYP27B1, THE 25-HYDROXYVITAMIN D-1α-HYDROXYLASE, SUPPORTS A ROLE FOR LOCAL SYNTHESIS OF 1,25-DIHYDROXYVITAMIN D IN GROWTH PLATE DEVELOPMENT, by

Roy-Pascal Naja, Olivier Dardenne, Alice Arabian, and René St-Arnaud

(The submission confirmation and a copy of the manuscript are attached in Appendix A)

The second part of the results section (Fracture repair in Cyp24a1-deficient mice) is currently being prepared to be submitted for publication with myself as first author.

Contribution of authors

With the exception of the initial engineering of the Cyp24a1 knockout and Cyp27b1 floxed strains, ALL the experiments presented in this thesis were performed by myself. The floxed Cyp27b1 mouse was engineered by Dr. Olivier Dardenne. Complete characterization of the phenotype was done by myself. Myself, Dr. René St-Arnaud, and Alice Arabian, planned the engineering of the chondrocyte-specific Cyp27b1 overexpression model. I conducted all the subcloning experiments. The pronuclear injections were done at the McGill mouse transgenic facility. Complete characterization of the phenotype of the different transgenic strains was performed by myself. Alice Arabian and Dr. René St-Arnaud engineered the Cyp24a1 knockout mouse (Fig.40). I performed all the surgical procedures and the follow-up characterization of the fracture repair phenotype in these mice. Mireille Dussault measured the serum calcium and phosphate levels in the mice (Fig.41).

All the figures (except Fig.40 & Fig.41) in the results and discussion sections of this thesis are the experimental outcome of my own work. The experiments conducted by myself include:

1) Genotyping using Southern Blots and PCR (Fig. 29)

2) ATDC5 cell-culture transfections (Fig. 28)

3) Molecular cloning experiments (Construction of the Cyp27b1 transgene) (Fig. 27)

4) Immunoblotting (Fig. 30B)

5) RT-qPCR (Fig. 12, 21, 23, 24, 25, 30A, 34, 35, 37, 38, 39, 44, 46, 51, 55, Table 1, Table2)

6) Histological preparations and histomorphometric analysis (Fig. 13, 15, 18, 19, 20, 31, 32, 33, 43, 45, 48, 49, 50, 52, 53, 54)

7) Immunohistochemistry (Fig.14, 22)

8) Surgical procedure of fracture stabilization (Fig. 39, 42, 43, 45, 47, 48, 49, 52, 53)

9) Microcomputed-tomography analysis (Fig. 16, 17, 36)

10) ELISA (Fig. 26)

11) RadioImmunoAssay (Fig. 56, Table 3)

I. Introduction

I. 1-Endochondral ossification and the growth plate

The mammalian skeletal organ is composed of two types of connective tissue, bone and cartilage. The formation of bones occurs either through intramembranous ossification (flat bones) or endochondral ossification (long bones). Endochondral ossification is the process where bone is formed after passing through a cartilage intermediate. Intramembranous ossification is the process where bone is formed directly after the condensation of mesenchymal cells into osteoblasts that secrete a matrix that is later on mineralized to form bone. My interest in this thesis is the process of endochondral ossification in long bones where the skeletal cartilage anlagen are replaced by bone (Erlebacher et al., 1995). These cartilage anlagen are formed after mesenchymal cells condense into chondrocytes. The anlagen elongate and expand in width by proliferation of chondrocytes that deposit a cartilage matrix formed mainly of collagen type II and the proteoglycan aggrecan. These proliferative chondrocytes in the central region of the cartilage undergo further differentiation to become hypertrophic chondrocytes. The hypertrophic chondrocytes exit the cell cycle and secrete collagen type X (Iyama et al., 1991) and later on angiogenic factors. The angiogenic factors, comprised mainly of vascular endothelial growth factor (VEGF), induce vessel invasion from the perichondrium into these almost avascular cartilage anlagen around embryonic day 15 in mice. The vascular invasion brings along osteoblasts, osteoclasts, and hematopoeitic cells resulting in the formation of the primary ossification center (Olsen et

al., 2000). Once this occurs, the hypertrophic cartilage matrix is degraded and the hypertrophic chondrocytes undergo apoptosis. The osteoblasts will replace the degraded hypertrophic cartilage with trabecular bone and the bone marrow is formed (Fig. 1). Around the same time, the osteoblasts in the perichondrium form a collar of compact bone around the middle portion (diaphysis) of the anlagen, so that the primary ossification center ends up being located inside a tube of bone. At both ends (epiphyses) of the bone rudiment, secondary ossification centers (in which secondary growth plates emerge) are formed leaving a plate of cartilage (primary growth plate) between epiphysis and diaphysis (Fig. 2).

Postnatally, in the epiphyseal primary growth plate, we can morphologically distinguish between four different layers of chondrocytes (Fig. 3): a first region of resting chondrocytes followed by a second zone of flat, proliferating chondrocytes. These proliferating chondrocytes will exit the cell cycle, enlarge, and differentiate into a third layer of hypertrophic chondrocytes that secrete a specialized matrix comprised mostly of collagen type X that will later on calcify. The terminal layer of hypertrophic chondrocytes bordering the chondro-osseous junction will release angiogenic factors (mainly VEGF) and undergo apoptotic cell death. Recruited blood vessels coming from the metaphysis will invade this chondro-osseous junction. An almost identical process to the embryonic one will result in the degradation of the calcified cartilage matrix and the formation of trabecular bone and bone marrow.

The development of the growth plate and the postnatal process of endochondral ossification are regulated by the coordinated function of several molecular players. The central molecule was shown to be Indian Hedgehog (Ihh). Ihh secreted from the

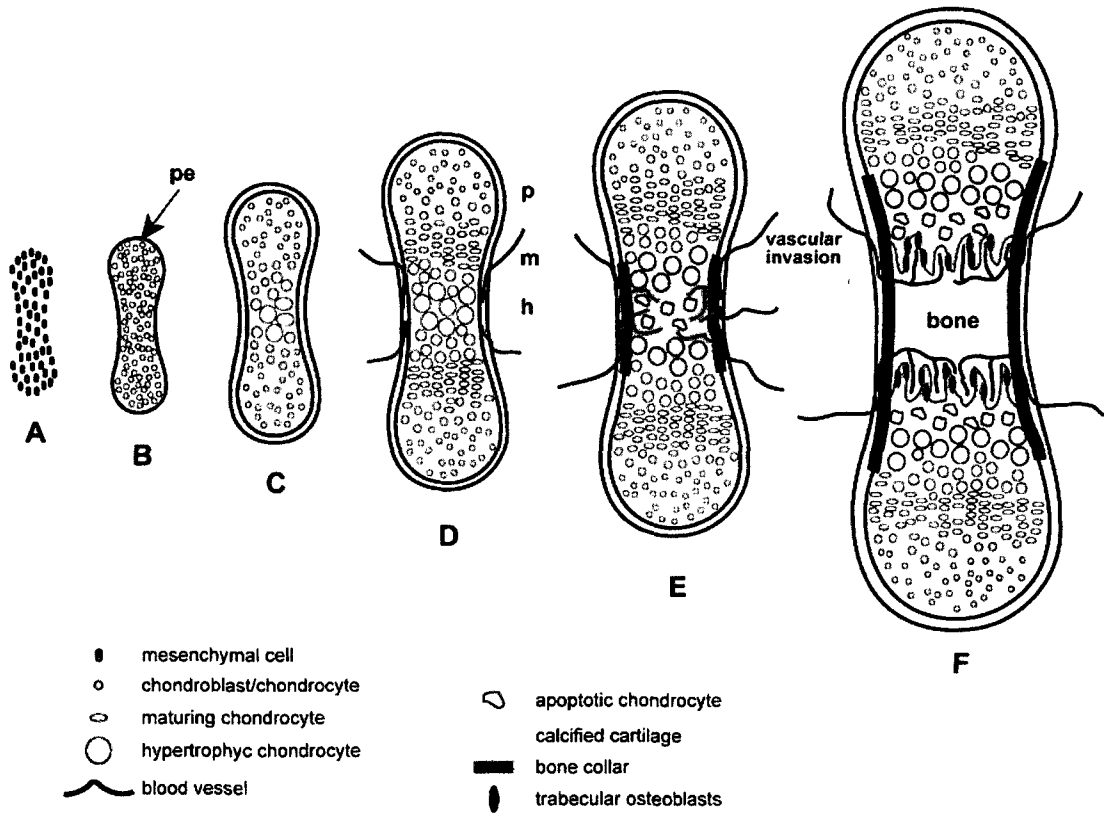

Figure 1 Schematic representation of the embryonic endochondral ossification process.

(**A**) Mesenchymal condensation start in cells committed to the chondrogenic fate. A perichondrium surrounding the chondroblast/chondrocyte appears in (**B**). Chondrocyte maturation starts in (**C**) where the mature hypertrophic chondrocytes localize in the center leaving both extremities to the proliferative chondrocytes. (**D**) Vascular invasion spurs from the perichondrium bringing with it osteoclasts and osteoblasts to replace the calcified matrix deposited by the hypertrophic chondrocytes that undergo apoptosis (**E**). (**F**) Formation of the primary ossification center and appearance of trabecular bone.

pe, perichondrium; p, proliferative zone; m, maturation zone; h, hypertrophic zone.

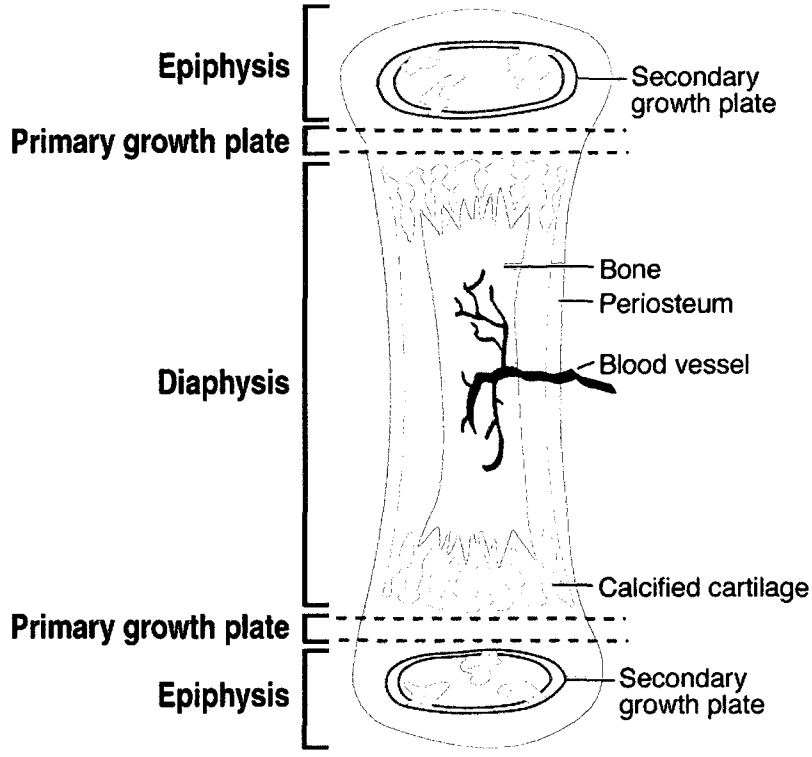

Figure 2 Anatomy of a postnatal long bone formed by endochondral ossification. The epiphyses at both ends contain the secondary growth plates (formed by secondary ossification). Going inward from the epiphyses are the two primary growth plates bordered by the central diaphysis. The diaphysis, surrounded by the bone periosteum, contains the calcified cartilage that will be replaced inward by vascularized trabecular bone.

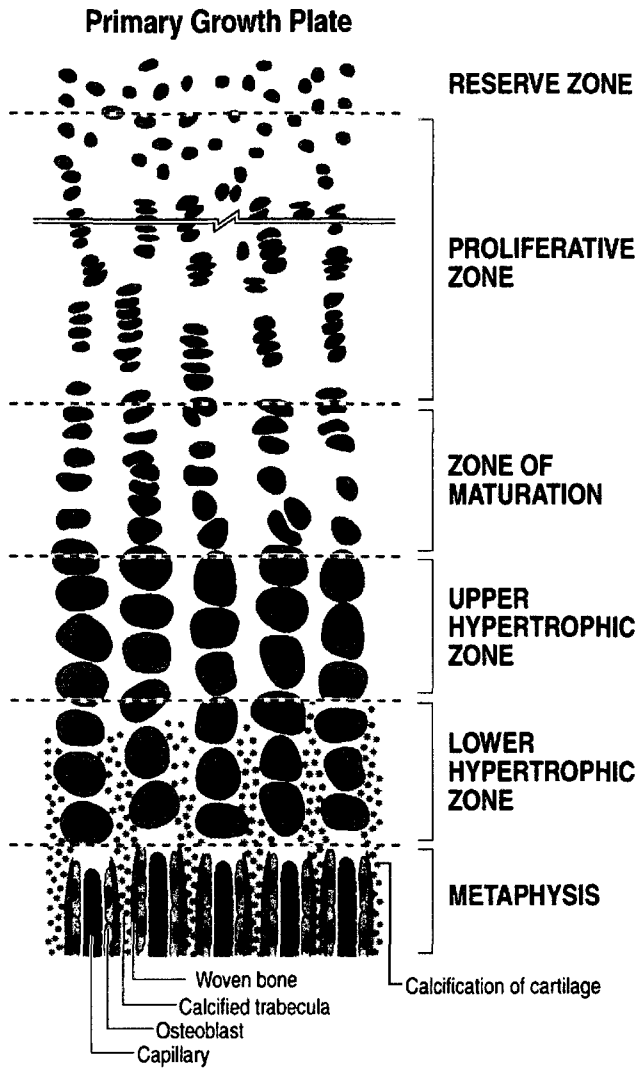

Figure 3 The primary epiphyseal growth plate consisting of the different types of chondrocytes.

From top to bottom or outward to inward: Reseve zone consists of resting non-proliferative chondrocytes. Proliferative zone consisted of mainly flat chondrocytes that enter the cell cycle. Zone of maturation (also known as prehypertrophic zone) consists of prehypetrophic chondrocytes that begin to differentiate and exit the cell cycle. Upper and Lower hypertrophic zone consists of fully differentiated chondrocytes that deposit a calcified matrix and undergo apoptosis in the lower zone. Underneath the growth plate is the metaphysis consists of calcified cartilage matrix, osteoblasts depositing woven bone, and capillaries.

prehypertrophic chondrocytes (Bitgood & McMahon, 1995) is a stimulator of chondrocyte proliferation and an inhibitor of chondrocyte hypertrophy. Mice that are homozygous for an inactivation of Ihh show severe dwarfism in axial and appendicular skeletal elements and no endochondral bone formation (St-Jacques et al., 1999). Ihh binds to its receptor complex (the patched/smoothened complex), leading to the release of parathyroid hormone related peptide (PTHrP) from the perichondrial cells. PTHrP also prevents chondrocyte hypertrophy and maintain a pool of proliferating chondrocytes just above the hypertrophic zone (Karp et al., 2000). Hence, Ihh and PTHrP appear to be part of a feedback loop (Fig. 4).

The process of endochondral ossification is also regulated by mineral homeostasis. Lack of calcium will inhibit mineralization leading to rickets in children and osteomalacia in adults (DeLuca, 1988). In infants, the symptoms include failure to thrive, bone pain, deformity of the thorax, softening of the skull, enlargement of the wrists and ankles, and if left untreated deformities of long bones. At the growth plate, the lack of calcium deposition in the extra cellular matrix (ECM) of the hypertrophic chondrocytes will lead to the unresorption of this ECM resulting in increase of chondrocyte proliferation and the width of the growth plate (Harris et al., 1965; Harris et al., 1965; Li et al., 1998). More than that, the underlying primary spongiosa will characteristically have less trabecular bone. The defect in mineralization will also lead to the widening of the osteoid seams in the cortical bone of the diaphysis (DeLuca, 1988).

Mineral homeostasis is mainly regulated by the parathyroid hormone (PTH) and vitamin D. Lack of vitamin D through the diet or any abnormality in its synthesis

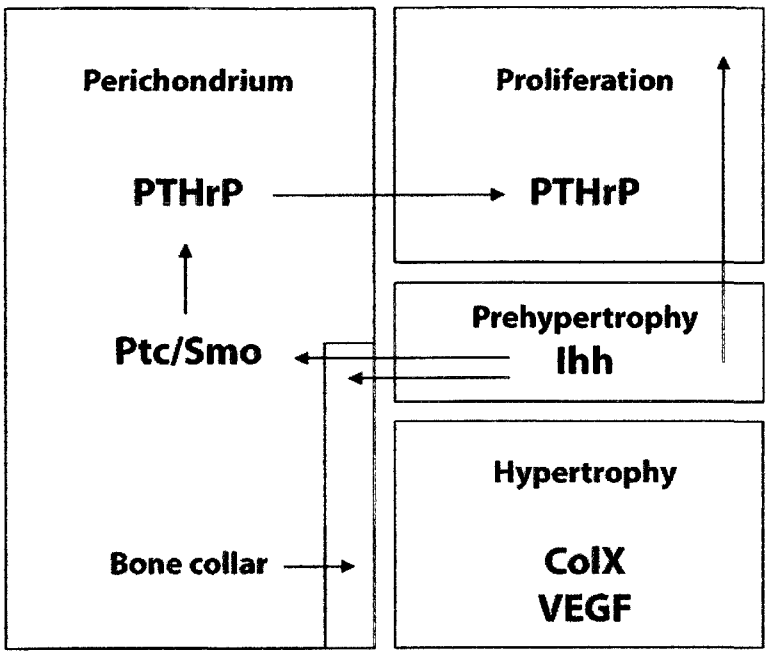

Figure 4 Diagram showing the role of several molecules in regulating the process of endochondral ossification. Expressed by prehypertrophic chondrocytes, indian hegehog (Ihh) is a central player that directly regulates chondrocyte proliferation. Ihh also acts on perichondrial and periarticular cells by binding to its Patched(Ptc)/Smoothnened (Smo) receptor complex to induce the synthesis and release of parathyroid hormone related peptide (PTHrP). PTHrP acts through its receptor in the proliferative chondrocytes to delay their passage into hypertrophy where they express collagen type X (ColX) and vascular endothelial growth factor (VEGF).
Adapted from (Olsen et al., 2000).

(Dardenne et al., 2001) or the synthesis of its receptor (Kato et al., 1998) will lead to rickets in children and osteomalacia in adults.

I. 2-Vitamin D. Historical view

Experimentation to know the causes of rickets, an old described illness in antiquity, lead to the discovery of vitamin D. The industrial revolution in 19th century Europe lead to polluted cities and an increase of rickets. In 1822, a polish physician, after observing that rickets was rare in unpolluted rural areas, experimented with children and concluded that sunbathing cured rickets. Other reports at that time showed that cod liver oil had beneficial action against rickets but was not given scientific credence due to the lack of understanding of the importance of micronutrients. Later on, German researchers showed in 1919 that artificially produced ultraviolet (UV) light could cure rickets. The link between the diet and UV irradiation was made after the experiment that showed feeding UV irradiated skin to rats cured rickets. In 1923, Goldblatt and Soames showed that irradiation of 7-dehydrocholesterol by UV produces an active vitamin D (unravelling the enigma of vitamin D. Beyond discovery, National Academy of Sciences, USA. www.beyonddiscovery.org/Icludes/DBLink.asp?ID=1176). The secosteroid structure of vitamin D_3, produced by UV irradiation of 7-dehydrocholesterol, was described in 1936 and shown to be structurally identical to the antirachitic component of cod liver oil. Secosteroids are based on the typical four rings steroid structure except that carbons C9 and C10 of the B-ring are not joined, thus opening up the structure (Fig. 5).

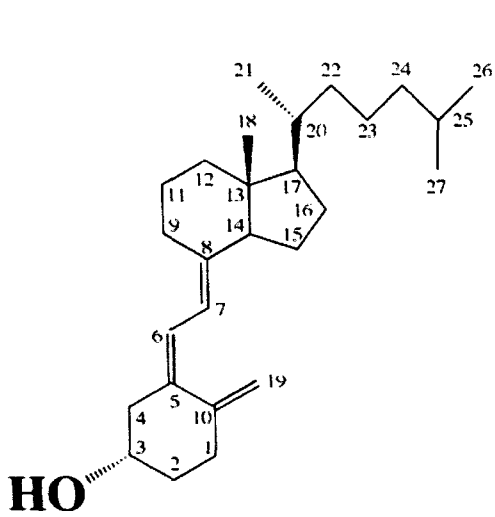

Vitamin D_3

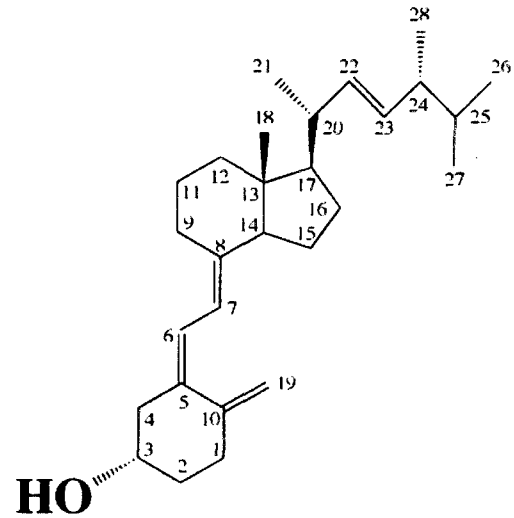

Vitamin D_2

Figure 5 Secosteroid chemical structure of the two existing isoforms of vitamin D.

I. 3-Vitamin D. Synthesis, circulation, and metabolism

Two forms of vitamin D exist: vitamin D_2 (ergocalciferol) formed by the UV irradiation of the plant product ergosterol and vitamin D_3 (cholecalciferol) formed in animal tissues from near-UV (290-310 nm) irradiation of 7-dehydrocholesterol found in keratinocytes (DeLuca, 2004). Both vitamins are secosteroids where vitamin D_2 has a 22,23 double bond and an additional methyl group attached to carbon 24 (Fig. 5). The majority of vitamin D synthesized and ingested is of the D_3 type and for the purpose of simplicity I will refer to either isoform as D (without subscript) in the rest of this dissertation. Once thermal isomerization converts 7-dehydrocholesterol to cholecalciferol, it enters the circulation by binding to the vitamin D binding protein (VDBP). The same occurs for ingested cholecalciferol and ergocalciferol once they enter circulation and the complexes are targeted to the liver to be catalyzed to 25-hydroxyvitamin D [25-(OH)D] by carbon 25 hydroxylation under the action of 25-hydroxylase. The identity of the hepatic 25-hydroxylase was unclear for more than 30 years with *CYP27A1* and *CYP2R1* as the best two candidate enzymes. *CYP27A1* is a cytochrome P450 mitochondrial enzyme that also exists in the microsomal element of the liver where it catalyzes cholesterol 27-hydroxylation in the bile-acid pathway (DeLuca & Schnoes, 1976). Mutations in both the human and mouse genes encoding the *CYP27A1*(human)/*Cyp27a1*(mouse) protein impair bile acid synthesis but have no consequences on vitamin D metabolism (Rosen et al., 1998) shifting the interest to microsomal *CYP2R1* as the plausible primary candidate enzyme for the majority of 25-hydroxylations. Cheng *et al.* recently reported a molecular analysis of a patient with low

circulating levels of 25-hydroxyvitamin D and classic symptoms of vitamin D deficiency. The patient was found to be homozygous for a transition mutation in exon 2 of the CYP2R1 gene (Cheng et al., 2004). The inherited mutation caused the substitution of a proline for the conserved leucine at amino acid position 99 in the *CYP2R1* protein and eliminated vitamin D 25-hydroxylase activity. These results showed that *CYP2R1* is in fact a biologically relevant hepatic enzyme for the 25-hydroxylation of vitamin D.

25-(OH)D released from the liver again binds to the VDBP and goes back into the circulation to the kidney where it is converted to 1α,25-dihydroxyvitamin D [1α,25-$(OH)_2$D] by the hydroxylating action of 1α-hydroxylase (officially termed *CYP27B1*) on carbon 1α (Fraser & Kodicek, 1970; Miller & Portale, 2000) and/or to 24R,25-dihydroxyvitamin D [24R,25-$(OH)_2$D)] by the hydroxylating action of 24-hydroxylase (officially termed *CYP24A1*) on carbon 24 (Fig. 6) (Makin et al., 1989). Again, both hydroxylases belong to the cytochrome P450 family of mitochondrial enzymes. The active form of vitamin D is 1α,25-$(OH)_2$D and is systemically produced in the proximal convoluted tubule of the renal nephron. The uptake/reabsorption of the 25-(OH)D-VDBP complex in the kidney proximal tubule from the glomerular filtrate is conducted by receptor-mediated endocytosis. Megalin/gp330, a type I cell receptor, along with Cubilin, a peripheral membrane glycoprotein, were shown to be the receptors mediating the endocytotic process. Megalin knockout mice develop vitamin D deficiency and bone disease due to inability of the proximal tubules to capture the complex from the glomerular filtrate (Nykjaer et al., 1999), and injection of anti-Cubilin antibodies inhibit the uptake of the complex by 70% (Nykjaer et al., 2001). Once the complex is internalized, the endocytotic vesicle is delivered to the lysosomal compartment of the

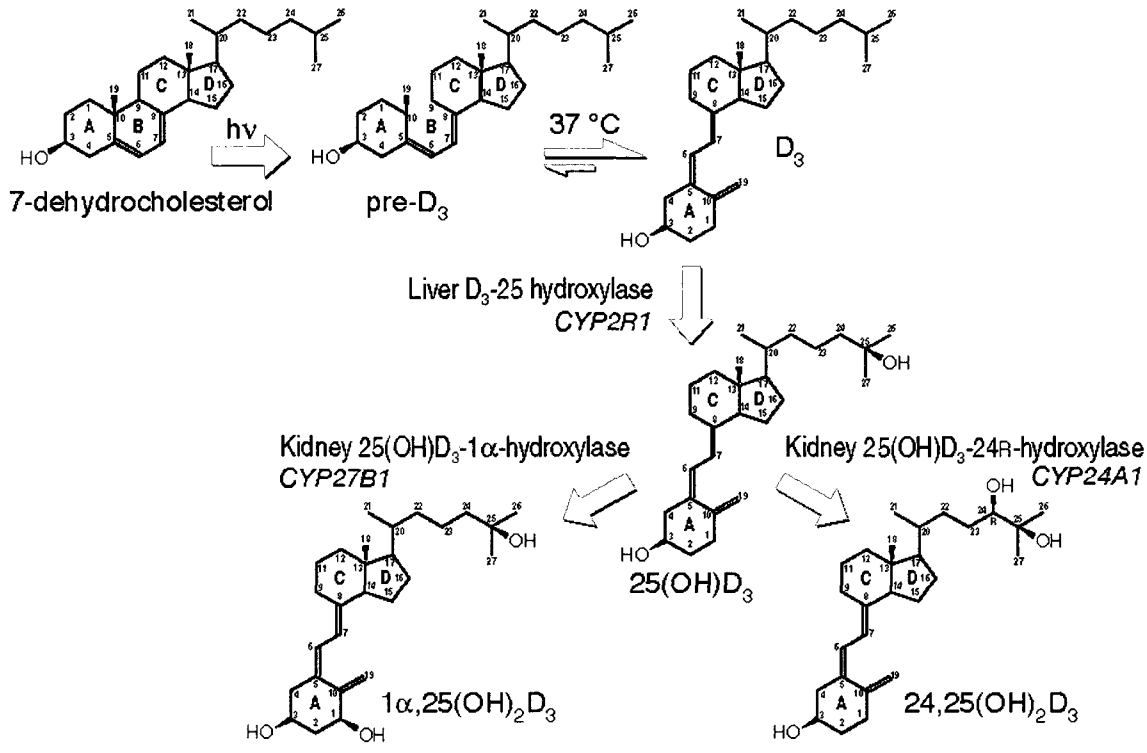

Figure 6 Synthesis of 1α,25-dihydroxyvitamin D3 (1α,25-(OH)$_2$D$_3$) begins in the skin.

UV irradiated 7-dehydrocholesterol is converted to previtamin D_3 (pre-D_3) that undergoes thermal isomerization at 37°C to give vitamin D_3 (also known as cholecalciferol). Vitamin D_3 enters the ciculation bound to the vitamin D binding protein (VDBP) and is targeted to the liver where it is converted to 25-hydroxyvitamin D (25(OH)D_3) by the action of the microsomal vitamin D3-25 hydroxylase (*CYP2R1*). 25(OH)D_3 again enters the circulation bound to the VDBP and is targeted to the kidney where it is converted to 1α,25-(OH)$_2$D$_3$ by the action of the mitochondrial 25(OH)D_3-1α-hydroxylase (*CYP27B1*) and/or to 24R,25-dihydroxyvitamin D_3 (24R,25(OH)$_2$D$_3$) by the action of the mitochondrial 25-(OH)D_3-24-hydroxylase (*CYP24A1*).

cell where the VDBP is degraded and the 25-(OH)D is released into the cytosol (Negri, 2006).

As mentioned above, the transport of vitamin D metabolites occurs through the VDBP. VDBP, referred to as the group-specific component of serum (Gc globulin) (Hirschfeld, 1959), is structurally related to albumin and α-fetoprotein, and the VDBP gene is a member of the linked albumin and α-fetoprotein gene family. Binding, solubilization, and serum transport of vitamin D sterols was always thought to be the only functions of VDBP, however, there is now evidence that VDBP may have a spectrum of biological functions, including roles in inflammation and the immune system. Like albumin and other serum proteins, VDBP is produced primarily in the liver and binds to the vitamin D metabolites through a single binding site with variable affinity (Bouillon et al., 1976). VDBP shows the greatest affinity for 25-(OH)D and 24R,25-$(OH)_2$D, followed by 1α,25-$(OH)_2$D and parent vitamin D.

The catabolism and subsequent degradation of 1α,25-$(OH)_2$D is catalyzed by *CYP24A1*. *CYP24A1* is a multicatalytic enzyme that catalyzes the side-chain oxidation of both 25-hydroxyvitamin D metabolites, namely 25-(OH)D and 1α,25-$(OH)_2$D. The catalytic process is initiated by side-chain hydroxylation of 1α,25-$(OH)_2$D at C-23 or C-24 (Prosser & Jones, 2004). The C-23 pathway is preferentially expressed in humans and the guinea pig (Beckman et al., 1996) and involves sequential 23- and 26-hydroxylations followed by formation of a 26,23-lactol and the final 1α,25-$(OH)_2$D -26,23-lactone product (Horst et al., 1984; Ishizuka & Norman, 1987; Yamada et al., 1987). Oxidation by the C-24 pathway, the main activity of the rat enzymes (Sakaki et al., 1999), results in the formation of calcitroic acid (Makin et al., 1989; Reddy & Tserng, 1989). Side-chain

cleavage occurs in the C-24 pathway and involves five separate steps that begin with 24-hydroxylation, followed by oxidation to C24-oxo, 23-hydroxylation to C23-OH/C24-oxo, followed by side-chain cleavage to the C23-alcohol, and finally oxidation to the C23-carboxylic acid. Four aliphatic hydrocarbons are cleaved in the C-24 pathway during the oxidation of 1α,25-$(OH)_2$D, which results in synthesis of the water-soluble oxidized-end-product calcitroic acid that is filtered and excreted in the kidney (Fig. 7). Similar C23/C24 oxidation pathways exist for 24R,25-$(OH)_2$D. On the other hand, the side-chain cleavage of plant vitamin D_2 metabolites with rat *Cyp24a1* does not proceed past the initial 24-hydroxylation step, hence, it is thought that other enzymes are required for the complete side-chain metabolism of D_2 metabolites.

I. 4-1α,25-dihydroxyvitamin D [1α,25-$(OH)_2$D]

I. 4. a-Receptor(s)

The genomic actions of 1α,25-$(OH)_2$D are mediated by the nuclear receptor, vitamin D receptor (VDR), which is the only nuclear protein that binds the vitamin D hormone with high affinity (Haussler et al., 1988). The VDR belongs to a large family of nuclear receptors that are also transcription factors (Evans, 1988). The 48 human members of this superfamily are the best-characterized genes of approximately 3000 mammalian genes involved in transcriptional regulation (Maglich et al., 2001) and

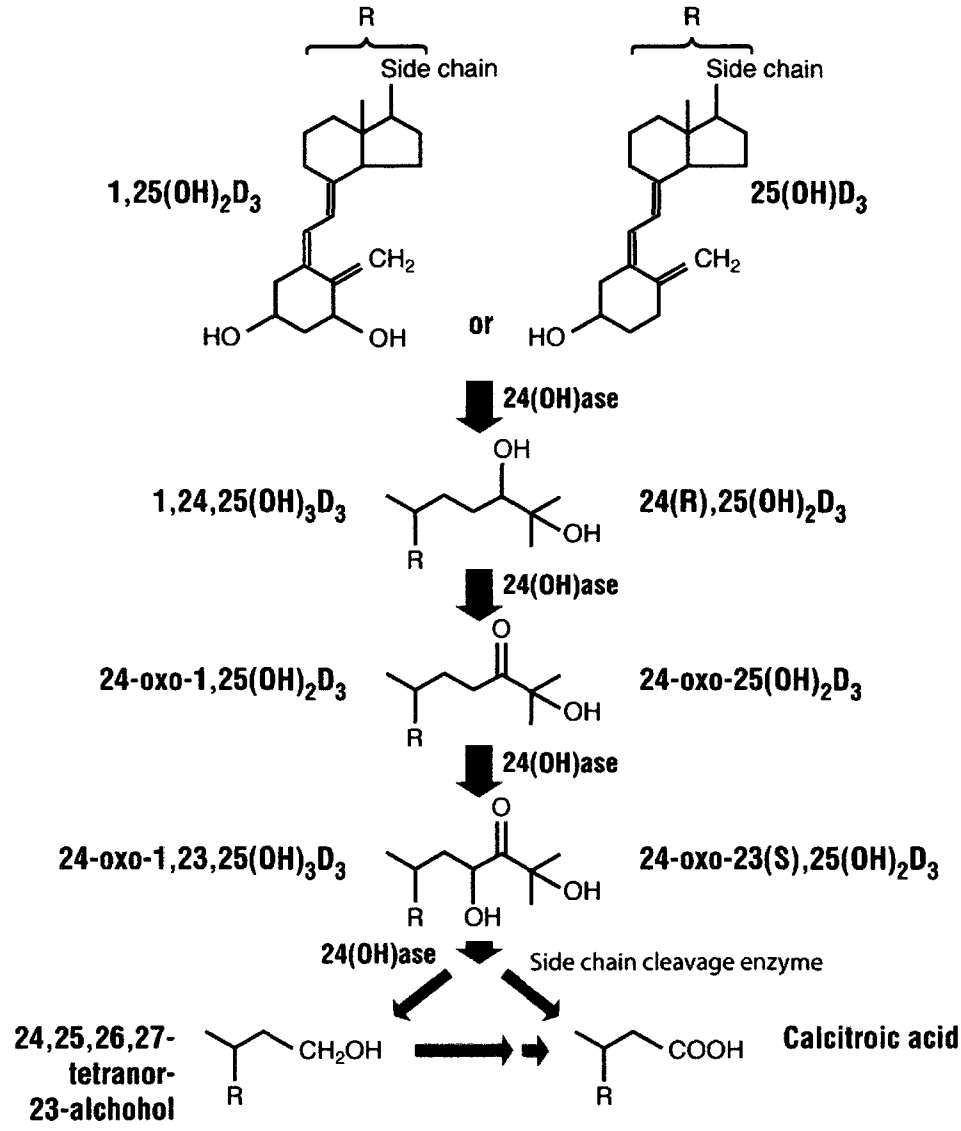

Figure 7 C-24 oxidative pathway of 1α,25-$(OH)_2$ D_3 and 25-(OH)D_3
All the enzymatic steps are catalyzed by 24-hydroxylase (24(OH)ase)/*CYP24A1*. 1,25$(OH)_2$ D_3 is converted to 1,24,25$(OH)_3D_3$ by hydroxylation on carbon position 24. The C24 hydroxyl group of 1,24,25$(OH)_3D_3$ is further oxidized to give 24-oxo-1,25$(OH)_2$ D_3 which is in turn hydroxylated on carbon position 23 to give 24-oxo-1,23,25$(OH)_3D_3$. Side chain cleavage of the resulting product occurs directly to give calcitroic acid or indirectly through an alcoholic intermediate (24,5,26,27-tetranor-23-alcohol) which in then oxidized to calcitroic acid.
Adapted from (Makin et al., 1989).

including the receptors for the nuclear hormones retinoic acid, thyroid hormone, estradiol, progeterone, testosterone, cortisol, and aldosterol.

Nuclear receptors are ligand activated with a conserved domain structure. The highly conserved DNA binding domain (DBD) contains two zinc fingers that form a structural domain containing an α-helix that in turn controls specific DNA sequence recognition (MacDonald et al., 1994). The VDR binding domain (ligand binding domain or LBD) binds ligands and contains a ligand-regulated C-terminal activating function-2 (AF-2) domain that is required to activate transcription (Barettino et al., 1994; Danielian et al., 1992; Durand et al., 1994) (Fig. 8). Members of the nuclear receptor class II family function as heterodimers with one of the three retinoid X receptors (RXR) α, δ, γ (Mangelsdorf & Evans, 1995). 1α,25-$(OH)_2$D target genes contain a specific receptor binding site in their promoter region referred to as the vitamin D response element (VDRE) (MacDonald et al., 1994). VDREs are composed of tandem motifs with the consensus PuG(G/T)TCA often arranged as direct repeats separated by three base pairs (DR3-type) or four base pairs (DR4-type). VDR has been shown to form homodimers (Carlberg et al., 1993) and heterodimers with the thyroid hormone receptor (Schrader et al., 1994) and retinoic acid receptor (Schrader et al., 1994), but by far the strongest binding partner of VDR is RXR. The trimeric complex of VDR, RXR and a VDRE is a switch for 1α,25-$(OH)_2$D target genes. VDR-RXR heterodimers bind to the above-mentioned DR3 and DR4 VDREs as well as to everted repeat (ER-type) REs with six spacing nucleotides (Fig. 8).

VDR and other nuclear receptors regulate target gene transcription by ligand-controlled recruitment of several coregulators required for the histone modifications,

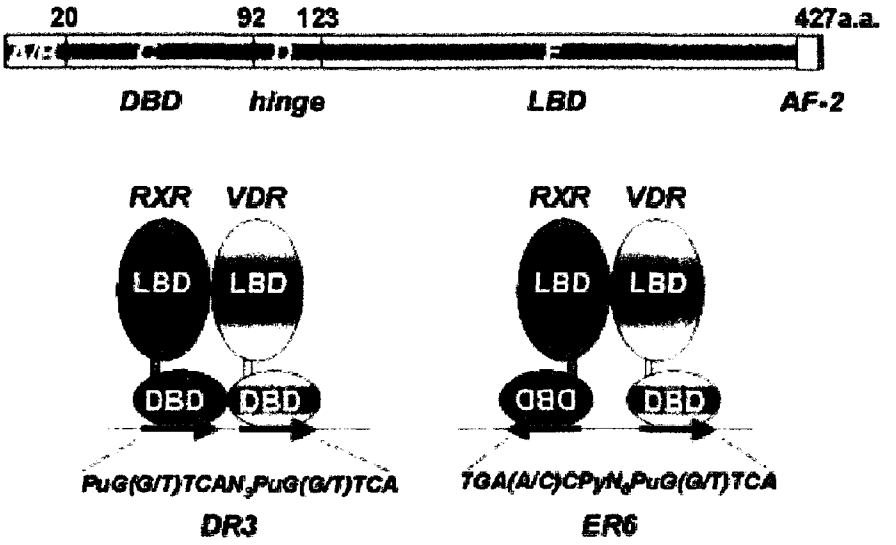

Figure 8 Schematic representation of the vitamin D receptor (VDR), its dimerization, and binding to the DNA.

Upper panel: The VDR is a 427 amino acid (a.a.) protein composed of several domains. At the N-terminal, the highly conserved DNA-binding domain (DBD) contains two zinc fingers that form a structural domain containing an α-helix that in turn controls specific DNA sequence recognition. By means of a hinge domain, the DBD is linked to the ligand binding domain (LBD) that binds ligands and contains a ligand-regulated C-terminal activating function-2 (AF-2) domain that is required to activate transcription. Lower panel: Dimerization of the VDR to the retinoid X receptor (RXR) occurs before binding to the vitamin D response elements (VDREs) in the form of direct repeats separated by 3 nucleotides (DR3) (left) and everted repeats separated by 6 basepairs (ER6) (right). Adapted from (Lin and White., 2004).

chromatin remodeling and recruitment of RNA polymerase necessary for the initiation of transcription. These coregulators, also known as VDR-interacting proteins (DRIPs) (Rachez et al., 1998), act via a sequential or combinatorial rather than simultaneous mechanism (Rosenfeld & Glass, 2001). Some DRIPs directly contact the VDR while others act as part of supercomplexes tethered to the VDR (Rachez et al., 1998). The recruitment of the DRIPs and the activation of gene expression occur in a cyclical manner. In the basal state, and in the absence of a ligand, the VDR-RXR complex is bound to a corepressor with the AF2 domains in the open inactive position (Masuyama et al., 1997). These corepressors that include the silencing mediator for retinoic acid and thyroid hormone receptors (SMRT) (Lusser & Kadonaga, 2003) and the hairless gene product (Hr) (Potter et al., 2002) associate with histone deacetylases (HDACs) that repress the chromatin (Lusser & Kadonaga, 2003). Surprisingly, the basal transcription factor IIb (TFIIB) also binds the unliganded VDR-RXR at two sites at this basal state (Masuyama et al., 1997). Once the VDR binds 1α,25-$(OH)_2$D, and is activated, a number of transformations occur including stronger association between the VDR and RXR, recognition of the VDREs by the liganded heterodimer, repositioning of the AF2 domains, and serine phosphorylation of the VDR. The corepressors/HDACs dissociate from the VDR-RXR complex in the active state and are replaced by coactivator(s) such as SRC-1 that binds the AF2 domain of complex (Chen & Evans, 1995). Next, CREB binding protein (CBP) binds SRC-1 and attracts polybromo- and BAF-containing complex (PBAF) (Lemon et al., 2001) resulting in an activating complex that acetylates and renders the chromatin accessible to the RNA polymerase II. Following acetylation, DRIP205 replaces the activating complex by binding to the AF2 domains of VDR-RXR.

DRIP205 is also believed to displace TFIIB and deliver it to RNA polymerase II (Masuyama et al., 1997) and to form a bridge composed of other DRIPs that link the RNA polymerase II to the VDR-RXR complex. Transcription is then initiated until completion where the DRIP complex is displaced along with 1α,25-$(OH)_2$D. Following this, the VDR is ubiquinated and targeted for degradation and the 1α,25-$(OH)_2$D metabolite is catabolized by *CYP24A1*.

It was recently described that some actions of 1α,25-$(OH)_2$D, namely the rapid ones, are effected through a membrane associated receptor. *In vitro* and in chondrocytes of the growth zone, binding of 1α,25-$(OH)_2$D to a membrane-associated vitamin D receptor molecule modulates gene expression through the ERK1/2 pathway activated by phospholipase C. In addition, protein kinase C (PKC) turns on the synthesis of prostaglandins that also increase ERK1/2 activities (Boyan et al., 2007). *In vivo,* the rapid non-genomic effects of 1α,25-$(OH)_2$D have been described in several tissues and species to a 1α,25-dihydroxyvitamin D–binding protein at the cell surface, which is called 1α,25-dihydroxyvitamin D membrane-associated rapid response steroid receptor [1α,25-$(OH)_2$D MARRS receptor] and which is also known as Erp57, GRp58, or Erp60 (Nemere et al., 2000). These *In vivo* rapid non-genomic effects include increased calcium transport, phosphate transport, PKC and MAPK activation (Nemere & Farach-Carson, 1998).

Additional support for the biological relevance of the MARRS receptor was reported by Nemere et al. measuring phosphate transport in cultured chick intestinal cells. The ability of these intestinal cells to take in phosphate was abolished once they were preincubated with Ab099, an antibody directed to the N-terminus of the MARRS

protein (Nemere et al., 2004). The physiological relevance of these mechanisms remains to be unequivocally established.

I. 4. b-1α,25-$(OH)_2$D target genes

The main systemic function of 1α,25-$(OH)_2$D is to regulate mineral homeostasis and bone integrity through its regulation of calcium-transporting proteins and bone-forming molecules such as the epithelial calcium channels, calbindin $D_{28k\&9k}$, osteocalcin, bone sialoprotein (BSP) and osteopontin (OPN) (Sutton & MacDonald, 2003).

The epithelial calcium channels (TRPV5 in kidney, TRPV6 in intestine) and calbindins were found to contain functional VDREs (Proudfoot et al., 2002). Studies in Caco-2 cells derived from a colon adenocarcinoma that mimic small intestinal cells in culture showed an mRNA increase of both TRPV6 and $calbindin_{9k}$ preceding calcium uptake in response to 1α,25-$(OH)_2$D (Giuliano & Wood, 1991).

The ostecocalcin VDRE is well characterized and resides in the distal promoter of the osteocalcin gene (osteocalcin is the main non-collagenous) matrix molecule secreted by differentiated osteoblasts that will be mentioned in more details in later sections). This VDRE was shown to be flanked by sequences recognized by Runx2 adding to the complexity of gene regulation at that site (Paredes et al., 2004). In fact, several other regulatory elements have been characterized in the osteocalcin gene promoter that contribute to the tissue-specific basal expression of the gene in response to 1α,25-$(OH)_2$D. One important regulatory element is an AP-1 site where once mutated

will inhibit the gene's responsiveness to 1α,25-$(OH)_2$D. It is also important to mention that the expression of the osteoclacin gene in response to 1α,25-$(OH)_2$D is clearly affected by the maturity state of the osteoblasts (mentioned in more detail in later sections). BSP and OPN are also matrix proteins deposited by oteoblasts and regulated by 1α,25-$(OH)_2$D. Both molecules contain a characterized VDRE (Li et al., 1998) and are differentially regulated by 1α,25-$(OH)_2$D. BSP mRNA was shown to be suppressed in contrary to OPN's induced mRNA in response to 1α,25-$(OH)_2$D in cultured osteoblasts (Chen et al., 1996).

The antiproliferative actions described for 1α,25-$(OH)_2$D are mediated through its upregulation of the cyclin-dependent kinase inhibitors p21 (Jiang et al., 1994) and p27. Three functional VDREs were identified in the p21 promoter in which two of them co-localize with p53 binding sequences (Saramaki et al., 2006). In fact, chromatin immuno-preciptitation assays in MCF-7 breast cancer cell lines using VDR & p53 antibodies showed that the two molecules interact to induce p21 mRNA expression in these cells (Saramaki et al., 2006).

Another molecule involved in the cell cycle and is regulated by 1α,25-$(OH)_2$D is cyclin C. The cyclin C-CDK8 complex is found associated with the RNA polymerase II basal transcriptional machinery and is a functional player in gene expression (Bourbon et al., 2004). Gene reporter studies in MCF-7 cell line have shown that the cyclin C promoter contains four VDREs that are responsive to 1α,25-$(OH)_2$D (Sinkkonen et al., 2005).

One of the mechanisms whereby 1α,25-$(OH)_2$D regulates itself is by inducing the expression of CYP24A1 that catalyzes its degradation. The induction by 1α,25-

$(OH)_2D$ is the strongest ever reported resulting from a complex and simultaneous VDR-RXR binding to several VDREs identified in the gene's promoter (Hahn et al., 1994).

Another target gene of 1α,25-$(OH)_2D$ is the peroxisome proliferator activated receptor (PPAR) δ having one potent DR3-type VDRE (Dunlop et al., 2005). The (PPAR) δ gene has been used as a marker of the efficacy of the treatment of breast and prostate cancer with VDR agonists. Other 1α,25-$(OH)_2D$ target genes include the rat atrial natriuretic factor (ANF) (Kahlen & Carlberg, 1996), the rat PTH (Nemere & Szego, 1981), the human parathyroid hormone (PTH) (Demay et al., 1992), and others.

I. 4. c-1α,25-$(OH)_2D$ classical systemic functions

Calcium is the fifth most prominent element in the human body, constituting 2% of body weight, with 99% of this calcium present in the skeleton in the form of insoluble calcium phosphate crystals. The organic matrix of the bone becomes rigid once the calcium mineral is deposited in it, making calcium essential in bone formation. Calcium also plays other important physiological and biochemical roles in the body such as regulating skeletal muscle contraction and relaxation, regulating heart functioning, blood clot formation, transmission of nervous impulses and being an important cofactor for proper enzyme functioning. It is well known that the serum calcium level in humans and animals ranges from 9 to 10 mg/dl. Intestine, bone, and kidneys are three major organs responsible for calcium homeostasis. 1α,25-$(OH)_2D$ plays an important role in regulating serum calcium homeostasis together with PTH and calcitonin and thereby acts on all these three major organs to increase serum calcium levels.

A key molecule involved in the process of calcium regulation is the calcium sensing receptor (CaSR) (Hebert et al., 1997). This molecule serves as the body's thermostat for calcium. It is a seven transmembrane cell surface receptor linked to a G protein capable of sensing very minor fluctuations in ionic extracellular calcium (Conklin & Bourne, 1994). CaSR is present in the chief cells of the parathyroid gland, the thyroid C-cells, and cells along the renal tubules that are involved in calcium transport (Bai et al., 1996) A proposed role of CaSR in response to calcium in the parathyroid chief cells is as follows: Increases in concentration of extracellular calcium activates the G proteins (Gi & Gq) linked to the CaSR resulting in the inhibition of adenylate cyclase and the stimulation of phospholipase C. The net result of this is the release of calcium from the intracellular stores into the cytosol inhibiting PTH production and release from these cells.

When the extra-cellular-fluid calcium is reduced, PTH is released from the parathyroid glands inducing the renal expression of 1α,25-$(OH)_2$D (Heaney, 1997) (The mechanism will be detailed in a later section). 1α,25-$(OH)_2$D increases calcium absorption from mainly the duodenual portion of the gut. The molecular basis behind this is the expression induction of TRPV6 by 1α,25-$(OH)_2$D that results in the uptake of calcium from the lumen into the epithelial cells (Peng et al., 1999) Other 1α,25-$(OH)_2$D intestinal induced factors involved in calcium entry exist, the most important being the change of epithelial brush border lipids and consequently membrane fluidity leading to an increase in calcium vesicle formation (Schedl et al., 1994).

The 1α,25-$(OH)_2$D actions on the kidney to increase calcium occurs through reabsorption in the distal convoluted tubule. The molecular mechanism of reabsorption

is the following: Apical entry of calcium is facilitated by TRPV5, calcium then binds to calbindin D_{28k} and the complex diffuses through the cytosol to the basolateral membrane where calcium is extruded by a sodium/calcium exchanger and a plasma membrane calcium-ATPase.

The bone is the last organ where 1α,25-$(OH)_2$D acts upon to increase plasma calcium by resorption of its matrix (this occurs in cases of supraphysiological doses of the metabolite). The mechanism through which the hormone does that is indirect through the activation of the osteoclasts. The primary target of 1α,25-$(OH)_2$D in this organ are the osteoblasts expressing the VDR, where the binding of the ligand to the receptor induces the transcription of the macrophage colony stimulation factor (M-CSF) and the receptor activator of NF-κB ligand (RANKL) (Suda et al., 1999). Both RANKL and M-CSF are needed to stimulate the proliferation and differentiation of the osteoclasts to resorb bone and release the calcium into the ECF. In fact, physiological doses of 1α,25-$(OH)_2$D on bone leads to the inhibition of PTH-induced bone resorption (Miles et al., 2000) and as mentioned will preferentially stimulate intestinal absorption of calcium without inducing bone resorption, which then stimulates bone mineralization.

The other mineral that 1α,25-$(OH)_2$D regulates is inorganic phosphate (P_i). P_i accounts for around 1% of adult body weight, or 600 to 700 g where 85% of that is in the skeleton and teeth. P_i is essential to cellular metabolism and bone mineralization where its ion is negatively charged and has to be efficiently transferred across hydrophobic membrane barriers. Ingested P_i is absorbed by the small intestine, deposited in bone, and filtered by the kidney where it is reabsorbed and excreted in quantities determined by the specific needs of the organism.

P_i transport across the intestinal mucosal membrane (mainly the duodenum and jejunum) is regulated by 1α,25-$(OH)_2$D and dietary intake of P_i (Cross et al., 1990). The molecular mechanism through which 1α,25-$(OH)_2$D controls this P_i transport is through its induction expression of the sodium phosphate cotransporter 2 b (NPT2b) in the epithelial apical membrane and consequently the cotransport of Na/P_i (Xu et al., 2002).

Transepithelial P_i transport in the proximal tubule of the nephron is basically unidirectional and involves uptake across the brush border membrane, translocation across the cell, and efflux at the basolateral membrane (Tenenhouse, 2005). P_i uptake at the apical cell surface is the rate-limiting step in the P_i reabsorptive process and the major site of its regulation. As in the case of the intestine, this process is controlled by the 1α,25-$(OH)_2$D induced expression of the sodium phosphate cotransporter 2 a (NPT2a).

1α,25-$(OH)_2$D also affects phosphate homeostasis by participating in a negative feedback loop with FGF23. FGF23 is a phosphaturic factor (Tenenhouse, 2005) that is mainly produced by bone (Mirams et al., 2004) and induces renal phosphate wasting by suppressing NPT2a expression (Saito et al., 2003). 1α,25-$(OH)_2$D stimulates the production of FGF23, which in turn suppresses renal CYP27B1 expression (Saito et al., 2003). Mice lacking VDR show decreased circulating FGF23 levels in agreement with the negative reciprocal regulation (Kolek et al., 2005). FGF23 imbalance is implicated in hypophosphatemic diseases such as X-linked hypophosphatemia (XLH). XLH is caused by mutations in PHEX, a Pi-regulating gene with homology to endopeptidases on the X-chromosome (Francis et al., 1997). This loss of PHEX function in patients of XLH results in significant increase of serum FGF23.

I. 4. d-Vitamin D deficiency

Vitamin D deficiency is a common cause of rickets and osteomalacia, but these disorders may also result from other conditions, such as various renal tubular disorders (Ferreira, 2006), familial hypophosphatemic (vitamin D–resistant) rickets (Pettifor, 2008), Autosomal dominant hypophosphatemic rickets (ADHR) (Pettifor, 2008), inadequate dietary calcium (Gilchrest, 2008), disorders or drugs that impair the mineralization of bone matrix (Lawson, 2002), and others. Vitamin D deficiency causes hypocalcemia, which stimulates production of PTH, causing hyperparathyroidism. Hyperparathyroidism increases absorption, bone mobilization, and renal conservation of calcium but increases excretion of phosphate. As a result, the serum level of calcium may be normal, but because of hypophosphatemia, bone mineralization is impaired (Glorieux, 1991).

Vitamin D deficiency may result from the following:

Inadequate sunlight exposure or dietary intake: Inadequate direct sunlight exposure (or sunscreen use) and inadequate dietary intake usually occur simultaneously to result in clinical deficiency (Gilchrest, 2008). Susceptible people include the elderly (who are often undernourished and are not exposed to enough sunlight), and certain communities (for example, women and children who are confined to the home or who wear clothing that covers the entire body and face) (Heath & Elovic, 2006). The recommended direct sunlight exposure is 5 to 15 min to arms and legs, or face, arms and hands, at least three times a week (Holick, 2004).

Malabsorption: Malabsorption can deprive the body of dietary vitamin D (Heath & Elovic, 2006).

Abnormal metabolism: Vitamin D deficiency may result from defects in the production of 25-(OH)D or 1α,25-$(OH)_2$D. People with a chronic renal disorder commonly develop rickets or osteomalacia because renal production of 1α,25-$(OH)_2$D is decreased and phosphate levels are decreased. Hepatic dysfunction can also interfere with the production of 25-(OH)D and consequently 1α,25-$(OH)_2$D.

Type I hereditary vitamin D-dependent rickets (VDDR-1) also known as pseudovitamin D-deficiency rickets (PDDR) is an autosomal recessive disease caused by absent or defective conversion of 25-(OH)D to 1α,25-$(OH)_2$D in the kidneys. It is characterized by growth retardation, failure to thrive, rickets, and osteomalacia (St-Arnaud et al., 2000). Serum biochemistry shows hypocalcemia, secondary hyperparathyroidism, and undetectable levels of 1α,25-$(OH)_2$D. The molecular basis behind this disease is inactivating mutations in the *CYP27B1* gene (Fu et al., 1997; Kitanaka et al., 1998).

X-linked familial hypophosphatemia is another rare inherited disorder characterized by impaired transport of phosphate and altered vitamin-D metabolism in the kidneys. In addition, calcium and phosphate are not absorbed properly in the intestines, which can lead to rickets and osteomalacia. As mentioned before, this disorder is caused by mutations on the X-linked PHEX gene.

Resistance to vitamin D: Type II hereditary vitamin D-dependent rickets (VDDR-2) also known as hereditary vitamin D-resistant rickets (HVDRR) is due to mutations in the VDR (Hughes et al., 1988). Individuals with HVDRR exhibit end organ resistance to

vitamin D and do not respond to treatment with vitamin D metabolites. Symptoms of this disorder are similar to PDDR with an addition of total scalp and body alopecia.

I. 4. e-Regulation of 1α,25-$(OH)_2$D

The production of 25-(OH)D in the liver is mostly unregulated and dependent on vitamin D substrate availability. Under normal physiological conditions, the systemic levels of 1α,25-$(OH)_2$D are tightly controlled by regulating renal CYP27B1. PTH, 1α,25$(OH)_2$D, calcium, phosphate, and calcitonin regulate the enzyme's expression whereby PTH and 1α,25-$(OH)_2$D are the two most important regulators.

Parathyroid Hormone: PTH increases the renal CYP27B1 mRNA expression through a cAMP dependent protein kinase A pathway (Murayama et al., 1999). Analysis of the Cyp27b1 promoter sequence showed several binding sites for transcription factors that could be phosphorylated by PKA (Brenza et al., 1998). Recently, a PTH target site has been identified in the –0.5 kb region of the human CYP27B1 promoter that involves a novel vitamin D inhibitor receptor (VDIR) present in the kidney (Murayama et al., 2004). It is proposed that VDIR functions in the absence 1α,25-$(OH)_2$D and in the presence of protein kinase A to upregulate CYP27B1 gene expression. When present, 1α,25-$(OH)_2$D would let the VDR/RXR heterodimeric complex interact with VDIR and inhibit gene expression by recruitment of a corepressor.

PTH not only induces the expression of CYP27B1, but also inhibits the renal expression of CYP24A1. The molecular mechanism by which PTH does that involves

the posttranscriptional modification of CYP24A1 mRNA to decrease its stability (Zierold et al., 2003).

1α,25-(OH)$_2$D: 1α,25-(OH)$_2$D downregulates CYP27B1 mRNA expression from the renal proximal tubules both *in vivo* and *in vitro* (Takeyama et al., 1997). VDR is essential for the hormone's inhibitory action due to the fact that in VDR-null mice there is no downregulation of CYP27B1 expression observed in the presence of high 1α,25-(OH)$_2$D levels. The mechanism of this downregulation has not been clearly elucidated. Several negative VDREs have been reported in the promoter sequence of CYP27B1(Murayama et al., 1998), however, none was identified with the inhibition by using 5'-flanking region reporter constructs. As mentioned above, a novel mechanism of repression was proposed in which VDIR bound to the CYP27B1 promoter facilitates recruitment of a corepressor in the presence of 1α,25-(OH)$_2$D (Murayama et al., 2004).

The feedback inhibition of 1α,25-(OH)$_2$D on Cyp27b1 expression is accompanied by the induced expression of Cyp24a1 in the renal proximal tubule adding additional control of circulating 1α,25-(OH)$_2$D levels (Akeno et al., 1997). This induction is dependent on VDR-1α,25-(OH)$_2$D complex and in both Cyp27b1 and VDR-null mice the expression of Cyp24a1 is dramatically reduced (Endres et al., 2000). The rat Cyp24a1 promoter contains two tandem VDREs (Kerry et al., 1996), where in the absence of 1α,25-(OH)$_2$D, the heterodimer VDR/RXR binds to one or both VDREs to recruit a corepressor and lower basal expression (Dwivedi et al., 1998). Once the VDR binds to its 1α,25-(OH)$_2$D ligand, the corepressor is replaced by a coactivator complex. When levels of 1α,25-(OH)$_2$D are elevated, both VDREs are activated to ensure high

Cyp24a1 expression and consequent degradation of the vitamin D hormone (Kerry et al., 1996).

Calcium: It is believed that extracellular calcium regulates CYP27B1 expression in a mechanism independent of PTH. In parathyroidectomized PTH-replete rats, the elevation of serum calcium inhibits circulating 1α,25-$(OH)_2$D levels, indicating a role for this mineral in regulating renal Cyp27b1 expression (Weisinger et al., 1989). A directly inverse relationship between calcium levels and CYP27B1 expression was shown in studies that used human kidney cell lines (Bland et al., 1999). These cell lines express the calcium sensing receptor that is sensitive to extracellular calcium fluctuations. Several downstream signaling pathways including PKC and MAPK are known to be activated by the calcium sensing receptor (Kifor et al., 2001) and could result in the activation of the CYP27B1 promoter.

Phosphate: Phosphate deprivation in rats results in increased serum 1α,25-$(OH)_2$D along with an increase of renal Cyp27b1 mRNA expression and protein in a mechanism independent of PTH (PTH is reduced under low phosphate conditions) (Yoshida et al., 2001). The signal for the kidney to synthesize more 1α,25-$(OH)_2$D is believed to be transduced via hormones of the pituitary gland in a poorly established mechanism.

Phosphate deprivation leads also to a decrease in renal CYP24A1 mRNA and protein eventhough levels of circulating 1α,25-$(OH)_2$D are high (Wu et al., 1996) due to the increased CYP27B1 expression in the hypophosphatemic state. The inability of 1α,25-$(OH)_2$D to induce CYP24A1 expression in this particular case is related to a reduced VDR content in low phosphate conditions. The molecular mechanism behind this is still not understood.

Calcitonin: Under normal calcemic conditions, calcitonin stimulates Cyp27b1 expression in the distal parts of the nephron (Shinki et al., 1999). 1α,25-$(OH)_2$D synthesis is increased by calcitonin in a cortical-collecting-duct cell line but not in a proximal tubule one (Bland et al., 2001). PKC signaling rather than PKA (Murayama et al., 1999) (employed by PTH) is the mechanism through which calcitonin upregulates CYP27B1 mRNA synthesis. On the other hand, Calcitonin does not affect CYP24A1 expression in the distal part of the nephron.

Lipopolysaccharide: It was recently reported that lipopolysaccharide (LPS) induces CYP27B1 expression in the cortical-collecting-duct cell line (HCD) with no effects in the proximal tubular cell line HKC-20 (Bland et al., 2001). This induction by LPS is insensitive to the negative feedback inhibition by 1α,25-$(OH)_2$D due to molecular mechanisms not yet fully understood.

The Klotho gene product: Mice having homozygous mutations in the Klotho gene display disorders similar to those observed in human aging, elevated plasma 1α,25-$(OH)_2$D and renal CYP27B1 mRNA levels. It has been shown that Klotho-deficient mice (Kuro-o et al., 1997) and Fgf23 knockout mice (Shimada et al., 2004) exhibit identical phenotypes. This observation led to the identification of Klotho as a cofactor essential for interactions between FGF23 and FGF receptors.

I. 4. f-Non-classical functions of 1α,25-$(OH)_2D$

The major site of 1α-hydroxylation of 25-(OH)D by *CYP27B1* and concomitant production of 1α,25-$(OH)_2D$ occurs as mentioned before in the proximal tubule of the renal nephron (Brunette et al., 1978). However, the expression of *CYP27B1* enzyme has been reported in many other cell types, namely, the osteoblasts (Turner et al., 1980), keratinocytes (Fu et al., 1997), macrophages and cells of the lympho-hematopoietic system (Reichel et al., 1991), chondrocytes (Pedrozo et al., 1999), cancerous cells, and other normal cells. The discovery of these extra-renal sites of CYP27B1 expression has led investigators to hypothesize an autocrine and/or paracrine role of 1α,25-$(OH)_2D$ on the proliferation and/or differentiation of the cells that produce it. In fact, a role for 1α,25-$(OH)_2D$ was recently described for most of these non-renal cell types:

Osteoblasts: The bone forming cells express the VDR and an effect of 1α,25-$(OH)_2D$ on these osteoblasts has been shown in both primary osteoblastic cultures and established osteoblastic cell lines *in vitro*. 1α,25-$(OH)_2D$ treatment inhibits collagen type I expression by osteoblasts (Kream et al., 1986; Kream et al., 1980) on the level of gene transcription. This inhibition involves the regulatory element within the alpha 1 chain of procollagen type I (Pavlin et al., 1994). On the other hand, 1α,25-$(OH)_2D$ was shown to induce the expression of several osteoblastic differentiation markers including alkaline phosphatase (Manolagas et al., 1981), osteopontin (Oldberg et al., 1989), osteocalcin (Demay et al., 1990), and matrix Gla protein (Fraser & Price, 1988). The stimulation of the expression of both osteopontin and osteocalcin has been well characterized and acts through the VDREs present in these matrix molecule's promoters. Other molecules

induced by 1α,25-$(OH)_2$D treatment in *vitro* include Insulin-like growth factor 1 (Kurose et al., 1990). The induction of the above mentioned molecules shows an overall 1α,25-$(OH)_2$D positive effect on osteoblast differentiation *in vitro*. Accordingly, 1α,25-$(OH)_2$D was shown to stimulate mineralization in cultures of clonal osteoblast-like cells (Matsumoto et al., 1991). This action of 1α,25-$(OH)_2$D involves genomic responses through the VDR due to the fact that the multifunctional protein calreticulin, which binds to the VDR DNA-binding domain to inhibit its transcriptional activating function, perturbs the vitamin D response and prevents the mineralization of the cultured osteoblasts (St-Arnaud et al., 1995).

There are a lot of contradictory reports on the *in vitro* effects of 1α,25-$(OH)_2$D on osteoblasts in the literature, with a few investigators reporting a stimulatory effect on collagen type I synthesis (Kurihara et al., 1986) while the majority report a decrease in collagen type I synthesis. Also, both increases and decreases (Majeska & Rodan, 1982) of alkaline phosphatase expression was reported in 1α,25-$(OH)_2$D treated osteoblastic cultures.

These discrepancies in the response of cultured osteoblasts to 1α,25-$(OH)_2$D appear to be due to the differentiated state of the osteoblast. Once put in culture, bone cells undergo an ordered developmental sequence characterized by the temporal expression of proliferation and differentiation markers to end up in the ability to mineralize the deposited ECM (Owen et al., 1990). Owen *et al.* showed that 1α,25-$(OH)_2$D treatment of primary osteoblasts in culture can both positively and negatively induce collagen type I and alkaline phosphatase depending on the differentiated state of these bone cells (Owen et al., 1990). The expression of these genes was inhibited in the

early preosteoblastic cultures and stimulated in the late-stage ones. Similar culture variations were observed for other osteoblast related markers upon 1α,25-$(OH)_2$D treatment, with osteopontin and matrix Gla protein expression being stimulated by the metabolite during early proliferation but exhibiting a blunted response at later stages. Osteocalcin in these studies did not respond to 1α,25-$(OH)_2$D early on in culture but was expressed in mid to late cultures.

The osteoblastic differential response to 1α,25-$(OH)_2$D is supported by other recent reports that used an osteoblast-specific VDR knockout model. Primary osteoblast cultures from this model show increased expression of alkaline phosphatase, BSP, and osteocalcin in addition to an earlier and sustained increase in mineralization (Sooy et al., 2005). This inhibition by 1α,25-$(OH)_2$D was also documented in another study that showed increased radiographic density and mineralized bone volume in VDR-deficient bones transplanted into wild-type mice as compared to the wild-type control bones (Tanaka & Seino, 2004). Another preliminary report also suggested increases in bone mass and bone mineral density in osteoblast-specific VDR-null mice (Yamamoto et al., 2004).

The effect of 1α,25-$(OH)_2$D on bone was also studied in an osteoblast-specific VDR transgenic model (by using the osteoclacin promoter expressed in mature osteoblasts) and was found out to induce bone formation (Gardiner et al., 2000; Yamamoto et al., 2004).

The different effects of 1α,25-$(OH)_2$D observed in the tissue-specific inactivation and overexpression models can be explained by the time of onset of VDR expression. In the early stages of osteoblastogenesis, VDR-dependent signaling may inhibit

differentiation, as its absence leads to enhanced differentiation of cells into the osteoblastic lineage. VDR overexpression in terminally differentiated osteoblasts, on the other hand, would increase osteoblast activity.

Keratinocytes: As mentioned earlier, 1α,25-$(OH)_2$D plays an important part in the differentiation of many normal and cancerous cells. Skin keratinocytes have been the main model used to show the action of 1α,25-$(OH)_2$D in promoting differentiation of nonmalignant cells. The keratinocytes express the VDR and all the enzymes necessary needed to convert 7-dehydrocholesterol to 1α,25-$(OH)_2D_3$ (Bikle et al., 2001). This expression varies with differentiation where it is reduced in the later stages. 1α,25-$(OH)_2$D increases involucrin, transglutaminase (TG) activity, and cornified envelope formation (markers of differentiation) at subnanomolar concentrations in preconfluant keratinocytes (Lemire et al., 1995). At these concentrations, 1α,25-$(OH)_2$D has also been found to have antiproliferative actions due to its decrease in the expression of c-myc and increase in the expression of the cell cycle inhibitors p21 and p27. *In vivo*, the absence of 1α,25-$(OH)_2$D in Cyp27b1-null mice resulted in a reduction in involucrin, filaggrin, and loricrin in the keratinocytes in addition to a reduction in the permeability barrier function of the epidermis (Bikle et al., 2004).

The antiproliferative actions of 1α,25-$(OH)_2$D are currently clinically used in the treatment of psoriasis (Brown & Slatopolsky, 2008).

The mechanisms by which 1α,25-$(OH)_2$D reglulates keratinocyte differentiation involves an autocrine function of 1α,25-$(OH)_2$D in inducing the calcium receptor and phospholipase C (PLC) that leads to the rise in intracellular calcium, inositol 1,4,5 triphoshate (IP_3), and diacylglycerol (DAG) (Tang et al., 1987). The rise in these second

messengers leads to protein kinase activation (PKC) in part by translocation of PKCs to their membrane receptors (RACK) and opening up of calcium channels in the plasma membrane (Yada et al., 1989). 1α,25-$(OH)_2D$, in combination with the increase in intracellular calcium and the AP-1 transcription factors activated by PKC, stimulates differentiation by inducing involucrin and loricrin substrates for cornified envelope formation as well as the enzyme TG, which cross-links these substrates into the cornified envelope (Bikle et al., 2004; Bikle et al., 2002; Bikle et al., 2001).

Macrophages: In 1895, the Danish scientist Niels Finsen found an effective way to treat tuberculosis. He exposed individuals with lupus vulgaris (tuberculosis of the skin) to high-intensity light produced from an electric arc lamp. Exposing a small area of affected skin to intense light produced moderate sunburn. The superficial skin layers subsequently peeled away leaving normal, healthy skin underneath. Almost more than a century later, the mechanism in which sunlight helps in treating tuberculosis became clearer. Liu *et al.*, in a recent issue of science propose that sunlight, by stimulating the synthesis of 1α,25-$(OH)_2D_3$, induces the expression of a microbe-fighting peptide (Liu et al., 2006). This microbe-fighting peptide was determined to be LL-37 (also known as cathelicidin) that has anti-infective properties useful in killing bacteria such as *Mycobacterium tuberculosis* (causative agent of tuberculosis). Studies on the LL-37 gene demonstrated the presence of VDREs in the promoter sequence which are activated by 1α,25-$(OH)_2D$ (Wang et al., 2004). LL-37 is produced by human neutrophils, macrophages, and skin keratinocytes. In fact, the mechanism (Zasloff, 2006) in which sunlight helps in fighting bacterial infection involves both the macrophages and keratinocytes and entails the following: Sunlight converts 7-dehydrocholesterol in the

skin to vitamin D_3, which is converted to 25-$(OH)D_3$ and then to 1α,25-$(OH)_2D_3$ within keratinocytes. Sunlight also induces expression of the VDR. 1α,25-$(OH)_2D_3$ and the VDR then together induce the expression of the gene encoding the human antimicrobial peptide LL-37. Also, vitamin D_3 produced in the keratinocytes is released and enters the circulation where it is converted to 25-$(OH)D_3$ by the liver. Circulating monocytes/macrophages are activated by toll-like receptor 2/1 (TLR2/1) agonists present on the surface of certain microbes. The genes encoding the VDR and CYP27B1 are induced in these activated macrophages. *CYP27B1* converts the 25-$(OH)D_3$ from the circulation to 1α,25-$(OH)_2D_3$ that binds to the VDR and activates the gene encoding LL-37, leading to an increase in cellular LL-37 and enhanced microbicidal activity of the phagocyte (Fig. 9).

These effects resulting from the collaborative role of two nonrenal cell types synthesizing 1α,25-$(OH)_2D_3$ are the first to show an essential intracrine role for this metabolite in the context of normal calcemia and phosphatemia.

Chondrocytes: There are several reports in the literature describing an effect of vitamin D metabolites on the proliferation and differentiation of growth plate chondrocytes. The laboratory of Boyan, through the use of cell biology and signal transduction methodologies on cultured cells, showed that both 1α,25-$(OH)_2D$ and 24R,25-$(OH)_2D$ regulate the proliferation and differentiation of chondrocytes isolated from different zones of the growth plate (Schwartz et al., 1989; Schwartz et al., 1988; Swain et al., 1992). Taking advantage of the visual differences between the maturation zones of the rat rib chondrocytes, the group used sharp dissection to separate cells in the uppermost resting zone (reserve zone) from those in the post-proliferative, prehypertrophic, and

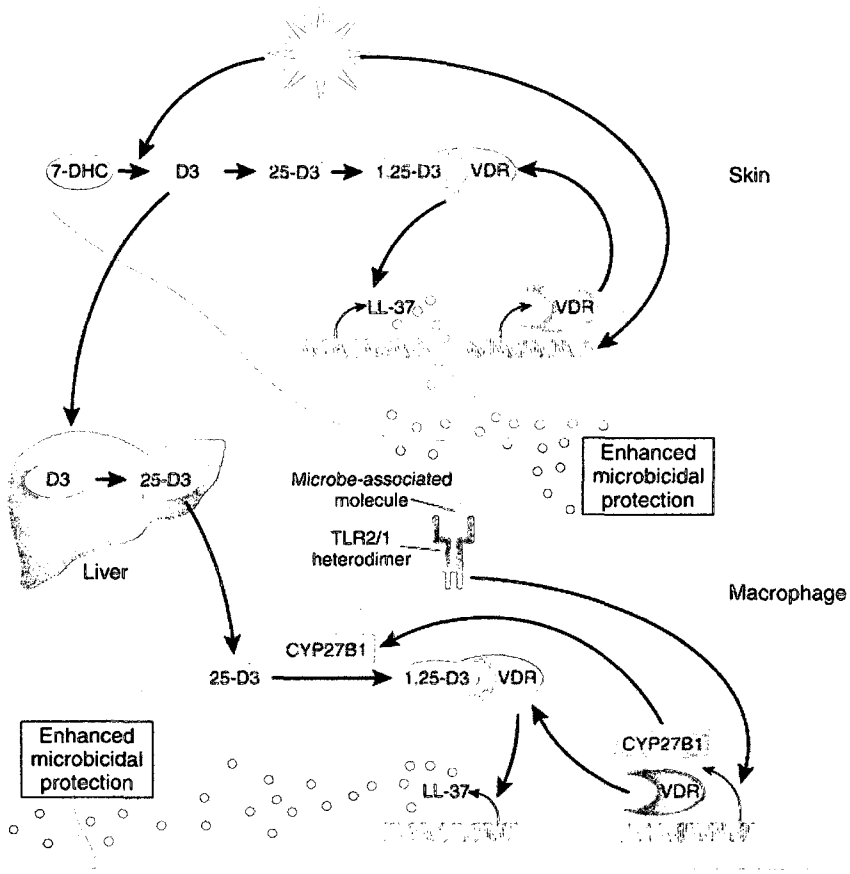

Figure 9 Schematic representation showing the role of $1\alpha,25\text{-}(OH)_2D_3$ in fighting infection through the coordinated function of both keratinocytes and macrophages.

Sunlight converts 7-dehydrocholesterol in the skin to vitamin D_3, which is converted to $25\text{-}(OH)D_3$ and then to $1\alpha,25\text{-}(OH)_2D_3$ within keratinocytes. Sunlight also induces expression of the VDR. $1\alpha,25\text{-}(OH)_2D_3$ and the VDR then together induce the expression of the gene encoding the human antimicrobial peptide LL-37. Also, vitamin D_3 produced in the keratinocytes is released and enters the circulation where it is converted to $25\text{-}(OH)D_3$ by the liver. Circulating monocytes/macrophages are activated by toll-like receptor 2/1 (TLR2/1) agonists present on the surface of certain microbes. The genes encoding the VDR and CYP27B1 are induced in these activated macrophages. *CYP27B1* converts the $25\text{-}(OH)D_3$ from the circulation to $1\alpha,25\text{-}(OH)_2D_3$ that binds to the VDR and activates the gene encoding LL-37, leading to an increase in cellular LL-37 and enhanced microbicidal activity of the phagocyte.

$25\text{-}D_3$, $25\text{-}(OH)D_3$; $1\text{-}25\text{-}D_3$, $1\alpha,25\text{-}(OH)_2D_3$. Adapted from (Zasloff, 2006).

upper hypertrophic zones (collectively termed the growth zone) and place them in culture. Their studies showed that 1α,25-$(OH)_2$D inhibits the proliferation of both resting and growth zone cells and affects primarily the differentiation of growth zone cells, whereas, 24R,25-$(OH)_2$D affects primarily the differentiation of resting zone cells (Boyan et al., 2002). In addition 24R,25-$(OH)_2$D initiates a differentiation cascade that results in down-regulation of responsiveness to 24R,25-$(OH)_2$D itself and upregulation of responsiveness to 1α,25-$(OH)_2$D (Boyan et al., 2002). 1α,25-$(OH)_2$D regulates growth zone chondrocytes both through the nuclear VDR, and through a membrane-associated receptor that mediates its effects via a PKC signal transduction pathway (Sylvia et al., 1996; Sylvia et al., 1993). PKCα is increased via a phosphatidylinositol-specific PLC-dependent mechanism, as well as through the stimulation of phospholipase A_2 (PLA_2) activity (Schwartz & Boyan, 1988). Arachidonic acid and its downstream metabolite prostaglandin E_2 (PGE_2) also modulate cell response to 1α,25-$(OH)_2$D (Boyan et al., 1998). In contrast, 24R,25-$(OH)_2$D exerts its effects on resting zone cells through a separate, membrane-associated receptor that also involves PKC pathways (Nemere et al., 1998). PKCα is increased via a phospholipase D (PLD)-mediated mechanism (Sylvia et al., 2001). The target-cell-specific effects of each metabolite are also seen in the regulation of matrix vesicles. Matrix vesicles are membrane-bound extracellular organelles produced by the chondrocytes. Their membrane phospholipid composition differs from that of the plasma membrane and there is a differential distribution of membrane and cellular enzymes as well. Unlike the chondrocyte plasma membrane, the PKC isoform involved in matrix vesicles is PKCδ, and its activity is

inhibited, providing a mechanism for differential autocrine regulation of the cell and its matrix vesicles by 1α,25-$(OH)_2$D and 24R,25-$(OH)_2$D.

In vivo effects of 1α,25-$(OH)_2$D on the growth plate chondrocytes and consequently on endochondral ossification were recently reported and will be discussed in section I. 4 g.

Cancerous cells: It was observed that expression of CYP27B1 is decreased in some types of cancers including prostate and colon cancers (Hsu et al., 2001). A negative correlation between UV-sunlight exposure, dietary vitamin D, and various cancers was also reported (Schwartz, 1992). These reports are the basis for current studies on the preventive and therapeutic actions of 1α,25-$(OH)_2$D in cancer. Both the VDR and the suggested membrane receptor of 1α,25-$(OH)_2$D are involved in the signaling of the anticancer actions of this metabolite. 1α,25-$(OH)_2$D was reported to regulate cell cycle regulators (e.g., p21, p27, cyclin C, CDKs), growth factors (e.g., inhibition of insulin growth factor -1 signaling pathway), apoptosis (e.g., bcl-2 down regulation), telomerase (e.g., decreased activity), and metastatic progression (e.g., decreased invasive action) (Hansen et al., 2001). Recent studies are aiming to synthesize vitamin D analogs that lack the 1α,25-$(OH)_2$D calciotropic effects and that retain the hormone's anticancer action.

Role of 1α,25-$(OH)_2$D in the immune system: Besides the macrophages, the VDR is expressed in most cells of the immune system including T lymphocytes and dentritic cells. Growing evidence indicates that 1α,25-$(OH)_2$D is a modulator of the immune system through its action in controlling cellular differentiation. This immunomodulatory function of 1α,25-$(OH)_2$D is evident by its effect in several animal models to prevent

autoimmune diseases, extend graft survival (Casteels et al., 1998), and downregulate immune responses in general (Overbergh et al., 2000). Immunosuppressive actions of 1α,25-$(OH)_2D$ appear to be mediated though dendritic cells that result in the decrease of T-cell responsiveness (Penna & Adorini, 2000).

The role of 1α,25-$(OH)_2D$ in the nervous system: Recent reports have suggested that 1α,25-$(OH)_2D$ acts on the central nervous system (CNS) and has neuroprotective effects. The VDR is expressed throughout the nervous system (Prufer et al., 1999) and is a strong inducer of nerve growth factor expression once bound to 1α,25-$(OH)_2D$ (Kumar, 2002). *In vivo* experiments in rodents have shown that 1α,25-$(OH)_2D$ retards age-related decreases in hippocampal neuronal density (Landfield & Cadwallader-Neal, 1998) and protects against neuronal cell death in a rodent model of stroke. Moreover, 1α,25-$(OH)_2D$ can act directly on primary cultures of rat hippocampal neurons to inhibit expression of markers associated with neuronal aging (Brewer et al., 2001).

I. 4. g-Role of 1α,25-$(OH)_2D$ in endochondral ossification

As mentioned earlier, vitamin D deficiency affects normal endochondral ossification, which results in rickets and osteomalacia. The abnormal mineralization accompanying the perturbed endochondral ossification is partly caused by the calcium deficiency due to the lack of vitamin D. Vascular invasion of mineralized cartilage is an essential step in endochondral ossification giving osteoclasts and osteoblasts access to resorb the cartilage matrix and lay down a new one. VEGF, a well-characterized angiogenic molecule, was shown to be a key player in this process. The White laboratory

showed that infusion of a dominant negative VEGF receptor would block vascular invasion and endochondral ossification in the growth plate of juvenile mice (Lin et al., 2002). The group also showed that 1α,25-$(OH)_2$D stimulates the mRNA transcription of VEGF-121 and -165 isoforms in the rat chondrocanial cell line CFK2. VEGF expression along with matrix metalloproteinase 9 (MMP9) was also enhanced in the tibial growth plate chondrocytes and osteoblasts of mice systemically treated with 1α,25-$(OH)_2$D. MMP9, produced by the osteoclasts bordering the chondro-osseous junction, cleaves VEGF stored in the cartilage matrix and makes it accessible to the neighboring endothelial cells that form the blood vessels. In summary, the group proposes the following mechanism: 1α,25-$(OH)_2$D produced and released from the hypertrophic chondrocytes will act on the hypertrophic chondrocytes themselves and neighboring osteoblasts to stimulate the synthesis and release of VEGF. The osteoblasts (through VEGF release and other mechanisms) will induce the osteoclasts to produce MMP9, which cleaves and renders VEGF accessible to the endothelial cells that form the vasculature (Fig. 10) (Lin et al., 2002).

The above observations are supported by the phenotype documented in the MMP9 knockout mouse-model. The phenotype is characterized by a substantial increase in growth plate hypertrophic chondrocytes, impaired endochondral ossification at the primary site with decreased vascular invasion, and a delay in the formation of the bone marrow (Vu et al., 1998).

Masuyama *et al.* used a genetic approach to address the direct role of VDR in growth plate development and endochondral ossification. They conditionally inactivated the VDR in chondrocytes using a Cre recombinase driven by a collagen type α_1(II)

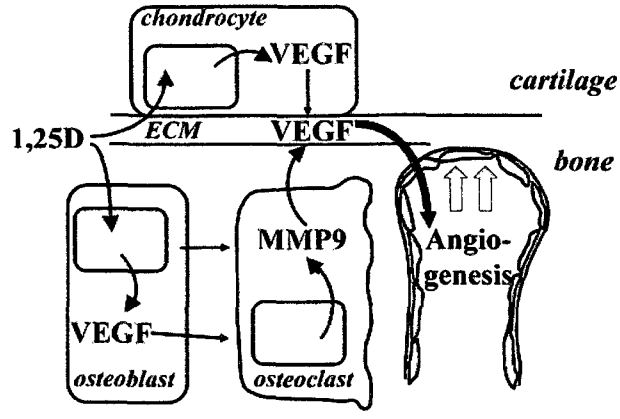

Figure 10 Schematic representation showing the role of $1\alpha,25\text{-}(OH)_2D$ in promoting vascular invasion.

$1\alpha,25\text{-}(OH)_2D$ (1,25D) produced and released from the hypertrophic chondrocytes will act on the hypertrophic chondrocytes themselves and neighboring osteoblasts to stimulate the synthesis and release of vascular endothelial growth factor (VEGF). The osteoblasts (through VEGF release and other mechanisms) will stimulate the osteoclasts to produce matrix metallo-proteinases 9 (MMP9), which cleaves and renders VEGF accessible to the endothelial cells that form the vasculature. Adapted from (Lin et al., 2002).

promoter. The growth plate development was not affected in their model, but vascular invasion was impaired and osteoclast number was reduced in juvenile mice, resulting in increased trabecular mass (Masuyama et al., 2006). The impaired vascular invasion due to the decreased chondrocytic VEGF expression only partly explained the reduced osteoclast number bordering the chondro-osseous junction. The group confirmed, by using a coculture system of splenocytes and chondrocytes derived from the VDR-null long bones, that VDR signaling in the chondrocytes directly regulated osteoclastogenesis by inducing RANKL expression. Interestingly, mineral homeostasis was also affected in the chondrocyte-specific VDR-null mice with serum phosphate and $1\alpha,25\text{-}(OH)_2D$ levels increased in the juveniles. mRNA analysis of VDR-null long bone epiphyses and of cocultures of osteoblasts and VDR-null chondrocytes showed that VDR inactivation in these chondrocytes reduced the expression of FGF23 by osteoblasts (in a mechanism not fully understood) and consequently led to increased renal expression of Cyp27b1 and NPT2a.

These findings show, *in vivo,* a role for VDR signaling in the process of endochondral ossification and bone formation. A support for these findings would be the characterization of the role played by the $1\alpha,25\text{-}(OH)_2D$ ligand in an *in vivo* condition.

I. 5-Role of 24R,25-$(OH)_2D$

I. 5. a-Historical view

Unlike the case of 1α,25-$(OH)_2D$, which has a well characterized nuclear receptor distributed throughout many tissues in the body exerting a pleiotropic action, 24R,25-$(OH)_2D$ has no known receptor. Hence, there is a lot of controversy in the literature on whether 24R,25-$(OH)_2D$ has a true physiological role or not. Some groups claim that the only function of this metabolite is to regulate 1α,25-$(OH)_2D$ levels by rendering 25-(OH)D unavailable. Other studies that support this claim involve the use of vitamin D analogs fluorinated at position 24 (thus preventing hydroxylation at this position) (Tanaka et al., 1979). These studies performed in rats have revealed that these fluorinated compounds produce the same biological response as those resulting from 25-(OH)D concerning the mineralization of vitamin D deficient bone, the mobilization of calcium from bone, and the intestinal calcium transport. Furthermore, the progeny of these animals also show no aberrant phenotype suggesting that 24-hyroxylation does not play a major role in bone growth and development in the rat. It can always be argued, however, that the fluoro compound might be a true 24R,25-$(OH)_2D$ agonist given the fact that position 24 is occupied. This counterargument is used by many groups that support a role of 24R,25-$(OH)_2D$. In fact, there are many reports suggesting a role of 24R,25-$(OH)_2D$ both *in vitro* and *in vivo*:

In vitro: The most dramatic *in vitro* experiments using 24R,25-$(OH)_2$D were performed by Boyan *et al.*. These studies, as mentioned earlier, were done on rat costochondral cultures and show a role for 24R,25-$(OH)_2$D in the regulation of the differentiation of growth plate chondrocytes (Schwartz et al., 1988). The "resting zone" chondrocytes respond to 24R,25-$(OH)_2$D that inhibits their proliferation and regulate several differentiation markers acting through a membrane receptor. These markers include increased collagen and proteoglycan synthesis, and regulation of plasma membrane and matrix vesicle fluidity and enzyme activity, such as alkaline phosphatase, phospholipase A_2 and protein kinase C (Schwartz & Boyan, 1988). More than that, it has been shown that growth plate chondrocytes express Cyp24a1 (24-hydroxylase) and are capable of converting 25-(OH)D to 24R,25-$(OH)_2$D (Schwartz, 1992). In summary, these studies suggest an autocrine regulation of chondrocytic differentiation and function in which 24R,25-$(OH)_2$D would induce immature resting zone chondrocytes to differentiate into mature growth zone chondrocytes.

Other *in vitro* experiments have reported an inhibitory effect of 24R,25-$(OH)_2$D on osteoclastogenesis. In these experiments, the addition of 24R,25-$(OH)_2$D inhibited the 1α,25-$(OH)_2$D induced fusion of pre-osteoclastic cells into fully mature multinucleated osteoclasts (Yamato et al., 1993).

In vivo: The first reports on a unique biological role of 24R,25-$(OH)_2$D involved the inhibition of PTH secretion in many animal models (Canterbury et al., 1978; Chertow et al., 1980) and the regression of hypertrophied parathyroid glands that are present in vitamin D-deficient hypocalcemic chicks (Henry et al., 1977).

24R,25-$(OH)_2D$ was shown to be required, in combination with 1α,25-$(OH)_2D$, for normal egg hatchability in both White Leghorn chickens and in Japanese quail (Henry & Norman, 1978). Moreover, it was found out that the naturally occurring 24R,25-$(OH)_2D$ and not its artificial epimer 24S,25-$(OH)_2D$ contribute to the normal egg hatchability (Norman et al., 1983).

Other recent studies with 24R,25-$(OH)_2D$ focuses on a biological role in bone and cartilage cells. The local administration of 24R,25-$(OH)_2D$ into bone was reported to heal rachitic lesions of chick tibiae (Ornoy et al., 1978), while 1α-hydroxyvitamin D alone could not produce the same effect. 24R,25-$(OH)_2D$ given in pharmalogical doses to ovariectomized beagle dogs has been shown to increase bone mass (Nakamura et al., 1992) and bone strength in rabbits. A Cyp24a1-knockout mouse strain was developed by the laboratory of St-Arnaud (St-Arnaud et al., 2000) where a defect in intramembranous ossification was reported. This defect was characterized by an increase in unmineralized osteoid in the calvaria, clavical and periosteal surface of the femur. Further crossing of the Cyp24a1-deficient mice with VDR knockout mice rescued the abnormal phenotype suggesting that the defect in bone mineralization was due to increased 1α,25-$(OH)_2D$ levels and not due to the lack of 24R,25-$(OH)_2D$.

I. 5. b-Role of 24R,25-$(OH)_2D$ in fracture repair

A putative biological function of 24R,25-$(OH)_2D$ is its involvement in healing in a fracture repair chick model (Seo & Norman, 1997). Seo *et al.* have established a tibial fracture-healing model in white leghorn chicks. After the infliction of a tibial osteotomy,

both the mRNA levels of renal CYP24A1 and the serum levels of 24R,25-$(OH)_2D$ started to gradually rise and peak at day 10 post-fracture (a three-fold statistically significant difference) in the chicks that received the osteotomy as compared to chicks that did not. At day 15 post-fracture, the level of renal CYP24A1 mRNA was similar in the two groups at baseline levels (Fig. 11). Moreover, these differences at day 10 post-fracture were not observed for 25-(OH)D or 1α,25-$(OH)_2D$. Exposure of primary chick kidney cells in culture to serum obtained from chicks with a tibial fracture for 20 hours resulted in an almost 40% increase in the activity of the CYP24A1 as compared with cells exposed to serum from control birds.

Follow up mechanical experiments by the Norman group in a vitamin D-depleted chick model showed that 24R,25-$(OH)_2D$ [and not its synthetic epimer 24S,25-$(OH)_2D$] along with 1α,25-$(OH)_2D$ improved mechanical strength parameters (torsional strength, angular deformation, and stiffness) (Seo et al., 1997). They also reported the presence of a receptor/binding protein for each of 24R,25-$(OH)_2D$ and 1α,25-$(OH)_2D$ in the membrane fraction of the tibial callus (Kato et al., 1998).

The group proposes a model in which 24R,25-$(OH)_2D$ is involved in the early process of fracture repair. The model involves some form of physiological communication between the fractured bone and the kidney so as to increase the renal *CYP24A1* enzyme levels and the circulating concentration of 24R,25-$(OH)_2D$.

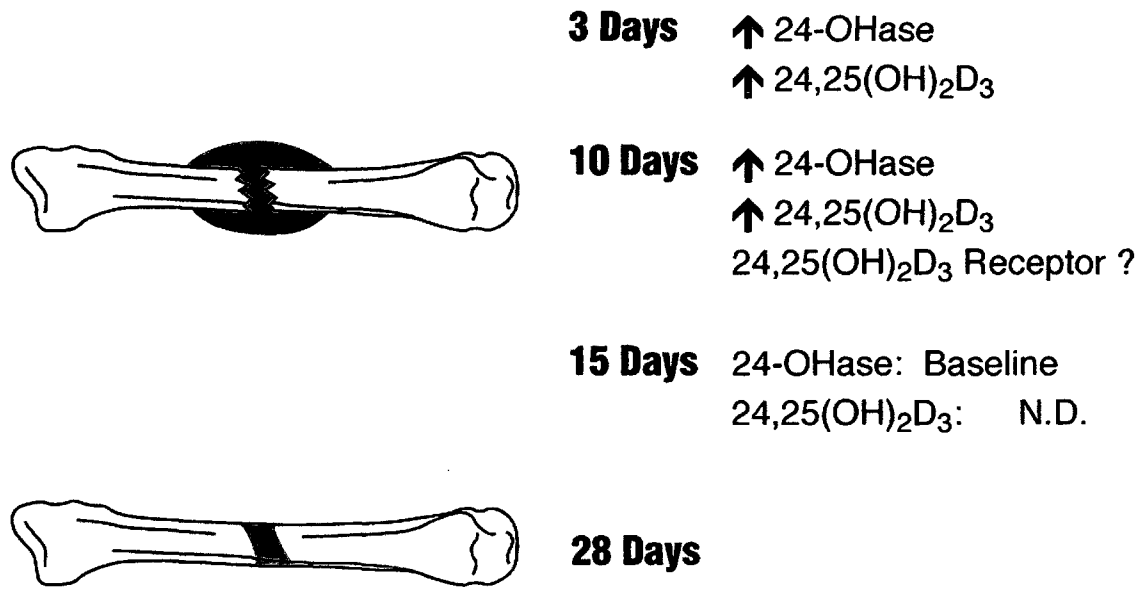

Figure 11 Schematic representation showing the levels of renal 25-hydroxyvitamin D-24-hydroxylase (24-OHase) and serum $24,25(OH)_2D$ in a chicken model of fracture repair.

After the infliction of a tibial osteotomy, both the levels of renal 24-OHase (CYP24A1) and the serum levels of $24,25(OH)_2D$ started to gradually rise at day 3 post-fracture to peak at day 10 post-fracture (a three-fold statistically significant difference) in the chicks that received the osteotomy as compared to chicks that did not. At day 15 post-fracture, the level of renal 24-OHase was similar in the two groups at baseline levels.

24-OHase, CYP24A1; $24,25(OH)_2D$, $24R,25\text{-}(OH)_2D$.

I. 5. c-Fracture repair

Bone formation begins during early fetal development, continues throughout the life of an animal as skeletal remodeling and, if injury occurs, is reinitiated during the process of fracture repair. Unlike soft tissues that heal mostly through the generation of scar tissue, bone heals through the generation of new bone. The process of fracture repair is divided into three phases: the reactive phase, the reparative phase, and the remodeling phase.

Reactive phase: After fracture, the blood vessels at the fracture site constrict to stop any further bleeding (Brighton & Hunt, 1997). Following vascular constriction, the extravascular blood cells, known as hematoma, form a blood clot. Within the area of the clot, the extravascular cells will degenerate and the neighboring fibroblasts will multiply forming a loose aggregate of cells interspersed with small blood vessels known as granulation tissue.

Reparative phase: Several days after fracture, the cells of the periosteum proximal to the fracture site will proliferate and differentiate into chondroblasts that deposit hyaline cartilage, whereby, the cells of the periosteum distal to the fracture site will proliferate and differentiate into osteoblasts that deposit woven bone (Brighton & Hunt, 1997). The fibroblasts within the granulation site also develop into chondroblasts. These newly formed tissues will grow in size and unite with their counterparts from other pieces of the fracture to form what is known as the *fracture callus.* The next step of the reparative phase is the replacement of the hyaline cartilage and woven bone with lamellar bone. The replacement process in case of the hyaline cartilage is known as endochondral

ossification that goes through the woven bone intermediate. In the case of the osteoblastic woven bone, the replacement process is known as intramembranous ossification and usually takes less time than the endochondral ossification process. The osteoblasts that come with the vasculature invading the mineralized matrix will deposit the lamellar bone that is in the form of trabecular bone (Brighton & Hunt, 1997). Eventually, all of the woven bone and cartilage of the original fracture callus will be replaced by trabecular bone, restoring most of the bone's original strength.

Remodeling phase: In this phase, the trabecular bone is replaced by compact bone. This trabecular bone is first resorbed by osteoclasts creating a resorption pit known as Howship's lacuna. Folllowing this, the osteoblasts deposit compact bone within the resorption pit. Eventually, the fracture callus is remodeled into a shape, which closely duplicates the bone's original shape and strength.

I. 5. d-Stabilized versus non-stabilized fractures

Fracture repair models to study the effect of many metabolites and hormones have been recently adapted in mice and other mammalian animals. These models, at the site of osteotomy, involve extensive skeletal regeneration that is greatly influenced by the mechanical environment. Cyclic motion and its associated shear stress, a characteristic of non-stabilized fractures, appear to favor the formation of a cartilaginous callus that is remodeled and thus healing occurs through endochondral ossification. On the other hand, low to moderate tensile strain and stress, a characteristic of stabilized

fractures, result in direct repair through intramembranous ossification (Carter et al., 1988).

The apparatus used in many stabilized fracture repair models is adapted from the Ilizarof model. Ilizarof, a Russian orthopedic surgeon, devised an apparatus to correct fractured and deformed bones in humans. His initial model was based on two bicycle wheel frames surgically placed on the distal and proximal part of the long bone and linked together via metallic rods. This apparatus was further adapted for distraction osteogenesis, a surgical process used to reconstruct skeletal deformities and lengthen the long bones of the body (zazimko, 1978, Klin Khir).

Our laboratory has a long-standing interest in the study of vitamin D metabolism and bone function. We have developed powerful genetic models to address the putative role of vitamin D metabolites hydroxylated at position 24 in fracture repair and to examine the contribution of vitamin D metabolic enzymes expressed in chondrocytes to the processes controlling growth plate development. In my work, I have modulated Cyp27b1 expression in chondrocytes (inactivation or overexpression) and examined the consequences of such genetic manipulations on growth plate development. I have also studied fracture repair in mice deficient for the vitamin D metabolic enzyme, *Cyp24a1*.

Hypotheses

1) Locally produced 1α,25-$(OH)_2D$ regulates the growth and differentiation of growth plate chondrocytes and/or angiogenesis in the growth plate.
2) 24R,25-$(OH)_2D$ plays a physiological role in mammalian fracture repair.

Objectives

1) Engineering of a tissue-specific loss-of-function model of Cyp27b1 in growth plate chondrocytes.
2) Engineering of a tissue-specific overexpression model of *Cyp27b1* in growth plate chondrocytes.
3) Analysis of the impact of *in vivo* Cyp27b1 modulation on the growth and differentiation of growth plate chondrocytes and the neovascularization of the growth plate.
4) Development of a mouse fracture repair model in the absence of 24R,25-$(OH)_2D$.
5) Analysis of the healing process in mice having 24R,25-$(OH)_2D$ as compared to mice lacking 24R,25-$(OH)_2D$.
6) Rescue of the phenotype produced by treatment with 24R,25-$(OH)_2D$ and 1α,25-$(OH)_2D$.

II. Materials & Methods

II. 1-Mating strategy

The mating strategy used to obtain a tissue-specific knockout model of Cyp27b1 was conducted as follows: mice heterozygous for Cyp27b1 null allele (previously engineered in our lab (St-Arnaud et al., 2000) were mated with transgenic mice (referred to as Col2Cre (Terpstra et al., 2003)) expressing the Cre recombinase under the control of the collagen α_1(II) chondrocyte-specific promoter (Niederreither et al., 1992) (i.e. $Cyp27b1^{+/-}$ x Col2Cre). The progeny obtained with the genotype of a heterozygous Cyp27b1 null allele and Col2Cre transgene were further mated with mice homozygous for floxed Cyp27b1 alleles (i.e. Col2Cre;$Cyp27b1^{+/-}$ x $Cyp27b1^{fl/fl}$). This final cross resulted in a proportion of a progeny having one Cyp27b1 null allele, one floxed Cyp27b1 allele and transgenic for Col2Cre (i.e. Col2Cre;$Cyp27b1^{-/fl}$ mutants that will be referred to as $Cyp27b1^{-/CH\Delta}$ in this study).

II. 2-Engineering of Cyp27b1 recombinant molecule & transgenic strains

1586 base pairs of Cyp27b1 cDNA (excluding the 5'UTR sequences and fused in frame with a FLAG epitope at the 3'end) was excised from pCR 2.1-TOPO (Invitrogen) cloning vector using BamH1 (New England Biolabs Ltd.,Mississauga, ON) digestion. The resulting fragment was blunt-ended and subcloned into a Sma1 site of the pSI vector

(Promega, Madison, WI). The Cyp27b1 cDNA fragment along with an upstream chimeric intron and a downstream SV40 Poly A sequence were excised from the pSI vector using HindIII (New England Biolabs) and BamH1 (New England Biolabs) digestion. The resulting fragment was blunt-ended and subcloned into a SpeI (New England Biolabs) site of pBluescript 2 (Stratagene, La Jolla, CA) between the collagen α_1(II) promoter and collagen α_1(II) intron 1 sequences that were previously cloned there. The resulting 8 kb molecule was linearized from the pBluescript 2 by XhoI (New England Biolabs) digestion (Fig. 27). The linearized recombinant molecule was then purified and used for pronuclear injections performed at the transgenic facility of McGill University (McGill University, Montreal, QC). The collagen α_1(II) promoter and enhancer sequences originated from the de Crombrugghe lab (Niederreither et al., 1992).

II. 3-Genotyping by PCR

All the PCR primers were purchased from AlphaDNA (AlphaDNA, Montreal, QC) and the PCR reagents from Invitrogen.

The Cyp27b1 tissue-specific knockout mice ($Cyp27b1^{-/CH\Delta}$) & control littermates were genotyped by performing two PCR reactions with Cre & α-ko primer sets. The α-ko primers [Forward: 5'-GTCCAGACAGAGACATCCGT-3', Reverse: 5'-GCACCTGGCTCAGGTAGCTCTTC-3'] flank exon 8 sequences of the Cyp27b1 wild-type allele and generate a 988 bp amplicon. In case of a knocked-out allele, the resulting amplicon will have the size of 345 bps. The PCR mix contained the following: 2.5 µl of 10X PCR Buffer, 0.75 µl $MgCl_2$ (50 mM), 2.5 µl dNTP (2 mM), 2.5 µl of each of the α-

ko primers (5 mM), 0.25 μl of TaqMan enzyme, 1 μl genomic DNA, and 13.5 μl dH_2O. The mix was loaded into a thermowell tube and amplification using the GeneAmp PCR 9700 was done as follows: heating at 94°C for 3 min, 35 cycles of 94°C for 45 sec, 60°C for 30 sec, and 72 °C for 1 min, with a further extension of 72 °C for 10 minutes.

The Cre primers [Forward: 5'-TGAAGCATGTTTAGCTGGCCCA-3', Reverse: 5'-GACCGTACACCAAAATTTGCCTGC-3'] flank Cre sequences (present in $Cyp27b1^{-/CH\Delta}$) and generate a 500 bp amplicon. The PCR mix contained the following: 2.5 μl of 10X PCR Buffer, 0.75 μl $MgCl_2$ (50 mM), 2.5 μl dNTP (2 mM), 2.5 μl of each of the Cre primers (5 mM), 0.25 μl of Taqman enzyme, 1 μl genomic DNA, and 13.5 μl dH_2O. The mix was loaded into a thermowell tube and amplification using the GeneAmp PCR 9700 was done as follows: heating at 94°C for 3 min, 30 cycles of 94°C for 45 sec, 58 °C for 30 sec, and 72°C for 1 min, with a further extension of 72 °C for 7 minutes.

The Cyp27b1 tissue-specific transgenic mice & control littermates were genotyped by performing one PCR reaction with 1alpha1 primer sets [Forward: 5'-GCGTGCTTGCGATTGCTAAC-3', Reverse: 5'-CGGGCCCAGGGTCCAGGTAT-3'] giving a 393 bp amplicon of the recombinant Cyp27b1 in the case of transgenesis and a 818 bp amplicon of the wild-type Cyp27b1 allele. The PCR mix contained the following: 2.5 μl of 10X PCR Buffer, 0.75 μl $MgCl_2$ (50 mM), 2.5 μl dNTP (2 mM), 3.1 μl of forward primer (3.96 mM), 1.76 μl of reverse primer (7.08 mM), 0.25 μl of Taqman enzyme, 1 μl genomic DNA, and 13.19 μl dH_2O. The mix was loaded into a thermowell tube and amplification using the GeneAmp PCR 9700 was done as follows: heating at 94°C for 3 min, 30 cycles of 94°C for 45 sec, 60°C for 30 sec, and 72 °C for 30 sec, with a further extension of 72°C for 10 minutes.

II. 4-Embryonic sample collection, paraffin embedding & processing

Mice were placed together for the purpose of breeding. Plugs were checked on the following day and when detected, the females were moved to a separate cage. Pregnant females were sacrificed 14 or 15 days later to give 14.5- or 15.5-day-old embryos (E14.5 or E15.5) respectively. Uterine horns were placed in 10 ml petri dishes with 1X phosphate buffered saline (PBS) and individual embryos were dissected out and placed in a 10 ml falcon tube containing 4% paraformaldehyde (PFA) [4g paraformaldehyde (Fisher Scientific Inc., Fair Lawn, NJ) powder dissolved in 100 ml 1X PBS, PH 7.5] solution for overnight fixation (yolk sacs were kept for DNA extraction and subsequent genotyping). The hindlimbs of the embryos were dissected out by using a Leica MZ6 dissecting microscope (Leica Microsystems, Richmond Hill, ON) the following day and paraffin embedding was conducted as follows:

The samples were rinsed in 1X (PBS) (137 mM NaCl, 2.7 mM KCl, 4.3 mM Na2HPO4, 1.4 mM KH2PO4, pH 7.3) for 30 minutes (min)-1 hour (1hr) and then placed in a solution of 0.85% saline in 30% ethanol for 15 min. The samples were then gradually dehydrated using 50,70, 80, 90 and 100% ethanol solutions for 15 min each time. Clearing of the samples was done in a 1:1 solution of ethanol: xylene (Fisher Scientific) for 15 min and then in xylene solution for 15 min. Following clearing, the samples were washed with three changes of molten paraplast (OXFORD LABWARE, St-louis, Mo.) prior to being placed overnight (O/N) in paraplast under vaccum at 55°C. The next day the hindlimbs were oriented properly and placed in plastic cassettes filled with molten paraplast and left at 4°C for several hours to cool and harden.

The hardened paraffin blocks were subsequently mounted on a Leica RM 2255 microtome (Leica Microsystems) and 5 μm sections were taken and placed in a 30°C water bath for 30 seconds before being laid down on superfrost/plus microscopic slides (Scientific Device Laboratories, Des Plains, IL). Sections were then dried for two hrs before being placed on a 60°C hot plate for two hours for the paraffin to melt after which they were ready for H&E staining that was performed as follows:

The sections were cleared in two 10 min changes of xylene before being rehydrated in a decreasing ethanol solution of 100% and 70% for 5 min each time. Following rehydration, the sections were washed with distilled water (dH_2O) for 10 min prior to being dipped in Harris modified Hematoxylin (Fisher Scientific) for 20 seconds (sec). The sections were then placed under running dH_2O for 2 min, dipped in a freshly filtered 0.5% sodium-acetate solution for 1 min, washed twice in dH_2O for 30 sec and then placed in Eosin solution (Sigma-Aldrich, Oakville, ON) for 4 min. Subsequent washing with running dH_2O for 2 min and dehydration in two changes of 100% ethanol solution for 2 min each time was done before the sections were cleared with two 10 min washes of xylene. The samples were then mounted with a water-soluble mounting media.

II. 5-Postnatal sample collection, embedding & processing

Tibiae of different mice strains (Cyp27b1 tissue-specific knockouts and different Cyp27b1 tissue-specific transgenic strains) were collected at different ages (2,14, and 42 days old) and fixed in 4% PFA O/N. The following day, samples were processed to be either embedded in paraffin (when immunohistochemistry was performed) or methyl

methacrylate (MMA) (when Golder-Trichrome staining and further histomorphometry was performed). Paraffin embedding was done as follows: The samples were rinsed in 1X PBS for 30 min-1 hr and then demineralized with formic acid-based Immunocal™ (Decal Chemical Co., Tallman, NY) for a couple of days. The samples were then rinsed in 1X PBS for 30 min-1 hr before being gradually dehydrated using two changes of 50,70, 90 and 100% ethanol solutions for 1hr each time. Clearing of the samples was done in two 30 min washes of xylene. From hereon, the same was done as described in section II. 4.

MMA (Fisher Scientific) embedding was done as follows: The samples were rinsed in 1X PBS for 30 min-1 hr and then gradually dehydrated using two changes of 50,70, 90 and 100% ethanol solutions for 1hr each time. Clearing of the samples was done in three 40 min washes of xylene before consecutive O/N changes in purified 0, 0, 1 (13% v/v di- butyl-phtalate, 1% w/v benzoyl peroxide), 1, and 4.5% (17% v/v di-butyl-phtalate, 4.5% w/v benzoyl peroxide) MMA solutions at 4°C. Following this, the tibiae were properly oriented (to allow longitudinal sectioning) and placed in a new vial containing 4.5% MMA solution at room temperature (RT) for several days to harden. The hardened MMA blocks were subsequently cut and mounted on the Leica microtome where 5 μm sections were taken and placed in 70% ethanol on silane plus slides (Scientific Device Laboratories). The slides were dried O/N at 55°C and deplastified the next day using four 15 min changes of Ethyl Glycol Monoethyl Ether Acetate (EGMA) (Fisher Scientific).

II. 6-Image acquisition

All sections were viewed on a Leica DM-R microscope (Leica Microsystems) and the images were acquired by the OLYMPUS DP70 camera (GE Healthcare Bio-Sciences, Baie d'Urfe, QC) and processed by the DPController software.

II. 7-Goldner staining & histomorphometric analysis

The deplastified MMA embedded sections were stained in Goldner-Trichrome staining as follows: The sections were rehydrated in 5 min consecutive changes of 70 and 40% ethanol solutions before being well rinsed in dH_2O. The sections were then placed in Weigert Hematoxyline [1% Hematoxyline powder in 95% ethanol, and Chloral-Ferric powder (5.8g) dissolved in 500mL deionized water with 1% HCL] for 20 min, washed with dH_2O for 10 min, placed in Fushine-ponceau [Fushine acid powder (0.167g) and Ponceau powder (0.667g) dissolved in 500 mL deionized water] for 30 min, quickly rinsed in 1% acetic acid solution, placed in Orange G [Orange G powder (10g) dissolved in 500 mL deionized water] for 8 min, quickly rinsed with 1% acetic acid solution, placed in Light green [(0.03% Light green powder (1.5g) dissolved in 500 mL deionized water] for 45 min, and quickly rinsed with 1% acetic acid solution (all Goldner reagents were purchased from Fisher Scientific). The sections were then immediately passed through quick washes of tertiary butanol and then xylene before the slides were mounted with Microkitt (Fisher Scientific). The slides were then cleaned with xylene and dried at RT for several hours before being photographed by the

QIMAGING RETIGA 300 camera (Bioquant Image Analysis Corporation, Nashville, TN).

Histomorphometric analysis (growth plate width, bone volume/tissue volume and other parameters) on the photographed sections was done by using BioQuant Osteo II imaging software (BioQuant Image analysis Corporation, Nashville, TN).

II. 8-Microcomputed-tomography (μCT) analysis

Trabecular bone parameters [Bone volume/Tissue volume (BV/TV), trabecular number, trabecular thickness, and trabecular separation] of Cyp27b1 tissue-specific knockout two-day-old and 14-day-old tibiae as well as for two-day-old Cyp27b1 tissue-specific transgenic tibiae were analyzed by μCT. The tibiae were collected and placed in 4% PFA O/N. The samples were then washed in 1X PBS, and placed in 70% ethanol to be taken to the McGill center for Bone and Periodontal Research centre for the analysis. The instrument used was a SkyScan 1072, with a detector at 1024 x 1024 pixels, 12 bit cooled CCD – camera.

II. 9-Tartrate Resistant Acid Phosphatase (TRAP) staining

Osteoclast number was determined using TRAP staining. Cyp27b1 tissue-specific knockout ($Cyp27b1^{-/CH\Delta}$ & controls) E15.5 and two-day-old mice tibiae sections were deparaffinized by passing through four washes of xylene (2 min each wash)

followed by rehydration in 100, 95, and 70% ethanol solutions. The sections were then placed in acid washed coplin jars and incubated in a media consisting of Complete Burstone's Media + 50 mM sodium tartrate pH 5.0 for 1 hr at 37°C. The sections were then washed with dH_2O for 10 min. before being mounted with the water-soluble VECTASHIELD (Vector Laboratories Inc, Burlington, ON) mounting media.

II. 10-Proliferating Cell Nuclear Antigen (PCNA) staining

Chondrocyte proliferation in the Cyp27b1 tissue-specific knockout ($Cyp27b1^{-/CH\Delta}$ & controls) tibiae was assayed using the PCNA Staining Kit (Zymed Laboratories Inc., Markham, ON). E15.5 sections were deparaffinized and epitope retrieval was performed by incubating the sections in 10 mM sodium citrate buffer, pH 6.0 at 95°C for 10 minutes. The sections were then washed with dH_2O and stained for PCNA following the manufacturer's instructions.

II. 11-RNA isolation & Reverse Transcription

Total RNA was isolated from the rib-cartilage of Cyp27b1 tissue-specific knockouts (two &14 days old) and transgenics (two days old). Mice were euthanised by cervical dislocation. The thoracic cage was dissected out using fine tools cleaned with RNAseZap (Ambion, Austin, Tx) to inactivate RNAses. The cartilaginous clear section between the mineralized sternum and the rest of the rib was carefully cut and placed in

RNA*later* (Ambion) solution to be stored at -20°C or placed in 1 ml of TRizol reagent (Invitrogen, Carlsbad, CA) for immediate RNA extraction. Once in TRizol solution, the samples were completely homogenized using a Polytron PT-MR 3000 (Kinematica, Littau, Switzerland) at medium to high speed. Following homogenization, 200 μL of chloroform was added to each sample followed by strong shaking. The samples were then centrifuged at 12000 *g* for 15 min and the aqueous RNA-containing supernatant was carefully removed from the protein-containing organic phase. One -half mL of isopropyl alcohol was then added to the separated RNA. Once the RNA precipitated, the samples were centrifuged again at 12000 *g* for 15 minutes. The collected pellet from each sample was washed with 70% ethanol , centrifuged at 7500 *g*, vacuum-dried for 4 minutes, and then resuspended in 30 μL of RNAse-free water (Ambion). The concentration and purity of the total RNA was calculated by measuring the optical density of the samples at 260 and 280 μm. Samples were then ready for reverse transcription or storage at –80 ° C.

Samples were reverse transcribed using either the Applied Biosystems High Capacity cDNA Reverse Transcription Kit (Applied Biosystems, Foster City, CA) or the High Capacity cDNA Archive kit (Applied Biosystems). The RT reaction involved adding equal volumes of Master mix (RT buffer, dNTP mix, Random primers, and the MultiScribe™) and total extracted RNA (diluted in water) before loading into the GeneAmp PCR 9700 thermal cycler (Applied Biosystems).

The same procedure described above was done for RNA extracted from nine-day-old Cyp27b1 tissue-specific knockout epiphyses (in this case the epiphyses were cut off making sure to include the primary growth plate and placed in TRIzol).

II. 12-Reverse-Transcription Real-Time Quantitative PCR (RT-qPCR)

The relative expression of different bone differentiation markers, cartilage differentiation markers and others was quantified using RT-qPCR on the reverse transcribed mRNA from different samples with specific TaqMan (Applied Biosystems) probes [VEGF, KDR/VEGFr2, Mmp9, Ihh, Pthr1, Collagen type I (Col1a1), Collagen α_1(II) (Col2a1), Collagen type X (Col10a1), Hypoxia induced factor 1α (Hif1α), Osteocalcin (Ocn), Alkaline phosphatase (Alkphos), RANKL, Cyp27B1, Cyp24, Cre recombinase (Cre), and Fibroblast growth factor 23 (Fgf23)]. Following the manufacturer's instructions, 100 ng of double-stranded cDNA was added to a mix of TaqMan probes, Universal PCR Master Mix (Applied Biosystems), and RNAse free water. The Real-Time PCR reaction was performed in an Applied Biosystems 7500 instrument (Applied Biosystems). Along with every target gene Real-Time reaction, an endogenous gene (e.g. Gapdh) was also run (in a different well of the same plate) and used to normalize the amount of target mRNA in the sample. The Real-Time plate reader measures the fluorescent dyes incorporated into the primers during amplification, and as a result, provides a quantitative assessment of the mRNA of the gene of interest, called the Ct value. This Ct value of the target gene is then normalized to the Ct value of the endogenous gene (Cttarget – Ctendogenous = dCt). The dCt provides a relative expression in each sample for the target gene. To compare different sample populations (e.g. wild-type versus mutants), the dCt of each value is compared to a chosen calibrator value (usually the wild-type population) (dCtsample1 –Ctcalibrator = ddCt). This ddCt

value is then expressed in terms of a relative value that reflects the exponential nature of PCR that doubles at every Ct increase ($2^{\wedge -ddct}$ = final relative expression value).

II. 13-Immunohistochemistry

Platelet/endothelial cell adhesion molecule-1 (PECAM-1, also known as CD31) immunostaining was done on the tibial primary growth plate of two-day-old Cyp27b1 tissue-specific knockouts ($Cyp27b1^{-/CH\Delta}$) & control littermates. After deparaffinization, 3% Hydrogen peroxide in 1X PBS was added to the sections for 10 min in order to block any endogenous peroxidase activity. The sections were then washed with 1X PBS and blocked in a blocking solution of 1.5% horse serum in 1X PBS. Following blocking, the sections were incubated with 10 μg/ml of PECAM-1 (M-20) goat polyclonal primary antibody (Santa Cruz Biotechnology Inc., Santa Cruz, CA) in a humidified chamber for one hr at RT. The sections were then washed with 1X PBS and incubated with 5 μg/ml of biotinylated anti-goat secondary antibody (Vector Laboratories) in a humidified chamber for 30 min at RT. The sections were then washed with 1X PBS and signals were detected using the ABC Staining System Kit (Santa Cruz) following the maufacturer's recommendations.

II. 14-ATDC5 cell-culture transfections & Immunofluorescence

Before proceeding with pronuclear injections of the Cyp27b1 recombinant molecule, the molecule's expressivity was tested in the ATDC5 cell-line (chondrogenic cell-line derived from embryonic murine teratocarcinoma cells) (courtesy of Dr. Benoit St-Jacques). The cells were trypsinized with 0.05% trypsin-EDTA (Invitrogen) 10 days post-confluency and seeded at a density of 300,000 cells/well in a 6-well plate where coverslips treated with 0.1% gelatin (Invitrogen) were placed. The following day, 2 μg of pBluescript 2 plasmid containing the recombinant molecule was mixed with 375 μl DMEM (Invitrogen) and added to another mixture of 6 μl Lipofectamine (Invitrogen) with 375 μl DMEM to be incubated at RT for 30 minutes. The plated cells were then washed with DMEM before adding the DNA-lipid complex along with 750 μl of DMEM for an incubation of 5 hrs at 37°C in a 5% CO_2 incubator. Following this, 1.5 ml DMEM with 20% FCS was added and the cells incubated for 48 hrs (changing the medium once after 24 hrs) before immunofluorescence was performed.

Immunofluorescence was done as follows: cells were washed with PBS and then fixed with -20°C methanol (10 min) followed by -20°C acetone (1 min) to be washed again twice with PBS. Cells were then blocked (1% BSA in PBS) for 10 min before being incubated with rabbit (1/100) anti-FLAG primary antibody (Sigma) at RT for 1 hour. The cells were then washed 3 times with PBS before being incubated with (1/500) anti-rabbit IgG Rhodmine conjugated (Sigma) as a secondary antibody in PBS containing 1% BSA for 30 minutes. The cells were then washed 3 times with PBS before being mounted with a coverslip along with VECTASHIELD mounting medium for

fluorescence (Vector Laboratories). The signal was viewed using the Leica DM-R microscope with the appropriate filters for fluorescence.

II. 15-DNA extraction & Southern Blotting

DNA extraction was performed on the tail snips of suspected transgenic founders. Tail snips were placed in lysis buffer (pH 8.5, 100 mM Tris- HCl, 200 mM NaCl, 5 mM EDTA, 0.2% SDS, 100 μg/ml proteinase K) at 55°C overnight and were microcentrifuged for 10 minutes at 12,000 rpm the following day. The supernatant was mixed with an equal volume of isopropanol (Fisher Scientific), incubated for 10 minutes, and then microcentrigured for 10 minutes at 12000 rpm. The supernatant was discarded and the pellet was washed with 70% ethanol, air dried, and resuspended in TE buffer (pH 7.7, Tris-HCl 10 mM, EDTA 0.1 mM).

Genotyping was then done using the Southern Blot technique. Ten μl of the extracted genomic DNA was digested with Bamh1 and migrated on a 1% agarose gel. The gel was then placed on a gasket and the DNA fragments were transferred under vaccum to a hybond-N (Amersham Biosciences, Piscataway, NJ) membrane and cross-linked by UV exposure for 20 sec. The membrane was then placed in a glass tube were the specific radioactive probe [prepared from Cyp27b1 cDNA using the Amersham Megaprime Kit (Amersham Biosciences) following the manufacturer's instructions] was added and hybridized at 50°C for 1 hour. Subsequent washing with different stringency buffers to eliminate non-specific binding was done before placing the membrane in contact with a Kodak BioMax film (Kodak, Rochester, NY). The resulting exposed film

showed the characteristic 2 kb band in the transgenics where the recombinant molecule was successfully incorporated.

II. 16-Protein extraction and Western Blotting of Cyp27b1 recombinant molecule

Protein extraction was done on tail snips from Cyp27b1 tissue-specific transgenics and control littermates using TRIzol reagent. The protein-containing organic phase was taken and precipitated with 1.5 ml of isopropanol at RT for 10 minutes. The protein was then sedimented at 12000 *g* for 10 minutes. The supernatant was discarded and the protein pellet was washed 3 times with a 2 ml solution containing 0.3 M of guanidine hydrochloride in 95% ethanol (20 min incubation & 7500 *g* centrifugation). After the third wash, the protein pellet was vortexed and suspended in 2 ml ethanol for 20 minutes followed by sedimentation at 7500 *g* for 5 minutes. The pellet was then vacuum dried and dissolved in 1% SDS. Protein concentration was determined by using the Bio-Rad Protein assay (Bio-Rad Laboratories Inc., Hercules, CA).

Ten to fifteen ug of proteins were then mixed with 100 mM DTT, and loading buffer (125 mM Tris-HCl, 4% SDS, 50% Glycerol, and bromophenol blue until visible). Samples were boiled for 5 minutes and loaded into a western blotting apparatus. This consisted of migrating the proteins through first a stacking gel (4% polyacrylamide) and then a separating gel (7.5% polyacrylamide) by electrophoresis. The gels were loaded with Rainbow RPN800V (GE Healthcare Biosciences) marker to determine protein size on the gel. Following electrophoresis for one to two hours at initially 60 V and then at 120 V in migration buffer (25 mM Tris-HCl, Ph 8.3, 190 mM Glycine, 0.5% SDS), the

lower separating gel was removed from the apparatus and the proteins were transferred onto a nitrocellulose ECL membrane (Amersham Biosciences) for one hour at 60 V in transfer buffer (25 mM Tris-HCl, 190 mM Glycine, 0.05% SDS, 20% methanol).

Once the proteins were bound to the membrane, it was washed in 1X PBS and blocked for one hr in 1X PBS containing 5% skim milk, followed by overnight incubation at 4°C with the rabbit anti-FLAG primary antibody (1/200). Following this incubation, membranes were washed 3 times in 1X PBS, then incubated for 1 hr at RT in blocking solution with the anti-rabbit IgG used as a secondary antibody (1/10000) conjugated to horseradish peroxidase (Amersham Biosciences). The signal was then detected by ECL Western Blotting Detection Reagents (GE Healthcare Bio-Sciences), showing the 56 kD recombinant Cyp27b1 molecule.

II. 17- 25-(OH)D_3 supplementation

0.044 nmol (18 ng) of 25-hydroxyvitamin D_3 [25-(OH)D_3] (Hoechst Marion Roussel Inc., Cincinnati, OH) was daily injected subcutaneously into females starting one week from plug detection until delivery. Offsprings were sacrificed two days later and tibiae were collected and processed into 70% ethanol solution for μCT analysis. The ribcage was also collected at the two-day time-point and kept in RNAlater at -20°C for further RNA extraction and RT-qPCR.

II. 18- Fgf23 ELISA

Peripheral blood was collected from 10-day-old Cyp27b1$^{-/CH\Delta}$ mice and controls. The blood was spun for 10 min. at 6000 *g* after which the aqueous supernatant serum was kept. Fifty µl of the serum was used to measure the Fgf23 levels using the FGF-23 ELISA kit (KAINOS LABORATORIES, Japan) and following the manufacturer's recommendations.

II. 19-Surgical procedure

We adopted a stabilized fracture-repair model by using a miniature Ilizarof apparatus (Fig. 41) originally developed by the Helms group (Le et al., 2001). All surgical protocols were approved by the McGill committee on animal research. Twelve-16 week-old Cyp24a1-null mice [previously engineered in our lab (St-Arnaud et al., 2000)] and control littermates received a subcutaneous injection of 0.1 ml buprenorphine (1 mg/kg) (Sigma) and kept under isofluorane the whole length of the surgery. After shaving, the proximal and distal metaphyses of the left tibia were transfixed using four 0.25 mm insect pins, which were oriented perpendicular to the long axis of the tibia and to each other (Fig. 41). The first ring was positioned above the proximal pins and then secured to these pins by means of four hexagonal nuts. Next, three threaded rods were placed through the ring and tightened into place using hexagonal nuts. The second ring was positioned below the distal pins (~ 11mm away from the first ring) and secured to the threaded rods and insect pins using hexagonal nuts. An incision was then made in the

middle of the diaphyses to clear away the soft tissues and make the bone visible. Once the bone was visible, a hole was drilled using the insect pins on top of which a n# 11 surgical scalpel (Fisher Scientific) was used to entirely cut the remaining bone resulting in an osteotomy.

The rings were custom designed in a machine shop (Paolo Alto, CA) and the remaining parts were purchased from Fine Science tools Inc. (Fine Science Tools Inc., Foster city, CA).

It is important to acknowledge Dr. Jill Helms for providing us with the proper training and initial materials for this fracture stabilization technique.

After surgery (average time of 40 min), the mouse cage was placed on a heated pad where the mice were allowed to ambulate freely. The following day, the mice received another injection of buprenorphine and were checked for any signs of tissue necrosis or major swelling.

II. 20-Sample callus collections

Blood was collected through a cardiac puncture, and the mice were then euthanised by cervical dislocation at 8, 14, or 21 days post-fracture. The blood was incubated for at least 30 minutes at RT, then microcentrifuged at 6,000 g for 6 minutes. The plasma supernatant was collected and stored at -20°C. The calluses were collected and either used for MMA embedding or RNA extraction. In the case of MMA embedding and subsequent histological preparation, the sample callus was carefully dissected out to avoid any disruption of the fracture. Goldner-Trichrome staining was

performed on 5 μm sections of the hardened callus block and the BioQuant Osteo II imaging software was used for histomorphometric analysis. In the case of RNA extraction, the collected callus was freezed with liquid nitrogen before being crushed using a mortar and pestle and further homogenized by the polytron. The TRIzol reagent was used in the RNA extractions as described before.

II. 21-Serum biochemistry & RadioImmunoAssays (RIA)

Serum biochemistry of inorganic calcium and phosphorus was done at the McGill Animal Resources Centre. The levels of serum 1α,25-$(OH)_2D$ was measured using the iDS Gamma-B 1,25-Dihydroxy Vitamin D RIA kit (ImmunoDiagnostic Systems Inc., Fountain Hills, AZ) following exactly the manufacturer's instructions.

II. 22-Rescue experiments

Rescue experiments were done as follows: After surgery and the infliction of an osteotomy, the mice were subcutaneously injected with a 50 μl volume of 24R,25-$(OH)_2D_3$, 1α,25-$(OH)_2D_3$, or propylene glycol (Fisher Scientific) as the vehicle for 14 or 21 days. Propylene glycol and 24R,25-$(OH)_2D_3$ (6.7 μg/kg diluted in vehicle) were injected daily, while 1α,25-$(OH)_2D_3$ (67 ng/kg diluted in vehicle) was injected on alternate days to avoid hypercalcemia. The absolute doses of the supplemeted metabolites were an average of the doses used in Yamate *et al.'s* study with

hypophosphatemic mice (Yamate et al., 1994). The calluses were collected at the end of the treatment and processed for either histology (where histomorphometric analysis was done) or RNA extraction (where RT-qPCR of several markers was done).

II. 23-Serum quantitation of 25-$(OH)D_3$ and 24R,25$(OH)_2D_3$

Mice undergoing a rescue regimen (described in previous section) were sacrified 14 days after the infliction of the osteotomy. Blood was collected and serum levels of 25-$(OH)D_3$ were measured using the DiaSorin 25-Hydroxyvitamin D ^{125}I RIA Kit (DiaSorin, Stillwater, MN) following the manufacturer's instruction. The assay consistsed of a two-step procedure. The first step involves a rapid extraction of 25-$(OH)D_3$ and other hydroxylated metabolites from serum with acetonitrile. Following extraction, the treated sample is then assayed using an equilibrium RIA procedure. The RIA method is based on an antibody with specificity to 25-$(OH)D_3$. The sample, antibody and tracer are incubated for 90 minutes at 20-25°C. Phase separation is accomplished after a 20 minute incubation at 20-25°C with a second antibody precipitating complex. A NSB/Addition buffer is added after this incubation prior to centrifugation to aid in reducing non-specific binding.

The 25-$(OH)D_3$ antibody included in the DiaSorin kit has 100% cross reactivity with 24R,25$(OH)_2D_3$. This fact enabled us to measure the 24R,25$(OH)_2D_3$ levels after separating the monohydroxylated vitamin D compounds from the dihydroxylated ones.

II. 24-Statistics

Results are expressed as the mean ± SEM.. To assess the effect of genotype or treatment, data were compared by using the two-tailed student T-test or the one-way ANOVA using Graphpad Prism 4 software. $P<0.05$ was considered signififcant. The number of replicates (n) was the following: Fig.12 (A. n=15 Cre+, n=7 Cre- B. n=14 Control, n=9 Cyp27b1$^{-/CH\Delta}$), Fig. 13 (n=8 for both genotypes), Fig.14 (n=5 for both genotypes), Fig.15 (B. n=8 for both genotypes), Fig.16 (n=7 for both genotypes), Fig.17 (n=7 for both genotypes), Fig. 18 (A. n=8 for both genotypes B. n=7 for both genotypes) Fig.19 (n=3 Control, n=6 Cyp27b1$^{-/CH\Delta}$), Fig.20 (n=8 for both genotypes), Fig.21 (n=14 Control, n=9 Cyp27b1$^{-/CH\Delta}$), Fig.23 (n=14 Control, n=9 Cyp27b1$^{-/CH\Delta}$), Fig.23 (n=14 Control, n=9 Cyp27b1$^{-/CH\Delta}$), Fig.25 (n=9 for both genotypes), Fig.26 (n=7 for both genotypes), Fig.30 (n=9 for both genotypes), Fig.31 (n=7 wt, n=4 tg), Fig.32 (n=4 for both genotypes), Fig.33 (n=7 for both genotypes), Fig.34 (n=9 for both genotypes), Fig.35 (n=9 for both genotypes), Fig.36 (n=5 wt, n=10 tg), Fig.37 (n=9 wt, n=8 tg), Fig.38 (n=9 wt, n=8 tg), Fig.39 (n=6 contralateral, n=7 fracture), Fig.41 (n=17 wt, n=14 Cyp24a1$^{-/-}$), Fig.44 (A. n=17 for both genotypes B. n=23 for both genotypes C. n=20 wt, n=13 Cyp24a1$^{-/-}$), Fig.46 (A. n=7 wt, n=5 Cyp24a1$^{-/-}$ B. n=5 for both genotypes), Fig.50 (A. n=5 wt vehicle, n=3 Cyp24a1$^{-/-}$ vehicle, n=3 wt 1,25, n=4 Cyp24a1$^{-/-}$ 1,25, n=5 wt 24,25, n=6 Cyp24a1$^{-/-}$ 24,25 B. n=3 across all genotypes and treatments), Fig.51 (n>5 for all panels), Fig.54 (n=3 for all treatments and genotypes), Fig.55 (n>5 for all panels), Fig.56 (A. n=6 wt, n=4 Cyp24a1$^{-/-}$ B. n=7 wt, n=6 Cyp24a1$^{-/-}$).

III. Results

The results of this section were submitted for peer-review and publication to the journal *Endocrinology* (see Foreword & Appendix A).

First part. Role of Locally synthesized 1α,25-$(OH)_2D$ in chondrocyte development and function

III. 1-Generation of the tissue-specific loss-of-function model of Cyp27b1

The developing growth plate is an avascular structure where access to molecules from the circulation is restricted. The purpose of this study was to inactivate Cyp27b1 in the chondrocytes and to determine the putative role for locally produced $1\alpha,25\text{-}(OH)_2D$ in these cells and in the growth plate. To achieve this, a mating strategy was adopted to give rise to a strain of mice where 25% have one Cyp27b1 null allele, one floxed Cyp27b1 allele, and transgenic for Cre recombinase under the control of collagen α_1(II) promoter. The resulting mice that will be referred to as Cyp27b1$^{-/CH\Delta}$, thus have inactive Cyp27b1 in chondrocytes but have a floxed functional allele in all other tissues. The presence of Cre recombinase was assessed at the DNA level by PCR (data not shown) that showed an absence of a band in the case of wild-type mice. Cre expression was assessed and at the RNA level by RT-qPCR performed on RNA extracted from two-day-old rib chondrocytes that showed no Cre mRNA expression in the case of non-transgenic mice (Fig. 12 A). The efficiency of chondrocyte-specific Cyp27b1 inactivation was also assessed at both the DNA and RNA levels. Correct excision of the floxed Cyp27b1 exon was demonstrated by both Southern Blot analysis and PCR of tail-extracted DNA from 15-day-old Cyp27b1$^{-/CH\Delta}$ mice (data not shown), which was not observed in control mice. Analysis of Cyp27b1 mRNA was done by RT-qPCR on RNA extracted form two-day-old rib chondrocytes that showed a significant reduction in Cyp27b1 levels in Cyp27b1$^{-/CH\Delta}$ mice as compared to controls (Fig. 12 B). This Cyp27b1 mRNA expression was not brought down to zero in Cyp27b1$^{-/CH\Delta}$ mice most probably due to incomplete penetrance of the Col2-Cre-mediated excision or contamination from

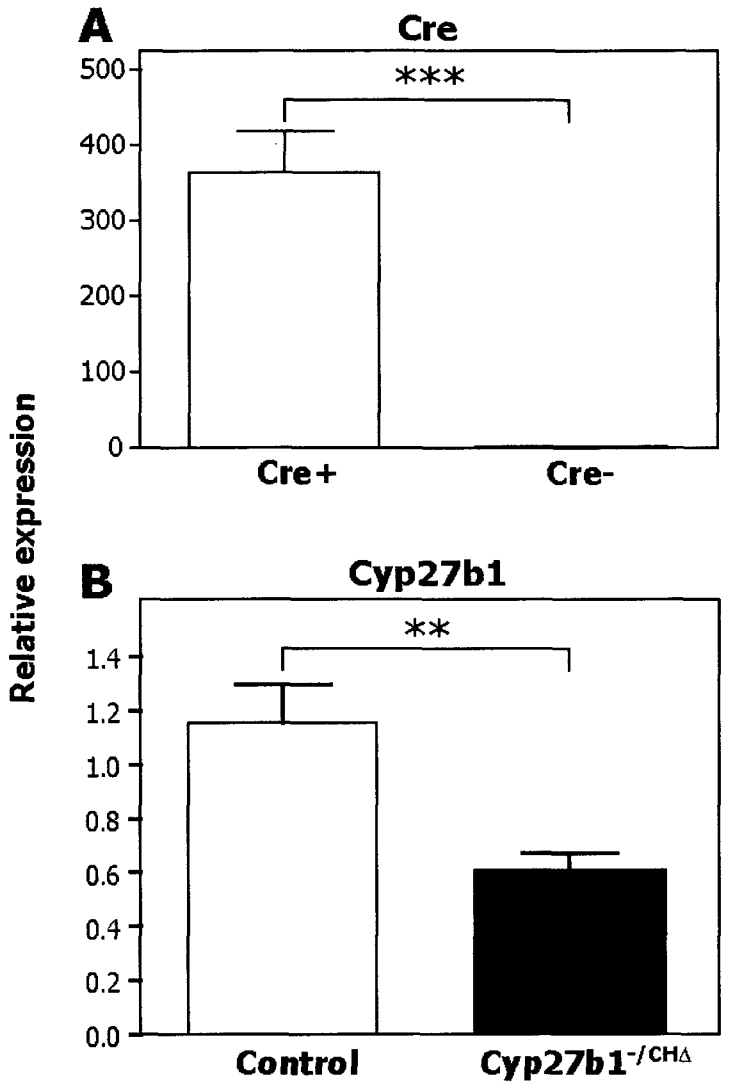

Figure 12 Expression of the Cre recombinase and of Cyp27b1 in control and Cyp27b1$^{-/CH\Delta}$ mice.

RT-qPCR on RNA extracted from two-day-old rib cartilage showing CRE expression only in mice with the CRE allele (**A**) and a decreased expression of Cyp27b1 in Cyp27b1$^{-/CH\Delta}$ as compared to controls (**B**). *p<0.05, *** p<0.001.

Cyp27b1$^{-/CH\Delta}$, chondrocyte-specific cyp27b1 knockdown mice; Cre, bacteriophage P1 Cre recombinase.

Cyp27b1 expressing osteoblasts (residing in the sternum and in the bony part of the ribs) dissected out along with the cartilaginous section of the ribs.

III. 2-Reduced Cyp27b1 levels affected chondrocyte development and endochondral ossification at embryonic and early neonatal time-points

In order to examine the effect(s) of reduced Cyp27b1 and presumably reduced 1α,25-$(OH)_2D$ on chondroctyte development and growth plate parameters, the murine long bones were collected at different time-points and carefully examined by both histomorphometry and μCT. Measurement of the hypertrophic zone of H&E stained E15.5 tibiae showed a significant increase of this zone in $Cyp27b1^{-/CH\Delta}$ mice as compared to controls (Fig. 13). In order to try to explain the reason behind this observation, PCNA staining was done to assess the proliferation of the chondrocytes that turned out to be almost identical between $Cyp27b1^{-/CH\Delta}$ mice and controls (Fig. 14). This difference in the early growth plate did not persist at the neonatal stage (Fig. 15 A) as shown by an almost identical hypertrophic zone width in H&E stained two-day-old tibiae of $Cyp27b1^{-/CH\Delta}$ mice and controls (Fig. 15 B). On the other hand, the metaphyseal trabecular bone was increased at postnatal day 2. Microcomputed-tomography of the region encompassing the primary and secondary spongiosa of the femurs showed an increase in BV/TV %, trabecular thickness, trabecular number, and a decrease in trabecular separation in the $Cyp27b1^{-/CH\Delta}$ mice as compared to the controls (Fig. 16 A,B,C,D). This phenotype was transient as shown by an almost identical BV/TV %, trabecular thickness, trabecular number, and trabecular separation in the tibiae of

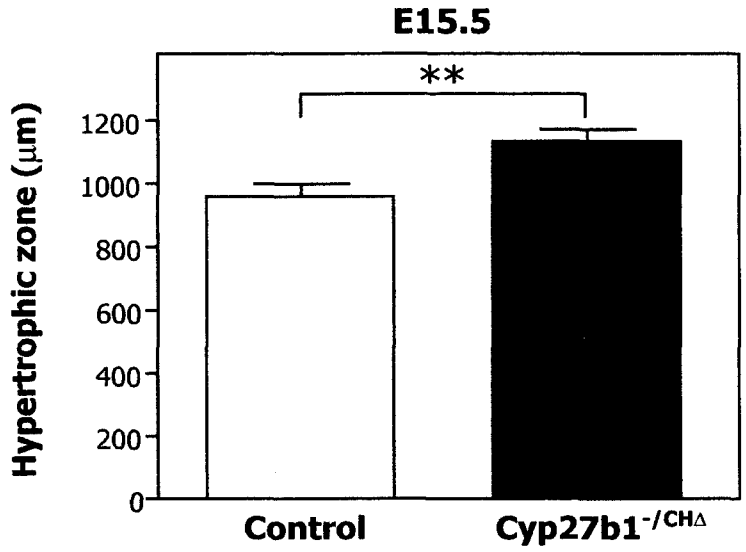

Figure 13 Chondrocyte-specific inactivation of Cyp27b1 affects hypertrophy.

Histomorphometric analysis of E15.5 tibiae showing a widened Hypertrophic zone in Cyp27b1$^{-/CH\Delta}$ mice as compared to controls. * $p<0.05$.

E15.5, Embryonic day 15.5.

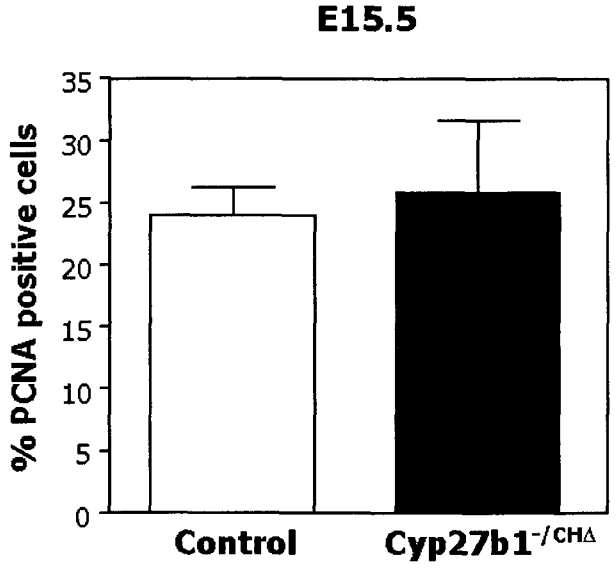

Figure 14 Inactivation of Cyp27b1 in chondrocytes does not affect proliferation.

Proliferating Cell Nuclear Antigen (PCNA) staining of E15.5 tibiae shows similar chondrocytic proliferation between $Cyp27b1^{-/CH\Delta}$ mice and their control littermates. Results are PCNA-positive cells expressed as percent of total cells in a fixed area across all samples.

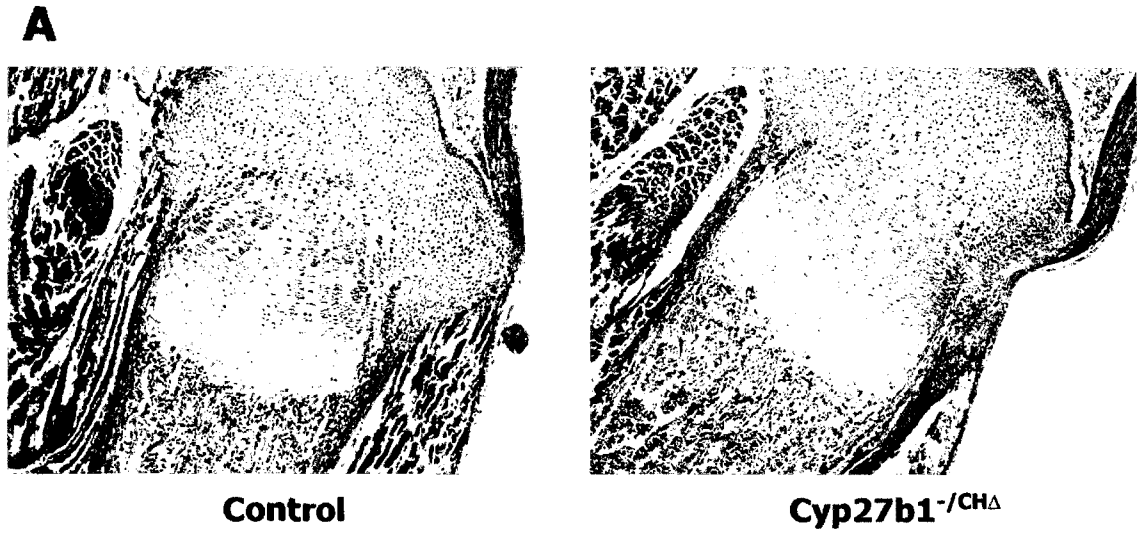

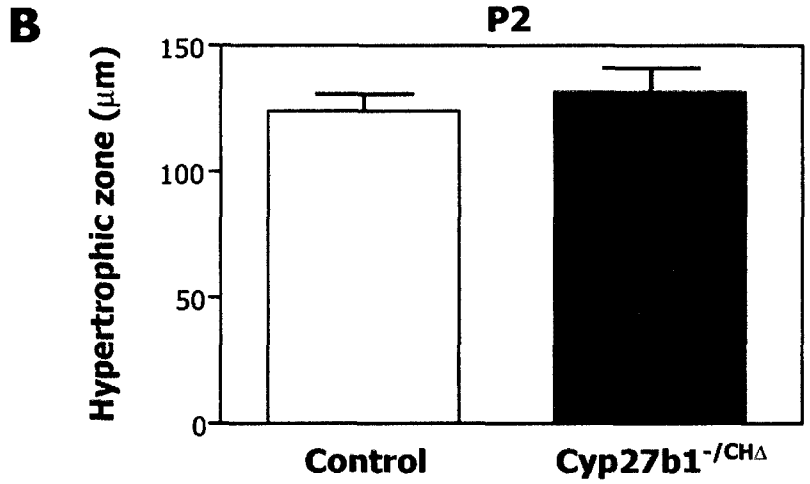

Figure 15 The changes induced by specific inactivation of Cyp27b1 in chondrocytes are transient.

Hematoxylin & Eosin staining of two-day-old femoral growth plates (**A**) showing no significant difference in the hypertrophic zone width between Cyp27b1$^{-/CH\Delta}$ and control mice when histomorphometric analysis was done (**B**).

P2, 2 days old.

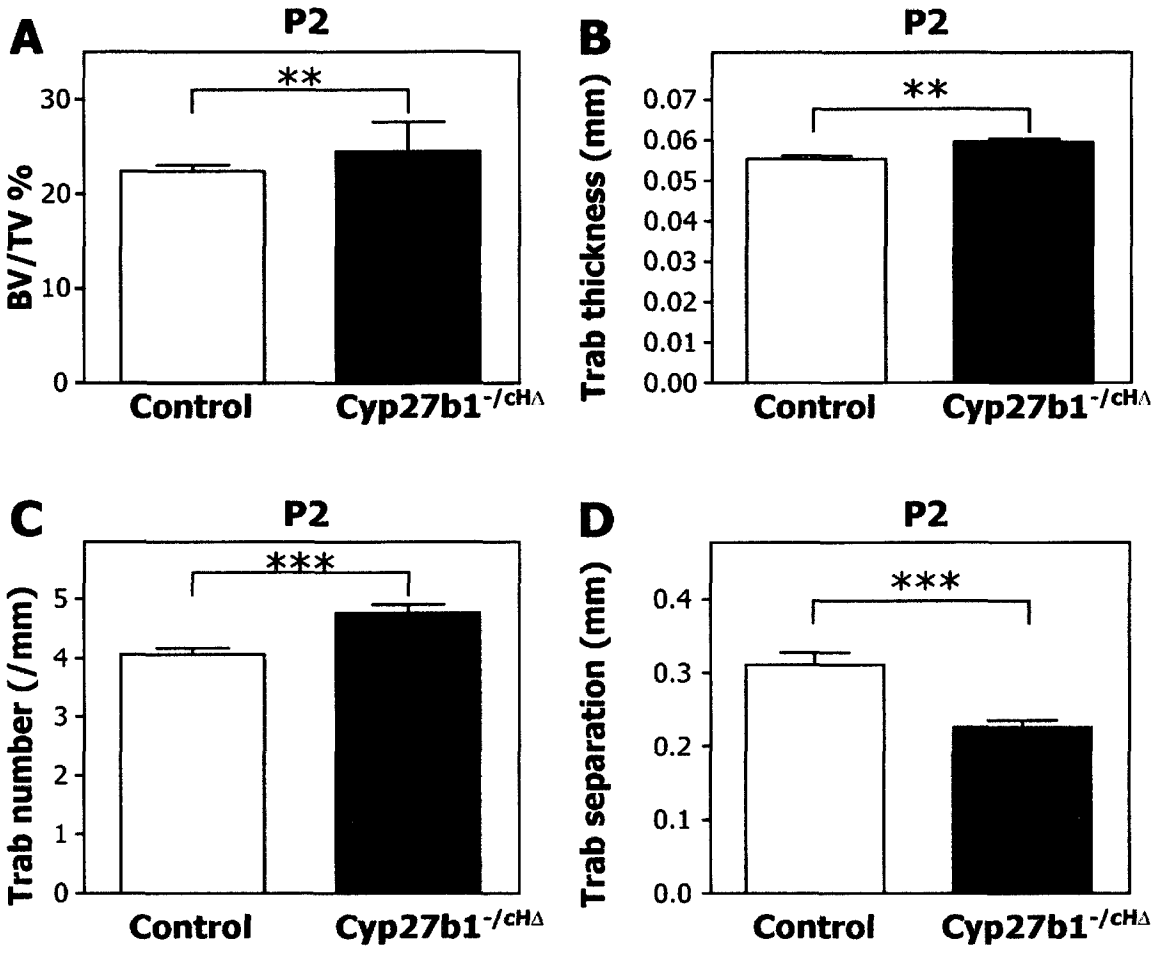

Figure 16 Chondrocyte-specific inactivation of Cyp27b1 leads to changes at the chondro-osseous junction.

Microcomputed-Tomography (μCT) of two-day-old femurs showing an increased BV/TV % (**A**), trabecular thickness (**B**), trabecular number (**C**) and a decreased trabecular separation (**D**) in Cyp27b1$^{-/cH\Delta}$ mice as compared to controls. **p<0.01, ***p<0.001.

BV/TV, Bone volume/Tissue volume; Trab, Trabecular; P2, postnatal day 2.

Cyp27b1$^{-/CH\Delta}$ mice and controls at 14 days of age (Fig. 17). Similarly, and at 42 days of age, histomorphometric measurements of the growth plate showed no difference in the growth plate width or the BV/TV % between Cyp27b1$^{-/CH\Delta}$ mice and controls (Fig. 18 A,B).

III. 3-Decreased Osteoclast recruitment in Cyp27b1$^{-/CH\Delta}$ mutant mice at embryonic and early neonatal time-points

Masuyama *et al.* (Masuyama et al., 2006) observed an increased bone mass phenotype in the chondrocytic VDR loss-of-function model, which they attributed to a decrease in osteoclast recruitment at the chondro-osseous junction at two days of age. This was also observed in the E15.5 cartilaginous anlagen. We used TRAP staining in order to detect activated osteoclasts, which were reduced at the E15.5 femoral ossification center in Cyp27b1$^{-/CH\Delta}$ mice as compared to controls (Fig. 19 A,B). TRAP staining was also performed on two-day-old femurs, where we observed a reduced number of osteoclasts bordering the last row of hypertrophic chondrocytes at the chondro-osseous junction in Cyp27b1$^{-/CH\Delta}$ mice as compared to controls (Fig. 20).

III. 4-Reduced/delayed vascularization in neonatal Cyp27b1$^{-/CH\Delta}$ mice

The ribcage contains a specialized growth plate that can be clearly and carefully dissected out to give a sample tissue almost entirely composed of chondrocytic cells. This was performed and RNA was extracted from that tissue for use in RT-qPCR

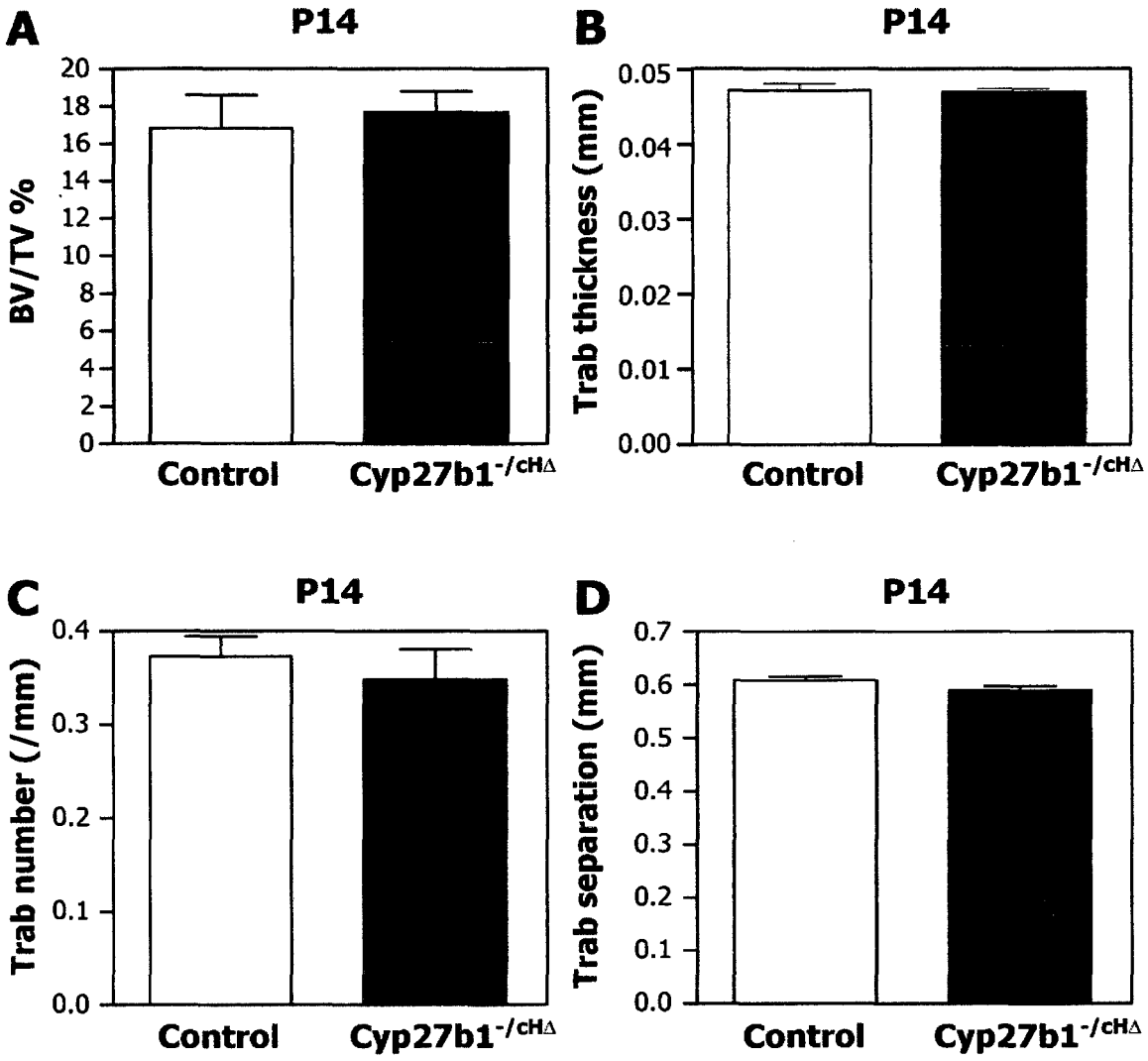

Figure 17 Normalization of histomorphometric parameters at postnatal day 14.

µCT of 14-day-old femurs showing no significant difference in BV/TV % (**A**), trabecular thickness (**B**), trabecular number (**C**), and trabecular separation (**D**) between Cyp27b1$^{-/CH\Delta}$ mice and their control littermates.

P14, postnatal day 14.

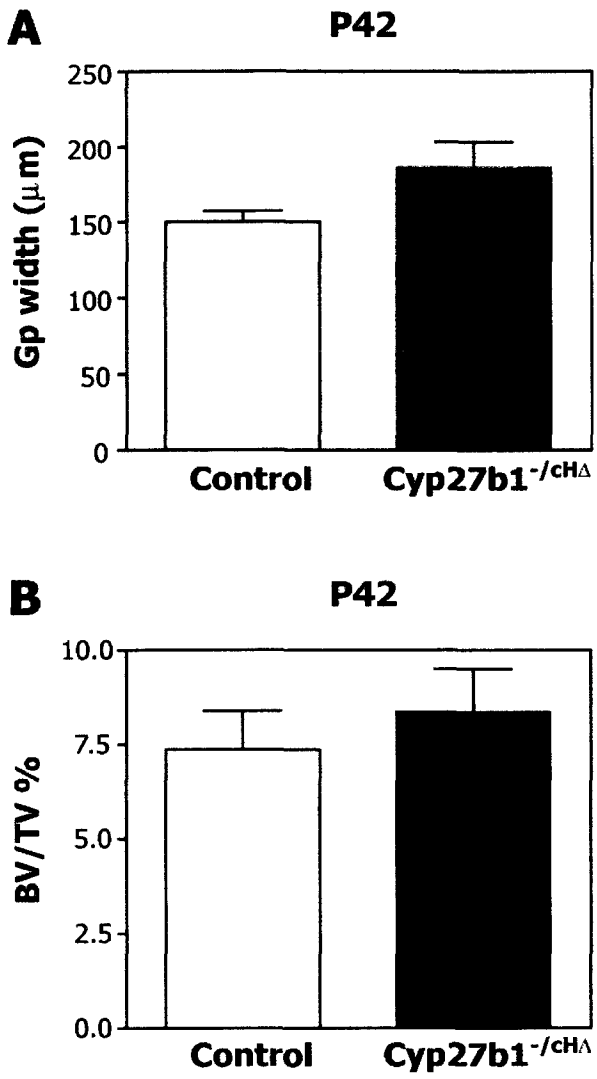

Figure 18 Chondrocyte-specific inactivation of Cyp27b1 does not affect growth plate function in young adults.

Histomorphometric analysis of 42-day-old tibial growth plates showing no significant change in growth plate width (**A**) and Bone volume/Tissue volume (**B**) between Cyp27b1$^{-/CH\Delta}$ mice and their control littermates.

Gp, Growth plate; P42, postnatal day 42.

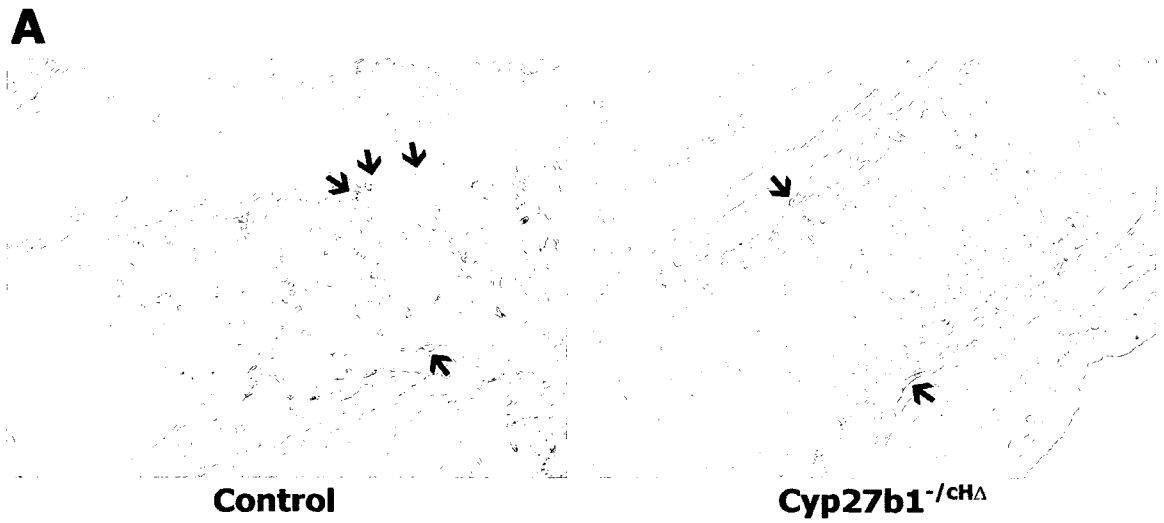

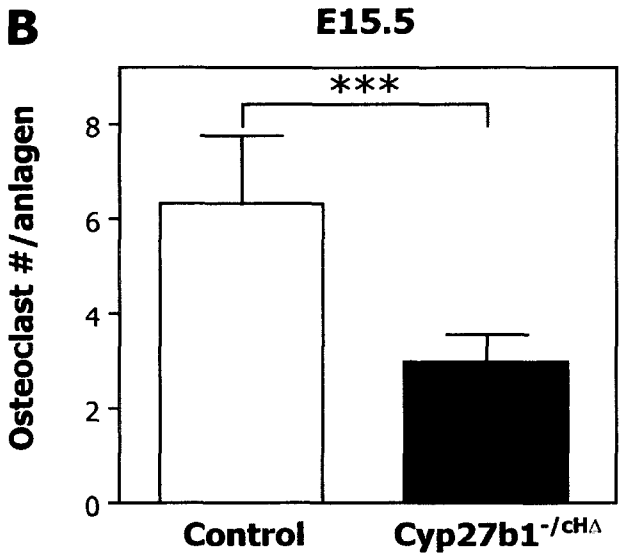

Figure 19 Tissue-specific ablation of Cyp27b1 in chondrocytes reduced embryonic osteoclastogenesis.

Tartrate Resistant Acid Phosphatase (TRAP) staining of E15.5 tibiae (**A**) showing a reduced number of osteoclasts at the primary ossification center in Cyp27b1$^{-/cH\Delta}$ mice as compared to controls (**B**). * $p<0.05$.

Oc, Osteoclast. Arrows are pointing at activated osteoclasts.

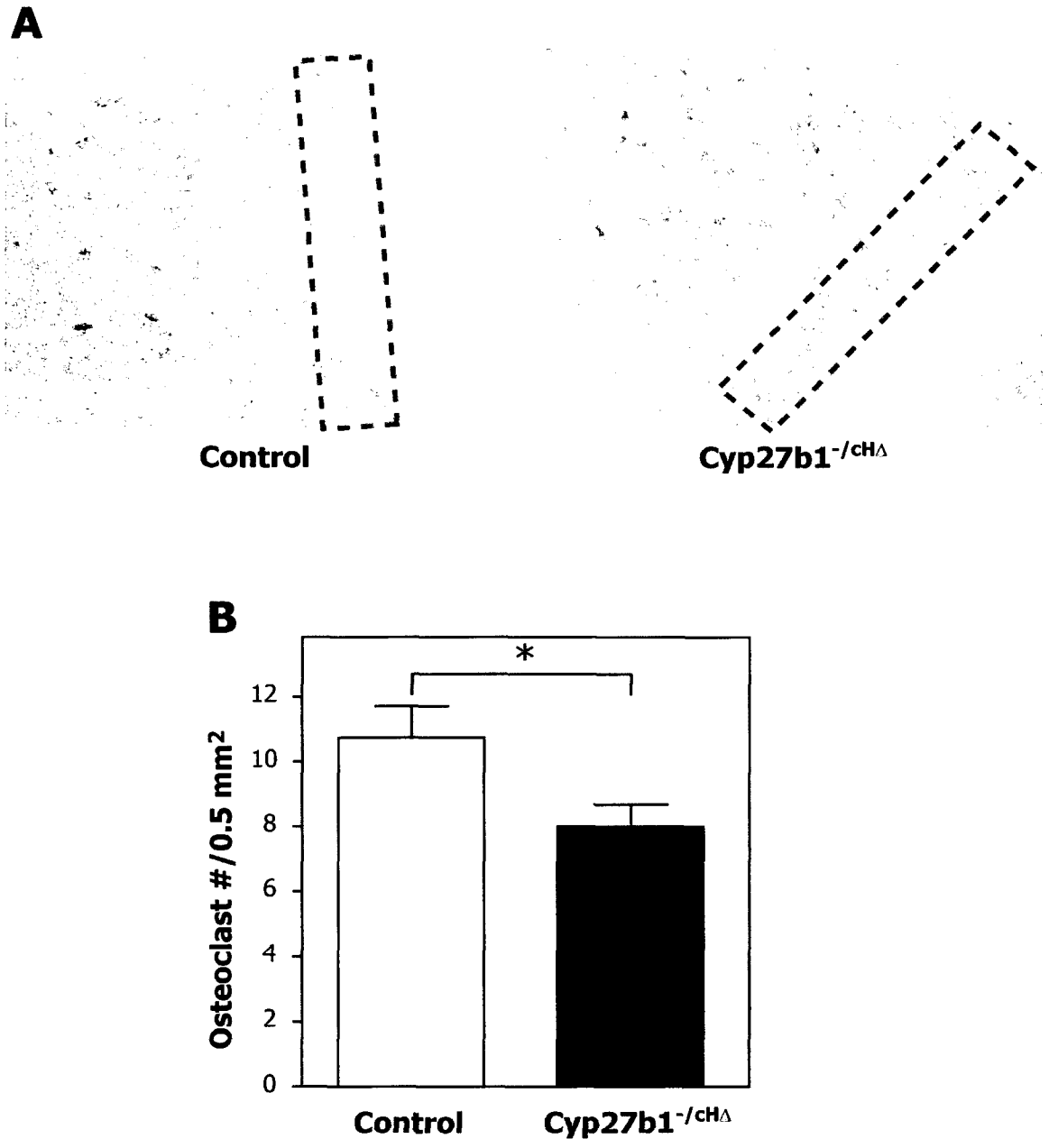

Figure 20 Reduced osteoclastogenesis at the chondro-osseous junction following specific inactivation of Cyp27b1 in chondrocytes.
TRAP staining of 2-day-old tibiae (**A**) showing a reduced number of osteoclasts (inside rectangle) near the last row of hypertrophic chondrocytes in Cyp27b1$^{-/cH\Delta}$ mice as compared to controls (**B**).

reactions. VEGF (a potent angiogenic molecule and a marker of chondrocyte differentiation) mRNA expression was found out to be reduced in Cyp27b1$^{-/CH\Delta}$ mice as compared to controls as well as its receptor (Kdr/VEGFR2). No change in Mmp13 (involved in angiogenesis and a marker of chondrocyte differentiation) (Tuckermann et al., 2000) expression was detected (Fig. 21 A,B,C). These differences in the angiogenic molecular markers prompted us to check the vascularization process using PECAM-1 immunostaining of two-day-old femurs. We observed a reduced staining in Cyp27b1$^{-/CH\Delta}$ mice as compared to controls (Fig. 22). PECAM-1, also known as CD31, is a marker of the endothelial cells forming the blood vessels and its reduction suggests a decrease in vascularization at the examined chondro-osseous junction.

III. 5-Decreased 1α,25-$(OH)_2$D perturbs neonatal chondrocyte differentiation

The difference in the zone of hypertrophic chondrocytes at E15.5 suggests a perturbation in chondrocyte differentiation secondary to a presumed lack of locally produced 1α,25-$(OH)_2$D. It is very difficult to isolate a chondrocyte-rich tissue at that time-point and examine what is happening at the molecular level. At postnatal day 2, chondrocytic markers were assayed by performing RT-qPCR on RNA extracted from rib chondrocytes. Ihh and Pthr1 (Pthr1 is the parathyroid hormone/parathyroid hormone related peptide receptor and is a marker of chondrocyte differentiation) mRNA expression was increased in Cyp27b1$^{-/CH\Delta}$ mice as compared to controls (Fig. 23 C,E). No difference in collagen α_1(II), collagen type X, and Hifα (Hif1α is a transcription

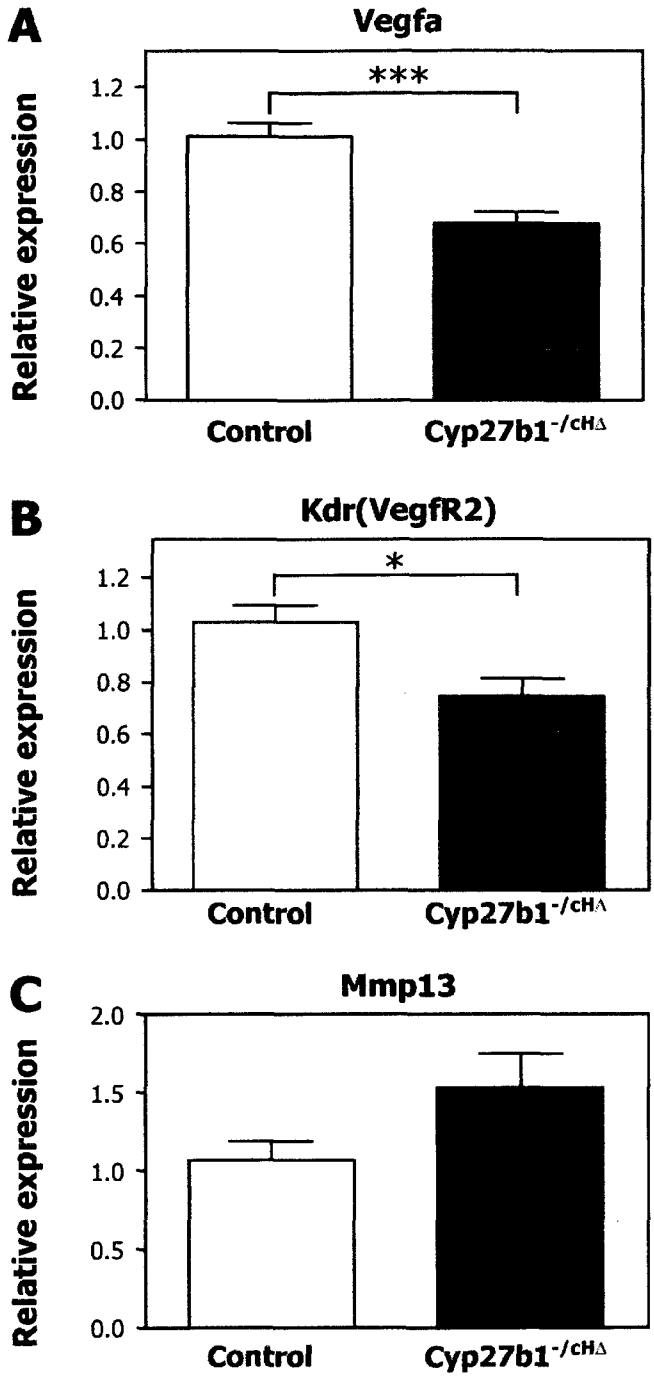

Figure 21 Impact of chondrocyte-specific inactivation of Cyp27b1 on the expression of angiogenic differentiation markers.

RT-qPCR on RNA extracted from 2-day-old rib cartilage showing a decreased expression of VEGF (**A**) and its receptor (**B**) in Cyp27b1$^{-/cH\Delta}$ mice as compared to controls with no significant difference in the case of Mmp13 expression (**C**). * $p<0.05$.

Vegfa, vascular endothelial growth factor a; Kdr/VegfR2, vascular endothelial growth factor receptor 2; Mmp13, matrix metallo-proteinase 13.

Control **Cyp27b1$^{-/cH\Delta}$**

Figure 22 Vascular invasion in control and Cyp27b1$^{-/cH\Delta}$ mice.
Platelet/endothelial cell adhesion molecule-1 (PECAM-1) immunostaining of two-day-old tibiae showing reduced growth plate vascular invasion in Cyp27b1$^{-/cH\Delta}$ mice as compared to controls.

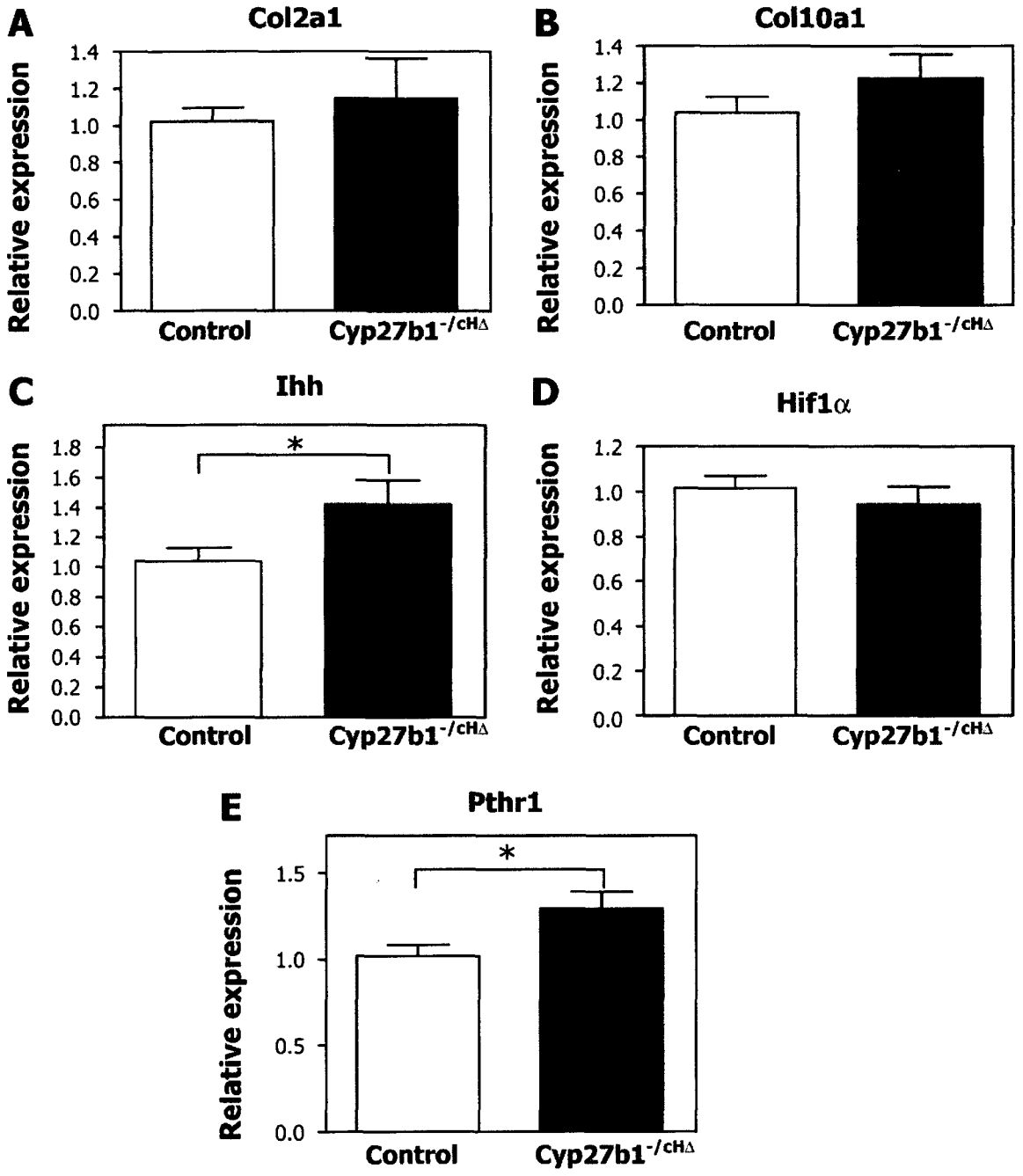

Figure 23 Expression of differentiation markers in control and Cyp27b1$^{-/cH\Delta}$ littermates.

RT-qPCR on RNA extracted from 2-day-old rib cartilage showing an increased expression of Ihh (**C**) and Pthr1 (**E**) in Cyp27b1$^{-/CH\Delta}$ mice as compared to controls with no significant difference in case of collagen type α_1(II) (**A**), collagen type X (**B**) and Hif1α (**D**) expression. * $p<0.05$.
Col2a1, collagen α_1(II); Col10a1, collagen type X; Ihh, indian hedgehog; Hif1α, hypoxia induced factor 1α; Pthr1, parathyroid hormone/parathyroid hormone related peptide receptor 1.

factor involved in hypoxia and is a marker of chondrocyte differentiation) (Schipani, 2006) expression levels (Fig. 23 A,B,D) was observed at this postnatal day 2. This perturbed chondrocyte differentiation did not persist beyond nenonatal time-points where both growth plate parameters (section. III. 2) and chondrocytic molecular markers did not change between Cyp27b1$^{-/CH\Delta}$ mice and controls at 14 or 42 days of age (data not shown).

Masuyama *et al.* (Masuyama et al., 2006) in the chondrocytic VDR loss-of-function model showed *in vivo* and *in vitro* that chondrocytes released RANKL influencing osteoclastogenesis at early stages of life. RANKL expression was assessed in two-day-old rib-cartilage using RT-qPCR. We did not measure any differences in the mRNA levels between Cyp27b1$^{-/CH\Delta}$ mice and controls (Fig. 24). Identical results were obtained using RNA extracted from nine-day-old epiphysial cartilage (Fig. 25 B), contrasting with the results reported by Masuyama *et al.*. That group also reported a reduction in Fgf23 (a phosphauric molecule that inhibits Npt2a expression) levels released from the osteoblasts due to the lack of VDR and consequently inactivity of the 1α,25-$(OH)_2$D. Fgf23 mRNA levels were not altered in epiphyseal cartilage from Cyp27b1$^{-/CH\Delta}$ mice and the reduction of VEGF expression was not reproducible in this tissue (Fig. 25 A,C).

The serum levels of Fgf23, however, were measured from 10-day-old mice and found to be significantly decreased in Cyp27b1$^{-/CH\Delta}$ mice as compared to controls (Fig. 26). Experiments are underway to measure the serum phosphate levels at the 10-day-old time-point.

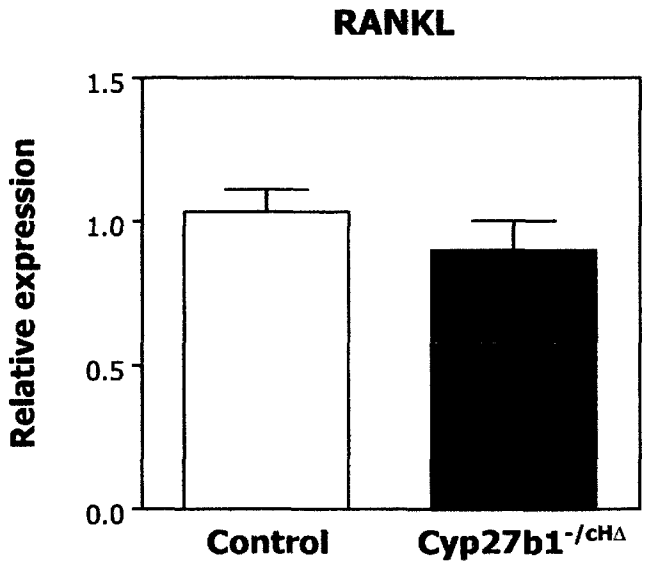

Figure 24 Chondrocyte-specific ablation of Cyp27b1$^{-/cH\Delta}$ does not affect RANKL expression.

RT-qPCR on RNA extracted from two-day-old rib cartilage showing no significant difference in RANKL expression between Cyp27b1$^{-/CH\Delta}$ mice and their control littermates.
RANKL, receptor activator of NF-KB ligand.

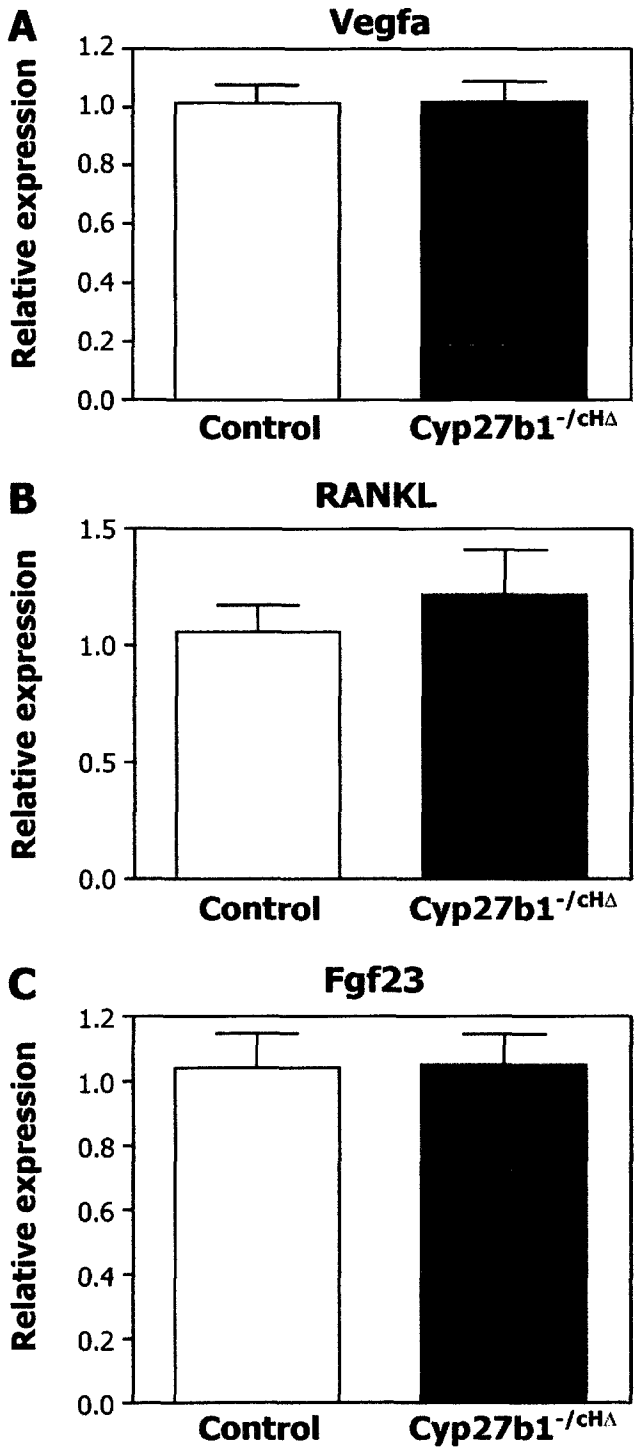

Figure 25 Marker gene espression in nine-day-old control and Cyp27b1$^{-/cH\Delta}$ littermates.

RT-qPCR on RNA extracted from nine-day-old tibial epiphyses showing no significant difference in VEGF (**A**), Fgf23 (**B**) and RANKL (**C**) expression between Cyp27b1$^{-/CH\Delta}$ mice and their control littermates.

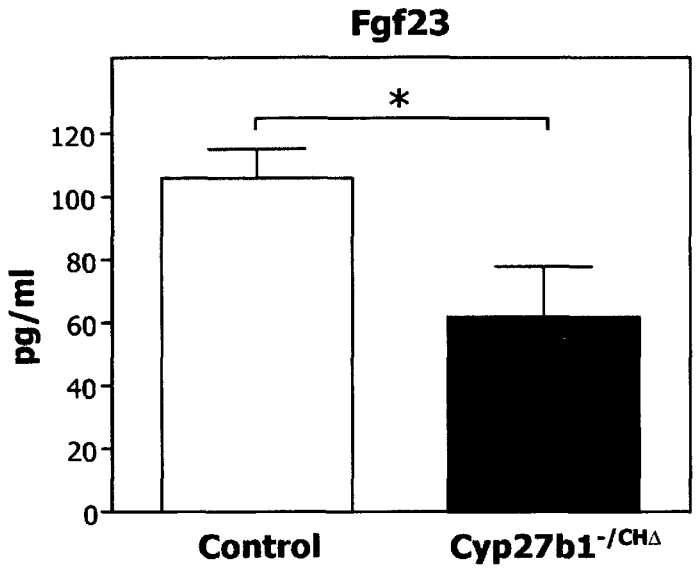

Figure 26 Fgf23 serum level is decreased in Cyp27b1$^{-/CH\Delta}$ mice as compared to controls.

Fgf23 ELISA performed on serum collected from 10-day-old Cyp27b1$^{-/CH\Delta}$ mice and controls showing a significant decrease in the case of Cyp27b1$^{-/CH\Delta}$ mice. *$p<0.05$.

III. 6-Engineering of a tissue-specific overexpression model of Cyp27b1

In order to validate the results obtained with the loss-of-function model of Cyp27b1, we engineered a recombinant molecule where the Cyp27b1 cDNA fused in frame with the FLAG epitope sequence at its 3'end was subcloned between a chimeric intron and a polyadenylation stop sequence under the control of the collagen α_1(II) promoter elements (Fig. 27). The expression of the transgenic recombinant molecule was first tested in transient transfections of the chondrocytic ATDC5 cell line (Shukunami et al., 1997). Anti-FLAG antibody was used as a primary antibody along with a secondary antibody conjugated to rhodamine to detect the *Cyp27b1* protein signal that was evident in cells transfected with the recombinant molecule. No signal was detected in cells transfected with the empty plasmid or untransfected cells (Fig. 28 A,B,C).

The transgene was then injected in fertilized eggs, which resulted in three transgenic mouse lines designated as 5Tg, 3Tg, and 1Tg (The strain 5tg was the highest expressor of *Cyp27b1* protein and will be the one referred to in this study). The molecule was successfully integrated in the mouse genome as shown by Southern Blot performed on 14-day-old tail-extracted genomic DNA where the recombinant molecule migrated as a band of 2 Kb in size (Fig. 29). The Cyp27b1 mRNA levels were quantified by RT-qPCR performed on RNA extracted from two-day-old rib-cartilage. The results showed more than a hundred fold increase in the transgenic mice as compared to the wild-type mice (Fig. 30 A). The recombinant *Cyp27b1* protein levels was detected by a Western Blot using anti-FLAG antibody on protein extracted from 14-day-old tail vertebral tissue where the collagen α_1(II) promoter is active. Both the 5Tg (highest expressor) and the

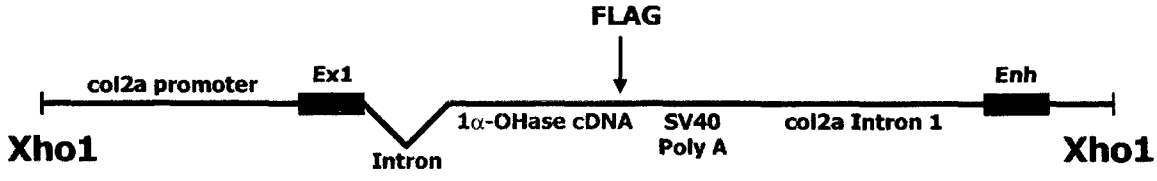

Figure 27 Cyp27b1 (1α-OHase) transgene.
1586 bp of 1α-OHase cDNA (excluding the 5'UTR sequences and fused in frame with a FLAG epitope at the 3'end) was subcloned downstream of a chimeric intron and upstream of an SV40 Poly A sequence. The resulting cDNA, chimeric intron, and the SV40 Poly A sequence were further subcloned downstream of the collagen α1(II) promoter (harboring exon 1) and upstream of the collagen α1(II) intron 1 (harboring the enhancer). The resulting molecule was linearized by Xho I (restriction enzyme) digestion prior to pronuclear injections.
Col2a, collagen α1(II); Ex1, Exon 1; SV40 Poly A, simian virus polyadenylation sequence; Enh, enhancer.

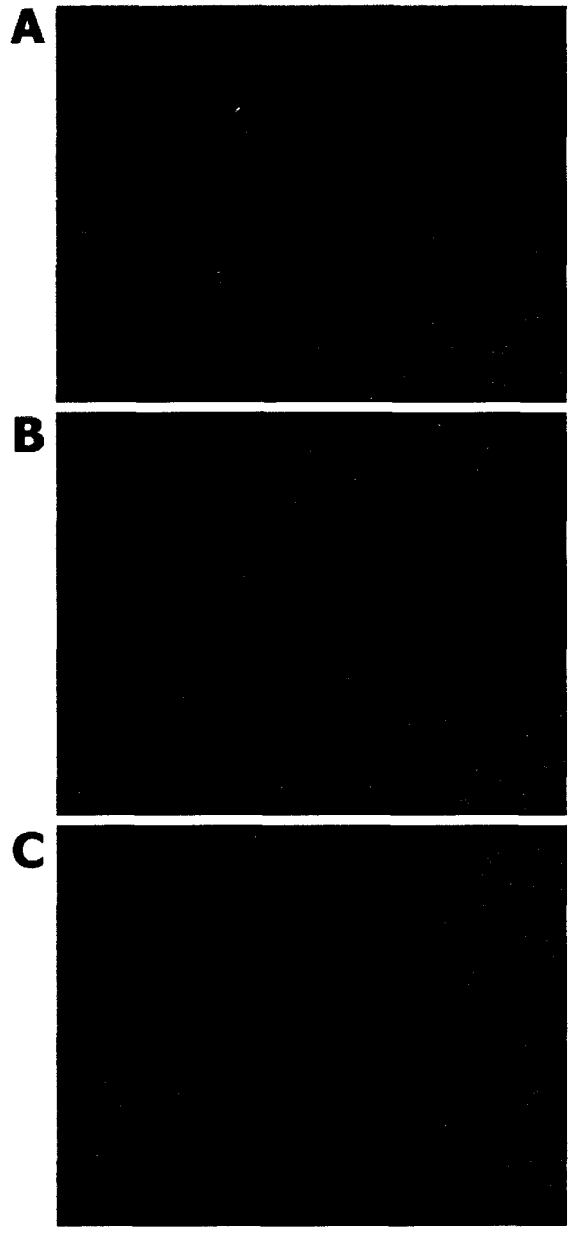

Figure 28 Test of Cyp27b1 transgene expression in ATDC5 chondrocytic cells.

Immunofluorescence using anti-FLAG and a rhodamine conjugated secondary antibody (red) showing the expression of the *Cyp27b1* recombinant molecule (**A**).

Figure 29 Identification of transgenic founders.
Southern Blot showing the migration of the recombinant Cyp27b1 (2 kb band) molecule in the transgenics where it was successfully incorporated.

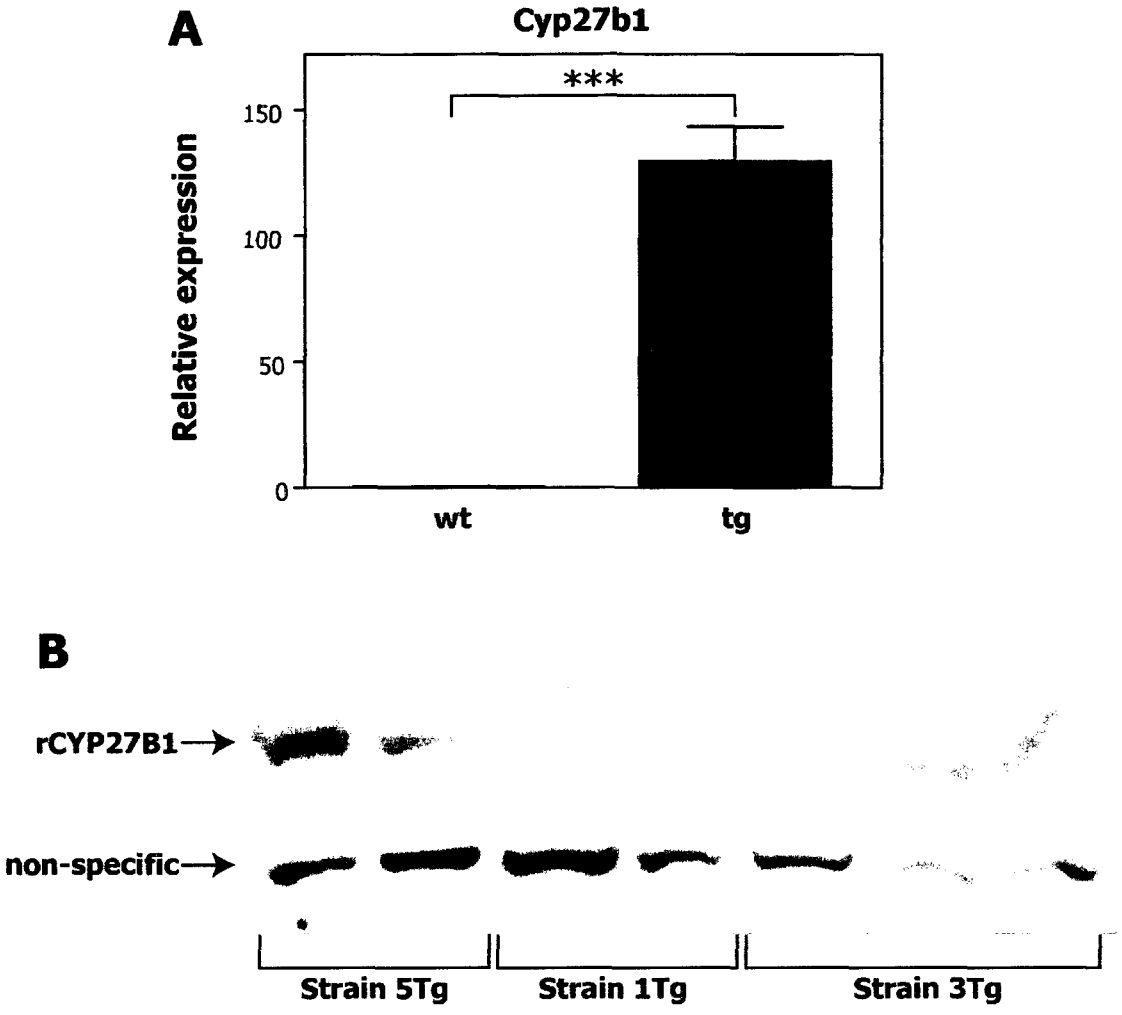

Figure 30 Cyp27b1 transgene expression.
(**A**) RT-qPCR on RNA extracted from 2-day-old rib cartilage showing the overexpression of the Cyp27b1 mRNA in the transgenic mice as compared to their wild-type littermates. (**B**) Western Blot showing the expression of the recombinant *Cyp27b1* protein (using anti-FLAG antibody), where it was highest in transgenic strain 5 Tg and nonexistant in strain 1 Tg. The lower band on the gel is non-specific and was used as a marker of equal loading.
wt, wild-type; rCYP27B1, recombinant *CYP27B1*; Tg/tg, transgenic.

3Tg strains expressed the protein with no expression evident in the case of the 1Tg strain (Fig. 30 B).

III. 7-Increased Cyp27b1 levels affected embryonic chondrocyte development.

In order to examine the effect(s) of increased Cyp27b1 levels and presumably increased local $1\alpha,25\text{-}(OH)_2D$ levels on the chondrocytes and growth plate, murine long bones were collected at different time-points and examined by both histomorphometry and μCT. Measurement of the hypertrophic zone of H&E stained E14.5 tibiae showed a reduction of this zone in transgenic mice as compared to wild-types (Fig. 31). This result is a mirror image of what we observed in the tissue-specific Cyp27b1 loss-of-function model. This reciprocal phenotype was also transient as the metaphyseal trabecular bone was not altered at postnatal day 2, where μCT of the primary and secondary spongiosa of the femurs showed no change in BV/TV % in the transgenic mice as compared to the wild-types (Fig. 32). At 42 days of age, the growth plate width was not changed in the transgenic mice as compared to the wild-types (Fig. 33).

No changes in the mRNA expression of VEGF, Kdr, and Mmp13 was measured between the transgenic and wild-type mice at postnatal day two (Fig. 34).

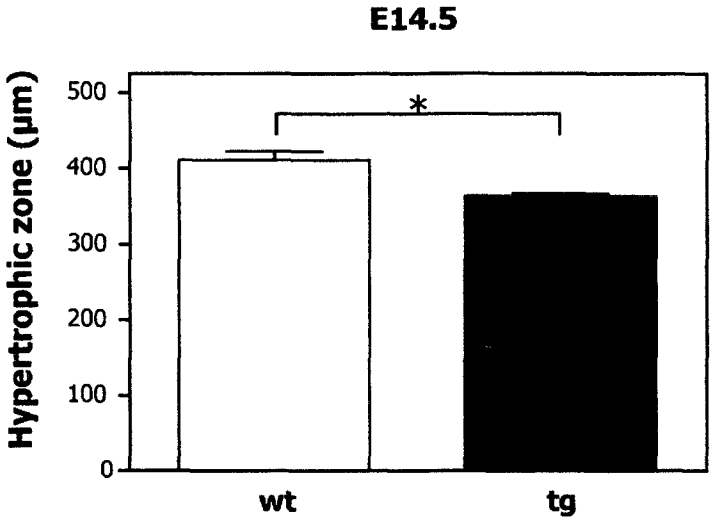

Figure 31 Chondrocyte-specific overexpression of Cyp27b1 affects hypertrophy.

Histomorphometric analysis of E14.5 tibiae showing a reduced Hypertrophic zone in transgenic mice as compared to wild types. *$p<0.05$.
tg, transgenic; wt, wild-type.

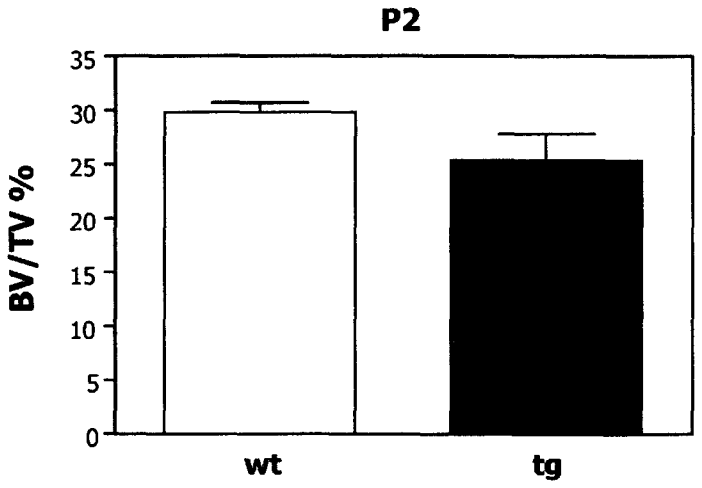

Figure 32 Chondrocyte-specific overexpression of Cyp27b1 leads to no changes at the chondro-osseus junction.
Microcomputed-tomography of two-day-old femurs showing no significant difference in BV/TV % between transgenic mice and their wild-type littermates.

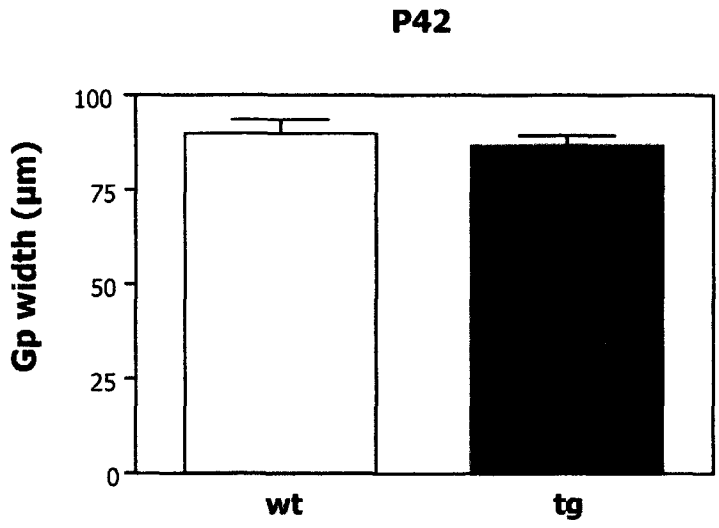

Figure 33 Chondrocyte-specific overexpression of Cyp27b1 does not affect growth plate function in young adults.
Histomorphometric analysis of 42-day-old tibial growth plates showing no significant change in growth plate width between the transgenic mice and their wild-type littermates.

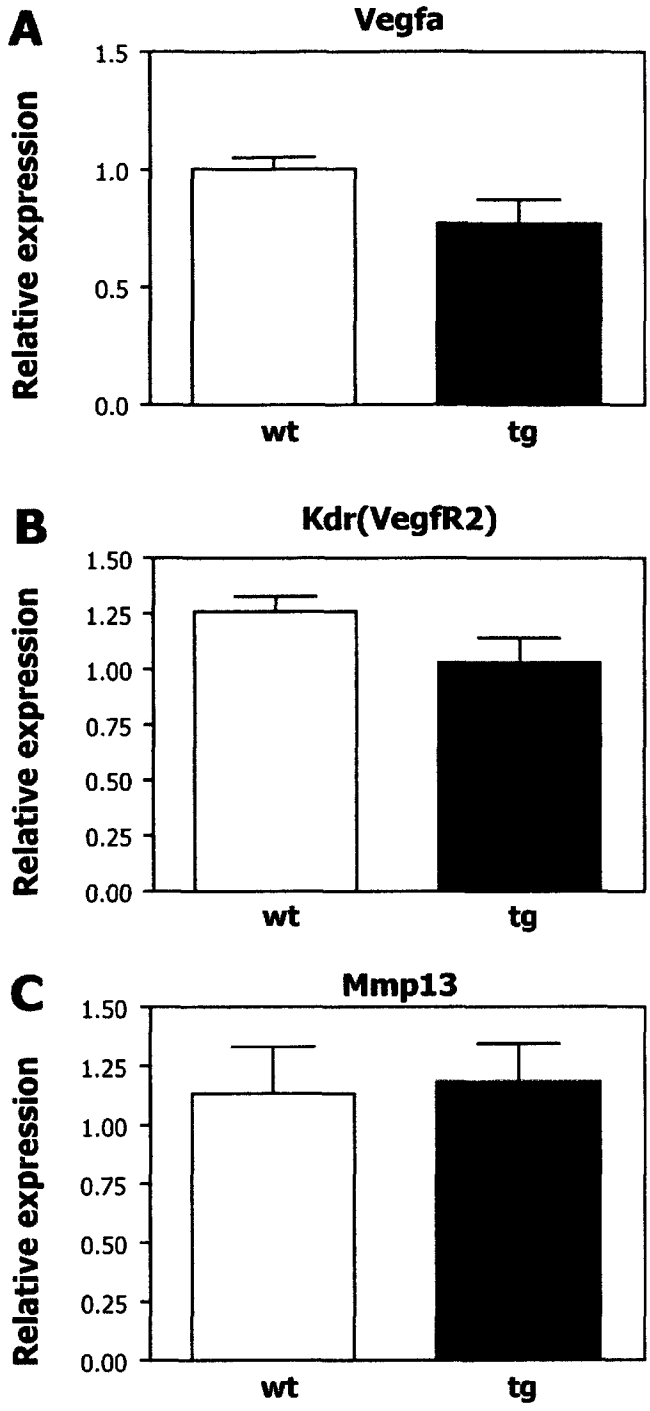

Figure 34 Impact of chondrocyte-specific inactivation of Cyp27b1 on the expression of differentiation markers.

RT-qPCR on RNA extracted from two-day-old rib cartilage showing no significant difference in VEGF (**A**), VEGFR2/Kdr (**B**), and Mmp13 (**C**) expression between the transgenic mice and their wild-type littermates.

III. 8-Increased Cyp27b1 perturbs neonatal chondrocyte differentiation

The difference in the zone of hypertrophic chondrocytes at E14.5 suggests a perturbation in chondrocyte differentiation due to a presumable increase in locally produced 1α,25-$(OH)_2$D. At postnatal day two, RT-qPCR was performed on RNA extracted from the rib-cartilage to examine expression of the same battery of chondrocytic markers used for the tissue-specific Cyp27b1 loss-of-function model. Ihh mRNA expression was decreased in transgenic mice as compared to wild-types (Fig. 35 C) giving a mirror image result to the tissue-specific Cyp27b1 loss-of-function model. Hif1α mRNA expression levels (Fig. 35 D) was also decreased in the transgenics as compared to the wild-types with no changes in collagen α_1(II), collagen type X, and Pthr1 expression (Fig. 35 A,B,E).

Similar to the lack-of-function model, the perturbed chondrocyte differentiation did not persist beyond nenonatal time-points where both growth plate parameters (section. III. 7) and chondrocytic molecular markers (data not shown) did not change between transgenic mice and wild-types at 14 or 42 days of age.

III. 9- 25-$(OH)D_3$ supplementation results in a metaphyseal bone phenotype in transgenic mice

One possible explanation for the absence of a mirror image change in metaphyseal bone mass in the overexpression model as compared to the loss-of-function model might be a limiting substrate availability for the overexpressed Cyp27b1

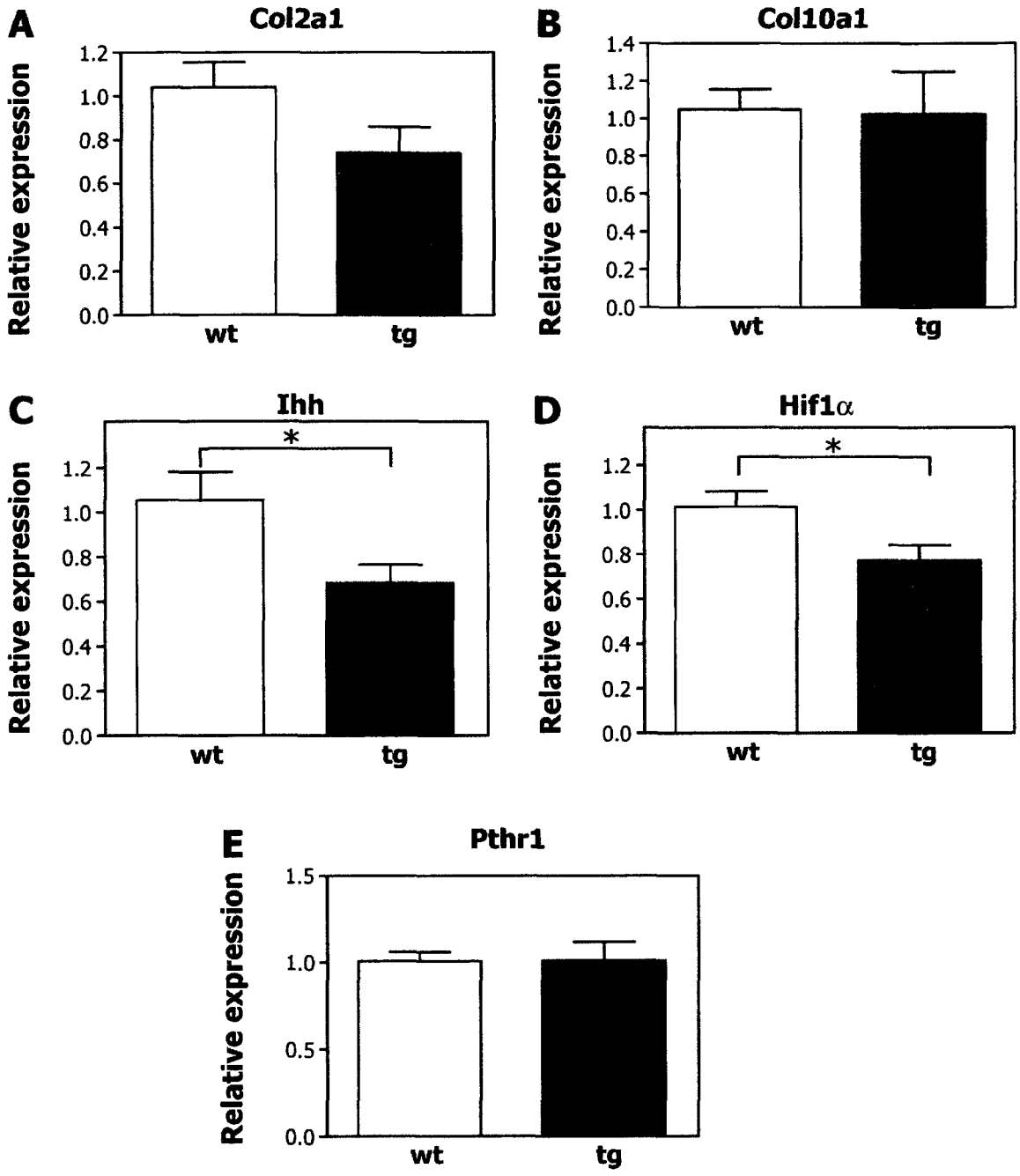

Figure 35 Expression of differentiation markers in wild-type and Cyp27b1 transgenic littermates.

RT-qPCR on RNA extracted from two-day-old rib cartilage showing a decreased expression of Ihh (**C**) and Hif1α (**D**) but no significant difference in the expression of collagen α_1(II) (**A**), collagen type X (**B**), and Pthr1 (**E**) between the transgenic mice and their wild-type littermates.

enzyme. In order to test this, 25-(OH)D_3, a metabolite that usually crosses the placenta (Haddad et al., 1971), was given to gestating females in order to boost Cyp27b1 substrate in the delivered offsprings. Microcomputed-tomography of the primary and secondary spongiosa of two-day-old femurs was done and revealed a decrease in BV/TV %, trabecular thickness, and trabecular number in the transgenic mice as compared to the wild-types (Fig. 36 A,B,C). This decrease in metaphyseal bone mass in the case of transgenics was a mirror image to what was observed in Cyp27b1$^{-/CH\Delta}$ mice. A change in the angiogenic markers was also expected to accompany this bone mass change, however, RT-qPCR performed on RNA extracted from the two-day-old rib-cartilage showed no difference in VEGF mRNA expression or its receptor (Fig. 37 A,B). In order to check if there was any change in osteoclastogenic markers, RANKL mRNA expression was also quantified and showed no difference between transgenic mice and wild-types (Fig. 38).

Taken together, our results suggest that 1α,25-$(OH)_2$D locally synthesized under the action of Cyp27b1 has a direct but non-essential role in the development of the growth plate.

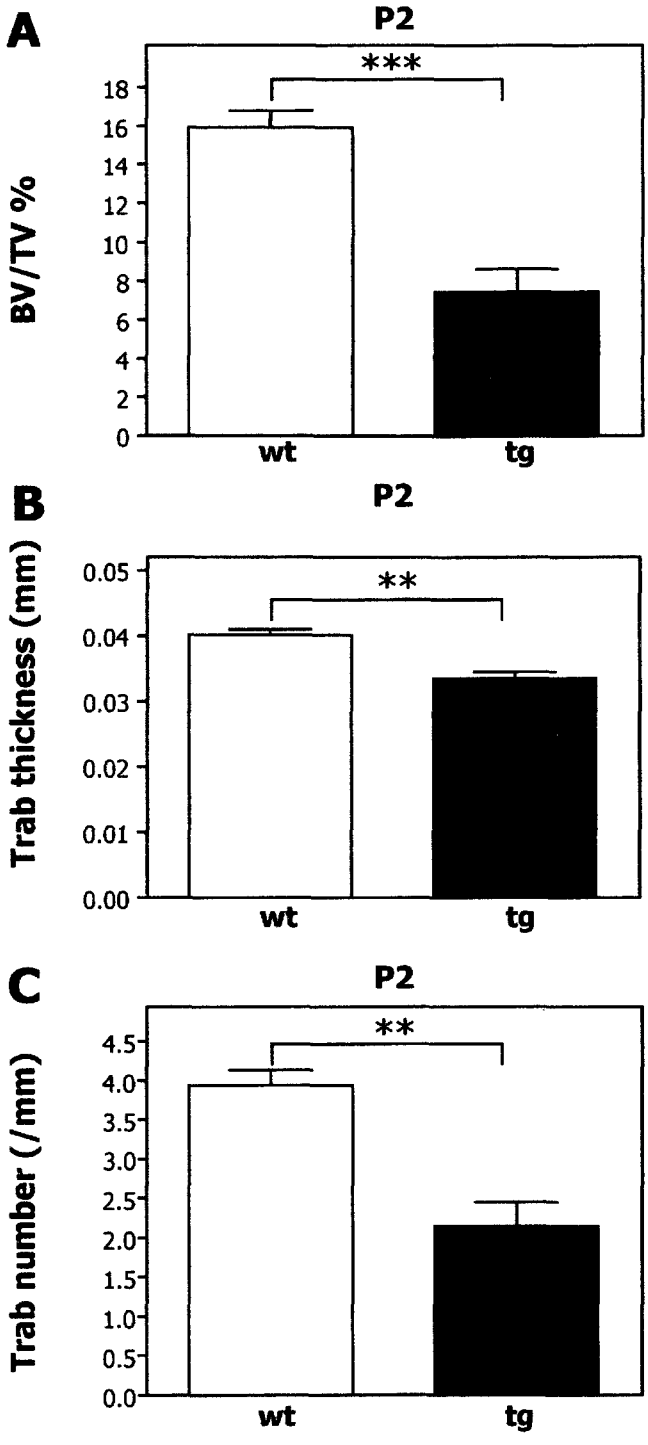

Figure 36 Chondrocyte-specific overexpression of Cyp27b1 leads to changes at the chondro-osseous junction in 25-(OH)D_3 supplemented mice.

Microcomputed-tomography of two-day-old femurs showing a decreased BV/TV % (**A**), trabecular thickness (**B**), and trabecular number (**C**) in transgenic mice as compared to wild-types (both genotypes were supplemented with 25-(OH)D_3 in this experiment). **p<0.01, ***p<0.001.

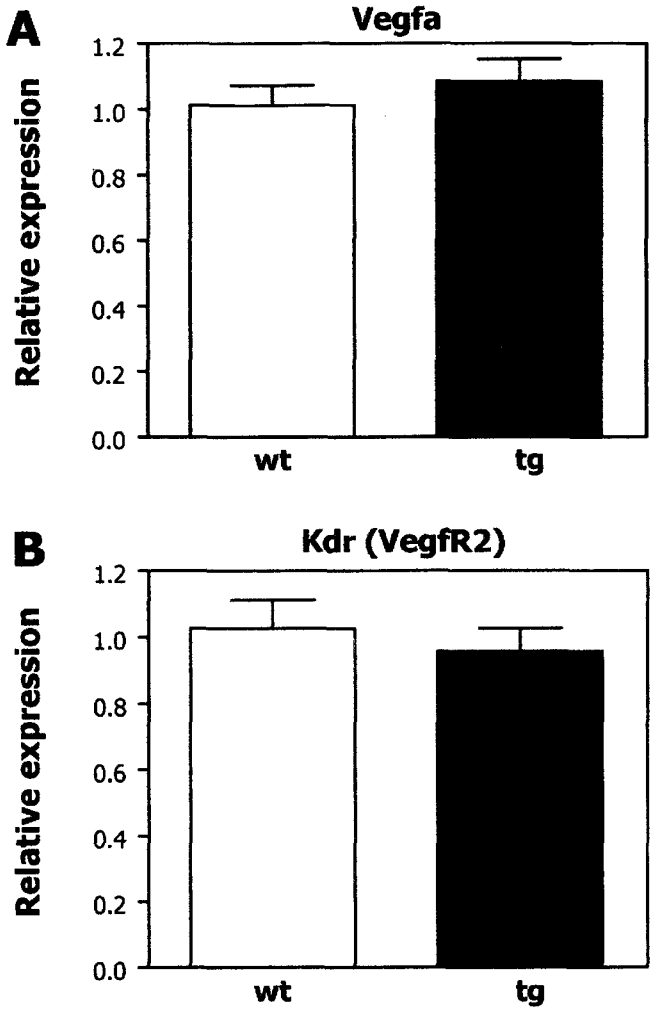

Figure 37 Angiogenic markers are not altered in Cyp27b1 transgenics supplemented with 25-(OH)D_3.

RT-qPCR on RNA extracted from two-day-old rib cartilage showing no significant difference in the expression of VEGF (**A**) and its receptor (**B**) between the transgenic mice and their wild-type littermates (both genotypes were supplemented with 25-(OH)D_3 in this experiment).

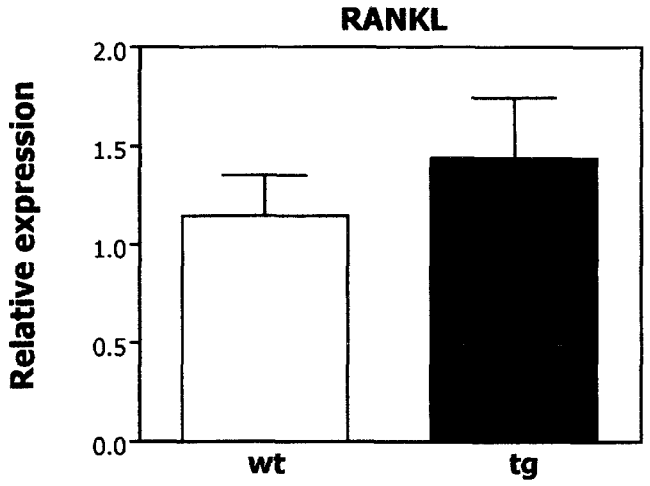

Figure 38 Chondrocyte-specific overexpression of Cyp27b1 does not affect RANKL expression.

RT-qPCR on RNA extracted from two-day-old rib cartilage showing no significant difference in the expression of RANKL between the transgenic mice and their wild-type littermates (both genotypes were supplemented with 25-(OH)D_3 in this experiment).

The results of this section are currently being prepared to be submitted as a manuscript with myself as first author.

Second part. Fracture repair in Cyp24a1-deficient mice

III. 10-Cyp24a1 mRNA expression is increased locally after the infliction of a fracture

The Cyp24a1 enzyme is involved in the catabolic breakdown of 1α,25-$(OH)_2$D but also synthesizes the 24R,25-$(OH)_2$D metabolite. Studies in chicken showed increases in serum levels of 24R,25-$(OH)_2$D and of the renal mRNA levels of CYP24A1 following fracture (Seo & Norman, 1997), suggesting a role for 24R,25-$(OH)_2$D in fracture repair. Using RT-qPCR on RNA extracted from the callus, we measured a significant increase in local expression of Cyp24a1 mRNA in the tibiae 14 days after being subjected to an osteotomy as compared to the unfractured contralateral tibiae (Fig. 39). We then used a Cyp24a1-deficient mouse strain to determine the putative role of 24-hydroxylated vitamin D metabolites during mammalian fracture repair.

III. 11-Generation of a Cyp24a1 knockout mouse-model

The Cyp24a1 gene was inactivated by eliminating the heme-binding domain sequences of exon 10 (Fig. 40). Animals homozygous for the Cyp24a1 mutation cannot effectively clear 1α,25-$(OH)_2$D from their circulation leading to perinatal lethality, most probably secondary to hypercalcemia. Fortunately, the perinatal lethality shows only partial penetrance suggesting that alternative pathways exist to degrade the elevated levels of 1α,25-$(OH)_2$D *in vivo*. The survival of some Cyp24a1 mutant mice ($Cyp24a1^{-/-}$) allowed the study to proceed. These animals had normal calcium and phosphate levels in their serum (Fig. 41), hence, we interpret that any phenotype observed would be due to

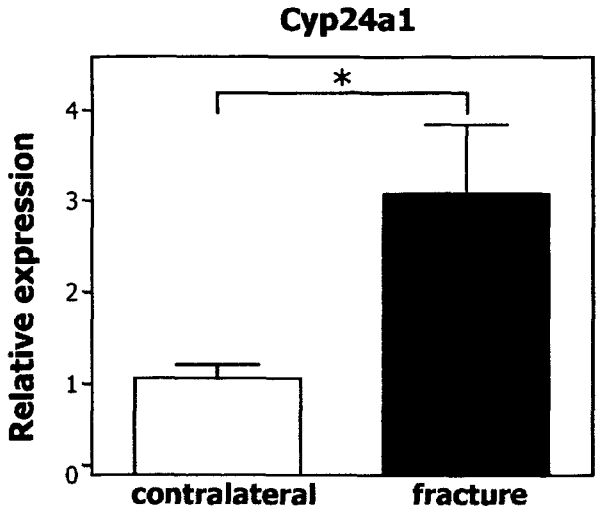

Figure 39 Cyp24a1 mRNA expression is increased after the introduction of an osteotomy.

RT-qPCR with Cyp24a1 TaqMan assay on RNA extracted from callus (fractured right tibia) and a diaphysial section of the bone (left nonfractured contralateral tibia) of wild type mice 14 days post-fracture. The expression of Cyp24a1 (24-hydroxylase) was siginificantly increased in the case of a fracture. *$p<0.05$.

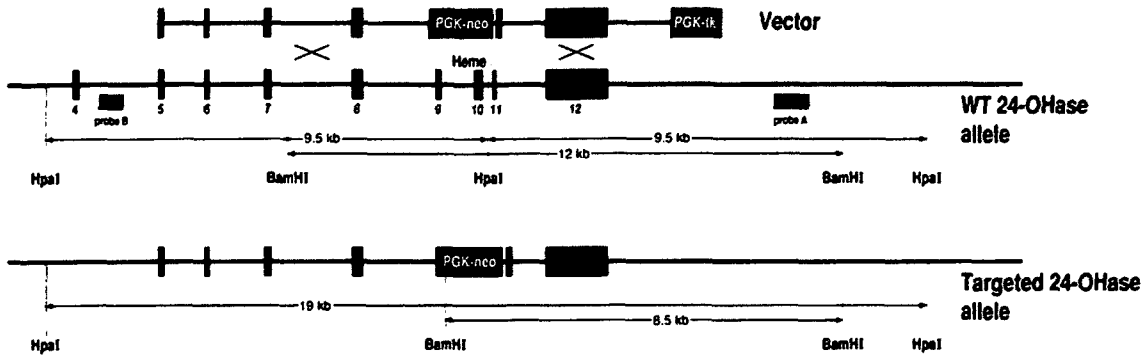

Figure 40 Targeted inactivation of the Cyp24a1 (24-OHase) gene in mice. Schematic representation of the targeting replacement-type vector, 24-OHase wild-type locus, and targeted 24-OHase locus after homologous recombination. The introduction of the PGK-neo cassette resulted in a new BamHI restriction site at the 24-OHase locus used in genotyping.

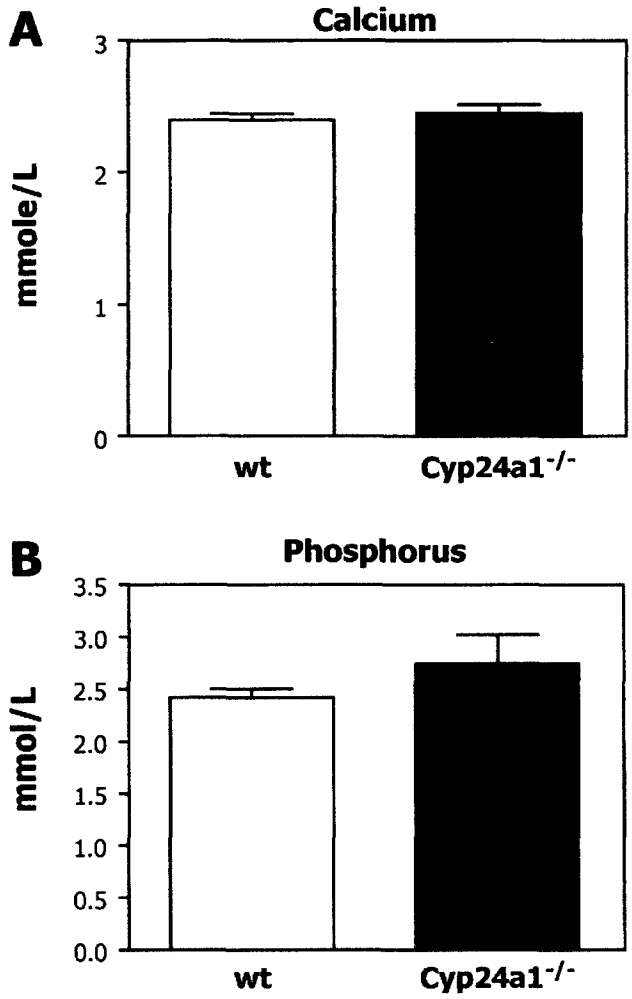

Figure 41 Serum biochemistry on blood collected from four-month-old mice 14 days after receiving a fracture.

The levels of both calcium (**A**) and phosphorus (**B**) were comparable in Cyp24a1$^{-/-}$ mice and their wild-type littermates.

Cyp24a1$^{-/-}$, Cyp24a1 knockout.

the abscence of a vitamin D metabolite hydroxylated at carbon position 24 such as 24R,25-$(OH)_2D$ and not secondary to abnormal mineral homeostasis.

III. 12-Mouse-model of stabilized fracture repair

Models to study the effect of many metabolites and hormones on fracture healing have been recently adapted in mice and other mammalian animals. These models involve extensive skeletal regeneration at the site of osteotomy that is greatly influenced by the mechanical environment. Different intensities of cyclic motion and its associated shear stress results in different callus formations and healing routes. In order to normalize for these variations, a stabilized model was adopted in our study to minimize movement. The model is based on the use of a miniaturized Ilizarof apparatus (Fig. 42 A) that also aligns the two ends of the fractured bone (alignment is another important factor that affects the callus formation). The surgical procedure, described in details in the materials and methods section, involved a stepwise fixation of the two-ringed apparatus by using insect pins and rods (Fig. 42 B).

III. 13-Delayed repair observed in Cyp24a1-deficient mice at 14 days post-osteotomy

Fourteen days after the surgery, the hard calluses were collected, sectioned and stained by Goldner. The histology revealed obvious differences between the Cyp24a1-deficient mice ($Cyp24a1^{-/-}$) and their wild-type littermates. In the wild-type mice, we can

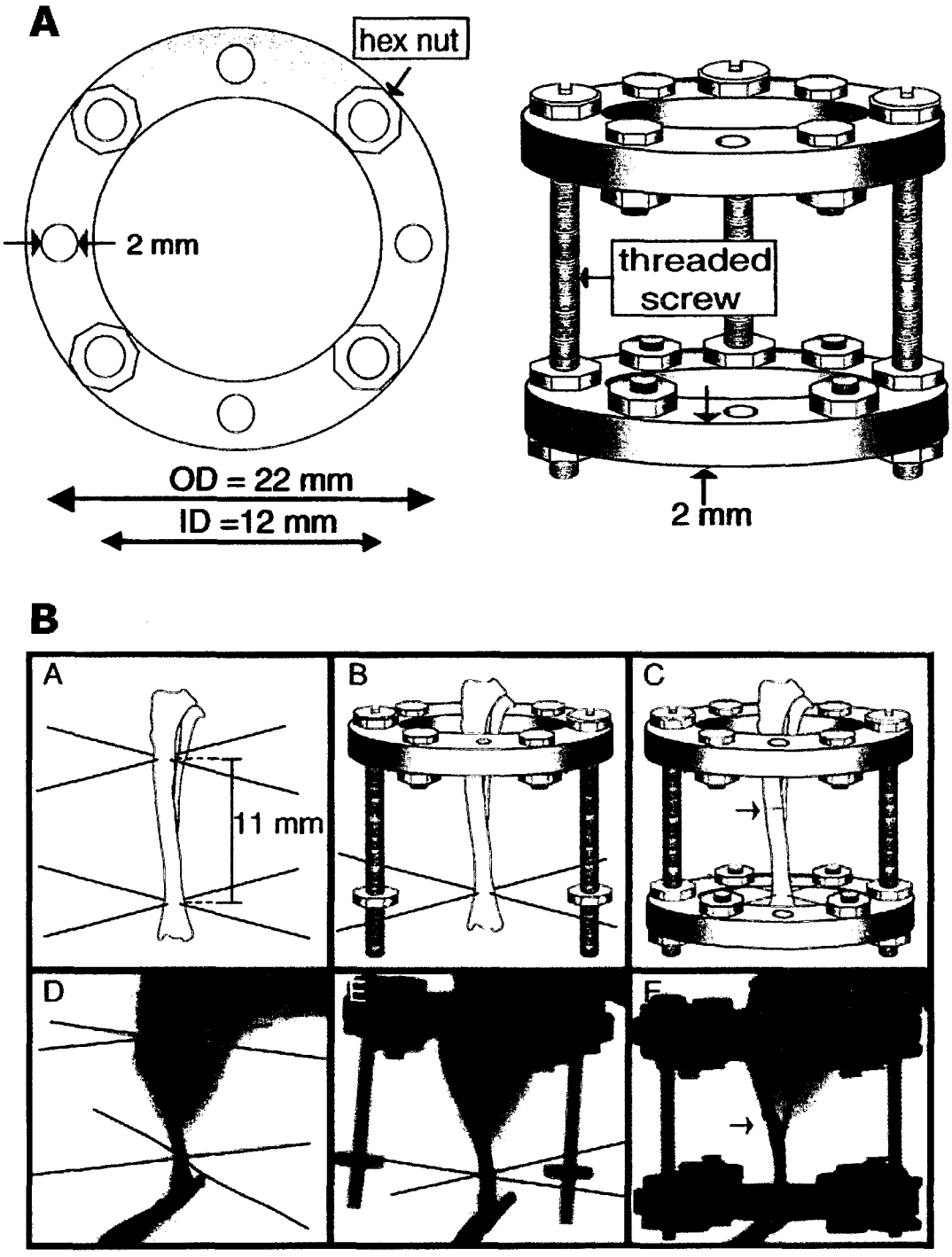

Figure 42

(**A**) Schematic presentation of the apparatus used in stabilizing the fractures. Left side shows the ring used and the positions where the threaded rods are fitted by means of hexagonal nuts. Right side shows the assembled apparatus where the two rings are attached by means of three threaded rods/screws. (**B**) Upper panel. Schematic presentation of the steps involved in the surgical procedure A,B,C . Lower panel. X rays taken at each of the surgical steps D,E,F.
hex nut, hexagonal nut; OD, outside diameter; ID, inside diameter. Adapted from (Thompson et al., 2002).

clearly observe the normal progression of a healthy callus at this 14-day post-osteotomy reparative phase. The callus is bulged from every side due to the inflammation that had occurred earlier in the reactive phase. Two types of connective tissue can be distinguished in this hard callus: the green islets of newly formed woven bone and the light yellow/light pink/light green hyaline cartilage. The green stained woven bone is deposited by the osteoblasts that were recruited from the periosteum once the osteotomy was inflicted. On the other hand, the lightly stained cartilage is deposited by periosteal cells that had differentiated into chondroblasts and further on into chondrocytes after the introduction of the fracture. In the cartilaginous areas, we can also observe different maturation stages of the cartilage anlagen where the light yellow/light pink reflects a collagen type II matrix produced by proliferative chondrocytes and the light green reflects a calcified collagen type X matrix produced by the mature hypertrophic chondrocytes. In addition, some areas of the callus harbor fibroblast like cells stained in light yellow/light pink that will preferentially differentiate into chondroblasts (Fig. 43 A). In the Cyp24a1$^{-/-}$ mice, the callus was poorly developed and practically non-existant with no newly formed bone or differentiated cartilage (Fig. 43 B).

RNA was extracted from the hard callus and the expression of several markers was assessed using RT-qPCR. Cyp27b1and Hif1α mRNA expression was increased in the Cyp24a1$^{-/-}$ mice as compared to the wild-types (Fig. 44 A,B). On the other hand, collagen type X mRNA expression was decreased in the Cyp24a1$^{-/-}$ mice as compared to the wild-types (Fig. 44 C). This decrease in the levels of collagen type X, a marker of differentiated chondrocytes (Chen et al., 1995), is a reflection of what was observed at the histological level where the wild-type callus had a more differentiated cartilaginous

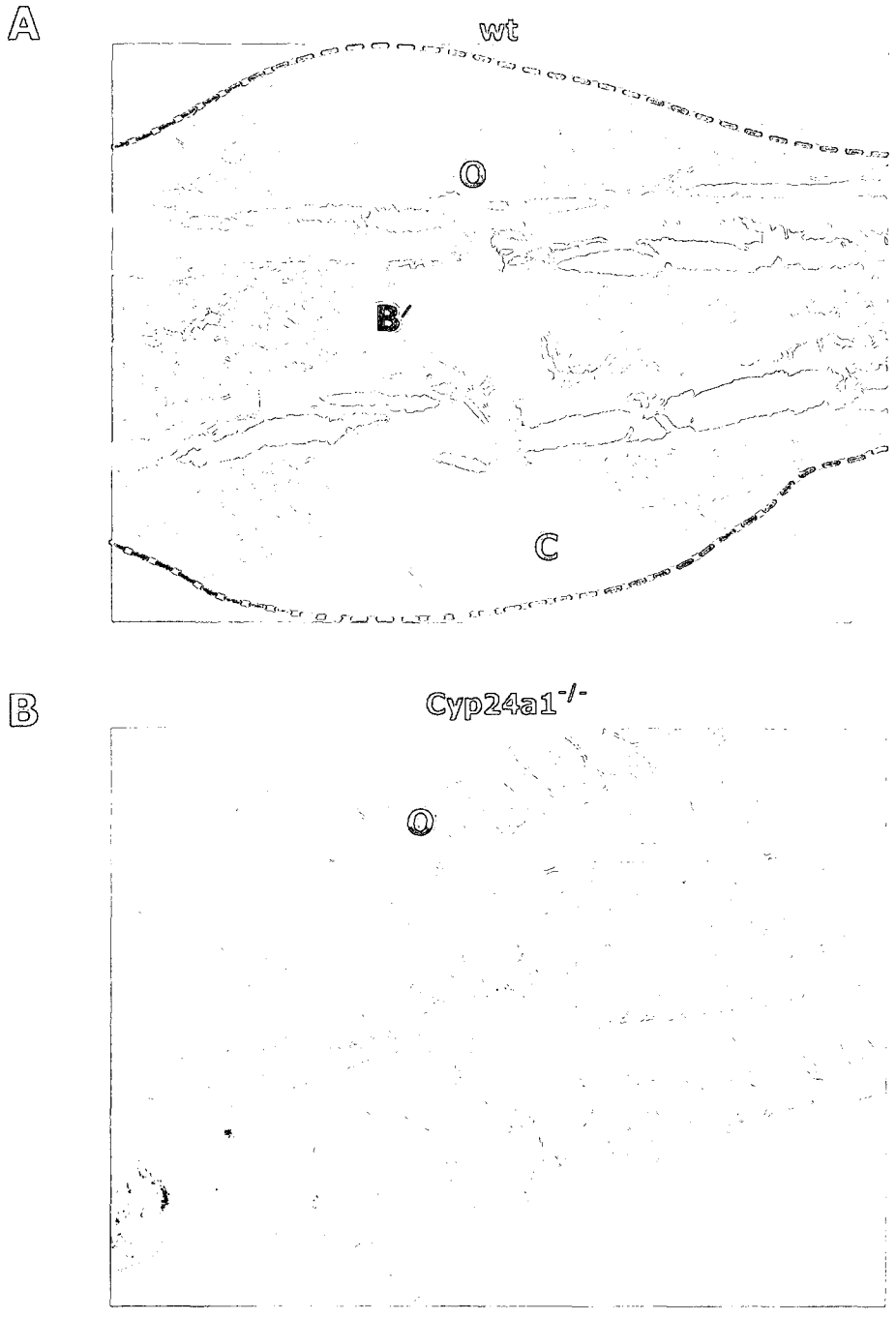

Figure 43 Delayed fracture repair in Cyp24a1-deficient mice at 14 days post-fracture.

Five µm transverse sections of 14 days post-fracture calluses stained with Goldner. (A) Wild-type mice show formation of a hard callus (area inside the dotted line) with cartilage and newly formed bone. Cyp24a1-/- mutant mice showed no evidence of callus formation at that time (B).
C, Cartilage; B, newly formed bone; O, location of the osteotomy.

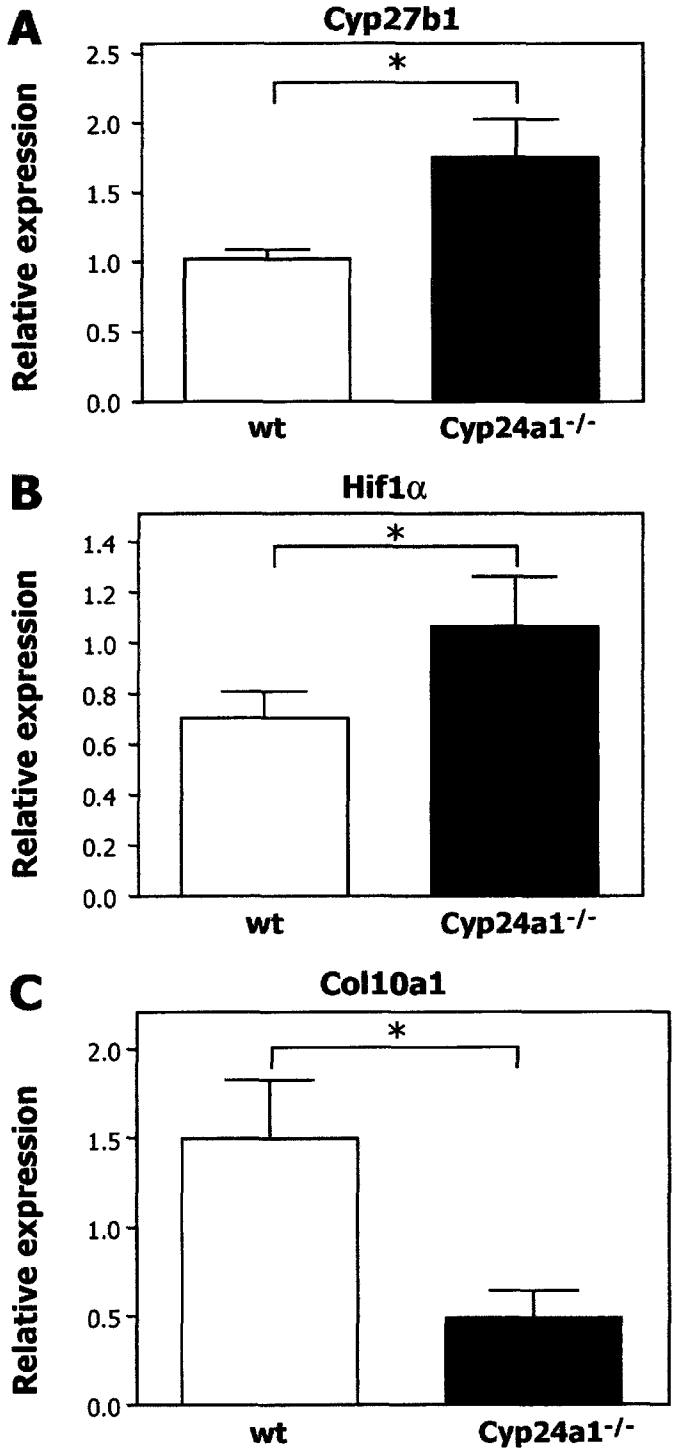

Figure 44 Marker gene expression perturbation of Cyp24a1$^{-/-}$ 14-day-old callus.

RT-qPCR on RNA extracted from calluses 14 days post-fracture showing a significant increase of Cyp27b1 (**A**) and Hif1α (**B**) mRNA levels and a significant decrease of collagen type X mRNA levels (**C**) in Cyp24a1$^{-/-}$ mice as compared to their wild-type littermates.

matrix as compared to the Cyp24a1$^{-/-}$ callus. In parallel, we measured the expression of several additional differentiation markers, and found no changes in their relative expression between genotypes (Table. 1).

III. 14-Delayed repair observed in Cyp24a1-deficient mice at 21 days post-osteotomy

Twenty-one days after the surgery, the calluses were collected, sectioned, and stained by Goldner. Again, the histology revealed obvious differences between the Cyp24a1$^{-/-}$ mice and their wild-type littermates giving further evidence for delayed fracture healing. In the wild-type mice, the callus has reached the remodeling phase. At this stage, the callus is at an advanced stage of resorption and is no longer bulged. In the area where the osteotomy was made, we notice the woven bone being remodeled and replaced by lamellar bone by the action of the osteoblasts. On the other hand, the cartilage section is completely resorbed and cannot be detected anymore. This phase precedes the final stage of union where the osteotomy is completely healed (Fig. 45 A). In the Cyp24a1$^{-/-}$ mice, repair has now picked up and the callus resembles the wild-type one at 14 days post-osteotomy. The callus is now bulged and we can recognize the two different connective tissues being produce in it, namely, bone and cartilage. However, and in this case of 24R,25-$(OH)_2$D deficiency, the woven bone being produced seem more prominent than that of the cartilage suggesting a possible preference for an intramembranous ossification rather than an endochondral one. In addition, one can observe pronounced osteoid seams in the mutant calluses (Fig. 45 B). This observation was quantified but did not reach statistical significance (data not shown).

Marker	Type	Relative expression
Collagen type II	Cartilage	No change
Indian hedgehog	Cartilage	No change
Alkaline phosphatase	Bone/Cartilage	No change
Runx2	Bone/Cartilage	No change
Collagen type I	Bone	No change
Osteocalcin	Bone	No change
Bone sialoprotein	Bone	No change
TRAP	Bone	No change
RANK	Bone	No change
Vitamin D receptor	Bone/Cartilage	No change

Table 1 Table summarizing the RT-qPCR reactions done on RNA extracted from callus 14 days post-fracture. The TaqMan assays of the different cartilaginous and bone markers showed no significant difference between Cyp24a1$^{-/-}$ mice and their wild-type littermates.

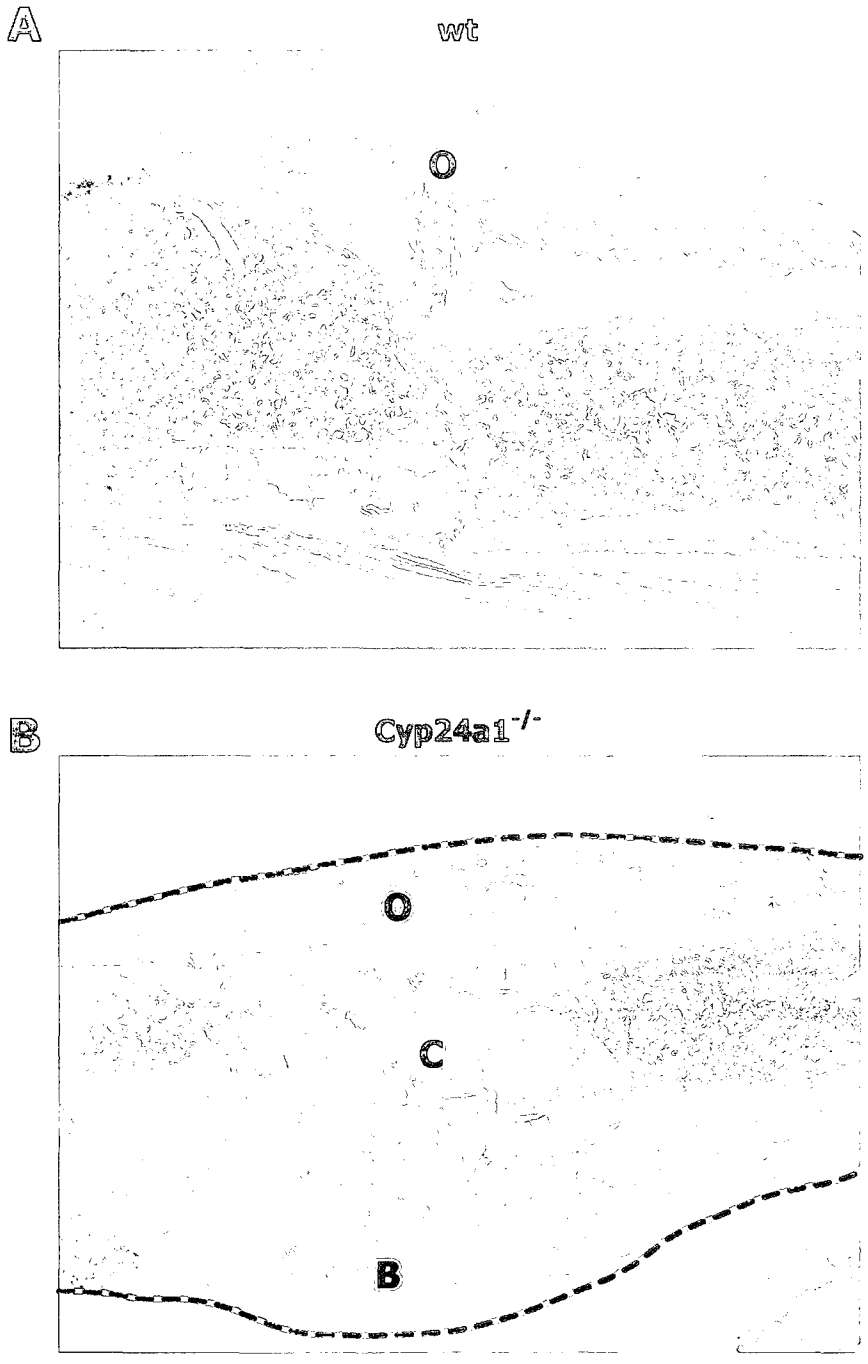

Figure 45 Delayed fracture repair in Cyp24a1-deficient mice at 21 days post-fracture.

Five µm transverse sections of 21 days post-fracture calluses stained with Goldner. (A) Wild-type animals show resorption of the hard callus and almost complete healing. The formation of a hard callus (area inside the dotted line) with cartilage and newly formed bone has now taken place in Cyp24a1-/- mutant mice (B).

C, Cartilage; B, newly formed bone; O, location of the osteotomy.

RNA was extracted from the calluses and the expression of several differentiation markers was assayed using RT-qPCR. Both osteocalcin and collagen type X mRNA expression was increased in Cyp24a1$^{-/-}$ calluses as compared to wild-types (Fig. 46 A,B). This increase in osteocalcin, an ECM molecule deposited by osteoblasts and a marker of bone formation (Aubin et al., 1995), reflects what was observed at the histological level where the Cyp24a1$^{-/-}$ callus showed newly formed bone at this 21-day post-fracture time-point. Similarly, the increase in collagen type X reflects the cartilage deposited by the chondrocytes in the Cyp24a1$^{-/-}$ callus. The various other markers assayed showed no significant change between genotypes and are summarized in Table 2.

III. 15-Specific rescue of the delayed fracture repair phenotype by treatment with 24R,25-$(OH)_2D_3$

The results obtained in the above sections suggest that the activity of *Cyp24a1*, and by extension a vitamin D metabolite hydroxylated at position 24, is important for the process of fracture healing, and that its absence leads to delayed healing. One of the products of the *Cyp24a1* enzymatic activity is 24R,25-$(OH)_2D$, a metabolite of unknown biological activity. We tested if treatment with 24R,25-$(OH)_2D$ could rescue the delayed fracture phenotype observed in Cyp24a1$^{-/-}$ mice.

Following surgery, the mice were subcutaneously injected with 24R,25-$(OH)_2D_3$ (6.7 μg/kg) or 1α,25-$(OH)_2D_3$ (67 ng/kg) [The different administered doses of the two metabolites is justified by the fact that the systemic levels of 1α,25-$(OH)_2D$ is always 10

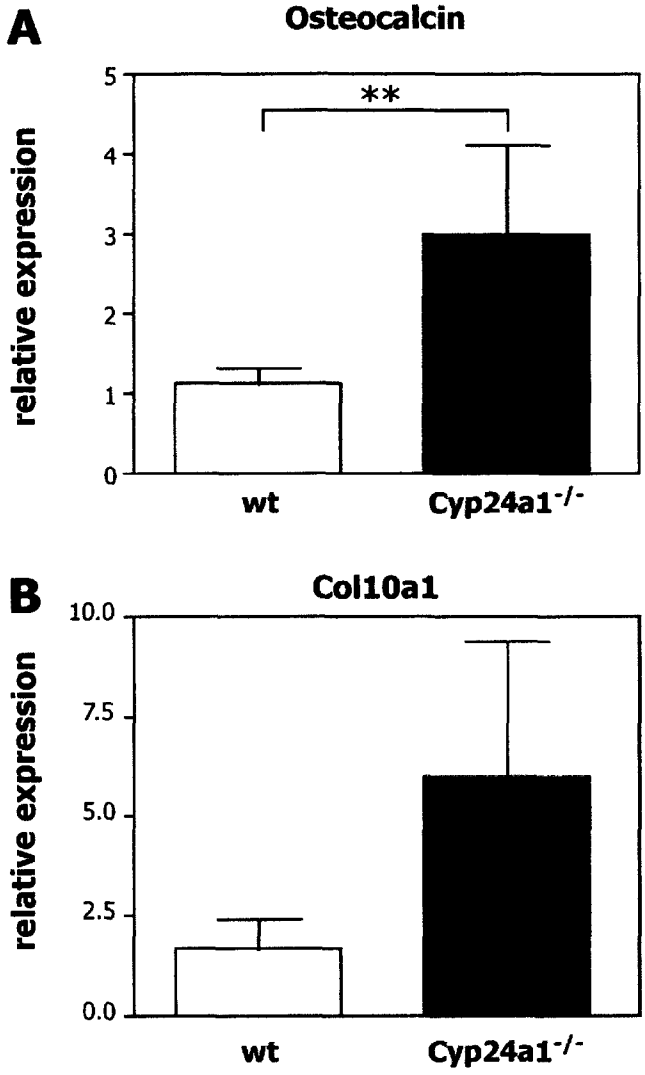

Figure 46 Marker gene expression perturbation of Cyp24a1$^{-/-}$ 21-day-old callus.

RT-qPCR on RNA extracted from calluses 21 days post-fracture showing a highly significant increase in osteocalcin (**A**) and an increase in collagen type X (**B**) mRNA levels in Cyp24a1$^{-/-}$ mice as compared to their wild-type littermates.

Marker	Type	Relative expression
Collagen type II	Cartilage	No change
Indian hedgehog	Cartilage	No change
Hipoxi induced factor 1α	Cartilage	No change
Alkaline phosphatase	Cartilage/Bone	No change
Runx2	Cartilage/Bone	No change
CYP27B1	Cartilage/Bone	No change
Vegfa	Cartilage/Vascular	No change
Collagen type I	Bone	No change
Bone sialoprotein	Bone	No change
TRAP	Bone	No change
RANK	Bone	No change
Vitamin D receptor	Bone/Cartilage	No change

Table 2 Table summarizing the RT-qPCR reactions done on RNA extracted from callus 21 days post-fracture. The TaqMan assays of the different cartilaginous and bone markers showed no significant difference between Cyp24a1$^{-/-}$ mice and their wild-type littermates.

to a 100 fold less than that of 24R,25-$(OH)_2D$ under normal physiological conditions]. Control groups were injected with propylene glycol (vehicle). Mice were sacrificed after 14 or 21 days of treatment and the calluses were collected and processed for either histology or mRNA profiling (Fig. 47). Blood was collected and assayed for circulating vitamin D metabolites. The levels of 24R,25-$(OH)_2D_3$ and 25-$(OH)D_3$ were found to be moderately increased in the treated Cyp24a1$^{-/-}$ mice as compared to the treated wild-types, however, within the same order of magnitude (Table 3).

Histological examination of the 14 days post-fracture time-point reveals changes in callus formation of the Cyp24a1$^{-/-}$ mice treated with 24R,25-$(OH)_2D_3$. These Cyp24a1$^{-/-}$ mice showed normal callus formation (Fig. 48 D) similar to what was observed in untreated wild-type mice (Fig. 43 A). Now in the reparative stage, the callus was bulged containing mainly two different connective tissue types: bone (stained in green) and cartilage (stained in light yellow/light pink/light green). The cartilage can also be divided into a mature one exhibiting a calcified type X collagen matrix (deposited by hypertrophic chondrocytes and stained in light green) and an immature one exhibiting a type II collagen matrix (produced by proliferative chondrocytes and stained in light pink/light yellow). The wild-types treated with either vehicle or 24R,25-$(OH)_2D_3$ had the same normal healthy phenotype contrary to the Cyp24a1$^{-/-}$ mice treated with the vehicle that retained the delayed healing phenotype (Fig. 48 A,B,C) implying that the vehicle treatment had no effect on the mice and the outcome of the callus.

We next compared the effect of 24R,25-$(OH)_2D_3$ with that of the active vitamin D metabolite, 1α,25-$(OH)_2D_3$. Treatment with 1α,25-$(OH)_2D_3$ did not rescue the delayed fracture healing phenotype in Cyp24a1$^{-/-}$ mice (Fig. 49 D). The callus was poorly formed

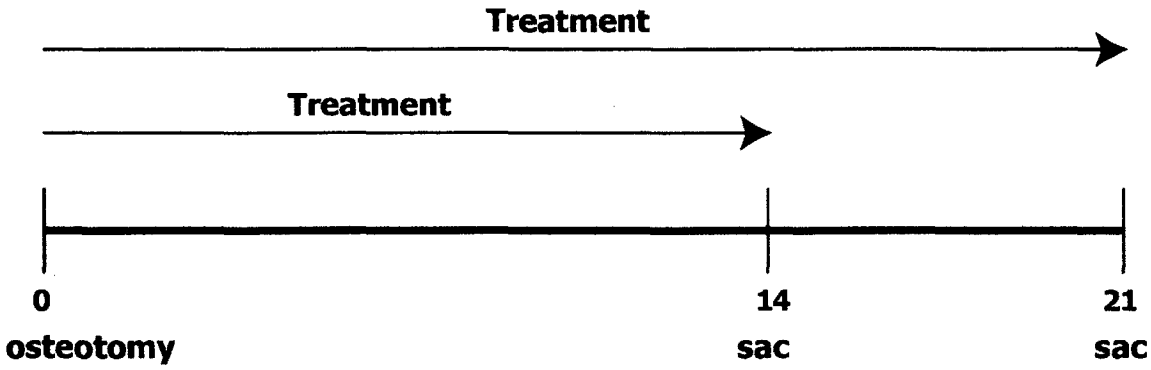

Figure 47 Schematic representation of the rescue protocol. After surgery and osteotomy (day 0), the mice were subcutaneously injected (treatment) with 24R,25(OH)$_2$D$_3$(6.7 µg/kg), 1α,25(OH)D$_3$(67 ng/kg), or propylene glycol (vehicle) for 14 or 21 days. The mice were then sacrificed and the calluses collected at the end of the treatment and processed for histology or RNA extraction.
14, 14 days; 21, 21 days; sac, sacrifice.

	Relative fold change	
	25-(OH)D	**24,25-$(OH)_2$D**
WT vehicle injected	1 (113.53±12 nmole/l)	1 (44.43±8.48 nmole/l)
WT 24R,25$(OH)_2D_3$ injected	~2	~4
Cyp24a1$^{-/-}$ vehicle injected	~1	0
Cyp24a1$^{-/-}$ 24R,25$(OH)_2D_3$ injected	~6	~6

Table 3 Serum vitamin D metabolites in operated mice are within the same order of magnitude across genotypes & treatments.

Table summarizing the 25-(OH)D and 24R,25-$(OH)_2D_3$ serum levels in operated mice treated with vehicle or 24R,25-$(OH)_2D_3$ for 14 days. The levels are expressed as fold change difference compared to wild-type (WT) mice receiving vehicle.

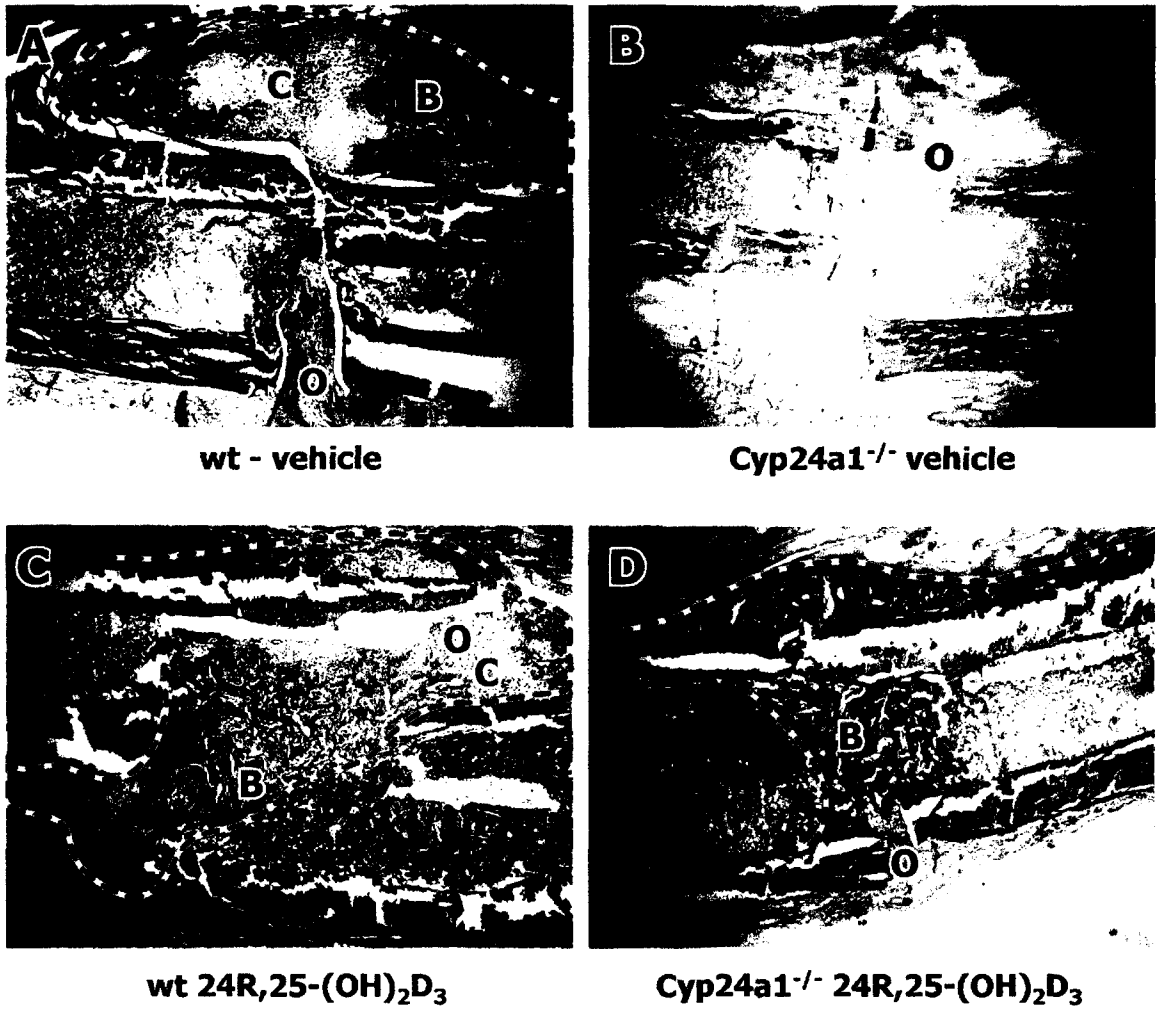

Figure 48 24R,25-$(OH)_2D_3$ treatment rescues the delayed fracture healing phenotype of Cyp24a1-deficient mice at 14 days post-osteotomy.

Histology of 14 days post-fracture calluses collected from mice treated with either propylene glycol (vehicle) or 24R,25$(OH)_2D_3$. (**A**) Shows the formation of a hard callus (area inside the dotted line) with cartilage and newly formed bone in wild-type mice treated with vehicle as compared to no callus formation in Cyp24a1$^{-/-}$ mice treated with vehicle (**B**). Lower panel shows the formation of a normal hard callus (area inside the dotted line) with cartilage and newly formed bone both in wild-type (**C**) and Cyp24a1$^{-/-}$ (**D**) mice treated with 24R,25-$(OH)_2D_3$.
C, cartilage; B, newly formed bone; O, location of the osteotomy.

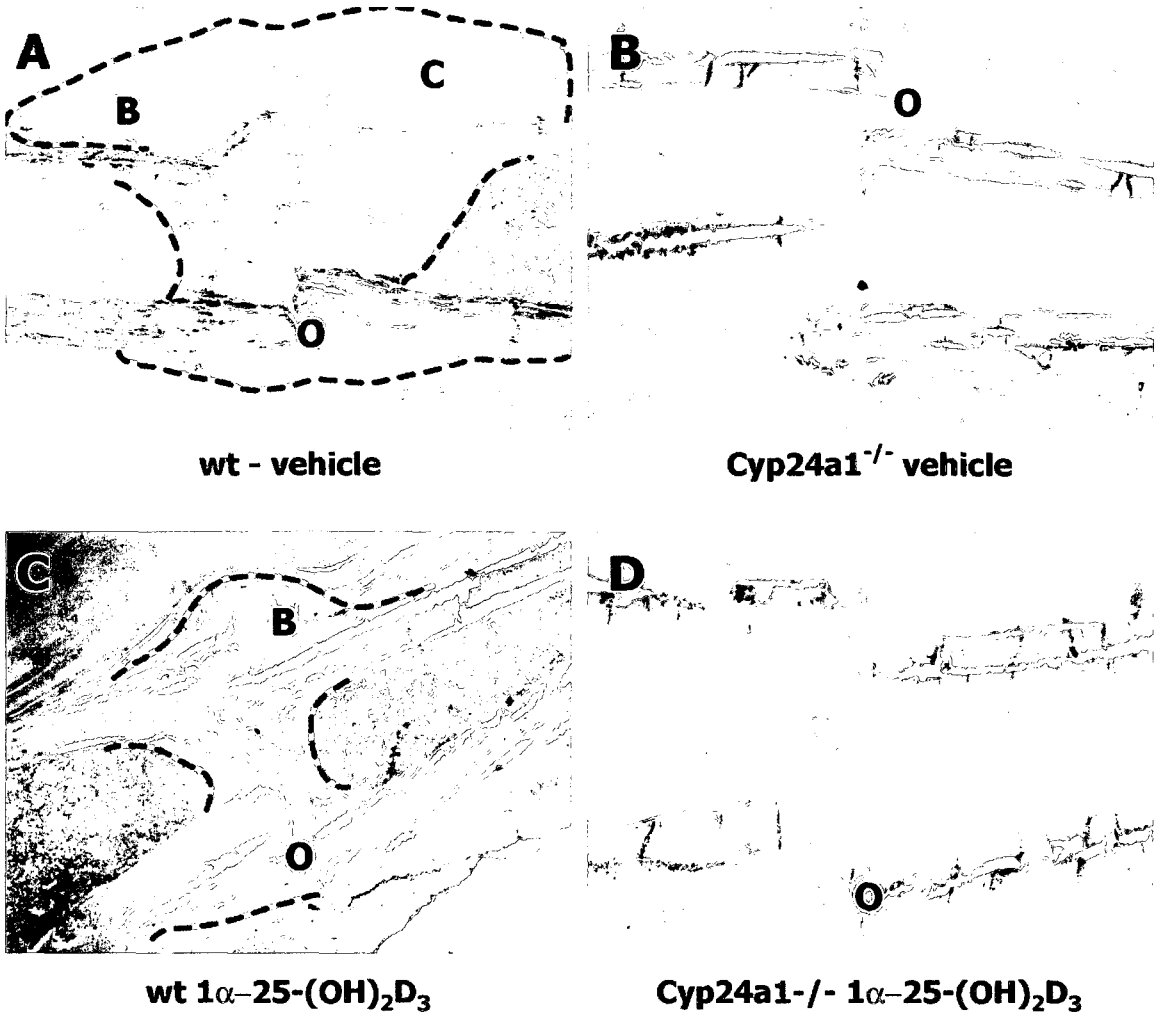

Figure 49 1α,25-$(OH)_2D_3$ treatment does not rescue the delayed fracture healing phenotype of Cyp24a1-deficient mice at 14 days post-osteotomy.

Histology of 14 days post-fracture calluses collected from mice treated with either propylene glycol (vehicle) or 1α,25-$(OH)_2D_3$. (**A,C**) Formation of a hard callus (area inside the dotted line) with cartilage and newly formed bone in wild-type mice treated with vehicle or 1α,25-$(OH)_2D_3$. Cyp24a1-deficient mice show the characteristic absence of callus formation at 14 days post-osteotomy (**B**) that is not rescued by treatment with 1α,25-$(OH)_2D_3$ (**D**).

C, cartilage; B, newly formed bone; O, location of the osteotomy.

showing minimal to no signs of newly formed bone and cartilage similar to what was observed in the untreated Cyp24a1$^{-/-}$ callus (Fig. 43 B). The wild-types treated with either vehicle or 1α,25-$(OH)_2D_3$ had the same normal phenotype contrary to the Cyp24a1$^{-/-}$ mice treated with the vehicle that retained the delayed healing phenotype (Fig. 49 A,B,C) implying that the vehicle treatment had no effect on the mice and the outcome of the callus.

We quantified the histological differences using histomorphometry. Bone volume (BV/TV %) and osteoid volume (OV/BV %) were measured at 14 days post-fracture. Bone volume at the fracture site was significantly reduced in Cyp24a1$^{-/-}$ mice (Fig. 50 A) reflecting the delay observed by histology. Treatment with 1α,25-$(OH)_2D_3$ did not influence the volume of bone at 14 days post-fracture in Cyp24a1$^{-/-}$ mutants (50 A) where fracture repair delay was still apparent (49 D). Remarkably, treatment with 24R,25-$(OH)_2D_3$ fully restored bone volume measured at 14 days post-fracture to wild-type levels. This quantitative, objective parameter demonstrates that the delay in fracture repair observed in Cyp24a1$^{-/-}$ mutant animals can be fully rescued by treatment with the 24-hydroxylated metabolite, 24R,25-$(OH)_2D_3$.

Osteoid volume within the callus was more variable and the measured parameter (OV/BV) showed no statistically significant differences across genotypes or treatments (50 B).

RT-qPCR of several osteogenic and cartilaginous markers was performed on RNA extracted from callus of treated mice 14 days post-fracture. The outcome of these experiments (that show no change between the different genotypes and treatments) is hard to interpret, however, the decreased mRNA levels of collagen type X in Cyp24a1$^{-/-}$

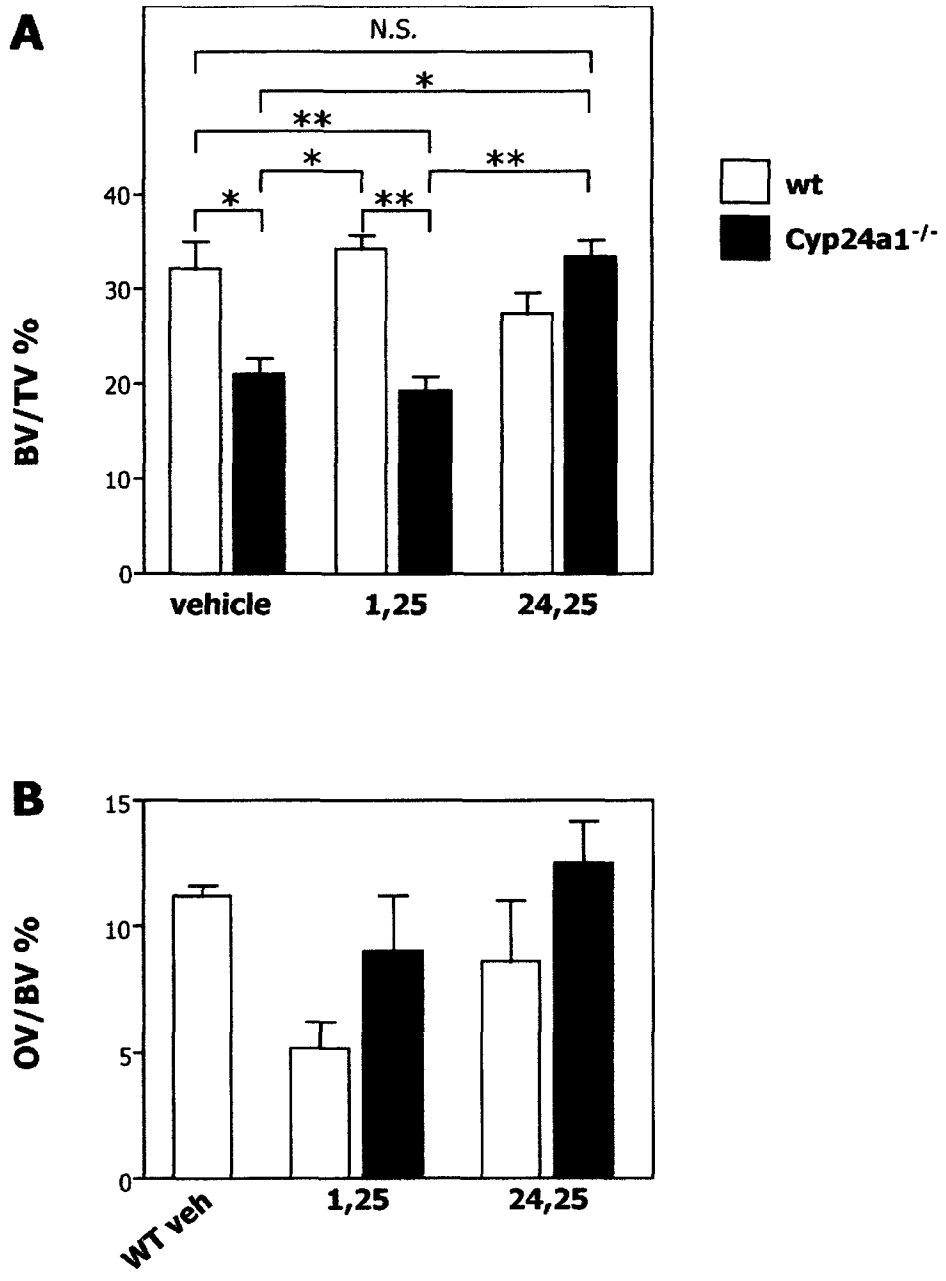

Figure 50 Bone volume is restored in Cyp24a1-deficient mice after 24R,25-$(OH)_2D_3$ treatment at 14 days post-osteotomy.

Histomorphometric analysis of 14 days post-fracture calluses collected from mice treated with vehicle, 1α,25-$(OH)_2D_3$, or 24R,25-$(OH)_2D_3$. (**A**) Shows the many significant changes of BV/TV % between the different treatments and genotypes (detailed explanation in the results section), while no significant changes were observed in case of the Osteiod volume/Bone volume OV/BV % parameter (**B**).

veh, vehicle treated; 1,25, 1α,25-$(OH)_2D$ treated; 24,25, 24R,25-$(OH)_2D_3$ treated.

mutant mice was found to be normalized by treatment with 24R,25-$(OH)_2D_3$, but not by treatment with 1α,25$(OH)_2D_3$ (Fig. 51 F).

At 21 days post-fracture, we observed changes in callus formation of the Cyp24a1$^{-/-}$ mutant mice treated with 24R,25-$(OH)_2D_3$. These Cyp24a1$^{-/-}$ mice now show a healthy callus at the remodeling phase. At this stage, the callus is at an advanced stage of resorption and is no longer bulged. In the area where the osteotomy was made, we notice the woven bone being remodeled and replaced by lamellar bone by the action of the osteoblasts. On the other hand, the cartilage section is completely resorbed and cannot be detected anymore (Fig. 52 D). This callus is similar to the untreated wild-type callus observed at 21 days post-osteotomy (Fig. 45 A), which is also shown here as the same sample of wild-type treated with vehicle (Fig. 52 A). The Cyp24a1$^{-/-}$ mice treated with vehicle showed a delayed callus formation (for this 21 days post-fracture time-point) that resembled the 14-day-old untreated wild-type callus in the reparative stage (Fig 43 A). The callus was bulged containing mainly two different connective tissue types: bone (stained in green) and cartilage (stained in light yellow/light pink/light green). The cartilage can also be divided into a mature one exhibiting a calcified type X collagen matrix (deposited by hypertrophic chondrocytes and stained in light green) and an immature one exhibiting a type II collagen matrix (produced by proliferative chondrocytes and stained in light pink/light yellow) (Fig. 52 B). This implies that the vehicle treatment had no effect on the mice and the outcome of the callus. The callus histology of wild-type mice treated with 24R,25-$(OH)_2D_3$ showed a delayed healing in this case (Fig. 52 C), which is most probably attributed to the misalignment of the fracture.

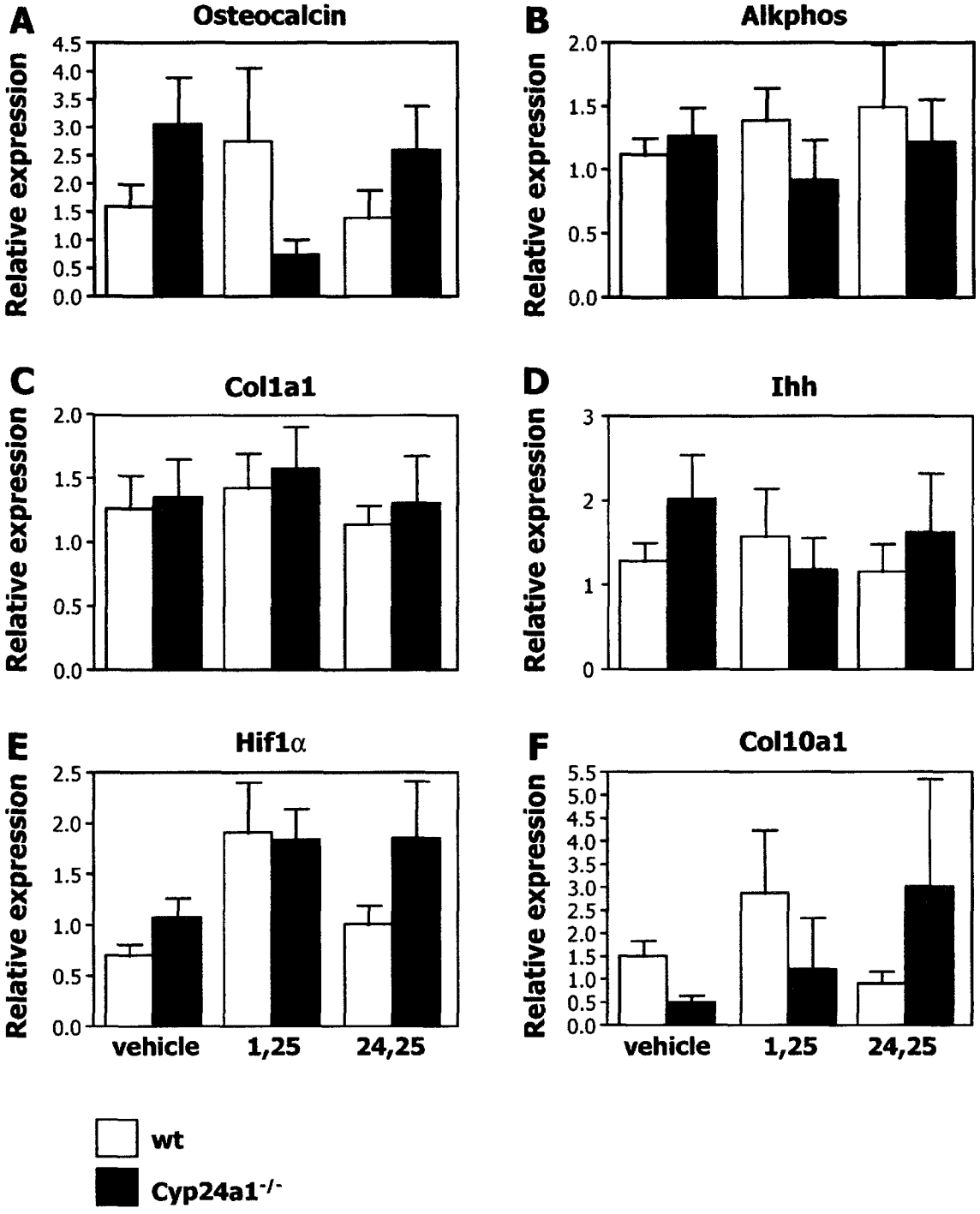

Figure 51 Collagen type X level is normalized with 24R,25-$(OH)_2D_3$ treatment at 14 days post-fracture.

RT-qPCR on RNA extracted from 14 days post-fracture calluses of mice treated with vehicle, 1α,25-$(OH)_2D_3$, or 24R,25-$(OH)_2D_3$. No significant change was observed in the markers assayed, however, the collagen type X (**F**) mRNA expression in the Cyp24a1$^{-/-}$ mice was normalized (the decreasing trend was reversed) to a certain extent when treated with 24R,25-$(OH)_2D_3$ and not 1α,25-$(OH)_2D_3$.

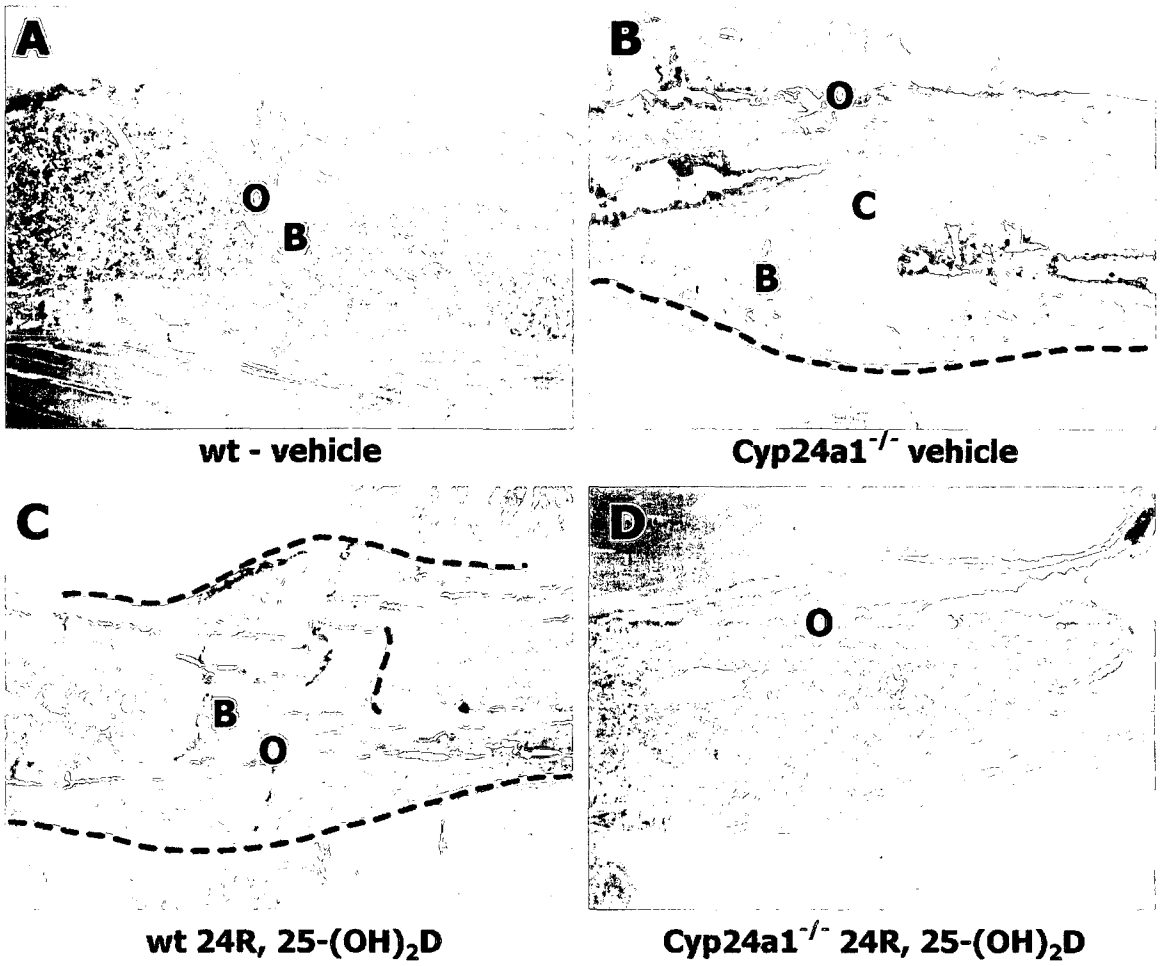

Figure 52 24R,25-$(OH)_2D_3$ treatment rescues the delayed fracture healing phenotype of Cyp24a1-deficient mice at 21 days post-osteotomy. Histology of 21 days post-fracture calluses collected from mice treated with either propylene glycol (vehicle) or 24R,25-$(OH)_2D_3$. Wild-type mice show complete or almost complete healing of the fracture at 21 days post-osteotomy (**A**), and this is not affected by treatment with 24R,25$(OH)_2D_3$ (**C**). Cyp24a1-deficient animals exhibit the delayed callus formation when treated with vehicle (**B**). Fracture repair was almost completely rescued by treatment with 24R,25-$(OH)_2D_3$(**D**).
C, cartilage; B, newly formed bone; O, location of the osteotomy.

These rescue results were not obtained with 1α,25-$(OH)_2D_3$ treatment where the Cyp24a1$^{-/-}$ mice showed a delayed callus formation (for this 21 days post-fracture time-point). The callus, still in the reparative stage, was bulged containing mainly two different connective tissue types: bone (stained in green) and cartilage (stained in light yellow/light pink/light green). The cartilage can also be divided into a mature type exhibiting a calcified type X collagen matrix (deposited by hypertrophic chondrocytes and stained in light green) and an immature type exhibiting a type II collagen matrix (produced by proliferative chondrocytes and stained in light pink/light yellow) (Fig. 53 D). This callus resembled the 14-day-old untreated wild-type callus (Fig. 43 A). The same retarded callus was observed for Cyp24a1$^{-/-}$ mice treated with vehicle (Fig 53 B). On the other hand, wild-type mice treated with vehicle showed the normal advanced remodeled callus (Fig. 53 A). This implies that vehicle treatment had no effect on the outcome of callus formation. The callus histology of wild-type mice treated with 1α,25-$(OH)_2D_3$ again showed a delayed healing in this case (Fig. 53 C), which is most probably attributed to the misalignment of the fracture.

Histomorphometric analysis showed no significant differences in bone volume (BV/TV %) (Fig. 54 A) or osteoid volume (OV/TV %) (Fig. 54 B) across the different treatments and genotypes. This could be due to some misalignments that affect the outcome of the callus.

RT-qPCR of several osteogenic and cartilaginous markers was performed on RNA extracted from callus of treated mice 21 days post-fracture. Similar to the 14 days post-fracture time-point, the outcome of these experiments (that show no change between the different genotypes and treatments) is hard to interpret, however, the

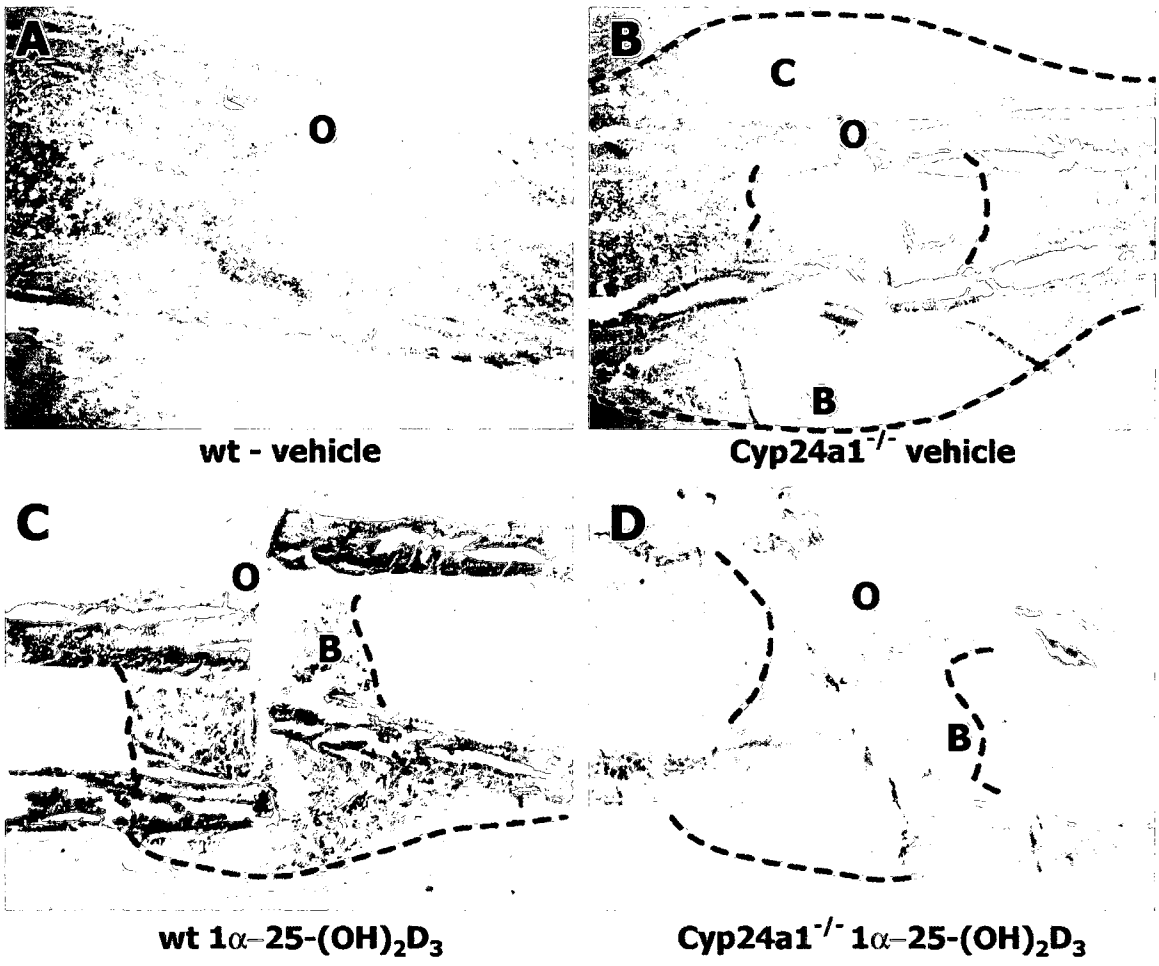

Figure 53 1α,25-$(OH)_2D_3$ treatment does not rescue the delayed fracture healing phenotype of Cyp24a1-deficient mice at 21 days post-osteotomy.

Histology of 21 days post-fracture calluses collected from mice treated with either propylene glycol (vehicle) or 1α,25-$(OH)_2D_3$. (**A, C**) Wild-type mice show complete or almost complete healing of the fracture at 21 days post-osteotomy. Following 1α,25-$(OH)_2D_3$ treatment, the incomplete healing in panel **C** is thought to be due to misalignement of the fracture. (**B**) Delayed callus formation in vehicle-treated Cyp24a1-/- mice. The healing was not accelerated by 1α,25-$(OH)_2D_3$ treatment (**D**).

C, cartilage; B, newly formed bone; O, location of the osteotomy.

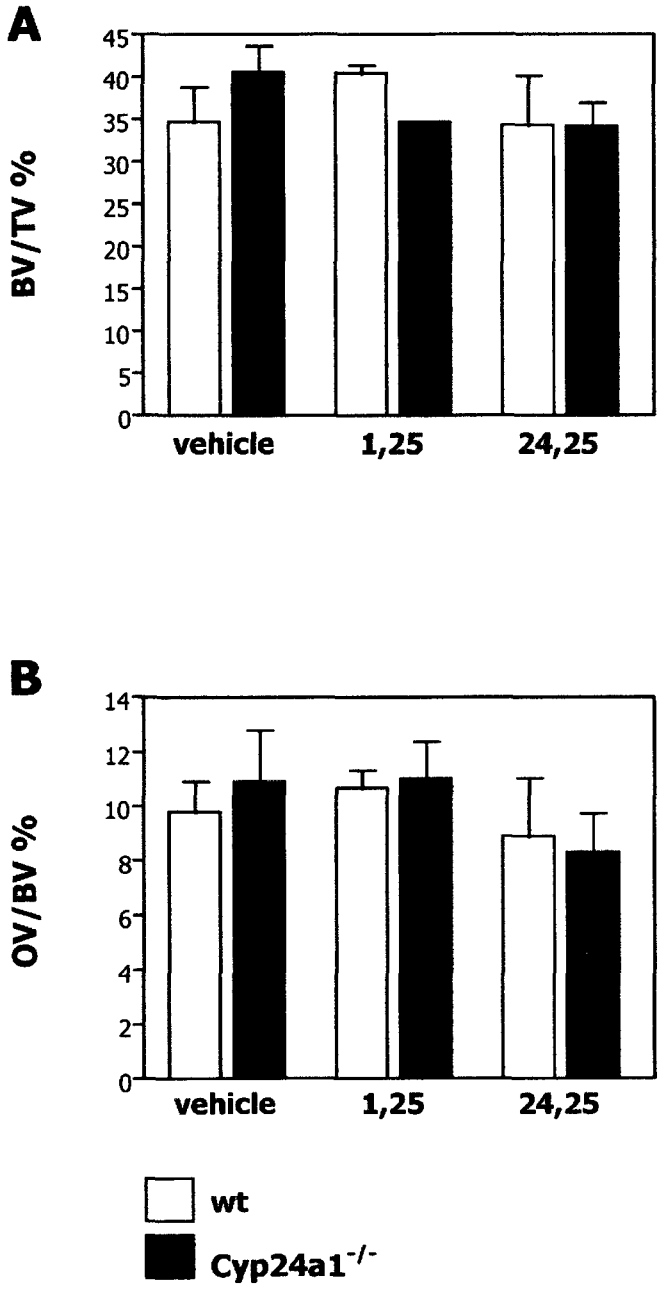

Figure 54 No change in histomorphometric parameters at 21 days post-fracture across the different genotypes and treatments.

Histomorphometric analysis of 21 days post-fracture calluses collected from mice treated with vehicle, 1α,25-$(OH)_2D_3$, or 24R,25-$(OH)_2D_3$ showing no significant changes across the different treatments and genotypes for either BV/TV % (**A**) or OV/BV % (**B**).

increased mRNA levels of collagen type X in Cyp24a1$^{-/-}$ mutant mice was found to be normalized by treatment with 24R,25-$(OH)_2D_3$ (Fig 55 F).

Again, these rescue studies suggest that a 24-hydroxylated metabolite of vitamin D, such as 24R, 25-$(OH)_2D$, is needed for normal fracture repair.

The discovery of a metabolite enhancing fracture repair could be helpful in human cases of fractures that do not heal properly or take a long time to repair. One example is the case of non-union fractures that don't repair properly. Another example is the case of distraction osteogenesis where the healing phase/consolidation phase is long and tedious on the patient. These two examples impair the patients's physical agility and have a negative effect on life style. The supplementation of a metabolite that enhances fracture repair would be useful in these two above-mentioned cases especially in vitamin D insufficient populations such as North Americans.

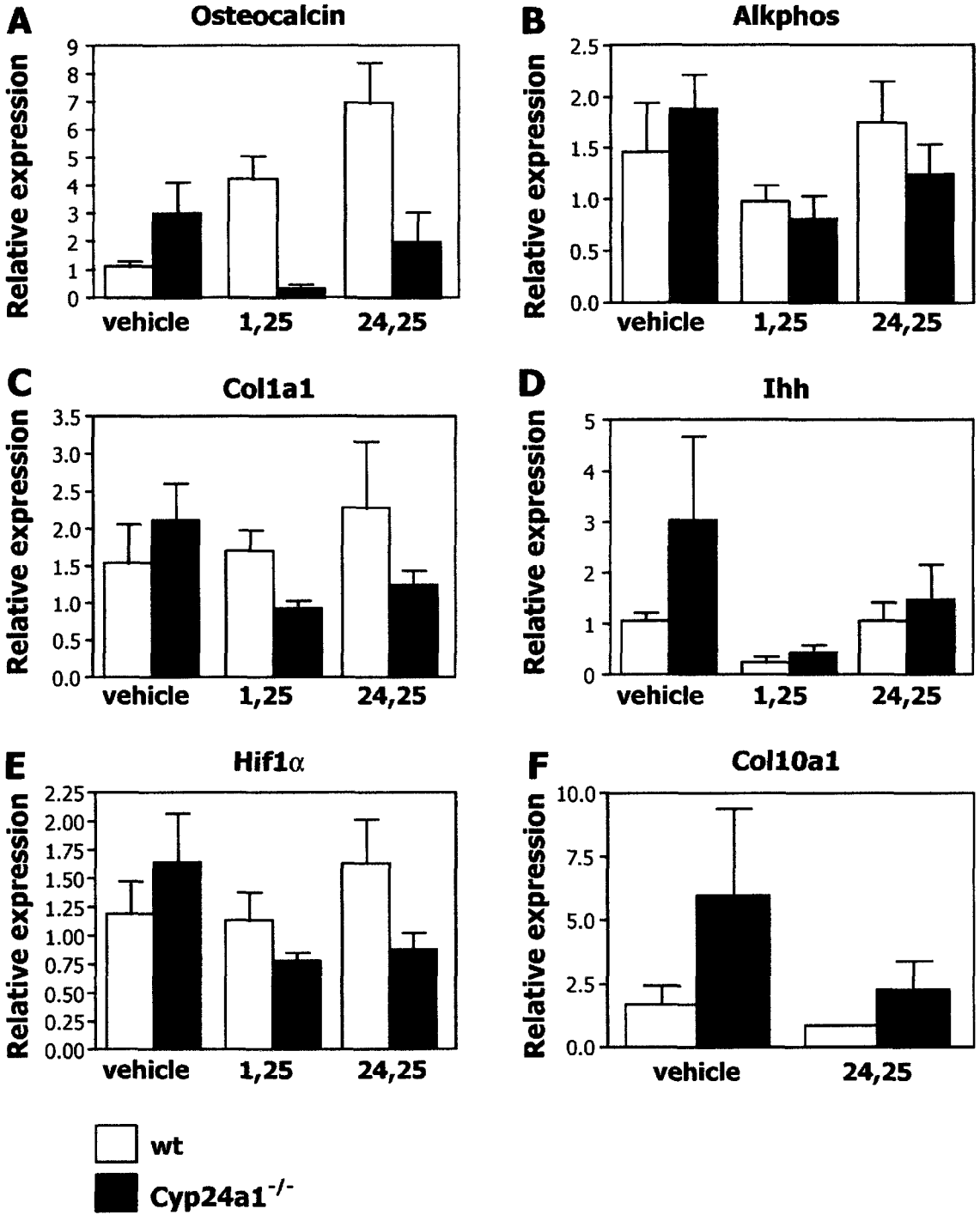

Figure 55 Collagen type X level is normalized with 24R,25-$(OH)_2D_3$ treatment at 21 days post-fracture.

RT-qPCR on RNA extracted from 21 days post-fracture calluses of mice treated with vehicle, 1α,25-$(OH)_2D_3$, or 24R,25-$(OH)_2D_3$. No significant change was observed in the markers assayed, however, the collagen type X (**F**) mRNA expression in the Cyp24a1$^{-/-}$ mice was normalized (the increased trend was minimized) to a certain extent when treated with 24R,25-$(OH)_2D_3$ and not 1α,25-$(OH)_2D_3$.

IV. Discussion

IV. 1-Modulation of Cyp27b1 expression in chondrocytes

1α,25-$(OH)_2$D has been widely known for decades for its main role in regulating calcium homeostasis. Recently, other subtle functions for the systemic 1α,25-$(OH)_2$D were also described and involved effects on the nervous system (Prufer et al., 1999) (Kumar, 2002) (Brewer et al., 2001), immune system (Casteels et al., 1998) (Overbergh et al., 2000) (Penna & Adorini, 2000), and cancer progression (Hsu et al., 2001) (Schwartz, 1992). In addition to that, the discovery of extra-renal CYP27B1 expression in different cell types and the characterization of a role for the locally produced 1α,25-$(OH)_2$D in these cells prompted us to test a putative autocrine/paracrine role for 1α,25-$(OH)_2$D in cartilage. We used a molecular genetic approach to create both a tissue-specific loss-of-function and overexpression model of Cyp27b1 in chondrocytes.

In the loss-of-function model we observed an increase in the size of the growth plate's hypertrophic zone at E15.5. We also detected at that time-point a reduction in the number of activated osteoclasts migrating towards the primary ossification center. The reduction in activated osteoclasts was also observed at the chondro-osseous junction of two-day-old tibiae. The mRNA levels of Ihh and Pthr1 were increased at postnatal day 2 along with a decrease in VEGF levels. This decrease in the angiogenic VEGF was accompanied by a decrease in blood vessel formation at the chondro-osseous junction as observed by a decrease in PECAM-1 immunostaining. The major phenotype obtained at postnatal day 2 was a highly significant increase in femoral trabecular bone mass.

In the overexpression model we observed a decrease in the size of the growth plate's hypertrophic zone at E14.5. The mRNA levels of Ihh and Hif1α were decreased at postnatal day 2. We also observed at this time-point a decrease in the femoral trabecular bone mass.

IV. 2-Cyp27b1 loss-of-function model

Possible intracrine role for 1α,25-$(OH)_2$D. One might propose that a major portion of the active 1α,25-$(OH)_2$D metabolite found in cartilage is derived systemically and that against the levels of circulating vitamin D hormone, any local synthesis may represent an insignificant contribution. During development, vitamin D and 25-(OH)D, but not 1α,25-$(OH)_2$D, cross the placenta (Haddad et al., 1971). Thus local synthesis of the active vitamin D metabolite may be essential to the regulation of target cell differentiation and function. Moreover, a recent concept in the field of sex steroids is intracrinology (Labrie et al., 2000). A significant proportion of androgens (approximately 50%) and estrogens (approximately 75% before menopause, and close to 100% after menopause) are produced in peripheral hormone-target tissues that express steroid metabolic enzymes. These locally produced bioactive androgens and/or estrogens exert their action in the cells where synthesis occurs without release in the extracellular space, including circulation. Thus despite steroidogenesis in the gonads, peripheral target tissues utilize 'on the spot' intracellular hormone synthesis/action to regulate their function (Labrie et al., 2000). Support for such a mode of action for vitamin D was recently obtained through the study of macrophage-mediated innate immunity (Liu et al.,

2006; Zasloff, 2006). Liu *et al.* identified both the VDR and CYP27B1 as induced genes in TLR-activated macrophages. The TLR-mediated upregulation of the expression of the VDR and CYP27B1 provokes intracrine 1α,25-$(OH)_2$D-dependent induction of cathelicidin and increased microbicidal activity of the macrophages (Zasloff, 2006). These results demonstrate the physiological relevance of extra-renal Cyp27b1 expression in peripheral target tissues.

Excision by Cre is not 100 % efficient. In the tissue-specific loss-of-function model, we used a mating strategy in order to obtain mutant mice having one Cyp27b1 null allele, one floxed Cyp27b1 allele, and transgenic for Cre under the control of collagen α_1(II) promoter. The mating strategy also gave three genotypically different control populations ($Cyp27b1^{+/fl}$; $Cyp27b1^{-/fl}$; Col2-Cre;$Cyp27b1^{+/fl}$). The phenotype of these three populations was identical and Cyp27b1 expression was not affected (data not shown), demonstrating the absence of gene dosage effects or any influence of the Col2-Cre transgene. It is known that Cre recombinase is not 100 % efficient in its excision of floxed alleles and that is the reason why we adopted a strategy to have one floxed allele to be excised with the homologous one being completely inactivated. Despite that, we still observed Cyp27b1 mRNA expression in the $Cyp27b1^{-/CH\Delta}$ rib-cartilage, even though significantly lower than that of the controls. Besides the low efficiency of Cre excision, another reason for this expression might be contamination from surrounding fibrous tissue covering the ribs and osteoblasts from the "bony" part of the rib that might express the Cyp27b1 mRNA.

Experiments are underway to measure: 1) the Cyp27b1 protein levels from two-day-old rib chondrocytes in order to confirm that the observed reduction of Cyp27b1

mRNA ultimately results in the reduction of the translated protein, 2) the levels of 1α,25-$(OH)_2$D from two-day-old rib chondrocytes or long bone primary growth plate to make sure there is no compensatory mechanism to restore this metabolite from neighboring cells such as the osteoblasts.

Transient phenotype. The phenotype obtained in the loss-of-function model can be basically divided into an effect on the chondrocytes *per se* and an effect on the growth plate's ability to be vascularized. In either case, the phenotype observed was transient being limited to embryonic and early neonatal stages of life. The reason behind the phenotype being transient could be explained by the following:

In the case of the growth plate, vascularization is delayed leading to differences in metaphyseal bone formation, however, blood vessels eventually are formed and the system will pick up and recover.

In the case of the chondrocytes, the Cyp27b1 expression is controlled by the collagen α_1(II) promoter whose activity was reported to be highest early on in life and to gradually decrease with age.

Chondrocyte development is affected by 1α,25-$(OH)_2$D. The observation of an increased chondrocytic hypertrophic zone in the Cyp27b1$^{-/CH\Delta}$ mice at E15.5 could be attributed to loss of the antiproliferative actions of 1α,25-$(OH)_2$D on these chondrocytes (Boyan et al., 1999). The hypothesis suggests that the lack of the metabolite would lead to increased proliferation of the chondrocytes ending in an enlarged hypertrophic zone of the long bone. PCNA staining did not reveal differences in chondrocytic proliferation between Cyp27b1$^{-/CH\Delta}$ mice and controls suggesting that other interpretations exist to account for this zone width difference. One interpretation would be decreased apoptosis

of the hypertrophic chondrocytes that can be verified in future experiments with caspase 3 immunoassays or other techniques.

The perturbation in the chondrocytic molecular markers (Ihh, Pthr1) observed at postnatal day 2 adds support to our claims that 1α,25-$(OH)_2$D plays a role to some extent in chondrocyte development. The disappearance of this effect of 1α,25-$(OH)_2$D on the chondrocytes at later stages in life might be due to several reasons. One reason might be linked to the activity of the collagen α_1(II) promoter. It has been reported that the activity of collagen α_1(II) promoter is strongest in early developmental and neonatal stages of life and gradually decreases with age. Another reason might be the presence of 1α,25-$(OH)_2$D that is produced by neighboring osteoblasts in late neonatal and adult stages of life and that leaks into the chondrocytic zone of the growth plate.

Vascularization of the growth plate is affected by 1α,25-$(OH)_2$D. The decrease in molecular angiogenic markers (VEGF and its receptor Kdr), endothelial cell/blood vessel marker (PECAM-1), osteoclast recuitment, and increase of metaphyseal bone mass in Cyp27b1$^{-/CH\Delta}$ long bones suggests the following model: In Cyp27b1$^{-/CH\Delta}$ mice, the reduction in VEGF expression and signaling leads to a decrease in blood vessel formation as seen by a decreased PECAM-1 immunostaining. This vasculature delay will reduce osteoclast invasion at the chondro-osseous junction. Since osteoclasts resorb the calcified cartilaginous matrix that serves as the scaffold for woven bone formation, a reduction in osteoclast invasion would result in an increased scaffold size that would lead to a larger bone volume at the primary spongiosa. This phenotype is transient as blood vessels eventually invade the chondro-osseous junction and normalize osteoclast recruitment and bone turnover.

In addition to our data, the results of Lin *et al.* support this model (Lin et al., 2002). These authors have observed an increase in VEGF expression in response to $1\alpha,25\text{-}(OH)_2D$. They also observed that blocking VEGF function (by infusion of a dominant negative VEGF receptor) leads to a delay in the vascularization of the juvenile growth plate.

One important future experiment to test our proposed model would be to cross the $Cyp27b1^{-/CH\Delta}$ mice with a strain of mice overexpressing VEGF in chondrocytes and try to rescue the observed embryonic and postnatal phenotype. Other future experiments to support this model would entail in situ localization of VEGF in the growth plate at postnatal day 2 and try to detect its reduced mRNA signal within the hypertrophic chondrocytes of the $Cyp27b1^{-/CH\Delta}$ mice. Immunostaining of VEGF can also be done to assay the release of the protein and try to document its decrease in the conditional knockout case.

Vascularization also occurs at embryonic time-points that lead to the resorption of the primary ossification center to result in the formation of the primary growth plate. At E15.5, we observed a reduction in the number of osteoclasts at the primary ossification center. Another future experiment would be to check for VEGF production and release from the hypertrophic zone and to immunostain for PECAM-1 at this primary ossification center at E15.5.

It is important to mention that Masuyama *et al.* (Masuyama et al., 2006) reported similar findings in the chondrocyte-specific VDR loss-of-function model. The group's findings are another support for our work. In our model, the delay in vascularization is a transient phenotype that gets rectified after the first week of life. This phenotype loss

was also documented by the group (In their case it was lost after the second week of life) and is not surprising. Again, a plausible explanation would be that vascularization is only temporarily delayed and once it is initiated the system will automatically pick up and recover.

The role of 1α,25-$(OH)_2$D in osteoclastogenesis. Masuyama *et al.* observed another phenotype in their model characterized by decreased osteoclastogenesis and an increase in serum phosphate and 1α,25-$(OH)_2$D levels. The decrease in osteoclastogenesis was evident by the decreased number of activated osteoclasts at the primary ossification center at E15.5 and later at the chondro-osseous junction of neonatal VDR conditional knockouts. According to their study, this osteoclast decrease is attributed to the combinatorial effect of decrease in blood vessel formation and RANKL release by the chondrocytes. The RANKL release by the chondrocytes is a novel finding and was reduced in the femoral growth plates of the VDR conditional knockouts. The expression of RANKL in our study was not changed when measured in the rib-cartilage. The growth plate in the ribs might behave differently than the primary growth plate of the long bones, however, we also dissected out the femoral epiphyses and did not detect by RT-qPCR any difference in RANKL expression between Cyp27b1$^{-/CH\Delta}$ mice and their control littermates. The unchanged RANKL levels in these epiphyses might be due to contamination from surrounding osteoblasts that secrete RANKL masking a difference in the signal. One important future experiment would be to establish a coculture of chondrocytes and splenocytes and to measure osteoclastogensis by TRAP staining.

The role of 1α,25-$(OH)_2$D in Fgf23 release. Masuyama *et al.* proposed a model where the chondrocytes release an unknown soluble factor that acts on the neighboring

osteoblasts triggering the production and release of Fgf23. Fgf23 mRNA levels was decreased in the femoral epiphyses of VDR conditional knockouts and in cocultures of chondrocytes (isolated from the conditional knockout) and osteoblasts. We detected no difference in Fgf23 expression in the femoral epiphyses. Again, several reasons might be behind this observation including possible contamination from neighboring tissues that might also release the same chondrocytic factor that triggers osteoblast Fgf23 synthesis and release. However, we measured serum levels of Fgf23, and in accordance with the VDR conditional knockout model, it was shown to be reduced in Cyp27b1$^{-/CH\Delta}$ mice as compared to controls. The remaining volume of serum after the Fgf23 ELISA did not allow me to measure circulating phosphate levels. This measurement will need to be performed in future experiments.

IV. 3-Cyp27b1 overexpression model

Engineering of the mouse-model. We engineered a chondrocyte-specific Cyp27b1 gain-of-funtion model. After the molecule was shown to be expressed in transfected ATDC5 cells, we proceeded in the pronuclear injections that resulted in four founder mice. The long bones of all four established transgenic strains were collected and analyzed at different time-points. The phenotype reported in this study was that of the strain (5tg) having the highest levels of *Cyp27b1* protein levels.

Chondrocyte development is transiently affected by 1α,25-(OH)$_2$D. At E14.5, we observed a decrease in the width of the hypertrophic zone in the transgenics as compared to the wild-types. This observation was reversed in the knockout setting at E15.5 and a

future experiment would be to make the measurements at exactly the same time-point in both models. Another experiment would be to assess the proliferation and apoptosis of the transgenic's chondrocytes by PCNA staining and Caspase 3 immunodetection respectively. At two days of age, the chondrocytic molecular markers were measured by RT-qPCR that showed Ihh (mirror image result of the conditional knockouts) and Hif1α to be decreased in the transgenics as compared to the wild-types. Similar to the conditional knockout case, this perturbation in chondrocyte development did not persist at later stages of life for similar reasons mentioned above.

The role of 1α,25-$(OH)_2$D in the vascularization of the growth plate and trabecular bone formation. Contrary to the tissue-specific knockout and at postnatal day 2, we did not observe a difference in the angiogenic molecular markers of the rib-cartilage or a difference in the metaphyseal bone mass of the femurs in the tissue-specific transgenics.. One reason for this difference might be the lack of substrate availability for this highly expressed *Cyp27b1*. For that, we supplemented the gestating females with the 25-$(OH)D_3$ substrate that crosses the placenta and collected the offspring at postnatal day 2. The metaphyseal bone mass was significantly decreased in the transgenics as compared to the wild-types giving a mirror image phenotype to that of the tissue-specific knockouts. However, VEGF expression in the rib-cartilage was shown to be unchanged (an increase is expected in this case). This result has several interepretations: 1) 1α,25-$(OH)_2$D is the cause of the decrease in bone mass acting through the same mechanism discussed above in the tissue-specific knockout case. The RT-qPCR experiment in this case has to be repeated with more samples to try to detect a change in VEGF expression. 2) 1α,25-$(OH)_2$D is the cause of the decrease in bone mass acting through another

unknown mechanism. 1) and 2) can be tested by crossing the transgenics with the chondrocyte-specific VDR knockout and try to normalize the reduction in bone mass. 3) The 25-$(OH)D_3$ substrate that crosses the placenta has a catabolic effect on bone causing a reduction in metaphyseal bone mass.

RANKL expression was also not altered in the transgenic case probably due to the same reasons discussed above for the tissue-specific knockout.

At any rate, our results from both overexpression and loss-of-function of Cyp27b1 in chondrocytes support a role for locally synthesized 1α,25-$(OH)_2D$ in the control of chondrocyte development and growth plate vascularization.

IV. 4-Cyp24a1 and mammalian fracture repair

Another vitamin D metabolite of interest is 24R,25-$(OH)_2D$. As mentioned earlier, there is a lot of controversy in the literature concerning a putative biological role for 24R,25-$(OH)_2D$. Studies in chicken showed increases in serum levels of 24R,25-$(OH)_2D$ and of the renal mRNA levels of CYP24A1 following fracture, suggesting a role for 24R,25-$(OH)_2D$ in fracture repair (Seo & Norman, 1997). We used a Cyp24a1-deficient mouse-model to address the putative role of 24R,25-$(OH)_2D$ in a mammalian system of fracture repair.

The tibial mRNA level of Cyp24a1 was found to be increased 14 days post-osteotomy. In Cyp24a1-deficient mice we observed a delay in callus formations and the process of fracture healing at 14 and 21 days post-osteotomy. At 14 days post-osteotomy, we observed a decrease in callus mRNA levels of collagen type X and an

increase in callus mRNA levels of Cyp27b1 and Hif1α. At 21 days post-osteotomy, we observed an increase in callus mRNA levels of collagen type X and osteocalcin.

We observed a rescue of the delayed fracture healing at 14 and 21 days post-osteotomy with 24R,25-$(OH)_2D_3$ tretament and not 1α,25-$(OH)_2D_3$. The mRNA levels of collagen type X was also observed to be normalized at both post-osteotomy time-points with the 24R,25-$(OH)_2D_3$ treatment and not 1α,25-$(OH)_2D_3$.

IV. 4-The role of 24R,25-$(OH)_2D$ in a mouse-model of fracture repair

Cyp24a1 expression is increased in fractured long bones. After the induction of an osteotomy, both the renal expression of Cyp24a1 and the serum levels of 24R,25-$(OH)_2D$ were shown to be increased in the chick-model of fracture repair (Seo & Norman, 1997). We observed a local increase of Cyp24a1 mRNA levels at 14 days post-osteotomy. This increase in Cyp24a1 (that needs to be verified at the protein level in future experiments) is either needed to synthesize a vitamin D metabolite hydroxylated at carbon position 24 such as 24R,25-$(OH)_2D$ to perform a certain function (in this case its involvement in fracture repair) or is induced by local activity of 1α,25-$(OH)_2D$. The latter claim is unlikely due to the following reasons: 1) 24R,25-$(OH)_2D$ is increased in the chicken following an osteotomy. 2) Gene expression monitoring in the callus does not support local 1α,25-$(OH)_2D$ activity (discussed below). 3) 1α,25-$(OH)_2D_3$ treatment does not rescue the delayed fracture repair phenotype.

Other future experiments in this regard would be to measure the renal Cyp24a1 mRNA and serum 24R,25-$(OH)_2D$ levels in wild-type mice after receiving an osteotomy.

Delayed fracture healing is observed in Cyp24a1-deficient mice. We reported an obvious delay in fracture repair in Cyp24a1-deficient mice as compared to wild-type at mainly the 14 and 21 days post-fracture time-points. Reports in the literature studying the role of other molecules in fracture repair focus mainly on these two post-fracture time-points with an additional post-fracture time-point at day eight (Colnot et al., 2003; Gerstenfeld et al., 2003; Komatsu & Hadjiargyrou, 2004). We also characterized the eight-day post-fracture time-point with no obvious difference between the two genotypes. A phenotype might exist at that time-point, but technical difficulties arise in extracting RNA from a small soft callus (characteristic of that time-point in mice) and in maintaining the integrity of this soft callus while being dissected out and processed for histology.

It is important to mention that the nature of the callus formed is affected by the alignment of the fracture. In this study we mostly analyzed aligned fractured samples. The variation in alignment can be avoided in future experiments by adopting other stabilized fracture models that involves rod introduction into the bone (Hiltunen et al., 1993).

At 14 days post-fracture, the fracture site of Cyp24a-deficient mice showed no callus formation. In the wild-types at that stage, a fully formed callus is observed with both hyaline cartilage being formed and woven bone being deposited. At 21 days post-fracture, the fracture site of Cyp24a1-deficient mice showed a callus resembling the 14-day post-fracture callus of untreated wild-types with a cartilaginous matrix and newly formed bone. In the case of the wild-type at 21 days post-osteotomy, and when the fracture is aligned, the callus was shown to be remodeled with the osteotomy close to

being healed (complete healing and consolidation occurs around day 27 in mice). The case of the wild-type with a misaligned fracture becomes more complicated making it resemble the knockout situation at this 21-day post-fracture time-point. So, the different fracture healing phenotype observed between wild-type and knockout at 21 days post-fracture is obvious in the case of an aligned fracture.

The delay in fracture repair observed in the Cyp24a1-deficient mice can be argued to be caused by either a lack of 24R,25-$(OH)_2D$ or an increase in the systemic or local levels of 1α,25-$(OH)_2D$. The systemic levels of 1α,25-$(OH)_2D$ were measured at 8 and 14 days post-fracture and found to be significantly decreased in the knockouts as compared to the wild-type (Fig. 56). This decrease in 1α,25-$(OH)_2D$ was reported before by our lab (St-Arnaud et al., 2000) where the viable Cyp24a1-deficient mice adapt an alternative mechanism than the C-24 oxidation pathway to degrade 1α,25-$(OH)_2D$ and render it to levels even lower than that of the wild-type. This decrease of 1α,25-$(OH)_2D$ in the knockout persisted post-osteotomy eliminating the possibility of an increase in 1α,25-$(OH)_2D$ systemic levels to be the cause of the delayed fracture healing. One can also argue that this low systemic 1α,25-$(OH)_2D$ might have a longer half-life or enhanced activity that can be causing the delay in repair. This, however, might not be the case due to the fact that the VDR mRNA expression remains unchanged in the callus at both the 14 and 21-day post-fracture time-points (Tables 1 & 2) and that Cyp27b1 mRNA expression is increased in the Cyp24a1-deficient callus at day 14 post-fracture (Fig. 44 A). Cyp27b1 and VDR are 1α,25-$(OH)_2D$ regulated genes and their expression in this system is opposite to what would be predicted by a sustained 1α,25-$(OH)_2D$ bioactivity. A future experiment would be to quantitate the *Cyp27b1* protein in the callus

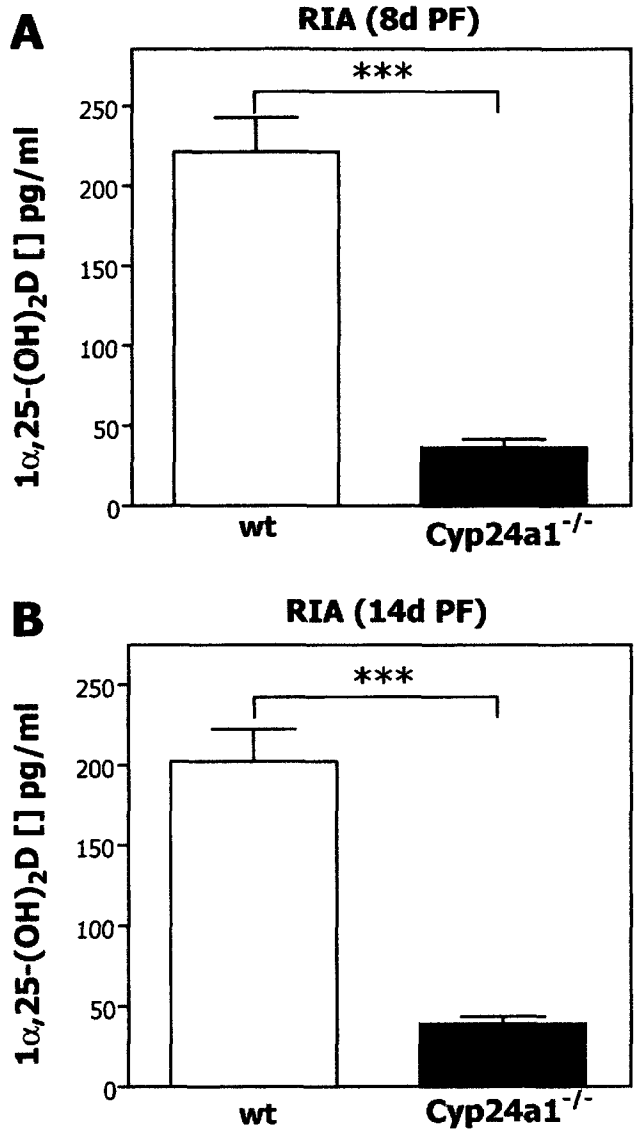

Figure 56 Serum levels of $1\alpha,25\text{-}(OH)_2D_3$ is decreased in Cyp24a1-deficient mice at 8 and 14 days post-fracture.

RadioImmunoAssay (RIA) on blood collected from four-month-old mice 8 days (a) and 14 days after receiving a fracture. At both time-points the levels of $1\alpha,25\text{-}(OH)_2D_3$ was significantly reduced in Cyp24a1$^{-/-}$ mice as compared to their wild type littermates. *** $p<0.001$.
8d PF, 8 days post-fracture; 14d PF, 14 days post-fracture.

in order to check the possibility of whether a locally produced 1α,25-$(OH)_2$D is directly involved in fracture delay or not.

Treatment with 24R,25-$(OH)_2D_3$ and not with 1α,25-$(OH)_2D_3$ rescued the delayed fracture healing. The rescue experiments conducted in this study strengthened the claim that the absence of a vitamin D metabolite hydroxylated at carbon position 24 is the cause of the delayed fracture healing. Treatment with 1α,25-$(OH)_2D_3$ did not correct the delayed healing suggesting that this metabolite does not play an important role in fracture repair.

It can always be argued that the observed rescue of the delayed fracture healing is due to 1α,24,25-$(OH)_3$D and not 24R,25-$(OH)_2$D. The supplemented 24R,25-$(OH)_2D_3$ will bind the VDBP and can be targeted to the kidney where it can be hydroxylated on carbon 1α by the action of *Cyp27b1* to produce 1α,24,25-$(OH)_3D_3$ [It has been shown that Cyp27b1 has even a higher affinity for 24R,25-$(OH)_2$D than 25-(OH)D (Sakaki et al., 1999)]. The 1α,24,25-$(OH)_3D_3$ then binds to the VDBP and can be targeted to the fracture site where it can bind the VDR (it was reported that the affinity of the VDR for 1α,24,25-$(OH)_3D_3$ is higher than for 24R,25-$(OH)_2D_3$ (Bouillon et al., 1995) and play a role in fracture repair. Also, the supplemented 24R,25-$(OH)_2D_3$ can be targeted directly to the fracture site where it can be changed to 1α,24,25-$(OH)_3D_3$ that can then bind the VDR and contribute in the process of fracture repair. However, 1α,24,25-$(OH)_3$D is a metabolite with a short half-life and is relatively quickly catabolized by the C-24 oxidation pathway making it less likely to have the sufficient time to be involved in the fracture healing process (Jones, 2008).

Additional future experiments. The role of 24R,25-$(OH)_2D$ or a vitamin D metabolite hydroxylated at C-24 in fracture repair can be strengthened with future experiments that includes treatment with the synthetic inactive 24S,25-$(OH)_2D_3$ metabolite and observing absence of rescue. Treatment with 1α,24,25-$(OH)_3D_3$ or 1α,24-$(OH)_2D_3$ can also be done to assess this metabolite's role in fracture repair.

As mentioned earlier, a receptor for 24R,25-$(OH)_2D$ was never well characterized and the results obtained in our study suggests a possible role for 24R,25-$(OH)_2D$ in fracture repair and provide a strong motive to try to identify a receptor for this metabolite. For that, a microarray could be done in the future on RNA extracted from the calluses of Cyp24a1-deficient and wild-type mice to measure differential gene expression. The idea would be to detect candidate genes that are overexpressed in the knockout case and try to acquire their full length cDNA transcript. The cDNA can be further subcloned in a vector and expressed in a eukaryotic cell line. The membrane fraction [where previous studies hinted at the presence of a receptor for 24R,25-$(OH)_2D$ (Seo et al., 1996)] can be purified and collected to perform binding assays with a radioactively labeled 24R,25-$(OH)_2D$. Once a "receptor" is found, the role of the 24R,25-$(OH)_2D$ ligand in fracture healing can be verified if the mouse knockout-model of this receptor results in a delay in fracture healing.

In summary, our studies contribute significantly to bone biology and vitamin D physiology by showing a novel *in vivo* role for 1α,25-$(OH)_3D$ in the development of the growth plate and by implicating 24R,25-$(OH)_2D$ or a vitamin D metabolite hydroxylated at C-24 in the mammalian process of fracture repair.

Claims of originality

This thesis contains the first reports of:

1) Chondrocyte-specific Cyp27b1 knockout mice
2) Characterization of the phenotype of these mice
3) Chondrocyte-specific Cyp27b1 transgenic mice
4) Characterization of the phenotype of these mice
5) Fracture healing in Cyp24a1 knockout mice
6) Rescue of the abnormal fracture healing phenotype of Cyp24a1 mice with 24R,25-$(OH)_2D_3$

Overall, my results strongly support a role for locally produced 1α,25-$(OH)_2D$ in the development of the growth plate and strongly suggest that a vitamin D metabolite hydroxylated at position 24, such as 24R,25-$(OH)_2D$, plays a role in fracture repair.

References

Akeno N, Saikatsu S, Kawane T, Horiuchi N 1997 Mouse vitamin D-24-hydroxylase: molecular cloning, tissue distribution, and transcriptional regulation by 1alpha,25-dihydroxyvitamin D3. Endocrinology 138:2233-2240

Aubin JE, Liu F, Malaval L, Gupta AK 1995 Osteoblast and chondroblast differentiation. Bone 17:77S-83S

Bai M, Quinn S, Trivedi S, Kifor O, Pearce SH, Pollak MR, Krapcho K, Hebert SC, Brown EM 1996 Expression and characterization of inactivating and activating mutations in the human Ca2+o-sensing receptor. J Biol Chem 271:19537-19545

Barettino D, Vivanco Ruiz MM, Stunnenberg HG 1994 Characterization of the ligand-dependent transactivation domain of thyroid hormone receptor. EMBO J 13:3039-3049

Beckman MJ, Tadikonda P, Werner E, Prahl J, Yamada S, DeLuca HF 1996 Human 25-hydroxyvitamin D3-24-hydroxylase, a multicatalytic enzyme. Biochemistry 35:8465-8472

Bikle DD, Chang S, Crumrine D, Elalieh H, Man MQ, Choi EH, Dardenne O, Xie Z, Arnaud RS, Feingold K, Elias PM 2004 25 Hydroxyvitamin D 1 alpha-hydroxylase is required for optimal epidermal differentiation and permeability barrier homeostasis. J Invest Dermatol 122:984-992

Bikle DD, Ng D, Oda Y, Hanley K, Feingold K, Xie Z 2002 The vitamin D response element of the involucrin gene mediates its regulation by 1,25-dihydroxyvitamin D3. J Invest Dermatol 119:1109-1113

Bikle DD, Ng D, Tu CL, Oda Y, Xie Z 2001 Calcium- and vitamin D-regulated keratinocyte differentiation. Mol Cell Endocrinol 177:161-171

Bitgood MJ, McMahon AP 1995 Hedgehog and Bmp genes are coexpressed at many diverse sites of cell-cell interaction in the mouse embryo. Dev Biol 172:126-138

Bland R, Walker EA, Hughes SV, Stewart PM, Hewison M 1999 Constitutive expression of 25-hydroxyvitamin D3-1alpha-hydroxylase in a transformed human proximal tubule cell line: evidence for direct regulation of vitamin D metabolism by calcium. Endocrinology 140:2027-2034

Bland R, Zehnder D, Hughes SV, Ronco PM, Stewart PM, Hewison M 2001 Regulation of vitamin D-1alpha-hydroxylase in a human cortical collecting duct cell line. Kidney Int 60:1277-1286

Bouillon R, Okamura WH, Norman AW 1995 Structure-function relationships in the vitamin D endocrine system. Endocr Rev 16:200-257

Bouillon R, Van Baelen H, Rombauts W, De Moor P 1976 The purification and characterisation of the human-serum binding protein for the 25-hydroxycholecalciferol (transcalciferin). Identity with group-specific component. Eur J Biochem 66:285-291

Bourbon HM, Aguilera A, Ansari AZ, Asturias FJ, Berk AJ, Bjorklund S, Blackwell TK, Borggrefe T, Carey M, Carlson M, Conaway JW, Conaway RC, Emmons SW, Fondell JD, Freedman LP, Fukasawa T, Gustafsson CM, Han M, He X, Herman PK, Hinnebusch AG, Holmberg S, Holstege FC, Jaehning JA, Kim YJ, Kuras L, Leutz A, Lis JT, Meisterernest M, Naar

AM, Nasmyth K, Parvin JD, Ptashne M, Reinberg D, Ronne H, Sadowski I, Sakurai H, Sipiczki M, Sternberg PW, Stillman DJ, Strich R, Struhl K, Svejstrup JQ, Tuck S, Winston F, Roeder RG, Kornberg RD 2004 A unified nomenclature for protein subunits of mediator complexes linking transcriptional regulators to RNA polymerase II. Mol Cell 14:553-557

Boyan BD, Sylvia VL, Curry D, Chang Z, Dean DD, Schwartz Z 1998 Arachidonic acid is an autocoid mediator of the differential action of 1,25-(OH)2D3 and 24,25-(OH)2D3 on growth plate chondrocytes. J Cell Physiol 176:516-524

Boyan BD, Sylvia VL, Dean DD, Del Toro F, Schwartz Z 2002 Differential regulation of growth plate chondrocytes by 1alpha,25-(OH)2D3 and 24R,25-(OH)2D3 involves cell-maturation-specific membrane-receptor-activated phospholipid metabolism. Crit Rev Oral Biol Med 13:143-154

Boyan BD, Sylvia VL, Dean DD, Pedrozo H, Del Toro F, Nemere I, Posner GH, Schwartz Z 1999 1,25-(OH)2D3 modulates growth plate chondrocytes via membrane receptor-mediated protein kinase C by a mechanism that involves changes in phospholipid metabolism and the action of arachidonic acid and PGE2. Steroids 64:129-136

Boyan BD, Wong KL, Fang M, Schwartz Z 2007 1alpha,25(OH)2D3 is an autocrine regulator of extracellular matrix turnover and growth factor release via ERp60 activated matrix vesicle metalloproteinases. J Steroid Biochem Mol Biol 103:467-472

Brenza HL, Kimmel-Jehan C, Jehan F, Shinki T, Wakino S, Anazawa H, Suda T, DeLuca HF 1998 Parathyroid hormone activation of the 25-hydroxyvitamin D3-1alpha-hydroxylase gene promoter. Proc Natl Acad Sci U S A 95:1387-1391

Brewer LD, Thibault V, Chen KC, Langub MC, Landfield PW, Porter NM 2001 Vitamin D hormone confers neuroprotection in parallel with downregulation of L-type calcium channel expression in hippocampal neurons. J Neurosci 21:98-108

Brighton CT, Hunt RM 1997 Early histologic and ultrastructural changes in microvessels of periosteal callus. J Orthop Trauma 11:244-253

Brown AJ, Slatopolsky E 2008 Vitamin D analogs: Therapeutic applications and mechanisms for selectivity. Mol Aspects Med

Brunette MG, Chan M, Ferriere C, Roberts KD 1978 Site of 1,25(OH)2 vitamin D3 synthesis in the kidney. Nature 276:287-289

Canterbury JM, Lerman S, Claflin AJ, Henry H, Norman A, Reiss E 1978 Inhibition of parathyroid hormone secretion by 25-hydroxycholecalciferol and 24,25-dihydroxycholecalciferol in the dog. J Clin Invest 61:1375-1383

Carlberg C, Bendik I, Wyss A, Meier E, Sturzenbecker LJ, Grippo JF, Hunziker W 1993 Two nuclear signalling pathways for vitamin D. Nature 361:657-660

Carter DR, Blenman PR, Beaupre GS 1988 Correlations between mechanical stress history and tissue differentiation in initial fracture healing. J Orthop Res 6:736-748

Casteels K, Waer M, Laureys J, Valckx D, Depovere J, Bouillon R, Mathieu C 1998 Prevention of autoimmune destruction of syngeneic islet grafts in spontaneously diabetic nonobese diabetic mice by a combination of a vitamin D3 analog and cyclosporine. Transplantation 65:1225-1232

Chen J, Thomas HF, Sodek J 1996 Regulation of bone sialoprotein and osteopontin mRNA expression by dexamethasone and 1,25-dihydroxyvitamin D3 in rat bone organ cultures. Connect Tissue Res 34:41-51

Chen JD, Evans RM 1995 A transcriptional co-repressor that interacts with nuclear hormone receptors. Nature 377:454-457

Chen Q, Johnson DM, Haudenschild DR, Goetinck PF 1995 Progression and recapitulation of the chondrocyte differentiation program: cartilage matrix protein is a marker for cartilage maturation. Dev Biol 172:293-306

Cheng JB, Levine MA, Bell NH, Mangelsdorf DJ, Russell DW 2004 Genetic evidence that the human CYP2R1 enzyme is a key vitamin D 25-hydroxylase. Proc Natl Acad Sci U S A 101:7711-7715

Chertow BS, Baker GR, Henry HL, Norman AW 1980 Effects of vitamin D metabolites on bovine parathyroid hormone release in vitro. Am J Physiol 238:E384-388

Colnot C, Thompson Z, Miclau T, Werb Z, Helms JA 2003 Altered fracture repair in the absence of MMP9. Development 130:4123-4133

Conklin BR, Bourne HR 1994 Homeostatic signals. Marriage of the flytrap and the serpent. Nature 367:22

Cross HS, Debiec H, Peterlik M 1990 Mechanism and regulation of intestinal phosphate absorption. Miner Electrolyte Metab 16:115-124

Danielian PS, White R, Lees JA, Parker MG 1992 Identification of a conserved region required for hormone dependent transcriptional activation by steroid hormone receptors. EMBO J 11:1025-1033

Dardenne O, Prud'homme J, Arabian A, Glorieux FH, St-Arnaud R 2001 Targeted inactivation of the 25-hydroxyvitamin D(3)-1(alpha)-hydroxylase gene (CYP27B1) creates an animal model of pseudovitamin D-deficiency rickets. Endocrinology 142:3135-3141

DeLuca HF 1988 The vitamin D story: a collaborative effort of basic science and clinical medicine. FASEB J 2:224-236

DeLuca HF 2004 Overview of general physiologic features and functions of vitamin D. Am J Clin Nutr 80:1689S-1696S

DeLuca HF, Schnoes HK 1976 Metabolism and mechanism of action of vitamin D. Annu Rev Biochem 45:631-666

Demay MB, Gerardi JM, DeLuca HF, Kronenberg HM 1990 DNA sequences in the rat osteocalcin gene that bind the 1,25-dihydroxyvitamin D3 receptor and confer responsiveness to 1,25-dihydroxyvitamin D3. Proc Natl Acad Sci U S A 87:369-373

Demay MB, Kiernan MS, DeLuca HF, Kronenberg HM 1992 Sequences in the human parathyroid hormone gene that bind the 1,25-dihydroxyvitamin D3 receptor and mediate transcriptional repression in response to 1,25-dihydroxyvitamin D3. Proc Natl Acad Sci U S A 89:8097-8101

Dunlop TW, Vaisanen S, Frank C, Molnar F, Sinkkonen L, Carlberg C 2005 The human peroxisome proliferator-activated receptor delta gene is a primary target of 1alpha,25-dihydroxyvitamin D3 and its nuclear receptor. J Mol Biol 349:248-260

Durand B, Saunders M, Gaudon C, Roy B, Losson R, Chambon P 1994 Activation function 2 (AF-2) of retinoic acid receptor and 9-cis retinoic acid receptor: presence of a conserved autonomous constitutive activating domain and influence of the nature of the response element on AF-2 activity. EMBO J 13:5370-5382

Dwivedi PP, Muscat GE, Bailey PJ, Omdahl JL, May BK 1998 Repression of basal transcription by vitamin D receptor: evidence for interaction of unliganded vitamin D receptor with two receptor interaction domains in RIP13delta1. J Mol Endocrinol 20:327-335

Endres B, Kato S, DeLuca HF 2000 Metabolism of 1alpha,25-dihydroxyvitamin D(3) in vitamin D receptor-ablated mice in vivo. Biochemistry 39:2123-2129

Erlebacher A, Filvaroff EH, Gitelman SE, Derynck R 1995 Toward a molecular understanding of skeletal development. Cell 80:371-378

Evans RM 1988 The steroid and thyroid hormone receptor superfamily. Science 240:889-895

Ferreira A 2006 Development of renal bone disease. Eur J Clin Invest 36 Suppl 2:2-12

Francis F, Strom TM, Hennig S, Boddrich A, Lorenz B, Brandau O, Mohnike KL, Cagnoli M, Steffens C, Klages S, Borzym K, Pohl T, Oudet C, Econs MJ, Rowe PS, Reinhardt R, Meitinger T, Lehrach H 1997 Genomic organization of the human PEX gene mutated in X-linked dominant hypophosphatemic rickets. Genome Res 7:573-585

Fraser DR, Kodicek E 1970 Unique biosynthesis by kidney of a biological active vitamin D metabolite. Nature 228:764-766

Fraser JD, Price PA 1988 Lung, heart, and kidney express high levels of mRNA for the vitamin K-dependent matrix Gla protein. Implications for the possible functions of matrix Gla protein and for the tissue distribution of the gamma-carboxylase. J Biol Chem 263:11033-11036

Fu GK, Lin D, Zhang MY, Bikle DD, Shackleton CH, Miller WL, Portale AA 1997 Cloning of human 25-hydroxyvitamin D-1 alpha-hydroxylase and mutations causing vitamin D-dependent rickets type 1. Mol Endocrinol 11:1961-1970

Fu GK, Portale AA, Miller WL 1997 Complete structure of the human gene for the vitamin D 1alpha-hydroxylase, P450c1alpha. DNA Cell Biol 16:1499-1507

Gardiner EM, Baldock PA, Thomas GP, Sims NA, Henderson NK, Hollis B, White CP, Sunn KL, Morrison NA, Walsh WR, Eisman JA 2000 Increased formation and decreased resorption of bone in mice with elevated vitamin D receptor in mature cells of the osteoblastic lineage. FASEB J 14:1908-1916

Gerstenfeld LC, Cho TJ, Kon T, Aizawa T, Tsay A, Fitch J, Barnes GL, Graves DT, Einhorn TA 2003 Impaired fracture healing in the absence of TNF-alpha signaling: the role of TNF-alpha in endochondral cartilage resorption. J Bone Miner Res 18:1584-1592

Gilchrest BA 2008 Sun exposure and vitamin D sufficiency. Am J Clin Nutr 88:570S-577S

Giuliano AR, Wood RJ 1991 Vitamin D-regulated calcium transport in Caco-2 cells: unique in vitro model. Am J Physiol 260:G207-212

Glorieux FH 1991 Rickets. Raven, New York

Haddad JG, Jr., Boisseau V, Avioli LV 1971 Placental transfer of vitamin D3 and 25-hydroxycholecalciferol in the rat. J Lab Clin Med 77:908-915

Hahn CN, Kerry DM, Omdahl JL, May BK 1994 Identification of a vitamin D responsive element in the promoter of the rat cytochrome P450(24) gene. Nucleic Acids Res 22:2410-2416

Hansen CM, Binderup L, Hamberg KJ, Carlberg C 2001 Vitamin D and cancer: effects of 1,25(OH)2D3 and its analogs on growth control and tumorigenesis. Front Biosci 6:D820-848

Harris F, Hoffenberg R, Black E 1965 Calcium kinetics in vitamin D deficiency rickets. I. Plasma kinetic studies after intravenous and oral Ca47. Metabolism 14:1101-1111

Harris F, Hoffenberg R, Black E 1965 Calcium kinetics in vitamin D deficiency rickets. II. Intestinal handling of calcium. Metabolism 14:1112-1121

Haussler MR, Mangelsdorf DJ, Komm BS, Terpening CM, Yamaoka K, Allegretto EA, Baker AR, Shine J, McDonnell DP, Hughes M, et al. 1988 Molecular biology of the vitamin D hormone. Recent Prog Horm Res 44:263-305

Heaney RP 1997 vitamin D: role in the calcium economy. In: Fieldman D, Glorieux FH, Pike JW (eds) Vitamin D. Academic Press, San Diego, pp 485-498]

Heath KM, Elovic EP 2006 Vitamin D deficiency: implications in the rehabilitation setting. Am J Phys Med Rehabil 85:916-923

Hebert SC, Brown EM, Harris HW 1997 Role of the Ca(2+)-sensing receptor in divalent mineral ion homeostasis. J Exp Biol 200:295-302

Henry HL, Norman AW 1978 Vitamin D: two dihydroxylated metabolites are required for normal chicken egg hatchability. Science 201:835-837

Henry HL, Taylor AN, Norman AW 1977 Response of chick parathyroid glands to the vitamin D metabolites, 1,25-dihydroxycholecalciferol and 24,25-dihydroxycholecalciferol. J Nutr 107:1918-1926

Hiltunen A, Vuorio E, Aro HT 1993 A standardized experimental fracture in the mouse tibia. J Orthop Res 11:305-312

Hirschfeld J 1959 A simple method of determining haptoglobin groups in human sera by means of agar-gel electrophoresis. Acta Pathol Microbiol Scand 47:169-172

Holick MF 2004 Vitamin D: importance in the prevention of cancers, type 1 diabetes, heart disease, and osteoporosis. Am J Clin Nutr 79:362-371

Horst RL, Wovkulich PM, Baggiolini EG, Uskokovic MR, Engstrom GW, Napoli JL 1984 (23S)-1,23,25-Trihydroxyvitamin D3: its biologic activity and role in 1 alpha,25-dihydroxyvitamin D3 26,23-lactone biosynthesis. Biochemistry 23:3973-3979

Hsu JY, Feldman D, McNeal JE, Peehl DM 2001 Reduced 1alpha-hydroxylase activity in human prostate cancer cells correlates with decreased susceptibility to 25-hydroxyvitamin D3-induced growth inhibition. Cancer Res 61:2852-2856

Hughes MR, Malloy PJ, Kieback DG, Kesterson RA, Pike JW, Feldman D, O'Malley BW 1988 Point mutations in the human vitamin D receptor gene associated with hypocalcemic rickets. Science 242:1702-1705

Ishizuka S, Norman AW 1987 Metabolic pathways from 1 alpha,25-dihydroxyvitamin D3 to 1 alpha,25-dihydroxyvitamin D3-26,23-lactone. Stereo-retained and stereo-selective lactonization. J Biol Chem 262:7165-7170

Iyama K, Ninomiya Y, Olsen BR, Linsenmayer TF, Trelstad RL, Hayashi M 1991 Spatiotemporal pattern of type X collagen gene expression and collagen deposition in embryonic chick vertebrae undergoing endochondral ossification. Anat Rec 229:462-472

Jiang H, Lin J, Su ZZ, Collart FR, Huberman E, Fisher PB 1994 Induction of differentiation in human promyelocytic HL-60 leukemia cells activates p21, WAF1/CIP1, expression in the absence of p53. Oncogene 9:3397-3406

Jones G 2008 Pharmacokinetics of vitamin D toxicity. Am J Clin Nutr 88:582S-586S

Kahlen JP, Carlberg C 1996 Functional characterization of a 1,25-dihydroxyvitamin D3 receptor binding site found in the rat atrial natriuretic factor promoter. Biochem Biophys Res Commun 218:882-886

Karp SJ, Schipani E, St-Jacques B, Hunzelman J, Kronenberg H, McMahon AP 2000 Indian hedgehog coordinates endochondral bone growth and morphogenesis via parathyroid hormone related-protein-dependent and -independent pathways. Development 127:543-548

Kato A, Seo EG, Einhorn TA, Bishop JE, Norman AW 1998 Studies on 24R,25-dihydroxyvitamin D3: evidence for a nonnuclear membrane receptor in the chick tibial fracture-healing callus. Bone 23:141-146

Kerry DM, Dwivedi PP, Hahn CN, Morris HA, Omdahl JL, May BK 1996 Transcriptional synergism between vitamin D-responsive elements in the rat 25-hydroxyvitamin D3 24-hydroxylase (CYP24) promoter. J Biol Chem 271:29715-29721

Kifor O, MacLeod RJ, Diaz R, Bai M, Yamaguchi T, Yao T, Kifor I, Brown EM 2001 Regulation of MAP kinase by calcium-sensing receptor in bovine parathyroid and CaR-transfected HEK293 cells. Am J Physiol Renal Physiol 280:F291-302

Kitanaka S, Takeyama K, Murayama A, Sato T, Okumura K, Nogami M, Hasegawa Y, Niimi H, Yanagisawa J, Tanaka T, Kato S 1998 Inactivating mutations in the 25-hydroxyvitamin D3 1alpha-hydroxylase gene in patients with pseudovitamin D-deficiency rickets. N Engl J Med 338:653-661

Kolek OI, Hines ER, Jones MD, LeSueur LK, Lipko MA, Kiela PR, Collins JF, Haussler MR, Ghishan FK 2005 1alpha,25-Dihydroxyvitamin D3 upregulates FGF23 gene expression in bone: the final link in a renal-gastrointestinal-skeletal axis that controls phosphate transport. Am J Physiol Gastrointest Liver Physiol 289:G1036-1042

Komatsu DE, Hadjiargyrou M 2004 Activation of the transcription factor HIF-1 and its target genes, VEGF, HO-1, iNOS, during fracture repair. Bone 34:680-688

Kream BE, Rowe D, Smith MD, Maher V, Majeska R 1986 Hormonal regulation of collagen synthesis in a clonal rat osteosarcoma cell line. Endocrinology 119:1922-1928

Kream BE, Rowe DW, Gworek SC, Raisz LG 1980 Parathyroid hormone alters collagen synthesis and procollagen mRNA levels in fetal rat calvaria. Proc Natl Acad Sci U S A 77:5654-5658

Kumar R 2002 1Alpha,25-dihydroxyvitamin D(3) - not just a calciotropic hormone. Nephron 91:576-581

Kurihara N, Ishizuka S, Kiyoki M, Haketa Y, Ikeda K, Kumegawa M 1986 Effects of 1,25-dihydroxyvitamin D3 on osteoblastic MC3T3-E1 cells. Endocrinology 118:940-947

Kuro-o M, Matsumura Y, Aizawa H, Kawaguchi H, Suga T, Utsugi T, Ohyama Y, Kurabayashi M, Kaname T, Kume E, Iwasaki H, Iida A, Shiraki-Iida T, Nishikawa S, Nagai R, Nabeshima YI 1997 Mutation of the mouse klotho gene leads to a syndrome resembling ageing. Nature 390:45-51

Kurose H, Yamaoka K, Okada S, Nakajima S, Seino Y 1990 1,25-Dihydroxyvitamin D3 [1,25-(OH)2D3] increases insulin-like growth factor I (IGF-I) receptors in clonal osteoblastic cells. Study on interaction of IGF-I and 1,25-(OH)2D3. Endocrinology 126:2088-2094

Labrie F, Luu-The V, Lin SX, Simard J, Labrie C, El-Alfy M, Pelletier G, Belanger A 2000 Intracrinology: role of the family of 17 beta-hydroxysteroid dehydrogenases in human physiology and disease. J Mol Endocrinol 25:1-16

Landfield PW, Cadwallader-Neal L 1998 Long-term treatment with calcitriol (1,25(OH)2 vit D3) retards a biomarker of hippocampal aging in rats. Neurobiol Aging 19:469-477

Lawson J 2002 Drug-induced metabolic bone disorders. Semin Musculoskelet Radiol 6:285-297

Le AX, Miclau T, Hu D, Helms JA 2001 Molecular aspects of healing in stabilized and non-stabilized fractures. J Orthop Res 19:78-84

Lemire JM, Archer DC, Beck L, Spiegelberg HL 1995 Immunosuppressive actions of 1,25-dihydroxyvitamin D3: preferential inhibition of Th1 functions. J Nutr 125:1704S-1708S

Lemon B, Inouye C, King DS, Tjian R 2001 Selectivity of chromatin-remodelling cofactors for ligand-activated transcription. Nature 414:924-928

Li JJ, Kim RH, Zhang Q, Ogata Y, Sodek J 1998 Characteristics of vitamin D3 receptor (VDR) binding to the vitamin D response element (VDRE) in rat bone sialoprotein gene promoter. Eur J Oral Sci 106 Suppl 1:408-417

Li YC, Amling M, Pirro AE, Priemel M, Meuse J, Baron R, Delling G, Demay MB 1998 Normalization of mineral ion homeostasis by dietary means prevents hyperparathyroidism, rickets, and osteomalacia, but not alopecia in vitamin D receptor-ablated mice. Endocrinology 139:4391-4396

Lin R, Amizuka N, Sasaki T, Aarts MM, Ozawa H, Goltzman D, Henderson JE, White JH 2002 1Alpha,25-dihydroxyvitamin D3 promotes vascularization of the chondro-osseous junction by stimulating expression of vascular endothelial growth factor and matrix metalloproteinase 9. J Bone Miner Res 17:1604-1612

Lin R, White JH 2004 The pleiotropic actions of vitamin D. Bioessays 26:21-28

Liu PT, Stenger S, Li H, Wenzel L, Tan BH, Krutzik SR, Ochoa MT, Schauber J, Wu K, Meinken C, Kamen DL, Wagner M, Bals R, Steinmeyer A, Zugel U, Gallo RL, Eisenberg D, Hewison M, Hollis BW, Adams JS, Bloom BR, Modlin RL 2006 Toll-like receptor triggering of a vitamin D-mediated human antimicrobial response. Science 311:1770-1773

Lusser A, Kadonaga JT 2003 Chromatin remodeling by ATP-dependent molecular machines. Bioessays 25:1192-1200

MacDonald PN, Dowd DR, Haussler MR 1994 New insight into the structure and functions of the vitamin D receptor. Semin Nephrol 14:101-118

Maglich JM, Sluder A, Guan X, Shi Y, McKee DD, Carrick K, Kamdar K, Willson TM, Moore JT 2001 Comparison of complete nuclear receptor sets from the human, Caenorhabditis elegans and Drosophila genomes. Genome Biol 2:RESEARCH0029

Majeska RJ, Rodan GA 1982 The effect of 1,25(OH)2D3 on alkaline phosphatase in osteoblastic osteosarcoma cells. J Biol Chem 257:3362-3365

Makin G, Lohnes D, Byford V, Ray R, Jones G 1989 Target cell metabolism of 1,25-dihydroxyvitamin D3 to calcitroic acid. Evidence for a pathway in kidney and bone involving 24-oxidation. Biochem J 262:173-180

Mangelsdorf DJ, Evans RM 1995 The RXR heterodimers and orphan receptors. Cell 83:841-850

Manolagas SC, Burton DW, Deftos LJ 1981 1,25-Dihydroxyvitamin D3 stimulates the alkaline phosphatase activity of osteoblast-like cells. J Biol Chem 256:7115-7117

Masuyama H, Jefcoat SC, Jr., MacDonald PN 1997 The N-terminal domain of transcription factor IIB is required for direct interaction with the vitamin D receptor and participates in vitamin D-mediated transcription. Mol Endocrinol 11:218-228

Masuyama R, Stockmans I, Torrekens S, Van Looveren R, Maes C, Carmeliet P, Bouillon R, Carmeliet G 2006 Vitamin D receptor in chondrocytes promotes osteoclastogenesis and regulates FGF23 production in osteoblasts. J Clin Invest 116:3150-3159

Matsumoto T, Igarashi C, Takeuchi Y, Harada S, Kikuchi T, Yamato H, Ogata E 1991 Stimulation by 1,25-dihydroxyvitamin D3 of in vitro mineralization induced by osteoblast-like MC3T3-E1 cells. Bone 12:27-32

Miles RR, Sluka JP, Santerre RF, Hale LV, Bloem L, Boguslawski G, Thirunavukkarasu K, Hock JM, Onyia JE 2000 Dynamic regulation of RGS2 in bone: potential new insights into parathyroid hormone signaling mechanisms. Endocrinology 141:28-36

Miller WL, Portale AA 2000 Vitamin D 1 alpha-hydroxylase. Trends Endocrinol Metab 11:315-319

Mirams M, Robinson BG, Mason RS, Nelson AE 2004 Bone as a source of FGF23: regulation by phosphate? Bone 35:1192-1199

Murayama A, Kim MS, Yanagisawa J, Takeyama K, Kato S 2004 Transrepression by a liganded nuclear receptor via a bHLH activator through co-regulator switching. EMBO J 23:1598-1608

Murayama A, Takeyama K, Kitanaka S, Kodera Y, Hosoya T, Kato S 1998 The promoter of the human 25-hydroxyvitamin D3 1 alpha-hydroxylase gene confers positive and negative responsiveness to PTH, calcitonin, and 1 alpha,25(OH)2D3. Biochem Biophys Res Commun 249:11-16

Murayama A, Takeyama K, Kitanaka S, Kodera Y, Kawaguchi Y, Hosoya T, Kato S 1999 Positive and negative regulations of the renal 25-hydroxyvitamin D3 1alpha-hydroxylase gene by parathyroid hormone, calcitonin, and 1alpha,25(OH)2D3 in intact animals. Endocrinology 140:2224-2231

Nakamura T, Nagai Y, Yamato H, Suzuki K, Orimo H 1992 Regulation of bone turnover and prevention of bone atrophy in ovariectomized beagle dogs by the administration of 24R,25(OH)2D3. Calcif Tissue Int 50:221-227

Negri AL 2006 Proximal tubule endocytic apparatus as the specific renal uptake mechanism for vitamin D-binding protein/25-(OH)D3 complex. Nephrology (Carlton) 11:510-515

Nemere I, Farach-Carson MC 1998 Membrane receptors for steroid hormones: a case for specific cell surface binding sites for vitamin D metabolites and estrogens. Biochem Biophys Res Commun 248:443-449

Nemere I, Farach-Carson MC, Rohe B, Sterling TM, Norman AW, Boyan BD, Safford SE 2004 Ribozyme knockdown functionally links a 1,25(OH)2D3 membrane binding protein (1,25D3-MARRS) and phosphate uptake in intestinal cells. Proc Natl Acad Sci U S A 101:7392-7397

Nemere I, Larsson D, Sundell K 2000 A specific binding moiety for 1,25-dihydroxyvitamin D(3) in basal lateral membranes of carp enterocytes. Am J Physiol Endocrinol Metab 279:E614-621

Nemere I, Schwartz Z, Pedrozo H, Sylvia VL, Dean DD, Boyan BD 1998 Identification of a membrane receptor for 1,25-dihydroxyvitamin D3 which mediates rapid activation of protein kinase C. J Bone Miner Res 13:1353-1359

Nemere I, Szego CM 1981 Early actions of parathyroid hormone and 1,25-dihydroxycholecalciferol on isolated epithelial cells from rat intestine: I. Limited lysosomal enzyme release and calcium uptake. Endocrinology 108:1450-1462

Niederreither K, D'Souza RN, de Crombrugghe B 1992 Minimal DNA sequences that control the cell lineage-specific expression of the pro alpha 2(I) collagen promoter in transgenic mice. J Cell Biol 119:1361-1370

Norman AW, Leathers V, Bishop JE 1983 Normal egg hatchability requires the simultaneous administration to the hen of 1 alpha,25-dihydroxycholecalciferol and 24R,25-dihydroxycholecalciferol. J Nutr 113:2505-2515

Nykjaer A, Dragun D, Walther D, Vorum H, Jacobsen C, Herz J, Melsen F, Christensen EI, Willnow TE 1999 An endocytic pathway essential for renal uptake and activation of the steroid 25-(OH) vitamin D3. Cell 96:507-515

Nykjaer A, Fyfe JC, Kozyraki R, Leheste JR, Jacobsen C, Nielsen MS, Verroust PJ, Aminoff M, de la Chapelle A, Moestrup SK, Ray R, Gliemann J, Willnow TE, Christensen EI 2001 Cubilin dysfunction causes abnormal metabolism of the steroid hormone 25(OH) vitamin D(3). Proc Natl Acad Sci U S A 98:13895-13900

Oldberg A, Jirskog-Hed B, Axelsson S, Heinegard D 1989 Regulation of bone sialoprotein mRNA by steroid hormones. J Cell Biol 109:3183-3186

Olsen BR, Reginato AM, Wang W 2000 Bone development. Annu Rev Cell Dev Biol 16:191-220

Ornoy A, Goodwin D, Noff D, Edelstein S 1978 24, 25-dihydroxyvitamin D is a metabolite of vitamin D essential for bone formation. Nature 276:517-519

Overbergh L, Decallonne B, Valckx D, Verstuyf A, Depovere J, Laureys J, Rutgeerts O, St-Arnaud R, Bouillon R, Mathieu C 2000 Identification and immune regulation of 25-hydroxyvitamin D-1-alpha-hydroxylase in murine macrophages. Clin Exp Immunol 120:139-146

Owen TA, Aronow M, Shalhoub V, Barone LM, Wilming L, Tassinari MS, Kennedy MB, Pockwinse S, Lian JB, Stein GS 1990 Progressive development of the rat osteoblast phenotype in vitro: reciprocal relationships in expression of genes associated with osteoblast proliferation and differentiation during formation of the bone extracellular matrix. J Cell Physiol 143:420-430

Paredes R, Arriagada G, Cruzat F, Olate J, Van Wijnen A, Lian J, Stein G, Stein J, Montecino M 2004 The Runx2 transcription factor plays a key role in the 1alpha,25-dihydroxy Vitamin D3-dependent upregulation of the rat osteocalcin (OC) gene expression in osteoblastic cells. J Steroid Biochem Mol Biol 89-90:269-271

Pavlin D, Bedalov A, Kronenberg MS, Kream BE, Rowe DW, Smith CL, Pike JW, Lichtler AC 1994 Analysis of regulatory regions in the COL1A1 gene responsible for 1,25-dihydroxyvitamin D3-mediated transcriptional repression in osteoblastic cells. J Cell Biochem 56:490-501

Pedrozo HA, Boyan BD, Mazock J, Dean DD, Gomez R, Schwartz Z 1999 TGFbeta1 regulates 25-hydroxyvitamin D3 1alpha- and 24-hydroxylase activity in cultured growth plate chondrocytes in a maturation-dependent manner. Calcif Tissue Int 64:50-56

Peng JB, Chen XZ, Berger UV, Vassilev PM, Tsukaguchi H, Brown EM, Hediger MA 1999 Molecular cloning and characterization of a channel-like transporter mediating intestinal calcium absorption. J Biol Chem 274:22739-22746

Penna G, Adorini L 2000 1 Alpha,25-dihydroxyvitamin D3 inhibits differentiation, maturation, activation, and survival of dendritic cells leading to impaired alloreactive T cell activation. J Immunol 164:2405-2411

Pettifor JM 2008 What's new in hypophosphataemic rickets? Eur J Pediatr 167:493-499

Potter GB, Zarach JM, Sisk JM, Thompson CC 2002 The thyroid hormone-regulated corepressor hairless associates with histone deacetylases in neonatal rat brain. Mol Endocrinol 16:2547-2560

Prosser DE, Jones G 2004 Enzymes involved in the activation and inactivation of vitamin D. Trends Biochem Sci 29:664-673

Proudfoot NJ, Furger A, Dye MJ 2002 Integrating mRNA processing with transcription. Cell 108:501-512

Prufer K, Veenstra TD, Jirikowski GF, Kumar R 1999 Distribution of 1,25-dihydroxyvitamin D3 receptor immunoreactivity in the rat brain and spinal cord. J Chem Neuroanat 16:135-145

Rachez C, Suldan Z, Ward J, Chang CP, Burakov D, Erdjument-Bromage H, Tempst P, Freedman LP 1998 A novel protein complex that interacts with the vitamin D3 receptor in a ligand-dependent manner and enhances VDR transactivation in a cell-free system. Genes Dev 12:1787-1800

Reddy GS, Tserng KY 1989 Calcitroic acid, end product of renal metabolism of 1,25-dihydroxyvitamin D3 through C-24 oxidation pathway. Biochemistry 28:1763-1769

Reichel H, Bishop JE, Koeffler HP, Norman AW 1991 Evidence for 1,25-dihydroxyvitamin D3 production by cultured porcine alveolar macrophages. Mol Cell Endocrinol 75:163-167

Rosen H, Reshef A, Maeda N, Lippoldt A, Shpizen S, Triger L, Eggertsen G, Bjorkhem I, Leitersdorf E 1998 Markedly reduced bile acid synthesis but maintained levels of cholesterol and vitamin D metabolites in mice with disrupted sterol 27-hydroxylase gene. J Biol Chem 273:14805-14812

Rosenfeld MG, Glass CK 2001 Coregulator codes of transcriptional regulation by nuclear receptors. J Biol Chem 276:36865-36868

Saito H, Kusano K, Kinosaki M, Ito H, Hirata M, Segawa H, Miyamoto K, Fukushima N 2003 Human fibroblast growth factor-23 mutants suppress Na+-dependent phosphate co-transport activity and 1alpha,25-dihydroxyvitamin D3 production. J Biol Chem 278:2206-2211

Sakaki T, Sawada N, Nonaka Y, Ohyama Y, Inouye K 1999 Metabolic studies using recombinant escherichia coli cells producing rat mitochondrial CYP24 CYP24 can convert 1alpha,25-dihydroxyvitamin D3 to calcitroic acid. Eur J Biochem 262:43-48

Sakaki T, Sawada N, Takeyama K, Kato S, Inouye K 1999 Enzymatic properties of mouse 25-hydroxyvitamin D3 1 alpha-hydroxylase expressed in Escherichia coli. Eur J Biochem 259:731-738

Saramaki A, Banwell CM, Campbell MJ, Carlberg C 2006 Regulation of the human p21(waf1/cip1) gene promoter via multiple binding sites for p53 and the vitamin D3 receptor. Nucleic Acids Res 34:543-554

Schedl HP, Ronnenberg W, Christensen KK, Hollis BW 1994 Vitamin D and enterocyte brush border membrane calcium transport and fluidity in the rat. Metabolism 43:1093-1103

Schipani E 2006 Hypoxia and HIF-1alpha in chondrogenesis. Ann N Y Acad Sci 1068:66-73

Schrader M, Muller KM, Nayeri S, Kahlen JP, Carlberg C 1994 Vitamin D3-thyroid hormone receptor heterodimer polarity directs ligand sensitivity of transactivation. Nature 370:382-386

Schwartz GG 1992 Multiple sclerosis and prostate cancer: what do their similar geographies suggest? Neuroepidemiology 11:244-254

Schwartz Z, Boyan B 1988 The effects of vitamin D metabolites on phospholipase A2 activity of growth zone and resting zone cartilage cells in vitro. Endocrinology 122:2191-2198

Schwartz Z, Schlader DL, Ramirez V, Kennedy MB, Boyan BD 1989 Effects of vitamin D metabolites on collagen production and cell proliferation of growth zone and resting zone cartilage cells in vitro. J Bone Miner Res 4:199-207

Schwartz Z, Schlader DL, Swain LD, Boyan BD 1988 Direct effects of 1,25-dihydroxyvitamin D3 and 24,25-dihydroxyvitamin D3 on growth zone and resting zone chondrocyte membrane alkaline phosphatase and phospholipase-A2 specific activities. Endocrinology 123:2878-2884

Seo EG, Einhorn TA, Norman AW 1997 24R,25-dihydroxyvitamin D3: an essential vitamin D3 metabolite for both normal bone integrity and healing of tibial fracture in chicks. Endocrinology 138:3864-3872

Seo EG, Kato A, Norman AW 1996 Evidence for a 24R,25(OH)2-vitamin D3 receptor/binding protein in a membrane fraction isolated from a chick tibial fracture-healing callus. Biochem Biophys Res Commun 225:203-208

Seo EG, Norman AW 1997 Three-fold induction of renal 25-hydroxyvitamin D3-24-hydroxylase activity and increased serum 24,25-dihydroxyvitamin D3 levels are correlated with the healing process after chick tibial fracture. J Bone Miner Res 12:598-606

Shimada T, Kakitani M, Yamazaki Y, Hasegawa H, Takeuchi Y, Fujita T, Fukumoto S, Tomizuka K, Yamashita T 2004 Targeted ablation of Fgf23 demonstrates an essential physiological role of FGF23 in phosphate and vitamin D metabolism. J Clin Invest 113:561-568

Shinki T, Ueno Y, DeLuca HF, Suda T 1999 Calcitonin is a major regulator for the expression of renal 25-hydroxyvitamin D3-1alpha-hydroxylase gene in normocalcemic rats. Proc Natl Acad Sci U S A 96:8253-8258

Shukunami C, Ishizeki K, Atsumi T, Ohta Y, Suzuki F, Hiraki Y 1997 Cellular hypertrophy and calcification of embryonal carcinoma-derived chondrogenic cell line ATDC5 in vitro. J Bone Miner Res 12:1174-1188

Sinkkonen L, Malinen M, Saavalainen K, Vaisanen S, Carlberg C 2005 Regulation of the human cyclin C gene via multiple vitamin D3-responsive regions in its promoter. Nucleic Acids Res 33:2440-2451

Sooy K, Sabbagh Y, Demay MB 2005 Osteoblasts lacking the vitamin D receptor display enhanced osteogenic potential in vitro. J Cell Biochem 94:81-87

St-Arnaud R, Arabian A, Travers R, Barletta F, Raval-Pandya M, Chapin K, Depovere J, Mathieu C, Christakos S, Demay MB, Glorieux FH 2000 Deficient mineralization of intramembranous bone in vitamin D-24-hydroxylase-ablated mice is due to elevated 1,25-dihydroxyvitamin D and not to the absence of 24,25-dihydroxyvitamin D. Endocrinology 141:2658-2666

St-Arnaud R, Prud'homme J, Leung-Hagesteijn C, Dedhar S 1995 Constitutive expression of calreticulin in osteoblasts inhibits mineralization. J Cell Biol 131:1351-1359

St-Jacques B, Hammerschmidt M, McMahon AP 1999 Indian hedgehog signaling regulates proliferation and differentiation of chondrocytes and is essential for bone formation. Genes Dev 13:2072-2086

Suda T, Takahashi N, Udagawa N, Jimi E, Gillespie MT, Martin TJ 1999 Modulation of osteoclast differentiation and function by the new members of the tumor necrosis factor receptor and ligand families. Endocr Rev 20:345-357

Sutton AL, MacDonald PN 2003 Vitamin D: more than a "bone-a-fide" hormone. Mol Endocrinol 17:777-791

Swain LD, Schwartz Z, Boyan BD 1992 1,25-(OH)2D3 and 24,25-(OH)2D3 regulation of arachidonic acid turnover in chondrocyte cultures is cell maturation-specific and may involve direct effects on phospholipase A2. Biochim Biophys Acta 1136:45-51

Sylvia VL, Schwartz Z, Del Toro F, DeVeau P, Whetstone R, Hardin RR, Dean DD, Boyan BD 2001 Regulation of phospholipase D (PLD) in growth plate chondrocytes by 24R,25-(OH)2D3 is dependent on cell maturation state (resting zone cells) and is specific to the PLD2 isoform. Biochim Biophys Acta 1499:209-221

Sylvia VL, Schwartz Z, Ellis EB, Helm SH, Gomez R, Dean DD, Boyan BD 1996 Nongenomic regulation of protein kinase C isoforms by the vitamin D

metabolites 1 alpha,25-(OH)2D3 and 24R,25-(OH)2D3. J Cell Physiol 167:380-393

Sylvia VL, Schwartz Z, Schuman L, Morgan RT, Mackey S, Gomez R, Boyan BD 1993 Maturation-dependent regulation of protein kinase C activity by vitamin D3 metabolites in chondrocyte cultures. J Cell Physiol 157:271-278

Takeyama K, Kitanaka S, Sato T, Kobori M, Yanagisawa J, Kato S 1997 25-Hydroxyvitamin D3 1alpha-hydroxylase and vitamin D synthesis. Science 277:1827-1830

Tanaka H, Seino Y 2004 Direct action of 1,25-dihydroxyvitamin D on bone: VDRKO bone shows excessive bone formation in normal mineral condition. J Steroid Biochem Mol Biol 89-90:343-345

Tanaka Y, DeLuca HF, Kobayashi Y, Taguchi T, Ikekawa N, Morisaki M 1979 Biological activity of 24,24-difluoro-25-hydroxyvitamin D3. Effect of blocking of 24-hydroxylation on the functions of vitamin D. J Biol Chem 254:7163-7167

Tang W, Ziboh VA, Isseroff RR, Martinez D 1987 Novel regulatory actions of 1 alpha,25-dihydroxyvitamin D3 on the metabolism of polyphosphoinositides in murine epidermal keratinocytes. J Cell Physiol 132:131-136

Tenenhouse HS 2005 Regulation of phosphorus homeostasis by the type iia na/phosphate cotransporter. Annu Rev Nutr 25:197-214

Terpstra L, Prud'homme J, Arabian A, Takeda S, Karsenty G, Dedhar S, St-Arnaud R 2003 Reduced chondrocyte proliferation and chondrodysplasia in mice lacking the integrin-linked kinase in chondrocytes. J Cell Biol 162:139-148

Thompson Z, Miclau T, Hu D, Helms JA 2002 A model for intramembranous ossification during fracture healing. J Orthop Res 20:1091-1098

Tuckermann JP, Pittois K, Partridge NC, Merregaert J, Angel P 2000 Collagenase-3 (MMP-13) and integral membrane protein 2a (Itm2a) are marker genes of chondrogenic/osteoblastic cells in bone formation: sequential temporal, and spatial expression of Itm2a, alkaline phosphatase, MMP-13, and osteocalcin in the mouse. J Bone Miner Res 15:1257-1265

Turner RT, Puzas JE, Forte MD, Lester GE, Gray TK, Howard GA, Baylink DJ 1980 In vitro synthesis of 1 alpha,25-dihydroxycholecalciferol and 24,25-dihydroxycholecalciferol by isolated calvarial cells. Proc Natl Acad Sci U S A 77:5720-5724

Vu TH, Shipley JM, Bergers G, Berger JE, Helms JA, Hanahan D, Shapiro SD, Senior RM, Werb Z 1998 MMP-9/gelatinase B is a key regulator of growth plate angiogenesis and apoptosis of hypertrophic chondrocytes. Cell 93:411-422

Wang TT, Nestel FP, Bourdeau V, Nagai Y, Wang Q, Liao J, Tavera-Mendoza L, Lin R, Hanrahan JW, Mader S, White JH 2004 Cutting edge: 1,25-dihydroxyvitamin D3 is a direct inducer of antimicrobial peptide gene expression. J Immunol 173:2909-2912

Weisinger JR, Favus MJ, Langman CB, Bushinsky DA 1989 Regulation of 1,25-dihydroxyvitamin D3 by calcium in the parathyroidectomized, parathyroid hormone-replete rat. J Bone Miner Res 4:929-935

Wu S, Finch J, Zhong M, Slatopolsky E, Grieff M, Brown AJ 1996 Expression of the renal 25-hydroxyvitamin D-24-hydroxylase gene: regulation by dietary phosphate. Am J Physiol 271:F203-208

Xu H, Bai L, Collins JF, Ghishan FK 2002 Age-dependent regulation of rat intestinal type IIb sodium-phosphate cotransporter by 1,25-(OH)(2) vitamin D(3). Am J Physiol Cell Physiol 282:C487-493

Yada Y, Ozeki T, Meguro S, Mori S, Nozawa Y 1989 Signal transduction in the onset of terminal keratinocyte differentiation induced by 1 alpha,25-dihydroxyvitamin D3: role of protein kinase C translocation. Biochem Biophys Res Commun 163:1517-1522

Yamada S, Yamamoto K, Takayama H, Hayashi T, Miyaura C, Tanaka H, Abe E, Suda T 1987 Isolation, identification, and chemical synthesis of 8 alpha,25-dihydroxy-9,10-seco-4,6,10(19)-cholestatrien-3-one. A new metabolite of 25-hydroxyvitamin D3 produced by mouse myeloid leukemia cells (M1). J Biol Chem 262:12939-12944

Yamamoto Y, Yoshizawa T, Fukuda T, Kawano H, Nakamura T, Yamada T, Karsenty G, Kato S 2004 A genetic evidence of direct VDR function in osteoblasts - Generation and analysis of osteoblast-specific VDRKO mice. J Bone Miner Res 19:S26

Yamate T, Tanaka H, Nagai Y, Yamato H, Taniguchi N, Nakamura T, Seino Y 1994 Bone-forming ability of 24R,25-dihydroxyvitamin D3 in the hypophosphatemic mouse. J Bone Miner Res 9:1967-1974

Yamato H, Okazaki R, Ishii T, Ogata E, Sato T, Kumegawa M, Akaogi K, Taniguchi N, Matsumoto T 1993 Effect of 24R,25-dihydroxyvitamin D3 on the formation and function of osteoclastic cells. Calcif Tissue Int 52:255-260

Yoshida T, Yoshida N, Monkawa T, Hayashi M, Saruta T 2001 Dietary phosphorus deprivation induces 25-hydroxyvitamin D(3) 1alpha-hydroxylase gene expression. Endocrinology 142:1720-1726

Zasloff M 2006 Fighting infections with vitamin D. Nat Med 12:388-390

Zierold C, Mings JA, DeLuca HF 2003 Regulation of 25-hydroxyvitamin D3-24-hydroxylase mRNA by 1,25-dihydroxyvitamin D3 and parathyroid hormone. J Cell Biochem 88:234-237

List of presentations at meetings

1- Canadian Connective Tissue Conference (CCTC), Montreal 2005 (Poster Presentation)
2- Gordon Research Conference (GRC) on Bones & Teeth, Biddeford 2005 (Poster Presentation)
3- CCTC, Ottawa 2006 (Poster Presentation)
4- Bone and Oral Healthcare Conference, Trois Riviere 2006 (Poster Presentation)
5- GRC on Bones & Teeth, Biddeford 2007 (Poster Presentation)
6- Advances in Mineral Metabolism (AIMM), Snowmass 2008, (Oral Presentation)
7- CCTC, Montreal 2008 (Oral Presentation)
8- American Society for Bone and Mineral Research, Montreal 2008 (Poster Presentation). R.P.Naja , A.Arabian, R.St-Arnaud 2008. Impaired fracture healing in the absence of the vitamin D-24-hydroxylase, Cyp24a1. J Bone Miner Res 2008; vol 23S1: S428.

Appendix A

Manuscript submitted to the journal

Endocrinology

CHONDROCYTE-SPECIFIC MODULATION OF THE EXPRESSION OF CYP27B1, THE 25-HYDROXYVITAMIN D-1α-HYDROXYLASE, SUPPORTS A ROLE FOR LOCAL SYNTHESIS OF 1,25-DIHYDROXYVITAMIN D_3 IN GROWTH PLATE DEVELOPMENT

Roy Pascal Naja[1,2], Olivier Dardenne[3], Alice Arabian[1], and René St-Arnaud[1,2,4,5]

[1]Genetics Unit, Shriners Hospital for Children, Montreal (Quebec) Canada H3G 1A6
[2]Department of Human Genetics, McGill University, Montreal, (Quebec) Canada H3A 2T5
[3]Current address: Liege University Center of Immunology, Institute of Pathology (CHU-B23), B-4000 Liege, Belgium
[4]Departments of Medicine and Surgery, McGill University, Montreal, (Quebec) Canada H3A 2T5

[5]Correspondence: René St-Arnaud
Genetics Unit
Shriners Hospital for Children
1529 Cedar Avenue
Montreal (Quebec) Canada H3G 1A6

Tel: (514) 282-7155
Fax: (514) 842-5581
E-Mail: rst-arnaud@shriners.mcgill.ca

Abbreviated title :role of Cyp27b1 in chondrocytes

Keywords: vitamin D; 25-hydroxyvitamin D-1-alpha-hydroxylase; Cyp27b1; chondrocytes; growth plate; endochondral bone formation.

Support: Shriners of North America (grant No. 8560)

ABSTRACT

The Cyp27b1 enzyme (25-hydroxyvitamin D-1alpha-hydroxylase) that converts 25-hydroxyvitamin D into the active metabolite, $1,25(OH)_2D_3$, is expressed in kidney, but also in other cell types such as chondrocytes. This suggests that local production of $1,25(OH)_2D_3$ could play an important role in the differentiation of these cells. To test this hypothesis, we have engineered mutant mice that do not express the *Cyp27b1* gene in chondrocytes. Inactivation of both alleles of the *Cyp27b1* gene led to decreased osteoclastogenesis, increased width of the hypertrophic zone of the growth plate at embryonic day 15.5, increased bone volume in neonatal long bones, and increased expression of the chondrocytic differentiation markers Indian Hedgehog and PTH/PTHrP receptor. The expression of the angiogenic marker VEGF was decreased, accompanied by decreased PECAM-1 staining in the neonatal growth plate, suggesting a delay in vascularization. In parallel, we have engineered strains of mice overexpressing a *Cyp27b1* transgene in chondrocytes by coupling the *Cyp27b1* cDNA to the collagen α_1(II) promoter. The transgenic mice showed a mirror image phenotype when compared to the tissue-specific inactivation, i.e. a reduction in the width of the hypertrophic zone of the embryonic growth plate, decreased bone volume in neonatal long bones, and inverse expression patterns of chondrocytic differentiation markers. These results support an intracrine role of $1,25(OH)_2D_3$ in endochondral ossification and chondrocyte development *in vivo*.

INTRODUCTION

The mitochondrial cytochrome P450 enzyme, 25-hydroxyvitamin D-1α-hydroxylase (Cyp27b1), catalyzes the conversion of $25OHD_3$ to 1,25-dihydroxyvitamin D_3 [$1,25(OH)_2D_3$], the hormonal form of the vitamin (1). This active metabolite, acting through its well-characterized vitamin D receptor (VDR) (2), is responsible for intestinal calcium and phosphorus absorption, mobilization of calcium from bone, and renal reabsorption of calcium and phosphorus (1). Expression of Cyp27b1 has long been thought to be confined to the proximal convoluted tubules of the kidney, and circulating concentrations of $1,25(OH)_2D_3$ primarily reflect its renal synthesis (1). However, Cyp27b1 expression was detected throughout the nephron (3) as well as in keratinocytes, macrophages, chondrocytes and osteoblasts (4). The identification of these extra-renal sites of expression of Cyp27b1 has led investigators to hypothesize that local production of $1,25(OH)_2D_3$ could play an important autocrine or paracrine role in the differentiation and function of these cells. Strong support for this model has been obtained for Toll-like receptor-mediated innate immunity in macrophages (5, 6). In bone, the classical view is that vitamin D exerts its effects indirectly via control of calcium and phosphate homeostasis, despite expression of Cyp27b1 and the VDR in osteoblasts and chondrocytes (7-9). However, recent molecular genetic studies have revealed direct, but non-essential roles for $1,25(OH)_2D_3$-mediated signaling in growth plate chondrocytes. Specific inactivation of the VDR in collagen type II-expressing chondrocytes leads to delayed osteoclastogenesis, which causes a transient increase in bone volume at the primary spongiosa (10).

We have generated both chondrocyte-specific *Cyp27b1* loss-of-function and overexpression mice models to further substantiate the physiological role of the 25-hydroxyvitamin D-1α-hydroxylase in growth plate chondrocytes. Our results agree with the phenotype observed in chondrocyte-specific VDR-ablated mice (10) and support a role for locally synthesized $1,25(OH)_2D_3$ in the neovascularization of the growth plate.

MATERIALS AND METHODS

Animals. Animal care and use followed the ethical guidelines of the Canadian Council on Animal Care and were reviewed and approved by the Institutional Animal Care and Use Committee. Mice heterozygous for the *Cyp27b1* null allele (11) were mated with Col2-Cre transgenic mice expressing the Cre recombinase under the control of the collagen α_1(II) chondrocyte-specific promoter (12) to obtain the Col2-Cre;$Cyp27b1^{+/-}$ genotype. These were mated to mice homozygous for a floxed Cyp27b1 allele (13) to yield mutant mice having one Cyp27b1 null allele, one floxed Cyp27b1 allele and transgenic for Col2-Cre (genotype: Col2Cre;$Cyp27b1^{-/fl}$; referred to as $Cyp27b1^{-/CH\Delta}$ herein).

The Col2-Cyp27b1 transgenic strain was engineered by subcloning the 1.6 kb *Cyp27b1* mouse cDNA fused in-frame with a C-terminal FLAG epitope between the β-globin intron and the SV40 polyadenylation signal of the pSI expression vector (Promega Corp. Madison, WI). The resulting minigene was excised and inserted between the collagen α_1(II) promoter fragment/first exon sequences and the collagen α_1(II) intron 1 and enhancer sequences (14). Plasmid construction details are available upon request. The transgene was excised, purified, and used for pronuclear injection performed by the Quebec Transgenesis Research Network (McGill University, Montréal, QC). Genotyping of all strains was performed using PCR under standard conditions (primer sequences available upon request).

Embryonic sample collection. Vaginal plugs were used as evidence of mating. Pregnant females were sacrificed 14 or 15 days later to give 14.5- or 15.5-day-old embryos (E14.5 or E15.5), respectively. Uterine horns were placed in 10 ml Petri dishes with 1X phosphate buffered saline (PBS) and individual embryos were dissected out and placed in a 10 ml falcon tube containing 4% paraformaldehyde (PFA) solution for overnight fixation (yolk sacs were kept for DNA extraction and subsequent genotyping). Embryonic hindlimbs were dissected out by using a Leica MZ6 dissecting microscope (Leica Microsystems, Richmond Hill, ON), to be embedded in paraffin. The paraffinized samples were sectioned at 5 μm and stained with Harris H&E.

Postnatal sample collection and processing. Tibias were collected at different ages (2, 14, and 42 days old) and fixed in 4% PFA overnight. The following day, samples were processed to be either

embedded in paraffin or methyl methacrylate (MMA).

Histomorphometry. The MMA embedded samples were sectioned at 5 μm. Histomorphometric analysis was performed using the BioQuant Osteo II imaging software (BioQuant Image analysis Corporation, Nashville, TN).

Microcomputed tomography (μCT) analysis. Scans were performed using a SkyScan 1072 instrument with a 12 bit cooled CCD – camera and a 1024 x 1024 pixels detector (Centre for Bone and Periodontal Research, McGill University).

Tartrate Resistant Acid Phosphatase (TRAP) staining. Osteoclast number was determined using TRAP staining. *Cyp27b1* chondrocyte-specific knockout ($Cyp27b1^{-/CH\Delta}$ & controls) E15.5 and two-day-old mice tibia sections were deparaffinized using four xylene washes (2 min each) followed by rehydration in 100, 95, and 70% ethanol solutions. The sections were then placed in acid-washed Coplin jars and incubated in media consisting of Complete Burstone's Media + 50 mM sodium tartrate pH 5.0 for 1 hr at 37°C. The sections were then washed with dH_2O for 10 min before being mounted with the water-soluble Vectashield (Vector Laboratories Inc, Burlington, ON) mounting media.

Proliferating Cell Nuclear Antigen (PCNA) staining. Chondrocyte proliferation was assayed using the PCNA Staining Kit (Zymed Laboratories Inc., Markham, ON). E15.5 sections were deparaffinized and epitope retrieval was performed by incubating the sections in 10 mM sodium citrate buffer, pH 6.0 at 95°C for 10 minutes. The sections were then washed with dH_2O and stained for PCNA following the manufacturer's instructions.

RNA isolation, Reverse Transcription and Real-Time PCR. Total RNA was isolated from the rib cartilage of $Cyp27b1^{-/CH\Delta}$ knockouts (2 and 14 days old) and Col2-Cyp27b1 transgenics (2 days old). The thoracic cage was dissected out using fine tools cleaned with RNAseZap (Ambion, Austin, Tx) to inactivate RNAses. The cartilaginous clear section between the mineralized sternum and the rest of the rib was carefully cut and placed in RNA*later* (Ambion) solution to be stored at -20°C or placed in 1 ml of Trizol reagent (Invitrogen, Carlsbad, CA) for immediate RNA extraction using the manufacturer's recommendations. Samples were then reverse-transcribed using either the Applied Biosystems High Capacity cDNA Reverse Transcription Kit (Applied Biosystems, Foster City, CA) or the High Capacity cDNA Archive kit (Applied Biosystems). The relative expression of different chondrocyte differentiation markers and housekeeping genes was quantified using Reverse Transcription-quantitative PCR (RT-qPCR) on the reverse transcribed mRNA from different samples with specific TaqMan (Applied Biosystems) probes. Following the manufacturer's instructions, 100 ng of double-stranded cDNA was added to a mix of TaqMan probes, Universal PCR Master Mix (Applied Biosystems), and RNAse free water. The RT-qPCR reaction was performed in an Applied Biosystems 7500 instrument (Applied Biosystems). Quantitative analysis was done using the comparative ΔC_t method and relative expression was normalized to *Gapdh*.

Immunohistochemistry. Platelet/endothelial cell adhesion molecule-1 (PECAM-1, also known as CD31) immunostaining was performed on the tibial primary growth plate of two-day-old $Cyp27b1^{-/CH\Delta}$ knockouts and control littermates. After deparaffinization, 3% hydrogen peroxide in 1X PBS was added to the sections for 10 min in order to block endogenous peroxidase activity. The sections were then washed with 1X PBS and blocked in a solution of 1.5% horse serum in 1X PBS. Following blocking, the sections were incubated with 10 μg/ml of PECAM-1 (M-20) goat polyclonal primary antibody (Santa Cruz Biotechnology Inc., Santa Cruz, CA) in a humidified chamber for one hr at room temperature. The sections were then washed with 1X PBS and incubated with 5 μg/ml of biotinylated anti-goat secondary antibody (Vector Laboratories) in a humidified chamber for 30 min at room temperature. The sections were then washed with 1X PBS and signals were detected using the ABC Staining System Kit (Santa Cruz) following the manufacturer's recommendations.

Fgf23 ELISA. Peripheral blood was collected from 10-day-old $Cyp27b1^{-/CH\Delta}$ mice and controls. The blood was spun for 10 min at 6000 *g* after which the aqueous supernatant serum was harvested. Fifty μl of serum were used to measure Fgf23 levels using the FGF23 ELISA kit (Kainos Laboratories, Japan) following the manufacturer's recommendations.

25OHD$_3$ supplementation. Eighteen ng (0.044 nmol) of 25-hydroxyvitamin D_3 (25OHD$_3$) (Hoechst Marion Roussel Inc., Cincinnati, OH) was subcutaneously injected daily into females starting one week after plug detection, until delivery.

Offsprings were sacrificed two days later and tibias were collected and processed into 70% ethanol solution for μCT analysis. The ribcage was also collected and kept in RNA*later* at -20°C for further RNA extraction and RT-qPCR.

Image acquisition. All sections were viewed on a Leica DM-R microscope (Leica Microsystems) and the images were acquired using an Olympus DP70 camera (GE Healthcare Bio-Sciences, Baie d'Urfe, QC) and processed by the DPController software.

Statistics. Results are expressed as the mean ± SEM. To assess the effect of genotype, data were compared by using the two-tailed student *t* test with the Graphpad Prism 4 software. $P<0.05$ was accepted as significant.

RESULTS

Chondrocyte-specific *Cyp27b1* loss-of-function. To examine the putative paracrine, autocrine, or intracrine role of locally synthesized $1,25(OH)_2D_3$ in growth plate chondrocytes, we generated mice having one *Cyp27b1* null allele, one floxed *Cyp27b1* allele, and transgenic for Cre recombinase under the control of the collagen α_1(II) promoter. The resulting animals (referred to as $Cyp27b1^{-/CH\Delta}$) thus have inactive *Cyp27b1* in chondrocytes but have a floxed functional allele in all other tissues. The expression of the Cre recombinase in mutant animals was confirmed by RT-qPCR performed on RNA extracted from two-day-old rib chondrocytes (Supplementary Fig. 1A). The efficiency of chondrocyte-specific *Cyp27b1* inactivation was assessed at both the DNA and RNA levels. Correct excision of the floxed *Cyp27b1* exon was demonstrated by Southern Blot analysis and PCR amplification of tail-extracted DNA from 15-day-old $Cyp27b1^{-/CH\Delta}$ mice (data not shown). Analysis of *Cyp27b1* mRNA was done by RT-qPCR on RNA extracted form two-day-old rib chondrocytes. *Cyp27b1* expression and all parameters examined were similar in all control genotypes ($Cyp27b1^{+/fl}$; $Cyp27b1^{-/fl}$; Col2-Cre;$Cyp27b1^{+/fl}$) (Supplementary Fig. 1B and data not shown), and results from these animals are grouped and expressed as 'controls'. Expression of *Cyp27b1* was significantly reduced in samples from $Cyp27b1^{-/CH\Delta}$ mutant mice (Supplementary Fig. 1B).

Reduced *Cyp27b1* levels affects embryonic chondrocyte development and neonatal endochondral ossification. To examine the effect of reduced *Cyp27b1* expression on chondrocyte development, long bones were collected at intervals and examined using histomorphometry and μCT. Measurement of the hypertrophic zone of H&E stained embryonic day 15.5 (E15.5) tibia showed a significant increase in the size of this zone in $Cyp27b1^{-/CH\Delta}$ mice as compared to controls (Fig. 1A). This was not due to increased chondrocyte proliferation as PCNA staining was identical between $Cyp27b1^{-/CH\Delta}$ mice and controls (data not shown). The increased size of the hypertrophic zone in the developing limb did not persist at the neonatal stage (Fig. 1B). On the other hand, the metaphyseal trabecular bone was increased at postnatal day 2. Microcomputed tomography of the region encompassing the primary and secondary spongiosa of the bones showed an increase in bone volume, trabecular thickness, trabecular number, and a decrease in trabecular separation in $Cyp27b1^{-/CH\Delta}$ mice as compared to the controls (Fig. 2). This phenotype was transient and all histomorphometric parameters showed no statistically significant differences between controls and $Cyp27b1^{-/CH\Delta}$ mice at 14 or 42 days of age (data not shown).

Decreased osteoclast recruitment in embryonic and neonatal $Cyp27b1^{-/CH\Delta}$ mutant mice. Masuyama et al. (10) observed an increased bone volume in neonatal chondrocyte-specific VDR knockouts, which they attributed to a decrease in osteoclast recruitment at the chondro-osseous junction at two days of age. This was also observed in the E15.5 cartilaginous anlagen of $Cyp27b1^{-/CH\Delta}$ mice. We used TRAP staining to detect activated osteoclasts, which were reduced in number at the E15.5 femoral ossification center in $Cyp27b1^{-/CH\Delta}$ mice when compared to controls (Fig. 3A,B,E). TRAP staining was also performed on two-day-old long bones, where we observed a reduced number of osteoclasts bordering the last row of hypertrophic chondrocytes at the chondro-osseous junction in $Cyp27b1^{-/CH\Delta}$ mice as compared to controls (Fig. 3C,D,F).

Reduced/delayed vascularization in neonatal $Cyp27b1^{-/CH\Delta}$ mice. The ribcage contains a growth plate that can be dissected out to give a sample tissue enriched in chondrocytic cells. This was performed and RNA extracted from these samples was used in RT-qPCR reactions. Expression of Vascular Endothelial Growth Factor (VEGF) as well as its receptor (Kdr/VEGFR2) was reduced in $Cyp27b1^{-/CH\Delta}$ mice (Fig. 4A,B). No change in the expression of Mmp13, a marker of chondrocyte

differentiation involved in angiogenesis (15), was detected (Fig. 4C). The differences in the mRNA expression of angiogenic markers prompted us to check vascularization of the neonatal epiphysis using PECAM-1 immunostaining of two-day-old tibias. We observed reduced PECAM-1 staining in Cyp27b1$^{-/CH\Delta}$ mice (Fig. 4D,E). PECAM-1, also known as CD31, is a marker of the endothelial cells forming the blood vessels and its reduction suggests a decrease in vascularization at the chondro-osseous junction.

Decreased *Cyp27b1* expression perturbs neonatal chondrocyte differentiation. We also analyzed expression of chondrocytic markers by RT-qPCR on RNA extracted from rib chondrocytes at postnatal day 2. Indian Hedgehog (*Ihh*) and parathyroid hormone/parathyroid hormone related peptide receptor (*Pthr1*) mRNA expression were increased in Cyp27b1$^{-/CH\Delta}$ mice as compared to controls (Supplementary Fig. 2). No difference in collagen α_1(II), collagen type X, and *Hif1α* expression levels could be measured (Supplementary Fig. 2). The altered expression of chondrocyte differentiation markers did not persist beyond the early neonatal period and gene expression patterns were normalized at 14 or 42 days of age (data not shown). In contrast to what was reported in the chondrocyte-specific VDR-ablated mice (10), *RANKL* mRNA levels remained unchanged in neonatal Cyp27b1$^{-/CH\Delta}$ mice (not shown). The serum levels of Fgf23 were measured in 10-day-old mice and found to be significantly decreased in Cyp27b1$^{-/CH\Delta}$ mice as compared to controls (Fig. 5), a result that agrees with the findings in chondrocyte-specific VDR ablated mice (10).

Chondrocyte-specific Cyp27b1 overexpression. We contrasted the phenotype of the chondrocyte-specific ablation of *Cyp27b1* with that of transgenic mice specifically overexpressing *Cyp27b1* in chondrocytes. The *Cyp27b1* cDNA was fused in frame with the FLAG epitope sequence at its 3'end and subcloned between a chimeric intron and a polyadenylation stop sequence under the control of the collagen α_1(II) promoter elements (Supplementary Fig. 3A). The expression of the transgenic recombinant molecule was first confirmed in transient transfections of the chondrocytic ATDC5 cell line (16) (data not shown). The transgene was then injected in fertilized eggs, which resulted in a transgenic line expressing high levels of *Cyp27b1* mRNA and protein in chondrocytes (strain 5Tg, Supplementary Fig. 3B,C).

Increased Cyp27b1 levels affect embryonic chondrocyte development. We collected long bones from Col2-Cyp27b1 transgenics at intervals and examined their phenotype by histomorphometry and μCT. Measurement of the hypertrophic zone of H&E stained E14.5 tibia showed a reduction in the size of this zone in transgenic mice as compared to wild-types (Fig. 6A). Under euvitaminic conditions, the metaphyseal trabecular bone of Col2-Cyp27b1 transgenic mice was not altered at postnatal day 2 or 42 (data not shown). Similarly, no changes in the mRNA expression of *VEGF*, *Kdr*, or *Mmp13* were measured between the transgenic and wild-type mice at postnatal day 2 (data not shown). However, *Ihh* and *Hif1α* mRNA expression was decreased in transgenic mice (Supplementary Fig. 4C,D), a reciprocal gene expression pattern when compared to results obtained with the tissue-specific *Cyp27b1* loss-of-function model. No changes in collagen α_1(II), collagen type X, and *Pthr1* expression were detected (Supplementary Fig. 4A,B,E). Similar to what was observed in Cyp27b1$^{-/CH\Delta}$ mice, the altered expression of chondrocyte differentiation markers did not persist beyond the nenonatal period as mRNA levels were equal between transgenic mice and controls at 14 or 42 days of age (not shown).

25OHD$_3$ supplementation results in a metaphyseal bone phenotype in Col2-Cyp27b1 transgenic mice. One possible explanation for the absence of changes in metaphyseal bone volume in Col2-Cyp27b1 transgenics might be limiting substrate availability for the overexpressed Cyp27b1 enzyme. To test this possibility, 25OHD$_3$, a metabolite that crosses the placenta (17), was administered to gestating females. Microcomputed tomography of the primary spongiosa of 2-day old bones was then performed, which revealed a decrease in bone volume, trabecular thickness, and trabecular number in the treated transgenic mice as compared to wild-types (Fig. 6B,C,D). This decrease in metaphyseal bone volume in the transgenics represents a mirror image phenotype to what was observed in Cyp27b1$^{-/CH\Delta}$ mice. A change in the angiogenic markers was also expected to accompany this bone volume change, however, RT-qPCR performed on RNA extracted from the 2-day old rib cartilage showed no difference in *VEGF*, its

receptor *Kdr*, or *RANKL* mRNA expression (Supplementary Fig. 5).

DISCUSSION

Vitamin D is classically thought to exert its effects on bone indirectly via control of calcium and phosphate homeostasis, despite expression of Cyp27b1 and the VDR in osteoblasts and chondrocytes (7-9). However, aberrant growth plate development appears prior to the onset of hypocalcemia in VDR-deficient mice (18), supporting a defined role for $1,25(OH)_2D_3$-mediated signaling in endochondral bone formation. A role for $1,25(OH)_2D_3$ in growth plate function is further supported by the observation that rescuing mineral homeostasis of *Cyp27b1*-deficient mice with a high calcium, high lactose diet corrected all aspects of the phenotype, except long bone growth (19). Recently, chondrocyte-specific ablation of the VDR was shown to cause delays in osteoclastogenesis, creating neonatal increases in bone volume at the chondro-osseous junction (10). The source of the $1,25(OH)_2D_3$ ligand that affect chondrocytes remains undetermined, however. To test the hypothesis that local production of $1,25(OH)_2D_3$ plays a role in the growth, differentiation, or function of growth plate cells, we engineered mice strains in which *Cyp27b1* was either ablated or overexpressed in chondrocytes.

One might propose that a major portion of the active $1,25(OH)_2D_3$ metabolite found in cartilage is derived systemically and that against the levels of circulating D hormone, any local synthesis may represent an insignificant contribution. During development, vitamin D and $25OHD_3$, but not $1,25(OH)_2D_3$, cross the placenta (17). Thus local synthesis of the active vitamin D metabolite may be essential to the regulation of target cell differentiation and function. Moreover, a recent concept in the field of sex steroids is intracrinology (20). A significant proportion of androgens (approximately 50%) and estrogens (approximately 75% before menopause, and close to 100% after menopause) are produced in peripheral hormone-target tissues that express steroid metabolic enzymes. These locally produced bioactive androgens and/or estrogens exert their action in the cells where synthesis occurs without release in the extracellular space, including circulation. Thus despite central steroidogenesis in the gonads, peripheral target tissues utilize 'on the spot' intracellular hormone synthesis/action to regulate their function (20). Support for such a mode of action for vitamin D was recently obtained through the study of macrophage-mediated innate immunity (5, 6). Liu et al. (5) identified both the VDR and *CYP27B1* as induced genes in TLR-activated macrophages. The TLR-mediated up-regulation of the expression of the VDR and *CYP27B1* provokes the intracrine $1,25(OH)_2D_3$-dependent induction of cathelicidin and increased microbicidal activity of the macrophages (6). These results demonstrate the physiological relevance of extra-renal *Cyp27b1* expression in peripheral target tissues.

The mating strategy that yielded the chondrocyte-specific *Cyp27b1* mutant mice ($Cyp27b1^{-/CH\Delta}$) generated three genotypically different control populations ($Cyp27b1^{+/fl}$; $Cyp27b1^{-/fl}$; Col2-Cre;$Cyp27b1^{+/fl}$). The phenotype of these three populations was identical and *Cyp27b1* expression was not affected (data not shown), demonstrating the absence of gene dosage effects or of any influence of the Col2-Cre transgene. Results from these animals were thus pooled in a single control group. In the $Cyp27b1^{-/CH\Delta}$ mutant mice, the expression of *Cyp27b1* was reduced by 47%, a significant change that yielded a phenotypic manifestation. The remaining Cyp27b1 mRNA expression could be due to incomplete penetrance of the Col2-Cre-mediated excision or, more likely, to contamination from Cyp27b1 expressing osteoblasts (residing in the sternum and in the bony part of the ribs) dissected out along with the cartilaginous section of the ribs.

The phenotype observed in $Cyp27b1^{-/CH\Delta}$ mutant mice included enhanced *Ihh* expression and increased metaphyseal bone volume. Interestingly, these phenotypic manifestations were modulated in reciprocal fashion in the Col2-Cyp27b1 transgenic mice. This mirror image phenotype of the chondrocyte-specific overexpression model when compared to the tissue-specific ablation model provides further support for a role of locally synthesized $1,25(OH)_2D_3$. The effect of the Col2-Cyp27b1 transgene on decreasing metaphyseal bone volume was also observed in a different strain expressing lower levels of the recombinant protein (strain 3Tg, supplementary Fig. 3), confirming that the phenotype is not an artifact of the integration site (data not shown).

Ihh is a stimulator of chondrocyte proliferation and an inhibitor of chondrocyte hypertrophy (21). Despite a stimulation in the expression of *Ihh* mRNA, we measured an increase in the size of the

hypertrophic zone without changes in chondrocyte proliferation in Cyp27b1$^{-/CH\Delta}$ mutant mice (Fig. 1 and data not shown). Expression of hedgehog family members is highly regulated at both the post-transcriptional and post-translational levels (22, 23). We did not measure Ihh protein expression in the developing limbs of Cyp27b1$^{-/CH\Delta}$ or Col2-Cyp27b1 mice and it remains a possibility that the observed changes in mRNA levels were not accompanied by similar changes in protein levels, which would explain the apparent discrepancy.

Based on the phenotype of Cyp27b1$^{-/CH\Delta}$ mutant mice, we propose the following model: locally synthesized $1,25(OH)_2D_3$ regulates VEGF expression and signaling in the developing growth plate. In the absence of Cyp27b1, decreased VEGF expression would lead to a decrease in blood vessel formation. In turn, the vasculature delay reduces osteoclast invasion at the chondro-osseous junction. Since osteoclasts resorb the calcified cartilaginous matrix that serves as the scaffold for woven bone formation, a reduction in osteoclast invasion would result in an increased scaffold size and thus a larger bone volume at the primary spongiosa. The model predicts that this phenotype is transient as blood vessels eventually invade the chondro-osseous junction and normalize osteoclast recruitment and bone turnover.

This model is supported in part by our observations and by published results: we have measured decreased *VEGF* mRNA levels in chondrocytes from Cyp27b1$^{-/CH\Delta}$ mutant mice (Fig. 4). Similarly, *VEGF* mRNA levels were significantly reduced in mutant newborn growth plates from chondrocyte-specific VDR knockout mice (10). We also observed a reduction in the protein levels of the endothelial cell/blood vessel marker PECAM-1 (Fig. 4), which is consistent with decreased blood vessel formation. Immunodetection of endothelial cells in developing tibia of chondrocyte-specific VDR mutant mice revealed a similar reduction in the number of invading blood vessels in the growth plate (10). Both genetic models are consistent with and support the observation that short-term treatment of mice with $1,25(OH)_2D_3$, under conditions where calcemia is not perturbed, induces changes in *VEGF* expression and promotes vascularization of the chondro-osseous junction (24). It would prove interesting to attempt rescue of the decreased angiogenesis phenotype of Cyp27b1$^{-/CH\Delta}$ mice by mating to chondrocyte-specific VEGF transgenic mice.

In the chondrocyte-specific VDR-ablated mice, Masuyama et al. (10) reported a reduction in the number of osteoclasts and a decrease in *RANKL* expression. We also observed reduced osteoclastogenesis at E15.5 and at the chondro-osseous junction of neonatal Cyp27b1$^{-/CH\Delta}$ mutant mice (Fig. 3). However, we did not measure reduced expression of *RANKL* in rib cartilage or femoral epiphyses from Cyp27b1$^{-/CH\Delta}$ animals (data not shown). This result may be explained by contamination from surrounding osteoblasts that secrete RANKL, and would mask modest differences in expression levels from chondrocytes. The expression of Fgf23 was reduced in the metaphysis of chondrocyte-specific VDR mutant mice (10). In accordance with this report, we have also measured a decrease in serum levels of Fgf23 in 10 day-old Cyp27b1$^{-/CH\Delta}$ mice. The mechanisms that explain the regulation of Fgf23 expression by $1,25(OH)_2D_3$ at the growth plate remain to be completely determined but appear to involve a $1,25(OH)_2D_3$-induced secreted factor from chondrocytes that affects Fgf23 production by neighboring osteoblasts (10).

Taken together, the results from genetic manipulation of the expression of *Cyp27b1* (herein) or the VDR (10) in chondrocytes strongly support a direct role for locally synthesized $1,25(OH)_2D_3$, acting through the VDR, in vascular invasion and osteoclastogenesis during endochondral bone development.

ACKNOWLEDGMENTS

This work was supported by the Shriners of North America through grant No. 8560 to R.St-A. We thank Dr. Gerard Karsenty (Columbia University) for his generous gift of the plasmid containing the collagen α_1(II) promoter fragment/first exon sequences and the collagen α_1(II) intron 1 and enhancer sequences. Mia Esser, Louise Marineau, Nathalie Guevremont, and Nathalie Girard provided expert animal care assistance. Guylaine Bédard prepared the figures. R.P. Naja was a Canada Bone Scholar supported in part by the CIHR Skeletal Health Training Grant. We used the SkyScan μCT instrument from the Centre for Bone and Periodontal Research of McGill University.

REFERENCES

1. **DeLuca HF** 2004 Overview of general physiologic features and functions of vitamin D. Am J Clin Nutr 80:1689S-1696S

2. **Haussler MR, Whitfield GK, Haussler CA, Hsieh JC, Thompson PD, Selznick SH, Dominguez CE, Jurutka PW** 1998 The nuclear vitamin D receptor: biological and molecular regulatory properties revealed. J Bone Miner Res 13:325-349

3. **Zehnder D, Bland R, Walker EA, Bradwell AR, Howie AJ, Hewison M, Stewart PM** 1999 Expression of 25-hydroxyvitamin D3-1alpha-hydroxylase in the human kidney. J Am Soc Nephrol 10:2465-2473.

4. **Miller WL, Portale AA** 2000 Vitamin D 1alpha-Hydroxylase. Trends Endocrinol Metab 11:315-319

5. **Liu PT, Stenger S, Li H, Wenzel L, Tan BH, Krutzik SR, Ochoa MT, Schauber J, Wu K, Meinken C, Kamen DL, Wagner M, Bals R, Steinmeyer A, Zugel U, Gallo RL, Eisenberg D, Hewison M, Hollis BW, Adams JS, Bloom BR, Modlin RL** 2006 Toll-like receptor triggering of a vitamin D-mediated human antimicrobial response. Science 311:1770-1773

6. **Zasloff M** 2006 Fighting infections with vitamin D. Nat Med 12:388-390

7. **Boivin G, Mesguich P, Pike JW, Bouillon R, Meunier PJ, Haussler MR, Dubois PM, Morel G** 1987 Ultrastructural immunocytochemical localization of endogenous 1,25- dihydroxyvitamin D3 and its receptors in osteoblasts and osteocytes from neonatal mouse and rat calvaria. Bone Miner 3:125-136.

8. **Johnson JA, Grande JP, Roche PC, Kumar R** 1996 Ontogeny of the 1,25-dihydroxyvitamin D3 receptor in fetal rat bone. J Bone Miner Res 11:56-61.

9. **Narbaitz R, Stumpf WE, Sar M, Huang S, DeLuca HF** 1983 Autoradiographic localization of target cells for 1 alpha, 25- dihydroxyvitamin D3 in bones from fetal rats. Calcif Tissue Int 35:177-182

10. **Masuyama R, Stockmans I, Torrekens S, Van Looveren R, Maes C, Carmeliet P, Bouillon R, Carmeliet G** 2006 Vitamin D receptor in chondrocytes promotes osteoclastogenesis and regulates FGF23 production in osteoblasts. J Clin Invest 116:3150-3159

11. **Dardenne O, Prud'homme J, Arabian A, Glorieux FH, St-Arnaud R** 2001 Targeted inactivation of the 25-hydroxyvitamin D(3)-1(alpha)- hydroxylase gene (CYP27B1) creates an animal model of pseudovitamin D- deficiency rickets. Endocrinology 142:3135-3141

12. **Terpstra L, Prud'homme J, Arabian A, Takeda S, Karsenty G, Dedhar S, St-Arnaud R** 2003 Reduced chondrocyte proliferation and chondrodysplasia in mice lacking the integrin-linked kinase in chondrocytes. J Cell Biol 162:139-148

13. **St-Arnaud R, Dardenne O, Prud'homme J, Hacking SA, Glorieux FH** 2003 Conventional and tissue-specific inactivation of the 25-hydroxyvitamin D-1alpha-hydroxylase (CYP27B1). J Cell Biochem 88:245-251

14. **Niederreither K, D'Souza RN, de Crombrugghe B** 1992 Minimal DNA sequences that control the cell lineage-specific expression of the pro alpha 2(I) collagen promoter in transgenic mice. J Cell Biol 119:1361-1370

15. **Tuckermann JP, Pittois K, Partridge NC, Merregaert J, Angel P** 2000 Collagenase-3 (MMP-13) and integral membrane protein 2a (Itm2a) are marker genes of chondrogenic/osteoblastic cells in bone

formation: sequential temporal, and spatial expression of Itm2a, alkaline phosphatase, MMP-13, and osteocalcin in the mouse. J Bone Miner Res 15:1257-1265

16. **Shukunami C, Ishizeki K, Atsumi T, Ohta Y, Suzuki F, Hiraki Y** 1997 Cellular hypertrophy and calcification of embryonal carcinoma-derived chondrogenic cell line ATDC5 in vitro. J Bone Miner Res 12:1174-1188

17. **Haddad JG, Jr., Boisseau V, Avioli LV** 1971 Placental transfer of vitamin D3 and 25-hydroxycholecalciferol in the rat. J Lab Clin Med 77:908-915

18. **Li YC, Pirro AE, Amling M, Delling G, Baron R, Bronson R, Demay MB** 1997 Targeted ablation of the vitamin D receptor: an animal model of vitamin D-dependent rickets type II with alopecia. Proc Natl Acad Sci U S A 94:9831-9835

19. **Dardenne O, Prud'homme J, Hacking SA, Glorieux FH, St-Arnaud R** 2003 Correction of the abnormal mineral ion homeostasis with a high-calcium, high-phosphorus, high-lactose diet rescues the PDDR phenotype of mice deficient for the 25-hydroxyvitamin D-1alpha-hydroxylase (CYP27B1). Bone 32:332-340

20. **Labrie F, Luu-The V, Lin SX, Simard J, Labrie C, El-Alfy M, Pelletier G, Bélanger A** 2000 Intracrinology: role of the family of 17b-hydroxysteroid dehydrogenases in human physiology and disease. J Mol Endocrinol 25:1-16

21. **St-Jacques B, Hammerschmidt M, McMahon AP** 1999 Indian hedgehog signaling regulates proliferation and differentiation of chondrocytes and is essential for bone formation. Genes Dev 13:2072-2086.

22. **Ingham PW** 2001 Hedgehog signaling: a tale of two lipids. Science 294:1879-1881

23. **Murakami S, Nifuji A, Noda M** 1997 Expression of Indian hedgehog in osteoblasts and its posttranscriptional regulation by transforming growth factor-beta. Endocrinology 138:1972-1978

24. **Lin R, Amizuka N, Sasaki T, Aarts MM, Ozawa H, Goltzman D, Henderson JE, White JH** 2002 1Alpha,25-dihydroxyvitamin D3 promotes vascularization of the chondro-osseous junction by stimulating expression of vascular endothelial growth factor and matrix metalloproteinase 9. J Bone Miner Res 17:1604-1612

LEGENDS TO FIGURES

Figure 1. Chondrocyte-specific inactivation of *Cyp27b1* affects hypertrophy. Histomorphometric analysis of the hypertrophic zone of E15.5 (A) and postnatal day 2 (B) tibia in Cyp27b1$^{-/CH\Delta}$ mice and controls. **, $p<0.01$. E15.5, embryonic day 15.5; P2, postnatal day 2.

Figure 2. Chondrocyte-specific inactivation of *Cyp27b1* leads to changes at the chondro-osseous junction. Microcomputed tomography (μCT) of 2 day-old long bones showing increased bone volume (A), trabecular thickness (B), trabecular number (C), and decreased trabecular separation (D) in Cyp27b1$^{-/CH\Delta}$ mice as compared to controls. **, $p<0.01$; ***, $p<0.001$. BV/TV, bone volume/tissue volume; Trab, trabecular; P2, postnatal day 2.

Figure 3. Chondrocyte-specific inactivation of *Cyp27b1* reduces osteoclastogenesis. Tartrate Resistant Acid phosphatase staining of embryonic day 15.5 (E15.5, panels A, B) and postnatal day 2 (C, D) in control (A, C) and Cyp27b1$^{-/CH\Delta}$ mice (B, D). Panels E and F show the quantification for E15.5 and postnatal day 2, respectively. Numbers in panel F refer to osteoclasts at the chondro-osseous junction (boxed rectangle). *, $p<0.05$; ***, $p<0.001$. Arrows point to activated osteoclasts.

Figure 4. Impaired vascularization of the neonatal growth plate of Cyp27b1$^{-/CH\Delta}$ mice. RT-qPCR on RNA extracted from 2-day old rib cartilage was used to quantify mRNA levels of VEGF (A), Kdr (B), and Mmp13 (C) in Cyp27b1$^{-/CH\Delta}$ mice and controls. Platelet/endothelial cell adhesion molecule-1 (PECAM-1) immunostaining of 2-day old tibia in Cyp27b1$^{-/CH\Delta}$ mice (E) and controls (D). *, $p<0.05$; ***, $p<0.001$. Vegfa, vascular endothelial growth factor a; Kdr/VegfR2, vascular endothelial growth factor receptor 2; Mmp13, matrix metalloproteinase 13.

Figure 5. Fgf23 serum levels in Cyp27b1$^{-/CH\Delta}$ mice and controls. Fgf23 ELISA was performed on serum collected from 10-day old mice. *, $p<0.05$.

Figure 6. Chondrocyte-specific overexpression of Cyp27b1 affects growth plate development. Histomorphometric analysis of E14.5 tibia showing a reduced hypertrophic zone in transgenic mice as compared to wild-types (A). Pregnant females were injected daily with $25OHD_3$ starting one week after plug detection, until delivery. Offsprings were sacrificed two days later and tibias were collected for microcomputed tomography. Bone volume (B), trabecular thickness (C), and trabecular number (D) were decreased in transgenic mice as compared to wild-types. *, $p<0.05$; **, $p<0.01$; ***, $p<0.001$.
Tg, transgenic; wt, wild-type.

FIGURE 1

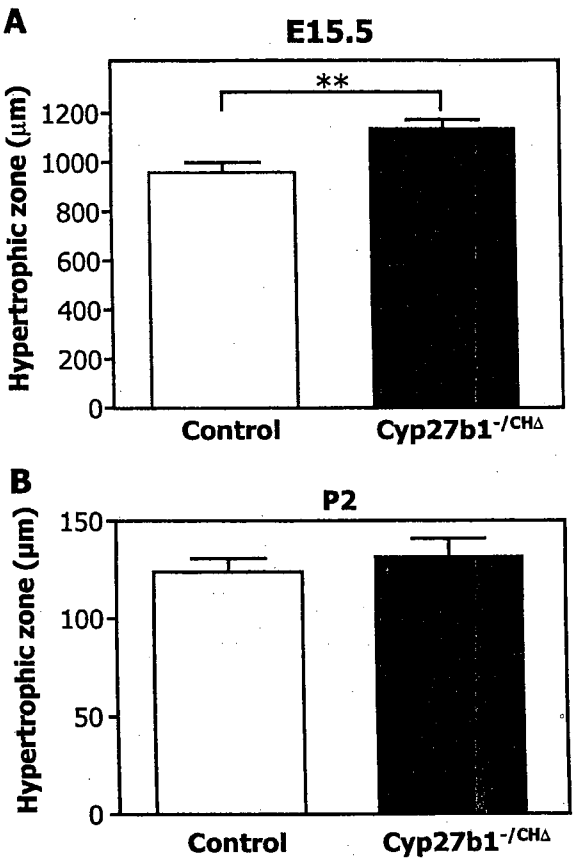
A
E15.5
**
Hypertrophic zone (μm)
1200
1000
800
600
400
200
0
Control
Cyp27b1-/CHΔ
B
P2
Hypertrophic zone (μm)
150
100
50
0
Control
Cyp27b1-/CHΔ

FIGURE 2

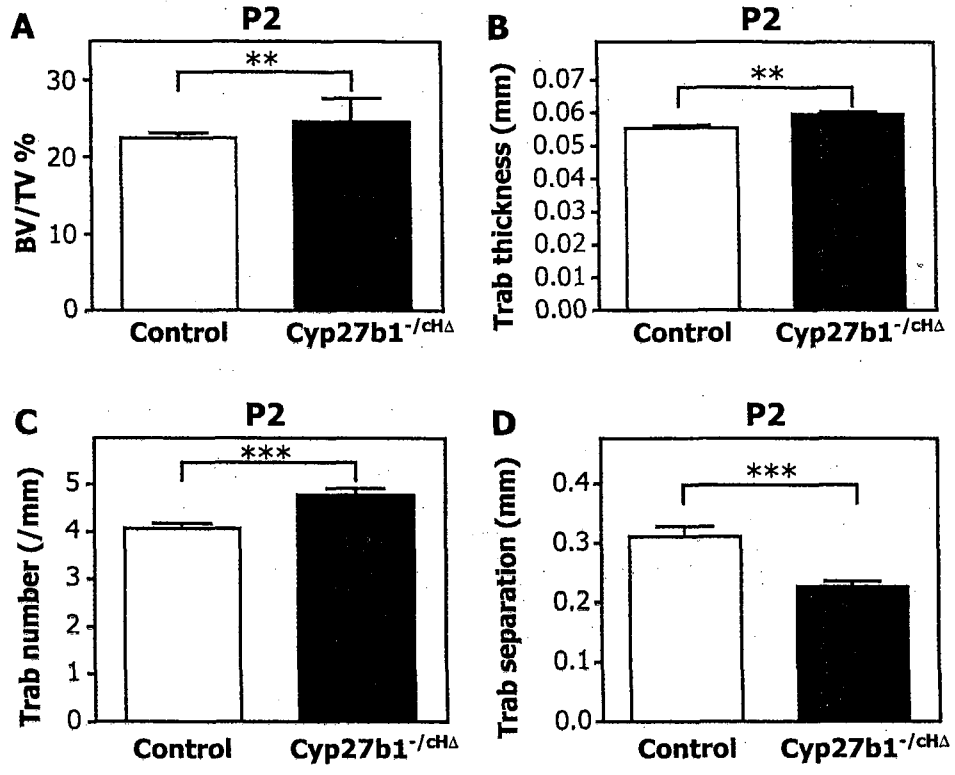
A
P2
**
BV/TV %
30
20
10
0
Control
Cyp27b1-/cHΔ
B
P2
**
Trab thickness (mm)
0.07
0.06
0.05
0.04
0.03
0.02
0.01
0.00
Control
Cyp27b1-/cHΔ
C
P2
***
Trab number (/mm)
5
4
3
2
1
0
Control
Cyp27b1-/cHΔ
D
P2
***
Trab separation (mm)
0.4
0.3
0.2
0.1
0.0
Control
Cyp27b1-/cHΔ

FIGURE 3

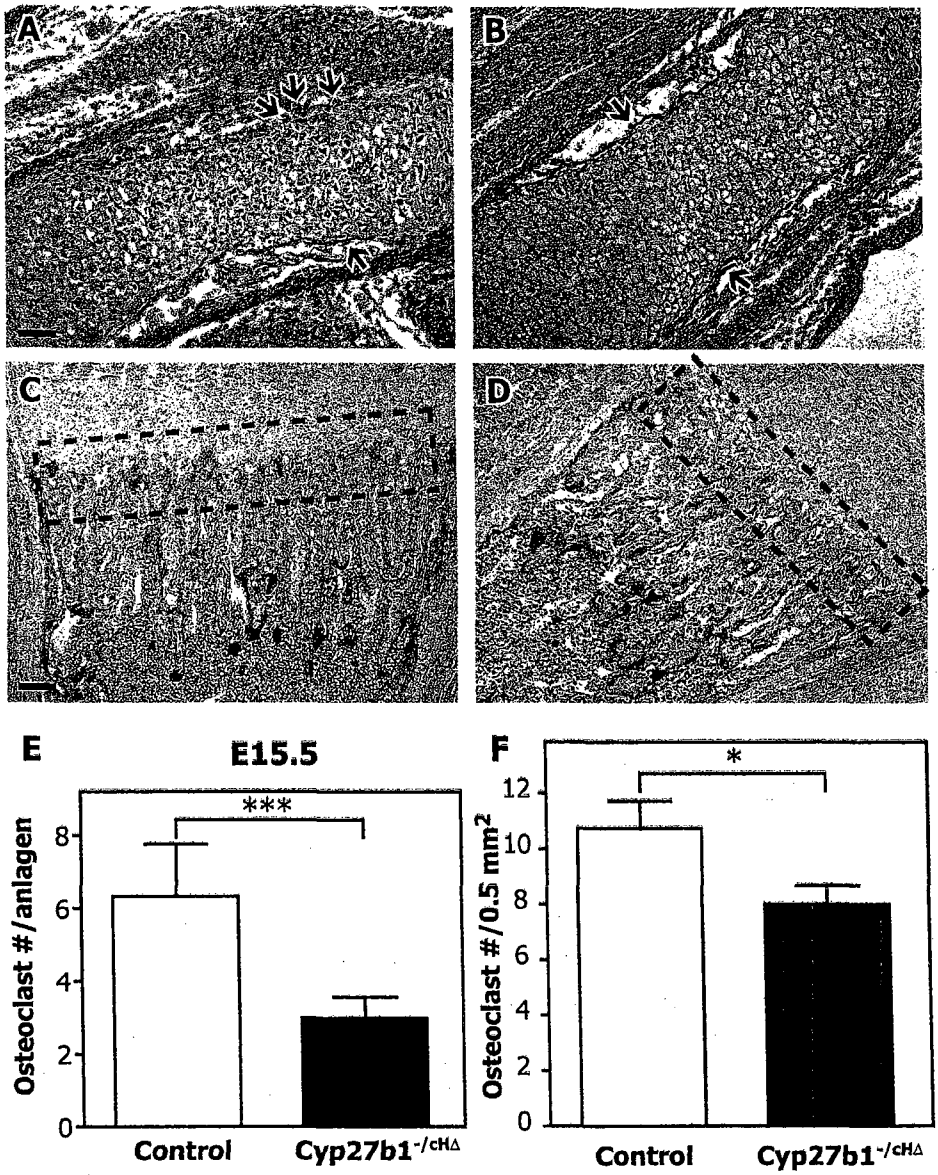
A
B
C
D
E
E15.5
***
Osteoclast #/anlagen
0
2
4
6
8
Control
Cyp27b1-/cHΔ
F
*
Osteoclast #/0.5 mm2
0
2
4
6
8
10
12
Control
Cyp27b1-/cHΔ

FIGURE 4

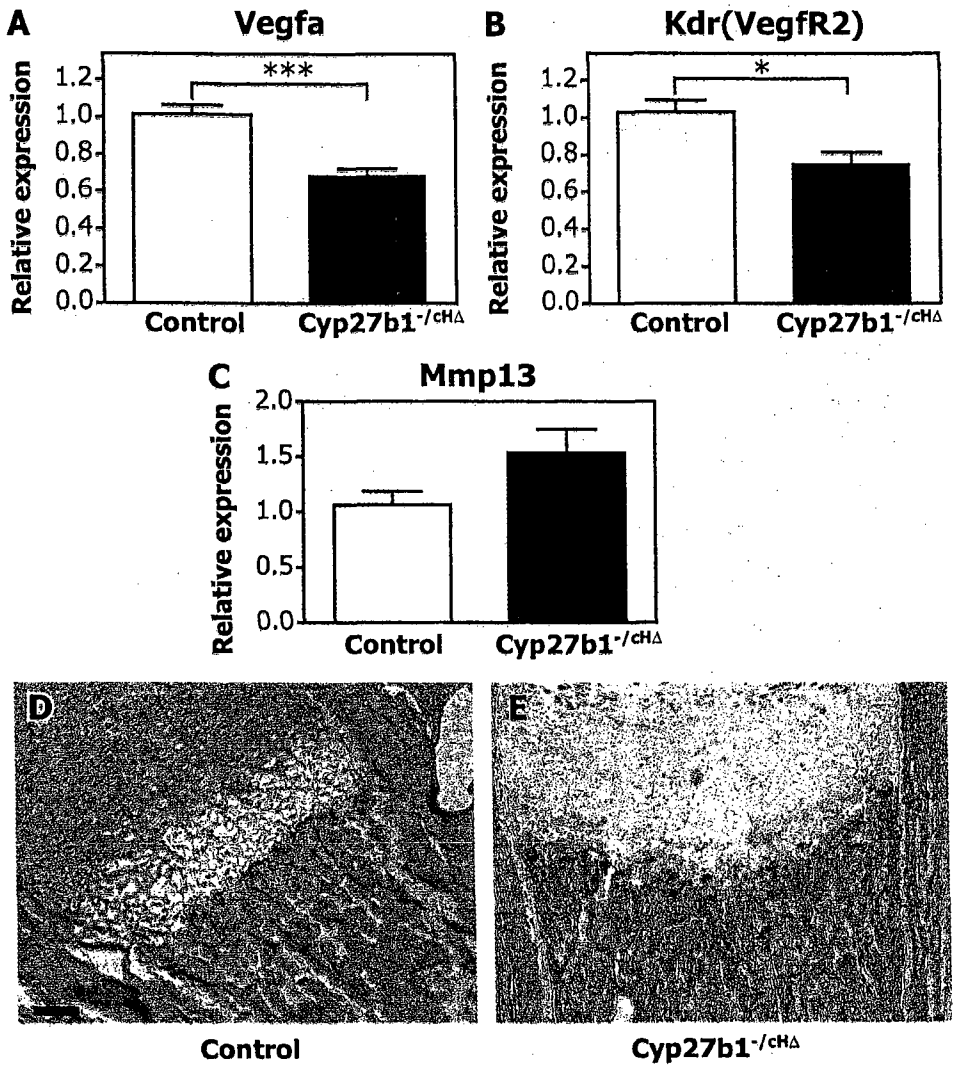
A
Vegfa
Relative expression
1.2
1.0
0.8
0.6
0.4
0.2
0.0
***
Control
Cyp27b1-/cHΔ
B
Kdr(VegfR2)
Relative expression
1.2
1.0
0.8
0.6
0.4
0.2
0.0
*
Control
Cyp27b1-/cHΔ
C
Mmp13
Relative expression
2.0
1.5
1.0
0.5
0.0
Control
Cyp27b1-/cHΔ
D
E
Control
Cyp27b1-/cHΔ

FIGURE 5

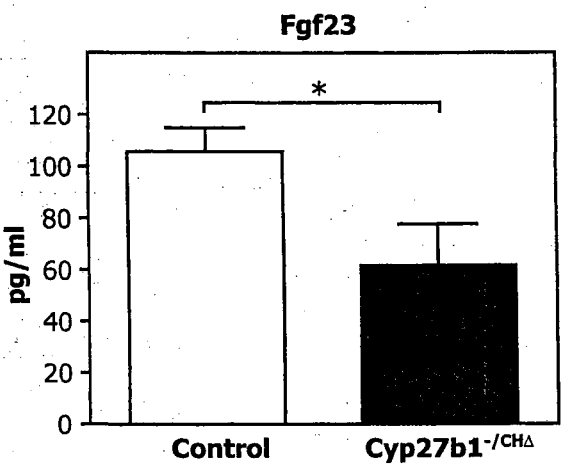

FIGURE 6

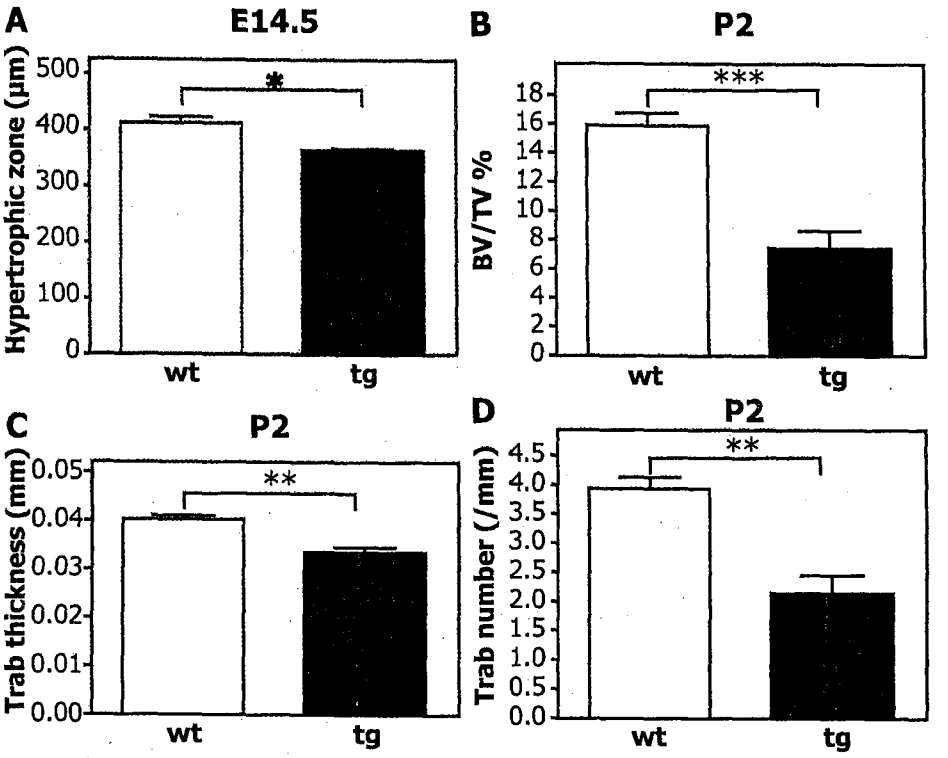
A
E14.5
Hypertrophic zone (µm)
500
400
300
200
100
0
*
wt
tg
B
P2
BV/TV %
18
16
14
12
10
8
6
4
2
0
***
wt
tg
C
P2
Trab thickness (mm)
0.05
0.04
0.03
0.02
0.01
0.00
**
wt
tg
D
P2
Trab number (/mm)
4.5
4.0
3.5
3.0
2.5
2.0
1.5
1.0
0.5
0.0
**
wt
tg

Supplementary Figure 1. Cre and Cyp27b1 expression in control and Cyp27b1$^{-/CH\Delta}$ mice. RT-qPCR on RNA extracted from 2-day old rib cartilage showing Cre expression only in mice with the Cre allele (A) and decreased expression of Cyp27b1 in Cyp27b1$^{-/CH\Delta}$ mice (B). **, $p<0.01$; ***, $p<0.001$. Cre, bacteriophage P1 Cre recombinase.

Supplementary Figure 2. Expression of differentiation markers in control and Cyp27b1$^{-/CH\Delta}$ littermates. RT-qPCR on RNA extracted from 2-day old rib cartilage was used to quantify expression of type II collagen (A), type X collagen (B), Ihh (C), Hif1α (D), and Pthr1 (E) in Cyp27b1$^{-/CH\Delta}$ mice and controls. *, $p<0.05$. Col2a1, collagen α_1(II); Col10a1, collagen type X; Ihh, Indian hedgehog; Hif1α, hypoxia induced factor 1α; Pthr1, parathyroid hormone/parathyroid hormone related peptide receptor.

Supplementary Figure 3. *Cyp27b1* (1α-OHase) transgene. (A) the 1586 bp *Cyp27b1* cDNA (excluding the 5'UTR sequences and fused in frame with a FLAG epitope at the 3'end) was subcloned downstream of a chimeric intron and upstream of an SV40 Poly A sequence. The resulting cDNA, chimeric intron, and the SV40 Poly A sequence were further subcloned downstream of the collagen α_1(II) promoter (harboring exon 1) and upstream of the collagen α_1(II) intron 1 (harboring the enhancer). The resulting molecule was linearized by Xho I digestion prior to pronuclear injection. (B) RT-qPCR on RNA extracted from 2-day old rib cartilage showing the overexpression of the *Cyp27b1* mRNA in 5Tg transgenic mice as compared to their wild-type littermates. (C) Western Blot using anti-FLAG antibody showing differential expression of the recombinant FLAG-tagged Cyp27b1 protein in various transgenic lines. The lower band on the gel is non-specific and was used as a marker of loading. Col2a, collagen α_1(II); Ex1, Exon 1; SV40 Poly A, simian virus 40 polyadenylation sequence; Enh, enhancer; rCYP27B1, recombinant Cyp27b1; Tg/tg, transgenic.

Supplementary Figure 4. Expression of chondrocyte differentiation markers in wild-type and Cyp27b1 transgenic littermates. RNA was extracted from 2-day old rib cartilage and RT-qPCR was used to quantify expression of collagen α_1(II) (A), collagen type X (B), Ihh (C), Hif1α (D), and Pthr1 (E) between transgenic mice and wild-type littermates. *, $p<0.05$. Col2a1, collagen α_1(II); Col10a1, collagen type X; Ihh, Indian hedgehog; Hif1α, hypoxia induced factor 1α; Pthr1, parathyroid hormone/parathyroid hormone related peptide receptor; wt, wild-type; tg, transgenic.

Supplementary Figure 5. Expression of angiogenic and osteoclastogenic markers in Col2-Cyp27b1 transgenics and control littermates. Pregnant females were injected daily with 25OHD$_3$ starting one week after plug detection, until delivery. Offsprings were sacrificed two days later and RNA was extracted from rib cartilage. RT-qPCR was used to quantify expression of VEGF (A), Kdr (B), and RANKL (C). Vegfa, vascular endothelial growth factor a; Kdr/VegfR2, vascular endothelial growth factor receptor 2; RANKL, receptor activator of Nf-κb ligand; wt, wild-type; tg, transgenic.

SUPPLEMENTARY FIGURE 1

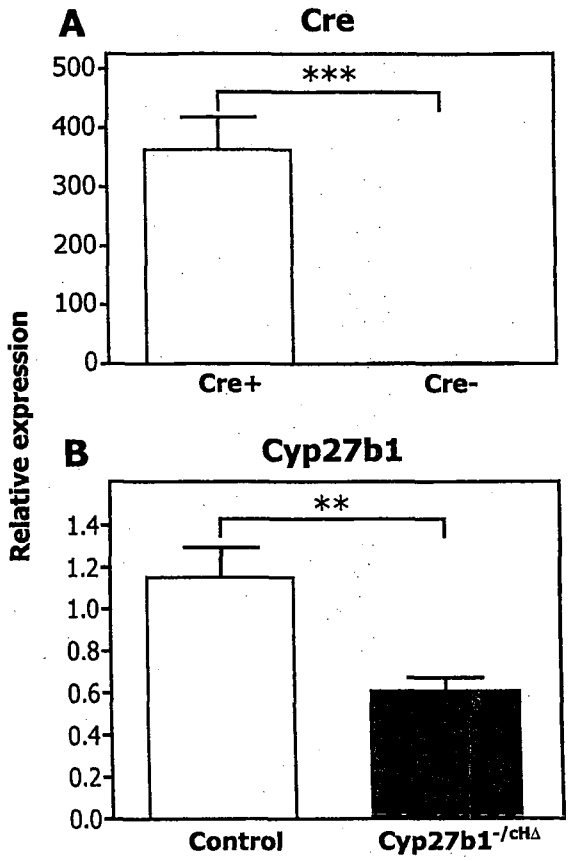

SUPPLEMENTARY FIGURE 2

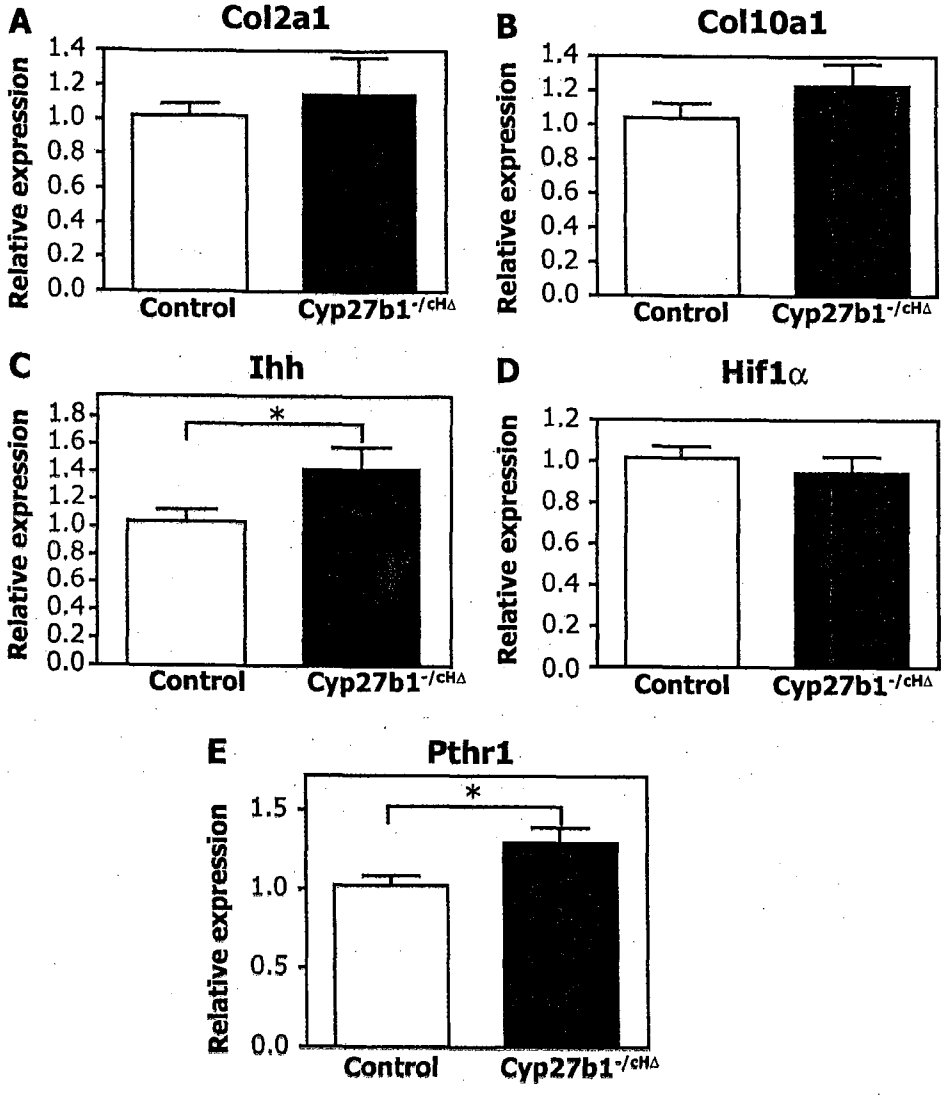

SUPPLEMENTARY FIGURE 3

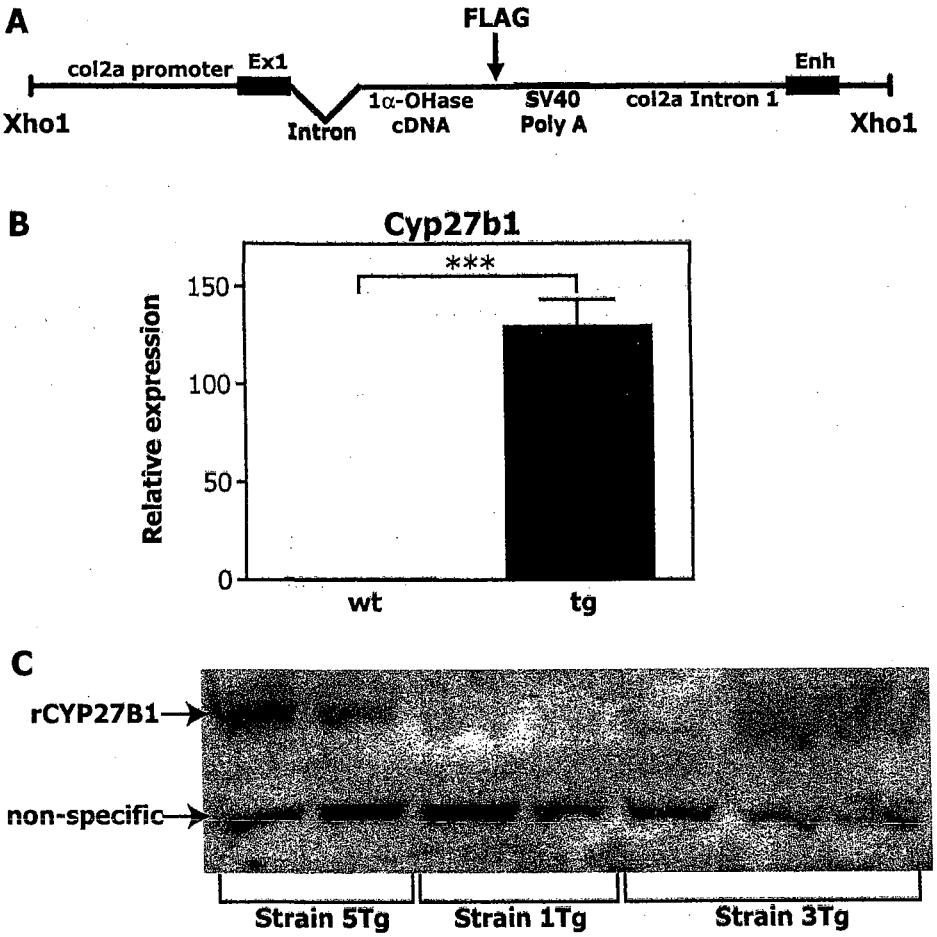

SUPPLEMENTARY FIGURE 4

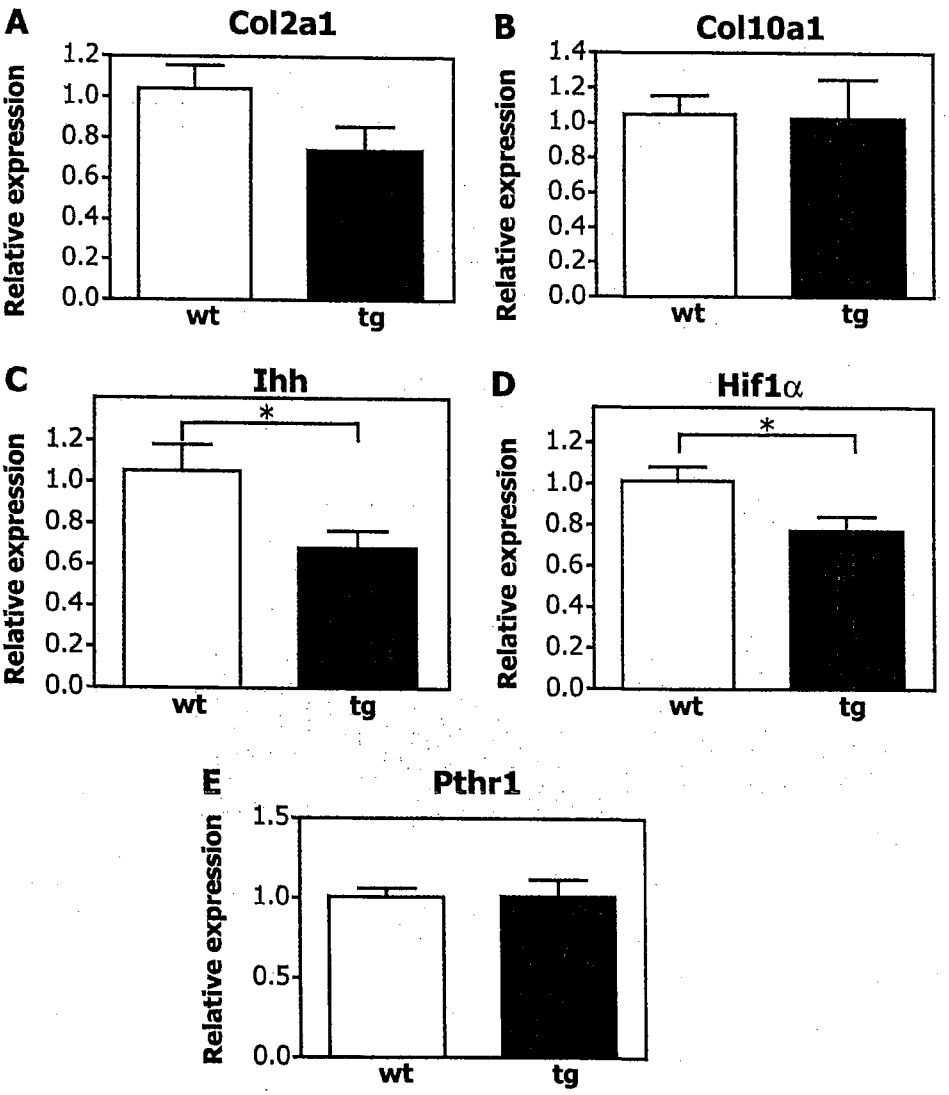

SUPPLEMENTARY FIGURE 5

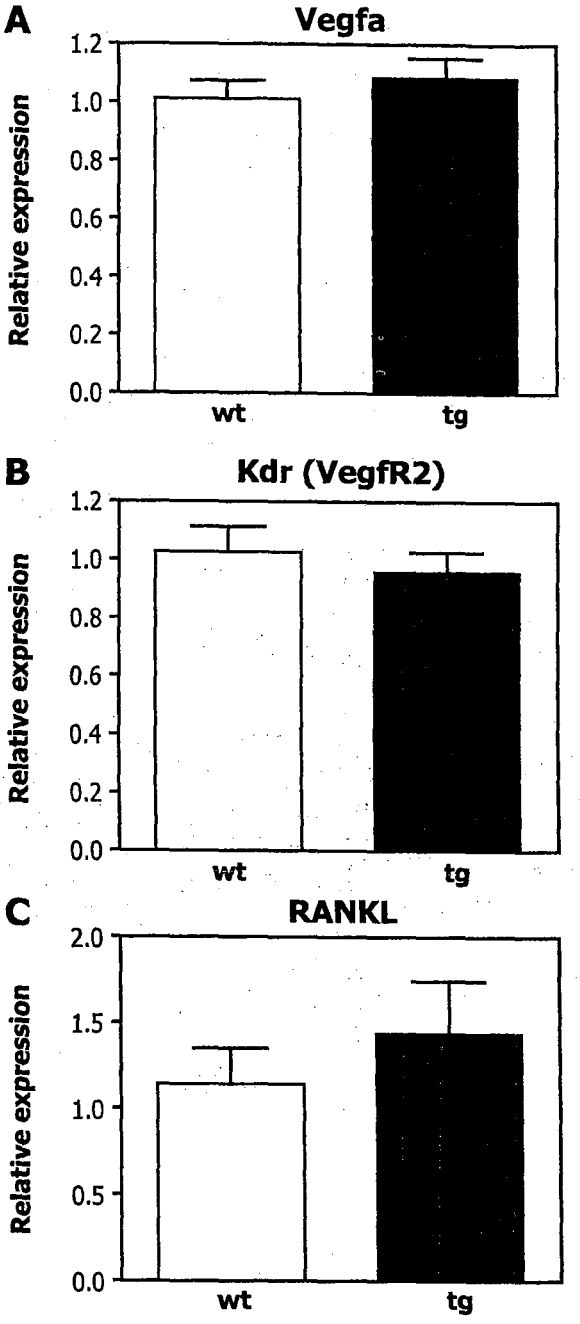

Appendix B

Certificates of Radiation Safety & ethics approval, and animal care protocols

www.mcgill.ca/researchoffice/compliance/animal/forms/

For Office Use Only:
Protocol #:
Approval end date:
Facility Committee:
Renewal#: 1st 2nd

McGill University Animal Care Committee
RENEWAL of Animal Use Protocol

For: Research ☒ Teaching ☐ project

Principal Investigator: René St-Arnaud **Protocol #** 4138

Protocol Title: Role of 24,25-dihydroxyvitamin D in fracture repair **Category:** D

Unit, Dept. & Address: Genetics Unit, Shriners Hospital for Children, 1529 Cedar Ave, Montreal (Quebec) H3G 1A6

Email: rst-arnaud@shriners.mcgill.ca **Phone:** 514-282-7155 **Fax:** 514-842-5581

Funding source: Shriners of North America

Start of Funding: January 2007 **End of Funding:** January 2010

Emergency contact #1 + work AND home phone #s: René St-Arnaud; work: 514-282-7155; home: 514-748-9129

Emergency contact #2 + work AND home phone #s: Mia Esser; work: 514-842-5964 ext.3305; home: 514-684-7590

1. Personnel and Qualifications

List the names of the Principal Investigator and of all individuals who will be in contact with animals in this study and their employment classification (investigator, technician, research assistant, undergraduate/ graduate student, fellow). Indicate if the Principal Investigator is not handling animals. If an undergraduate student is involved, the role of the student and the supervision received must be described. Training is mandatory for all personnel listed here. Refer to *www.animalcare.mcgill.ca* for details. Each person listed in this section must sign. ***(Space will expand as needed)***

Name	Classification	Animal Related Training Information		Occupational Health Program *	Signature *"Has read the original full protocol"*
		UACC on-line Theory course	Workshops + others		
René St-Arnaud	P.I.	03-11-2004	Will not handle live animals	SHC	
Mia Esser	AHT	07-11-2007	07-14-2004	SHC	
Nathalie Guevremont	AHT	07-11-2007	01-25-2007	SHC	
Nathalie Girard	Animal Attendant	May 2008	May 2008	SHC	
Roy-Pascal Naja	Graduate student	05-17-2004	02-03-2004	SHC	

*** Indicate for each person, if participating in the local Occupational Health Program, see http://www.mcgill.ca/researchoffice/compliance/animal/occupational/ for details.**

Approved by:

2. Approval Signatures

I will ensure that all collaborators and staff are aware of all changes to this protocol **Principal Investigator/ Course Director**		**Date:**
Chair, Facility Animal Care Committee		**Date:**
Animal Compliance Office		**Date:**
Chairperson, Ethics Subcommittee *(D level or Teaching Protocols Only)*		**Date:**
Approved Animal Use Period	**Start:**	**End:**

☐ **Renewal requires submission of full Animal Use Protocol form**

3. Summary (in language that will be understood by members of the general public)

AIMS AND BENEFITS: Describe, in a short paragraph, the overall aim of the study and its potential benefit to human/animal health or to the advancement of scientific knowledge *(was section 5a in main protocol).*

Vitamin D is either produced in the skin following exposure to sunlight, or is obtained from the diet. Before it can become active, the vitamin is transformed twice by the body, producing new forms of the vitamin, termed metabolites. Experimental results obtained in chicken suggest that one such metabolite, 24,25-dihydroxyvitamin D, is important for the repair of bone fractures. Confirming the role of this metabolite in other species would have great impact on health care and population health. We have engineered a mutant strain of mice that cannot produce the 24,25-dihydroxyvitamin D metabolite. We have begun to use this strain (cyp24-deficient mice) to compare fracture repair between the mutant mice and normal animals. Our preliminary results show delayed fracture repair in cyp24-deficient mice that can be rescued by treatment with 24,25(OH)2D. Fracture repair will be further analyzed in cyp24-deficient mice. We will attempt to rescue differences in fracture repair between wild-type and mutant mice by treatment with vitamin D metabolites. The characterization of a role for 24,25-dihydroxyvitamin D in fracture repair in mammals would have a major impact on the treatment of bone fractures.

4. Has there been any animal care issues?	**YES** ☐	**NO** ☒	**if yes, supply details:**

5. If creating genetically modified animals or new combinations of genetic modifications, complete and attach a *Phenotype Disclosure form.*

If mice expressing new phenotype have been produced, submit a *Phenotype Disclosure form.*

Blank forms at *http://www.mcgill.ca/researchoffice/compliance/animal/forms/*

6. Procedures

a) For B and C level of invasiveness,

The procedures are the same as the original protocol: **YES** ☐ **NO** ☐

IF NO, complete the following:

Detail new procedures that are different from section 10a of the original protocol, including amendments *(include a copy of the entire revised procedure section 10a of the original protocol with the changes and/or new procedures in CAPS):*

b) For D level of invasiveness,

Include here ALL procedures described in the original protocol. New and changed procedures in CAPS *(was section 10a in main protocol); Please only attach SOPs related to new and changed procedures to this renewal form.*

Breeding as per SOP UACC #4. Heterozygous animals will be used for breeding until six months of age. Wild-type animals and retired breeders will be sacrificed by CO2 asphyxia.

All surgery will be performed by the animal health technicians and Mr. Roy-Pascal Naja, which have trained in the laboratory of Dr. Jill Helms, who devised the mouse distraction osteogenesis model. The surgical procedure has been tested several times and animals recovered well and were fully mobile within 1 hour following surgery.

We have obtained the distraction osteogenesis device developed by the group of Jill Helms (Tay et al. 1998. J Orthop Res 16: 636). This device is a small scale version of the Ilizarov distraction device used in human patients. The custom-designed circular external fixators consist of two aluminum circular rings (outside diameter: 2.05 cm, inside diameter: 1.4 cm, thickness: 0.5 mm) held concentrically by two stainless-steel threaded rods (5/142 x 1.9 mm). Pins for transfixing the bone (0.25 mm) are attached to the frame with hexagonal bolts (2/56 inches). Total weight of the apparatus: 7 g.

Under sterile techniques in the procedures room, the proximal metaphysis of the tibia of anesthetized animals will be transfixed with 0.25 mm insect pins driven percutaneously from medial to lateral with a hand-held variable-speed drill. The orientation of the pins will be perpendicular to the long axis of the tibia (90 degrees at their intersection). Two pins, one on each side of the ring of the fixator device, will be used to transfix the bone proximally in the metaphysis and distally at the metaphyseal/diaphyseal junction. The pins will be secured to the rings by the hexagonal bolts with the tibias centered within the frame. A transverse osteotomy will be created using a number 11 scalpel blade in the proximal diaphysis of the tibia, between the two rings. This will be performed by way of an anterior longitudinal incision (2 mm in length) over the anterior compartment of the tibia. The underlying musculature will be dissected to expose the antero-lateral surface of the bone, and a neat transverse osteotomy will be performed. The underlying musculature will be closed with absorbable sutures and the skin closed with Tissue Glue.

Analgesia will be as follows: buprenorphin 0.05 mg/kg i.m. in a 50 microliter volume, 30 min before surgery, then every 12 h for a total of 36h.

Animals will be monitored three times daily during the first three days post-surgery, then daily until sacrifice.

In another series of experiments, animals will be injected with 24R,25-dihydroxyvitamin D, 24S,25-dihydroxyvitamin D (inactive epimer), or 1,25-dihydroxyvitamin D. Doses to be administered will be 6.7 ng/g body weight/day for 24,25-dihydroxyvitamin D (for both R and S epimers), a dose that yields circulating levels that are within the normal range in both wild-type and mutant mice. For 1,25-dihydroxyvitamin D, 67 pg/g body weight/every other day will be injected to avoid hypervitaminosis D. Vitamin D metabolites will be administered s.c. in a volume not exceeding 0.1 ml. Groups of animals will be sacrificed at the indicated time intervals by exsanguination under anaesthesia to allow to measure vitamin D metabolite levels in the blood. No animal will be kept for more than 28 days post-osteotomy.

For all procedures, mutant CYP24 (-/-) mice are the test animals, while heterozygous littermates (+/-) serve as controls. Mice are sacrificed at intervals following surgery (see 7b) and at least 5 mice per group are used. One series of experiments will use compound mutant mice (CYP24 -/-; VDR -/-) as test animals and littermate heterozygotes (CYP24 +/-; VDR +/-) as controls. The VDR strain will not be used in surgical treatments; it is only required to breed the VDR mutant allele onto the CYP24-deficient background.

7. Endpoints

a) For B and C level of invasiveness,

The procedures are the same as the original protocol: YES ☐ NO ☐

IF NO, supply new endpoints that are different from the original protocol:

Experimental endpoints:

Clinical endpoints:

b) For D level of invasiveness,

Include here ALL endpoints, including the ones described in the original protocol as well as new and changed endpoints in CAPS:

Experimental endpoints:

Animals will be sacrificed at 3, 7, 14, and 21 days post-surgery.

Clinical endpoints:

Animals will be sacrificed immediately if they exhibit signs of pain such as vocalizing and guarding, lose ambulation, cannot feed (weight loss >20%), or if swelling, self-mutilation, or signs of necrosis appear at the surgical site or the toes.

Frequency of monitoring: three times daily during the first three days post-surgery, then daily until sacrifice.

8. Hazards (check here if none are used: ☒)

a) Are the hazards different from original protocol? (infectious, radioactive, toxic, carcinogen, tumours)

YES ☐ NO ☐ if yes, supply details (material, risks, precautions):

b) Have the cell lines been tested for human and animal pathogens? YES:☐ NO:☐ None used:☒

9. Description of Animals to be used in the coming year (only):

Quality Control Assurance: To prevent introduction of infectious diseases into animal facilities, a health status report or veterinary inspection certificate may be required prior to receiving animals from all non-commercial sources or from commercial sources whose animal health status is unknown or questionable. Quarantine and further testing may be required for these animals. *If more than 6 columns are needed, please attach another page*

	Sp/strain 1	Sp/strain 2	Sp/strain 3	Sp/strain 4	Sp/strain 5	Sp/strain 6
Species	mouse	mouse	mouse			
Supplier/Source	breeding	Jackson labs	breeding			
Strain	cyp24 KO	VDR KO	cyp24/VDR compound			
Sex	m/f	m/f	m/f			
Age/Wt	up to 6 months	up to 6 months	up to 6 months			
# To be purchased	N/A	one breeding pair	N/A			
# Produced by in-house breeding	180	180	180			
# Other (e.g.field studies)	N/A	N/A	N/A			
TOTAL# /YEAR	**180**	**180**	**180**			

10. Explanation of Animal Numbers:

BASED ON THE EXPERIMENTAL OBJECTIVES OF THE PROJECT, describe the number of animals required for one year. Include information on experimental and control groups, # per group, and failure rates.

For breeding, specify how many adults are used, number of offspring produced, and how many offspring are used in experimental procedures. The arithmetic explaining how the total of animals for each column in the table above is calculated should be made clear.

All mice will be maintained as breeding colonies, from which experimental animals will be obtained. A breeding colony for mice in active experimental use contains approximately, on average, minimally 60 mice at one time, including active breeders, reserve stud males, males and females whose breeding success is under evaluation, pre-weaning litters and post-weaning juveniles awaiting screening. The minimum flow-through time is 10-15 weeks (gestation, weaning, screening); since three complete cycles can be completed in one year, the number of mice in one colony can be estimated at 3 x 60 = 180 mice/year.

Number of offspring used in experimental procedures: 40 wild-type and 40 mutants.

Submit to your local Facility Animal Care Committee. Please note that after two renewals, a full protocol needs to be submitted.

This approval does not imply that space will be made available. If a major increase of space needs is anticipated, please contact the appropriate animal facility manager.

6. Animals Use data for CCAC

6 a) Purpose of Animal Use (Check most appropriate one):

1. ☒ **Studies of a fundamental nature/basic research**
2. ☐ **Studies for medical purposes relating to human/animal diseases/disorders**
3. ☐ **Regulatory testing**
4. ☐ **Development of products/appliances for human/veterinary medicine**
5. **If for Teaching, use the Animal Use Protocol form for Teaching (www.mcgill.ca/research/compliance/animal/forms)**

6 b) Will field studies be conducted? NO ☒ YES ☐ If yes, complete "Field Study Form"
Will the project involve genetically altering animals? NO ☒ YES ☐ If yes, complete SOP #5 or #6
Will the project involve breeding animals? NO ☐ YES ☒ If breeding transgenics or knockouts, complete SOP#4

7. Animal Data

7 a) Please justify the need for live animals versus alternate methods (e.g. tissue culture, computer simulation)

Knockout strains allow to study the role of a particular gene product in the context of the physiology of a whole animal. No tissue culture system can reproduce these analyses.

7 b) Describe the characteristics of the animal species selected that justifies its use in the proposed study (consider characteristics such as body size, species, strain, data from previous studies or unique anatomic/physiological features)

The knockout technology is only available in mice. Mice breed well and rapidly, thus allowing the study to be completed in a reasonable amount of time.

7 c) Description of animals

Quality Control Assurance: To prevent introduction of infectious diseases into animal facilities, a health status report or veterinary inspection certificate may be required prior to receiving animals from all non-commercial sources or from commercial sources whose animal health status is unknown or questionable. Quarantine and further testing may be required for these animals.

If more than 6 columns are needed, please attach another page

	Sp/strain 1	Sp/strain 2	Sp/strain 3	Sp/strain 4	Sp/strain 5	Sp/strain 6
Species	mouse	mouse	mouse			
Supplier/Source	breeding	Jackson Labs	breeding			
Strain	cyp24 KO	VDR KO	cyp24/VDR compound			
Sex	m/f	m/f	m/f			
Age/Wt	up to 6 months	up to 6 months	up to 6 months			
# To be purchased	N/A	one breeding pair	N/A			
# Produced by in-house breeding	180	180	180			
# Other (e.g.field studies)	N/A	N/A	N/A			
#needed at one time	15	15	15			
# per cage	5	5	5			
TOTAL# /YEAR	**180**	**180**	**180**			

7 d) Explanation of Animal Usage: BASED ON THE EXPERIMENTAL OBJECTIVES OF THE PROJECT, describe the number of animals required for one year. Include information on experimental and control groups, # per group, and failure rates.

For breeding, specify how many adults are used, number of offspring produced, and how many offspring are used in experimental procedures.

The arithmetic explaining how the total of animals for each column in the table above is calculated should be made clear.
(Space will expand as needed)

All mice will be maintained as breeding colonies, from which experimental animals will be obtained. A breeding colony for mice in active experimental use contains approximately, on average, minimally 60 mice at one time, including active breeders, reserve stud males, males and females whose breeding success is under evaluation, pre-weaning litters and post-weaning juveniles awaiting screening. The minimum flow-through time is 10-15 weeks (gestation, weaning, screening); since three complete cycles can be completed in one year, the number of mice in one colony can be estimated at 3 x 60 = 180 mice/year.

8. Animal Husbandry and Care

8 a) If projects involves non-standard cages, diet and/or handling, please specify

The VDR KO strain and the cyp24-VDR compound mutants will be fed a high calcium, high phosphorus, 20% lactose diet.

8 b) Is there any component to the proposed procedures which will result in immunosuppression or decreased immune function (e.g. stress, radiation, steroids, chemotherapeutics, genetic modification of the immune system)?

NO ☒ YES ☐ **if yes, specify:**

8 c) Indicate area(s) where animal use procedures will be conducted:

Building: Shriners Hospital **Room:** Animal facility procedures room

Indicate area(s) all facilities where animals will be housed:

Building: Shriners Hospital **Room:** 306

If animal housing and animal use are in different locations, briefly describe procedures for transporting animals:

9. Standard Operating Procedures (SOPs)

Complete this section if you plan to use any of the UACC SOPs listed below. IT IS UACC POLICY THAT THESE SOPS BE USED WHEN APPLICABLE. Any proposed variation of the SOPs must be described and justified. The Standard Operating Procedures can be found at the UACC website at www.mcgill.ca/research/compliance/animal/procedures . The completed and signed SOP form must be attached to the protocol.

Check all SOPs that will be used:

Blood Collection UACC#1	☐	Collection of Amphibian Oocytes UACC#9	☐
Anaesthesia in rodents UACC#2	☐	Rodent Survival Surgery UACC#10	☒
Analgesia in rodents UACC#3	☐	Anaesthesia & Analgesia Neonatal Rodents UACC#11	☐
Breeding transgenics/knockouts UACC#4	☒	Stereotaxic Survival Surgery in Rodents UACC#12	☐
Transgenic Generation UACC#5	☐	Field Studies Form	☐
Knockout/in Generation UACC#6	☐	Phenotype Disclosure Form	☐
Production of Monoclonal Antibodies UACC#7	☐	Other, specify:	☐
Production of Polyclonal Antibodies UACC#8	☐		☐

10. Description of Procedures

10 a). IF A PROCEDURE IS COVERED BY AN SOP, WRITE "AS PER SOP", NO FURTHER DETAIL IS REQUIRED.

FOR EACH EXPERIMENTAL GROUP, DESCRIBE ALL PROCEDURES AND TECHNIQUES, WHICH ARE NOT PART OF THE SOPs, IN THE ORDER IN WHICH THEY WILL BE PERFORMED – surgical procedures, immunizations, behavioural tests, immobilization and restraint, food/water deprivation, requirements for post-operative care, sample collection, substance administration, special monitoring, etc. Appendix 2 of the Guidelines (www.mcgill.ca/research/compliance/animal/forms) provides a sample list of points that should be addressed in this section.

Breeding as per SOP UACC #4. Heterozygous animals will be used for breeding until six months of age. Wild-type animals and retired breeders will be sacrificed by CO2 asphyxia.

All surgery will be performed by the animal health technicians and Mr. Roy-Pascal Naja, which have trained in the laboratory of Dr. Jill Helms, who devised the mouse distraction osteogenesis model. The surgical procedure has been tested several times and animals recovered well and were fully mobile within 1 hour following surgery.

We have obtained the distraction osteogenesis device developed by the group of Jill Helms (Tay et al. 1998. J Orthop Res 16: 636). This device is a small scale version of the Ilizarov distraction device used in human patients. The custom-designed circular external fixators consist of two aluminum circular rings (outside diameter: 2.05 cm, inside diameter: 1.4 cm, thickness: 0.5 mm) held concentrically by two stainless-steel threaded rods (5/142 x 1.9 mm). Pins for transfixing the bone (0.25 mm) are attached to the frame with hexagonal bolts (2/56 inches). Total weight of the apparatus: 7 g.

Under sterile techniques in the procedures room, the proximal metaphysis of the tibia of anesthetized animals will be transfixed with 0.25 mm insect pins driven percutaneously from medial to lateral with a hand-held variable-speed drill. The orientation of the pins will be perpendicular to the long axis of the tibia (90 degrees at their intersection). Two pins, one on each side of the ring of the fixator device, will be used to transfix the bone proximally in the metaphysis and distally at the metaphyseal/diaphyseal junction. The pins will be secured to the rings by the hexagonal bolts with the tibias centered within the frame. A transverse osteotomy will be created using a number 11 scalpel blade in the proximal diaphysis of the tibia, between the two rings. This will be performed by way of an anterior longitudinal incision (2 mm in length) over the anterior compartment of the tibia. The underlying musculature will be dissected to expose the antero-lateral surface of the bone, and a neat transverse osteotomy will be performed. The underlying musculature will be closed with absorbable sutures and the skin closed with Tissue Glue.

Analgesia will be provided post-op: buprenorphin 0.05 mg/kg i.m. One pre-emptive administration prior to surgery, then every 12 h for the first 24h, and as needed thereafter.

Animals will be monitored three times daily during the first three days post-surgery, then daily until sacrifice.

In another series of experiments, animals will be injected with 24,25-dihydroxyvitamin D, 1,25-dihydroxyvitamin D, or a combination of both compounds. Doses to be administered will be 6.7 ng/g body weight/day for 24,25-dihydroxyvitamin D, a dose that yields circulating levels that are within the normal range in both wild-type and mutant mice. For 1,25-dihydroxyvitamin D, 67 pg/g body weight/every other day will be injected to avoid hypervitaminosis D. Vitamin D metabolites will be administered s.c. in a volume not exceeding 0.1 ml. Groups of animals will be sacrificed at the indicated time intervals by exsanguination under anaesthesia to allow to measure vitamin D metabolite levels in the blood. No animal will be kept for more than 28 days post-osteotomy.

For all procedures, mutant CYP24 (-/-) mice are the test animals, while heterozygous littermates (+/-) serve as controls. Mice are sacrificed at intervals following surgery (see 10b) and at least 5 mice per group are used. One series of experiments will use compound mutant mice (CYP24 -/-; VDR -/-) as test animals and littermate heterozygotes (CYP24 +/-; VDR +/-) as controls. The VDR strain will not be used in surgical treatments; it is only required to breed the VDR mutant allele onto the CYP24-deficient background.

10 b) Experimental endpoint – for each experimental group indicate survival time

Animals will be sacrificed at 3, 7, 14, and 21 days post-surgery. No animal will be maintained for mor than 28 days post-surgery.

10 c) Clinical endpoint – describe the conditions, complications, and criteria (e.g. >20% weight loss, maximum tumour size, vocalizing, lack of grooming) that would lead to euthanasia of an animal before the expected completion of the experiment (specify per species and project if multiple projects involved)

Animals will be sacrificed immediately if they **exhibit signs of pain such as vocalizing and guarding,** lose ambulation, cannot feed (weight loss >20%), or if swelling, self-mutilation, or signs of necrosis appear at the surgical site or the toes.

Frequency of monitoring: three times daily during the first three days post-surgery, then daily until sacrifice.

10 d) Specify person(s) who will be responsible for animal monitoring and post-procedural care ***(must also be listed in section 4)***

Name: Mia Esser	**Phone #:** 514-842-5964 ext. 3305 (work) 514-684-7590 (home)

10 e) Pre-Anesthetic/Anaesthetic/Analgesic Agents: List all drugs that will be used to minimize pain, distress or discomfort. *(Table will expand as needed)*

Species	Agent	Dosage (mg/kg)	Total volume(ml) per administration	Route	Frequency/Duration
mouse (strains 1-3)	Isoflurane	To effect	1 to 5 %	inhalation	during surgery
	ketamine xilazine acepromazine	50 mg/kg 5mg/kg 1 mg/kg	0.1 ml	i.m.	once, at sacrifice
	Buprenorphin	0.05 mg/kg	0.1 ml	i.m.	once, pre-surgery, every 12 h for one day, as needed after.

10 f) Administration of ALL other substances: List all non-anaesthetic agents under study in the experimental component of the protocol, including but not limited to drugs, infectious agents, viruses. *(Table will expand as needed)*

Species	Agent	Dosage (mg/kg)	Total volume(ml) per administration	Route	Frequency/Duration
mouse (strains 1-3)	24,25(OH)2D	6.7 ng/g bw	0.1 ml	i.m.	daily for up to 21 days
	1,25(OH)2D	67 pg/ g bw	0.1 ml	i.m.	every 2 days for up to 21 days

10 g) Method of Euthanasia

Specify Species	
	☐ **Anaesthetic overdose, list agent/dose/route:**
mouse, species 1-3	☒ **Exsanguination with anaesthesia, list agent/dose/route:** 50 mg/kg ketamine, 5 mg/kg xilazine, 1 mg/kg acepromazine i.m.
	☐ **Decapitation without anaesthesia *** ☐ **Decapitation with anesthesia, list agent/dose/route (including CO_2):**
	☐ **Cervical dislocation without anaesthesia *** ☐ **Cervical dislocation with anaesthesia, list agent/dose/route (including CO_2):**
	☐ **CO_2 chamber only**
	☐ **Other, specify:**
	☐ **Not applicable, explain:**

*** For physical method of euthanasia without anaesthesia, please justify:**

11. Category of Invasiveness: B ☐ C ☐ D ☒ E ☐

Categories of Invasiveness (from the CCAC ***Categories of Invasiveness in Animal Experiments*****). Please refer to this document for a more detailed description of categories.**

Category A: Studies or experiments on most invertebrates or no entire living material.

Category B: Studies or experiments causing little or no discomfort or stress. ***These might include holding animals captive, injection, percutaneous blood sampling, accepted euthanasia for tissue harvest, acute non-survival experiments in which the animals are completely anaesthetized.***

Category C: Studies or experiments involving minor stress or pain of short duration. ***These might include cannulation or catheterizations of blood vessels or body cavities under anaesthesia, minor surgery under anaesthesia, such as biopsy; short periods of restraint, overnight food and/or water deprivation which exceed periods of abstinence in nature; behavioural experiments on conscious animals that involve short-term stressful restraint.***

Category D: Studies or experiments that involve moderate to severe distress or discomfort. ***These might include major surgery under anaesthesia with subsequent recovery, prolonged (several hours or more) periods of physical restraint; induction of behavioural stresses, immunization with complete Freund's adjuvant, application of noxious stimuli, procedures that produce pain, production of transgenics (in***

accordance with University policy).
Category E: Procedures that involve inflicting severe pain, near, at or above the pain threshold of unanaesthetized, conscious animals. *Not confined to but may include exposure to noxious stimuli or agents whose effects are unknown; exposure to drugs or chemicals at levels that (may) markedly impair physiological systems and which cause death, severe pain or extreme distress or physical trauma on unanaesthetized animals.* According to University policy, E level studies are not permitted.

12. Potential Hazards to Personnel and Animals It is the responsibility of the investigator to obtain the necessary Biohazard and/or Radiation Safety permits before this protocol is submitted for review.
A copy of these certificates must be attached, if applicable.

No hazardous materials will be used in this study: ☒

12 a) Indicate which of the following will be used in animals:

☐ Toxic chemicals ☐ Radioisotopes ☐ Carcinogens
☐ Infectious agents (includes vectors) ☐ Transplantable tumours and/or tissues

12 b) Complete the following table for each agent to be used (use additional page as required):

Agent name			
Dosage			
Route of administration			
Frequency of administration			
Duration of administration			
Number of animals involved			
Survival time after administration			

12 c) After administration the animals will be housed in:

☐ the animal care facility ☐ laboratory under supervision of laboratory personnel

Please note that cages must be appropriately labeled at all times.

12 d) Describe potential health risk (s) to humans or animals:

12 e) Describe measures that will be used to reduce risk to the environment and all project and animal facility personnel:

12 f) If using cell lines, have they been tested?
☐ Yes If yes, What human and/or animal pathogens have been tested?

☐ No If no, justify:

13. Reviewer's Comments and Modifications (to be completed by ACC only): The Animal Care Committee has made the following modification(s) to this animal use procedure protocol during the review process. Please make these changes to your copy and comply with the recommended changes as a condition of approval.

- Obtain signature of Roy-Pascal Noja (section 4);
- Clarify vitamin D treatment in section 10a;
- Refine clinical endpoints for osteotomy (section 10a + SOP #10)

5 e) KEYWORDS: Using keywords only, list the procedures used on animals (e.g. anaesthesia, breeding colony, injection IP, gavage, drug administration, major survival surgery, euthanasia by exsanguination, behavioural studies). For a more complete list of suggested keywords refer to Appendix 1 of the Guidelines (www.mcgill.ca/researchoffice/compliance/animal/forms).

Breeding colony; survival surgery (nephrectomy); gavage; s.c. injections; treatment with non-toxic drugs (vitamin D analogs); euthanasia for tissue collection.

6. Animals Use data for CCAC

6 a) Purpose of Animal Use (Check most appropriate one):

1. ☐ **Studies of a fundamental nature/basic research**
2. ☒ **Studies for medical purposes relating to human/animal diseases/disorders**
3. ☐ **Regulatory testing**
4. ☐ **Development of products/appliances for human/veterinary medicine**
5. **If for Teaching, use the Animal Use Protocol form for Teaching (www.mcgill.ca/researchoffice/compliance/animal/forms)**

6 b) Will field studies be conducted? NO ☒ YES ☐ If yes, complete "Field Study Form"
Will the project involve genetically altering animals? NO ☒ YES ☐ If yes, complete SOP #5 or #6
Will the project involve breeding animals? NO ☐ YES ☒ If breeding transgenics or knockouts, complete SOP#4

7. Animal Data

7 a) Please justify the need for live animals versus alternate methods (e.g. tissue culture, computer simulation)

Knockout and transgenic strains allow to study the role of a particular gene product in the context of the physiology of a whole animal. No tissue culture system can reproduce these analyses. Furthermore, the cyp27b1-deficient mice represent a valid animal model for a complex disease, secondary hyperparathyroidism of renal failure, that cannot be obtained in vitro or through computer simulation.

7 b) Describe the characteristics of the animal species selected that justifies its use in the proposed study (consider characteristics such as body size, species, strain, data from previous studies or unique anatomic/physiological features)

The knockout technology is only available in mice. Mice breed well and rapidly, thus allowing the study to be completed in a reasonable amount of time.

7 c) Description of animals

Quality Control Assurance: To prevent introduction of infectious diseases into animal facilities, a health status report or veterinary inspection certificate may be required prior to receiving animals from all non-commercial sources or from commercial sources whose animal health status is unknown or questionable. Quarantine and further testing may be required for these animals.

If more than 6 columns are needed, please attach another page

	Sp/strain 1	Sp/strain 2	Sp/strain 3	Sp/strain 4	Sp/strain 5	Sp/strain 6
Species	KO mouse	KO mouse	KO mouse	KO mouse	Tg mouse	Tg mouse
Supplier/Source	Breeding	Breeding	Breeding	Breeding	Breeding	Breeding
Strain	Cyp27b1 KO	Cyp27b1 floxed	Col2-Cre-cyp27b1 floxed	Apo2E-Cre-cyp27b1 floxed	Col2-Cre	Apo2E-Cre
Sex	m/f	m/f	m/f	m/f	m/f	m/f
Age/Wt	Up to 6 months	Up to 6 months	Up to 6 months	Up to 6 months	Up to 6 months	Up to 6 months
# To be purchased	N/A	N/A	N/A	N/A	N/A	N/A
# Produced by in-house breeding	1632	48	180	180	48	48
# Other (e.g.field studies)	N/A	N/A	N/A	N/A	N/A	N/A
#needed at one time	80	Breeding pair	20	60	Breeding pair	Breeding pair
# per cage	5	5	5	5	5	5
TOTAL# /YEAR	**1632**	**48**	**180**	**180**	**48**	**48**

Additional table to add to 'Description of animals' in full Animal Use Protocol form as well as Renewal form

	Sp/strain 7	Sp/strain	Sp/strain	Sp/strain	Sp/strain	Sp/strain
Species	Tg mouse					
Supplier/Source	Breeding					
Strain	Col2-cyp27b1					
Sex	m/f					
Age/Wt	Up to 6 months					
# To be purchased	N/A					
# Produced by in-house breeding	180					
# Other (e.g.field studies)	N/A					
#needed at one time	20					
# per cage	5					
TOTAL# /YEAR	**180**					

Additional table to add to 'Description of animals' in full Animal Use Protocol form as well as Renewal form

	Sp/strain	Sp/strain	Sp/strain	Sp/strain	Sp/strain	Sp/strain
Species						
Supplier/Source						
Strain						
Sex						
Age/Wt						
# To be purchased						
# Produced by in-house breeding						
# Other (e.g.field studies)						
#needed at one time						
# per cage						
TOTAL# /YEAR						

7 d) Explanation of Animal Usage: BASED ON THE EXPERIMENTAL OBJECTIVES OF THE PROJECT, describe the number of animals required for one year. Include information on experimental and control groups, # per group, and failure rates.

For breeding, specify how many adults are used, number of offspring produced, and how many offspring are used in experimental procedures.

The arithmetic explaining how the total of animals for each column in the table above is calculated should be made clear.

(Space will expand as needed)

Strain 1 and 4:
17 litters/month, 8 pups/litter = 17 x 8 x 12 = 1632
50% of progeny (408 -/- and 408 +/-) used in experiments; 50% of progeny (remainder 408 +/- and 408 +/+) euthanized at weaning upon genotyping.
Calculations for experimental groups and treatments are provided in section 10a.

Strain 2, 5, 6:
6 litters/year, 8 pups/litter = 6 x 8 = 48

Strains 3, 4, 7:
These strains will be maintained as breeding colonies, from which experimental animals will be obtained. A breeding colony for mice in active experimental use contains approximately, on average, minimally 60 mice at one time, including active breeders, reserve stud males, males and females whose breeding success is under evaluation, pre-weaning litters and post-weaning juveniles awaiting screening. The minimum flow-through time is 10-15 weeks (gestation, weaning, screening); since three complete cycles can be completed in one year, the number of mice in one colony can be estimated at 3 x 60 = 180 mice/year.

8. Animal Husbandry and Care

8 a) If projects involves non-standard cages, diet and/or handling, please specify

Strains 1 and 4 will be fed from weaning to one week prior to treatment with a rescue diet: high calcium, high phosphorus, 20% lactose.

8 b) Is there any component to the proposed procedures which will result in immunosuppression or decreased immune function (e.g. stress, radiation, steroids, chemotherapeutics, genetic modification of the immune system)?

NO ☒ YES ☐ **if yes, specify:**

8 c) Indicate area(s) where animal use procedures will be conducted:

Building: Shriners Hospital **Room:** Animal facility procedure room

Indicate area(s) all facilities where animals will be housed:

Building: Shriners Hospital **Room:** Animal facility room 306

If animal housing and animal use are in different locations, briefly describe procedures for transporting animals:

9. Standard Operating Procedures (SOPs)

Complete this section if you plan to use any of the UACC SOPs listed below. IT IS UACC POLICY THAT THESE SOPS BE USED WHEN APPLICABLE. Any proposed variation of the SOPs must be described and justified. The Standard Operating Procedures can be found at the UACC website at www.mcgill.ca/researchoffice/compliance/animal/procedures . The completed and signed SOP form must be attached to the protocol.

Check all SOPs that will be used:

Blood Collection UACC#1	☐	**Collection of Amphibian Oocytes UACC#9**	☐
Anaesthesia in rodents UACC#2	☒	**Rodent Survival Surgery UACC#10**	☒
Analgesia in rodents UACC#3	☒	**Anaesthesia & Analgesia Neonatal Rodents UACC#11**	☐
Breeding transgenics/knockouts UACC#4	☒	**Stereotaxic Survival Surgery in Rodents UACC#12**	☐
Transgenic Generation UACC#5	☐	**Field Studies Form**	☐
Knockout/in Generation UACC#6	☐	**Phenotype Disclosure Form**	☐
Production of Monoclonal Antibodies UACC#7	☐	**Other, specify:**	☐
Production of Polyclonal Antibodies UACC#8	☐		☐

10. Description of Procedures

10 a) . IF A PROCEDURE IS COVERED BY AN SOP, WRITE "AS PER SOP", NO FURTHER DETAIL IS REQUIRED.

FOR EACH EXPERIMENTAL GROUP, DESCRIBE ALL PROCEDURES AND TECHNIQUES, WHICH ARE NOT PART OF THE SOPs, IN THE ORDER IN WHICH THEY WILL BE PERFORMED – surgical procedures, immunizations, behavioural tests, immobilization and restraint, food/water deprivation, requirements for post-operative care, sample collection, substance administration, special monitoring, etc Appendix 2 of the Guidelines (www.mcgill.ca/researchoffice/compliance/animal/guidelines) provides a sample list of points that should be addressed in this section.

For all strain, breeding as per SOP#4.

Species 1:
Weaned homozygote cyp27b1 mutant animals (n=5) and heterozygote littermates (n=5) (male or female based on availability) will be treated by subcutaneous injection or by gavage with vitamin D analogs (paricalcitol, cinacalcet, 1-OH-D2, or LR-103) for five weeks (age at onset of study: 3 weeks). Injection sites will be rotated. Doses to be tested : 30, 100, 300, 1000 pg/g body weight/ day. Animals will be sacrificed at the age of 8 weeks. To serve as an 'internal standard' for the rescue regimen, groups of 5 homozygote cyp27b1 mutant animals and 5 heterozygote littermates will receive 1,25(OH)2D3 by subcutaneous injection (500 pg/ g body weight/day). Control animals (n=5 for homozygote mutants and n=5 for heterozygotes) will be treated with the vehicle (propylene glycol). At sacrifice, blood, femurs, tibia, kidney and duodenum will be harvested from treated animals and untreated controls of the corresponding genotype. Number of animals required: 85 mice of the +/- genotype and 85 mice of the -/- genotype.

Surgical model of renal failure

Groups of homozygote cyp27b1 mutant animals and heterozygote littermates (8 to 10 weeks of age; male or female based on availability; n=5) will be partially nephrectomized according to the following procedure:

5/6 nephrectomy [Wada, M., Furuya, Y., Sakiyama, J., Kobayashi, N., Miyata, S., Ishii, H., and Nagano, N. (1997) J Clin Invest 100, 2977-2983]:
Under anesthesia, a 2.0 cm skin incision is made in the ventral midline, with its cranial terminus 1.0 cm caudal to the xyphoid process. Each kidney is dissected free through a dorsoventral incision of the muscles and fascia near the costal margin. The left kidney is removed following ligation of the renal blood vessels and ureter. The upper and lower poles of the right kidney are then resected using a cautery. This leaves intact the middle kidney segment. The musculofascial incisions are then sutured, and the skin incision is closed by metal clips. Clips are removed 5-7 days after surgery. Analgesia will be provided post-op: buprenorphin 0.05 mg/kg i.m. or 0.1 mg/kg s.c. One pre-emptive administration prior to surgery, then every 12 h for the first 24h, and as needed thereafter.

Nephrectomy will be performed by the animal health technicians.

Nephrectomized animals will be treated by gavage with vitamin D analogs (paricalcitol, cinacalcet, 1-OH-D2, or LR-103) for five or eight weeks. Doses to be tested : 30, 100, 300, 1000 pg/g body weight/ day. Control sham-operated animals (n=5 for homozygote mutants and n=5 for heterozygotes) will be treated with the vehicle. At sacrifice, blood, bone, heart, and duodenum will be collected. Number of animals required: 4 doses x 4 compounds x 5 mice/group x 2 time points, repeat once = 320 mice of the +/- genotype and 320 mice of the -/- genotype.

Total number of mice required, species 1: 85 + 320 = 405 mice of the -/- genotype
85 + 320 = 405 mice of the +/- genotype

Species 2, 5, 6:
Progeny will be genotyped using tail DNA (as per SOP UACC #4). Hemizygous (transgenic), heterozygote (+/floxed), and homozygote floxed animals will be used for breeding until six months of age. Wild-type animals and retired breeders will be sacrificed by CO2 asphyxia.

Species 3:
Groups of mutant animals (genotype: Cre fl/fl; n=10) and littermate controls (genotype: Cre +/fl; n=10) will be sacrificed at embryonic day 16.5 (E16.5), 2 days, 3 weeks, or 6 months to collect tissue for histology. All animals will be sacrificed by exsanguination under anesthesia. NOTE: animals of the appropriate genotype represent 25% of the progeny. We propose to study 40 mutant mice (4 time points at 10 mice per time point), so we need to breed 4 times more mice (4 x 40 = 160; breeding program plans for 180).

Species 4:
Mutant and wild-type littermate controls, intact or nephrectomized as described above, will be treated for 4 or 6 weeks by gavage with paricalcitol or 1-OH-D2 at the optimal dose determined in the studies with species 1. At sacrifice, blood, bone, heart, and duodenom will be collected. All animals will be sacrificed by exsanguination under anesthesia. NOTE: animals of the appropriate genotype represent 25% of the progeny. We propose to study 40 mutant mice (2 treatments, intact and NTX x 2 analogs x 2 time points x 5 mice/group = 40), so we need to breed 4 times more mice (4 x 40 = 160; the breeding program plans for 180).

Species 7:
Groups of transgenic animals (n=10) and littermate controls (n=10) will be obtained from the breeding colony and sacrificed at intervals (embryonic day 16.5, 2 days, 3 weeks, or 6 months to collect tissue for histology. All animals will be sacrificed by exsanguination under anesthesia (except E16.5 which are sacrificed by decapitation).

Gestating females will be treated with 25-hydroxyvitamin D at 0.6 ng/ g bw/ day s.c. (injected volume: 0.1 ml) from E10.5 to delivery (E21; total treatment time: 10.5 days). Pups will be sacrificed at post-natal day 2 by decapitation. We believe that the phenotype of these transgenic mice is not completely apparent due to rate-limiting amounts of the substrate of the transgenic enzyme, 25-hydroxyvitamin D-1-alpha-hydroxylase (cyp27b1). We wish to treat the transgenic mice with the substrate (25-hydroxyvitamin D) in order to maximize the phenotype, which we expect will be a reduction in the size of the growth plate and a decrease in trabecular bone volume. The phenotype should appear early after birth and could be transient, which is the rationale for treating the gestating females. Numbers of animals allocated to this study: 2 genotypes x 2 groups (controls and treated) x 10 mice/group = 40 mice total, obtained from the breeding colony.

10 b) Experimental endpoint – for each experimental group indicate survival time

Species 1: Wild-type animals are sacrificed at one month (after genotyping).
Animals used in treatment groups will be sacrificed after 5 or 8 weeks of treatment.
Retired breeders will be sacrificed at 6 months of age.

Species 2, 5, 6: Retired breeders will be sacrificed at 6 months of age.

Species 3, 7: Experimental animals will be sacrificed at intervals for tissue collection: E16.5, 2 days, 3 weeks, and 6 months.

Species 4: Wild-type animals are sacrificed at one month (after genotyping).
Animals used in treatment groups will be sacrificed after 4 or 6 weeks of treatment.
Retired breeders will be sacrificed at 6 months of age.

10 c) Clinical endpoint – describe the conditions, complications, and criteria (e.g. >20% weight loss, maximum tumour size, vocalizing, lack of grooming) that would lead to euthanasia of an animal before the expected completion of the experiment (specify per species and project if multiple projects involved)

Animals will be sacrificed earlier than specified in 10b above if signs of distress appear: necrosis of the surgical site, tremors, temperature loss, lack of grooming, weight loss (>20%), inability to feed, paralysis, etc.

Frequency of monitoring: daily, except animals that underwent surgery that will be monitored twice daily.

10 d) Specify person(s) who will be responsible for animal monitoring and post-procedural care ***(must also be listed in section 4)***

Name: Mia Esser | **Phone #:** 514-684-7590

10 e) Pre-Anesthetic/Anaesthetic/Analgesic Agents: List all drugs that will be used to minimize pain, distress or discomfort. *(Table will expand as needed)*

Species	Agent	Dosage (mg/kg)	Total volume(ml) per administration	Route	Frequency/Duration
mouse	Isoflurane	To effect	1 to 5 %	inhalation	during surgery
	ketamine xilazine acepromazine	50 mg/kg 5mg/kg 1 mg/kg	0.1 ml	i.m.	once, at sacrifice
	Buprenorphin	0.05 mg/kg	0.1 ml	i.m.	once, pre-surgery, every 12 h for one day, as needed after.

10 f) Administration of ALL other substances: List all non-anaesthetic agents under study in the experimental component of the protocol, including but not limited to drugs, infectious agents, viruses. *(Table will expand as needed)*

Species	Agent	Dosage (mg/kg)	Total volume(ml) per administration	Route	Frequency/Duration
mouse	1,25(OH)2D3	500 pg/g/day	0.1 ml	oral	once/ 2 days for up to 8 weeks
	vitamin D analogs: Paricalcitol	30 pg/g/day 100 pg/g/day 300 pg/g/day 1000 pg/g/day	0.1 ml	oral	once/ 2 days for up to 8 weeks
	cinacalcet	30 pg/g/day 100 pg/g/day 300 pg/g/day 1000 pg/g/day	0.1 ml	oral	once/ 2 days for up to 8 weeks
	1-OH-D2 (doxercalciferol)	30 pg/g/day 100 pg/g/day 300 pg/g/day 1000 pg/g/day	0.1 ml	oral	once/ 2 dayd for up to 8 weeks
	LR-103	30 pg/g/day 100 pg/g/day 300 pg/g/day 1000 pg/g/day	0.1 ml	oral	once/ 2 days for up to 8 weeks

10 g) Method of Euthanasia

Specify Species	
	☐ **Anaesthetic overdose, list agent/dose/route:**
mouse	☒ **Exsanguination with anaesthesia, list agent/dose/route:** ketamine/xylazine/acepromazine i.m.
mouse	☒ **Decapitation without anaesthesia *** Will be used with pups at or before 2 days of age. ☐ **Decapitation with anesthesia, list agent/dose/route (including CO_2):**
	☐ **Cervical dislocation without anaesthesia *** ☐ **Cervical dislocation with anaesthesia, list agent/dose/route (including CO_2):**
mouse	☒ **CO_2 chamber only**
	☐ **Other, specify:**
	☐ **Not applicable, explain:**

*** For physical method of euthanasia without anaesthesia, please justify:** Will be used with pups at or before 2 days of age.

11. Category of Invasiveness: B ☐ C ☐ D ☒ E ☐

Categories of Invasiveness (from the CCAC *Categories of Invasiveness in Animal Experiments*). Please refer to this document for a more detailed description of categories.

Category A: Studies or experiments on most invertebrates or no entire living material.

Category B: Studies or experiments causing little or no discomfort or stress. ***These might include holding animals captive, injection, percutaneous blood sampling, accepted euthanasia for tissue harvest, acute non-survival experiments in which the animals are completely anaesthetized.***

Category C: Studies or experiments involving minor stress or pain of short duration. ***These might include cannulation or catheterizations of blood vessels or body cavities under anaesthesia, minor surgery under anaesthesia, such as biopsy; short periods of restraint, overnight food and/or water deprivation which exceed periods of abstinence in nature; behavioural experiments on conscious animals that involve short-term stressful restraint.***

Category D: Studies or experiments that involve moderate to severe distress or discomfort. ***These might include major surgery under anaesthesia with subsequent recovery, prolonged (several hours or more) periods of physical restraint; induction of behavioural stresses, immunization with complete Freund's adjuvant, application of noxious stimuli, procedures that produce pain, production of transgenics (in accordance with University policy).***

Category E: Procedures that involve inflicting severe pain, near, at or above the pain threshold of unanaesthetized, conscious animals. ***Not confined to but may include exposure to noxious stimuli or agents whose effects are unknown; exposure to drugs or chemicals at levels that (may) markedly impair physiological systems and which cause death, severe pain or extreme distress or physical trauma on unanaesthetized animals.*** **According to University policy, E level studies are not permitted.**

12. Potential Hazards to Personnel and Animals It is the responsibility of the investigator to obtain the necessary Biohazard and/or Radiation Safety permits before this protocol is submitted for review.
A copy of these certificates must be attached, if applicable.

No hazardous materials will be used in this study: ☒

12 a) Indicate which of the following will be used in animals:

☐ Toxic chemicals ☐ Radioisotopes ☐ Carcinogens
☐ Infectious agents (includes vectors) ☐ Transplantable tumours and/or tissues

12 b) Complete the following table for each agent to be used (use additional page as required):

Agent name			
Dosage			
Route of administration			
Frequency of administration			
Duration of administration			
Number of animals involved			
Survival time after administration			

12 c) After administration the animals will be housed in:

☐ the animal care facility ☐ laboratory under supervision of laboratory personnel

Please note that cages must be appropriately labeled at all times.

12 d) Describe potential health risk (s) to humans or animals:

12 e) Describe measures that will be used to reduce risk to the environment and all project and animal facility personnel:

12 f) If using cell lines, have they been tested?
☐ Yes If yes, What human and/or animal pathogens have been tested?

☐ No If no, justify:

13. Reviewer's Comments and Modifications (to be completed by ACC only): The Animal Care Committee has made the following modification(s) to this animal use procedure protocol during the review process. Please make these changes to your copy and comply with the recommended changes as a condition of approval.